UiT
THE ARCTIC UNIVERSITY OF NORWAY

Faculty of Biosciences, Fisheries and Economics
Department of Arctic and Marine Biology

Potential drivers of the downward carbon and particle flux in Arctic marine ecosystems under contrasting hydrographical and ecological situations

—

Ingrid Wiedmann

A dissertation for the degree of Philosophiae Doctor – July 2015

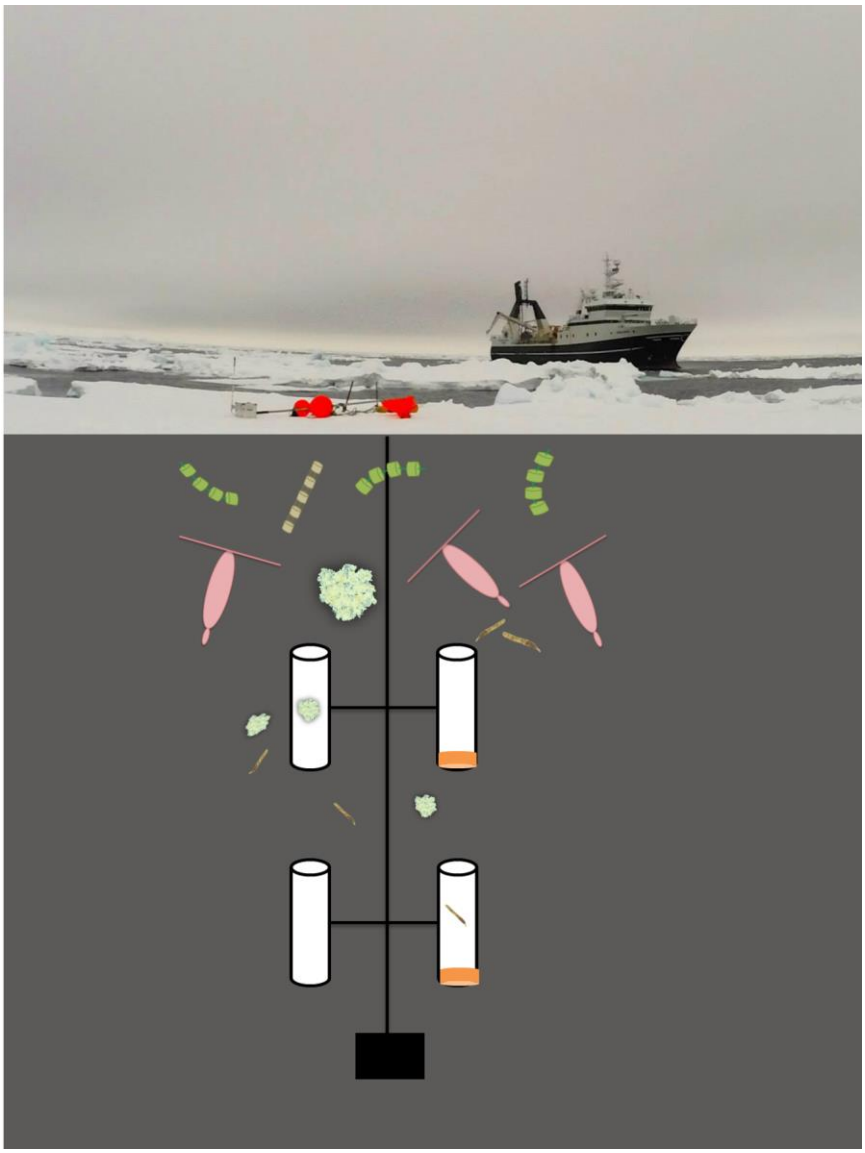

UNIVERSITY OF TROMSØ

Cover image kindly provided by Birgit Nesheim

Potential drivers of the downward carbon and particle flux in Arctic marine ecosystems under contrasting hydrographical and ecological situations

Ingrid Wiedmann

Thesis submitted in partial fulfillment of the requirements for

the degree Philosophiae Doctor in Natural Science

Tromsø, Norway

July 2015

Department of Arctic and Marine Biology
Faculty of Biosciences, Fisheries and Economics
UiT The Arctic University of Norway

ARCTOS Research School

SUPERVISORS

Prof. Marit Reigstad

UiT The Arctic University of Norway

Faculty of Biosciences, Fisheries and Economics

Department of Marine and Arctic Biology

Prof. Paul Wassmann

UiT The Arctic University of Norway

Faculty of Biosciences, Fisheries and Economics

Department of Marine and Arctic Biology

Dr. Sünnje Basedow

University of Nordland, Norway

ONCE YOU HAVE A TASTE FOR THE OCEAN,

THE INTOXICATION LASTS A LIFE LONG.

TREVOR NORTON

ACKNOWLEDGEMENTS

A PhD candidate in Germany usually has only one supervisor, called a "Doktorvater". Here in Tromsø, I was so lucky to get a whole "doctoral family" on my side. Marit Reigstad, my main supervisor, was an outstanding "doctoral mother". She always had an open door and open ear for my every day challenges in the world of particle fluxes and all the other issues in my PhD life. Thank you so much, Marit! It meant a lot to me that I could always come, ask for your opinion and advice, but still had the opportunity to decide myself. Paul Wassmann took the role as "doctoral father". Though not as involved as Marit in my daily PhD life, Paul played an important part in it. He introduced me to the scientific society through cozy dinners and international meetings, and opened many doors for me. Paul, thanks a lot for all these opportunities – in the past and in the future! It was/ is great to work with you and I am looking forward to all the things to come. Last, but not least, Sünnje Basedow perfectly filled the role as "older sister" in this "doctoral family". She was a great mentor in everything connected to numbers and particle, and is a fantastic mate. Sünnje, thanks for your help, for having fun at sea and on land, the possibility to crash on your sofa in Bodø and our 3-days-commune in Florence.

Apart from my supervisors, many other people substantially contributed to this thesis. I would like to thank my co-authors (Arild Sundfjord, Tove Gabrielsen, Miriam Marquardt, Anna Vader, Jean-Éric Tremblay), the skippers and the crews of the R/V Helmer Hanssen, R/V Johan Ruud, R/V Viking Explorer, K/V Svalbard, M/S Farm. Without your effort this doctoral thesis would not exist.

To all my colleagues and friends at the Department of Arctic and Marine Biology, to my office and cruise mates, the ARCTOS research school (especially to the previous and the current secretary, Daniel and Rike, who became very good friends during the last four years) and the ARCTOS network: Folks, thanks for all your help, your friendship, coffee breaks/ lunches/…and the good time we had together – you helped me to forget the lonesome struggles in front of my screen and made my PhD years a great time.

Further I would like to thank all my "non-scientific" friends, the people from "Kom og Dans Tromsø" as well as my family in Østfold and Bavaria, and in particular my parents. You managed to keep my feet firmly on the ground, and made me not forget that there is something beyond science and my office - something called life. This kept my mood up and put my "science problems" in the right perspective. Thank you so much for that.

Finally, dear Magnus, thank you so much for your endless support for all my projects, for always "catching me" when I had the feeling that the challenges got too big, for the conversations in our living room and for the decision (already a while ago) that you want to go this way of life together with me.

My research was financed by a scholarship from UiT The Arctic University of Norway. The field and lab work was financially supported by the Arctic Field Grant (RIS 5264), the Conflux project (Tromsø Forskningsstiftelse) and the MicroFUN project (UNIS).

Ingrid Wiedmann, Tromsø, July 2015

ABSTRACT

In Arctic marine ecosystems, hydrography, nutrient concentrations and ecological interactions of plankton change with season, which, in turn, affects the downward flux of particulate organic carbon (POC). Climate warming induces further changes, but detailed predictions of the future downward POC flux in Arctic regions are challenging due to the poor mechanistic understanding of potential drivers.

Here, short-term sediment traps, partly modified with gel-containing jars (gel traps), were deployed under contrasting hydrographical and ecological situations in the Barents Sea and Adventfjorden, Svalbard. In this way, the downward POC and the particle flux (≥ 0.05 mm equivalent spherical diameter determined in an image analysis, ESD_{image}) was quantified in a parallel manner, and POC sedimentation could be aligned with characteristics of sinking particles (e.g., size, POC: volume ratio) and be used to refine the understanding of potential drivers of the downward POC flux.

In the Barents Sea, three stations were investigated along a north-south gradient of stratification, turbulent mixing and phytoplankton bloom stage (late peak bloom, late bloom, post bloom, respectively). The highest downward POC flux (260-670 mg POC m^{-2} d^{-1}) occurred at the ice-free, weakly stratified and deeply mixed southernmost station. Sinking particles were here < 1.00 mm ESD_{image} and the particle volume flux was low (30-90 m: 40-130 x 10^3 mm^3 m^{-2} d^{-1}), resulting in a high POC: volume ratio of the sinking material. It is assumed that the high upward nitrate flux stimulated new production in the mixing layer, and that the produced biomass enhanced the downward POC flux in two ways. On the one hand, the biomass was fast transported to deeper layers by vertical mixing and on the other hand, zooplankton grazed and repackaged biomass into fast-sinking pellets, which matched the observed POC: volume ratio.

The seasonal study in Adventfjorden was conducted during winter, spring and autumn. The highest POC flux was found during autumn (mid-September, 770-1530 mg POC m^{-2} d^{-1}), when glacial run-off occurred. High volume flux (2150-6190 x 10^3 mm^3 m^{-2} d^{-1}) and large sinking particles (0.05-3.62 mm ESD_{image}) with a low POC: volume ratio were associated with this flux at two sampling depths. According to Stokes' Law, large particles tend to sink fast, and thus they may have caused a high downward POC flux despite the low POC: volume ratio. Further, entrained terrestrial POC apparently enhanced the downward POC flux in the fjord. The high downward flux was most likely also promoted by ballasting effects by

entrained lithogenic material as well as the formation of large aggregates by flocculation processes or pteropods, but further detailed investigation of these drivers is needed.

In conclusion, it is illustrated here that a high downward POC flux in Arctic marine ecosystems may occur during the phytoplankton bloom, but can also take place in deep-mixed waters during a post bloom situation or coastal regions affected by glacial run-off. The present study further shows that high POC downward flux is not necessarily caused by large sinking particles or a high sinking particle volume, but may also occur in form of small particles with a high POC: volume ratio.

TABLE OF CONTENTS

LIST OF PAPERS

PAPER I

Wiedmann I, Reigstad M, Sundfjord A, Basedow S (2014) Potential drivers of sinking particle's size spectra and vertical flux of particulate organic carbon (POC): Turbulence, phytoplankton and zooplankton. *Journal of Geophysical Research: Oceans*, 119: 6900-6917. doi: 10.1002/2013JC009754.

PAPER II

Wiedmann I, Tremblay JE, Sundfjord A, Reigstad M, Upward nitrate flux and downward particulate organic carbon (POC) flux along a gradient of stratification and turbulent mixing in an Arctic shelf sea, Barents Sea.
(Manuscript formatted to the standards of *Journal of Geophysical Research: Oceans*).

PAPER III

Wiedmann I, Reigstad M, Marquardt M, Vader A, Gabrielsen T M, Seasonality of vertical flux and sinking particle characteristics in an ice-free high Arctic fjord – different from sub-Arctic fjords?
(Submitted after revision to *Journal of Marine Systems*).

1 INTRODUCTION

The present scenario of climate warming causes considerable changes in the Arctic hydrographical environment (Carmack and McLaughlin, 2011; IPCC, 2013; Lique, 2015), its marine ecosystems (Kahru et al., 2011; Wassmann et al., 2011; Arrigo and van Dijken, in press), and the ability of the Arctic seas to function as a carbon sink (Wassmann and Reigstad, 2011). Especially the latter is challenging to predict, because it is controlled by various changing physical and biological factors, as illustrated by the following examples:

A reduced and weakened sea-ice cover exposes the Arctic seas to greater wind mixing and surface stress (Rainville et al., 2011; Martin et al., 2014). Direct mechanical wind mixing and wind-induced shelf upwelling potentially replenishes nutrient concentrations in the euphotic zone during the productive summer season (Sakshaug and Slagstad, 1992; Carmack et al., 2004; Spall et al., 2014). Pulsed nutrient renewal like this has been simulated in a mesocosm study, and there it caused an enhanced downward flux of biomass (chlorophyll *a* and particulate organic carbon) (Svensen et al., 2002).

At the same time, the Arctic surface waters tend to freshen due to increased melting of the sea-ice cover, stronger glacial melt water run-off and changes in the hydrological cycle (Arendt et al., 2002; Carmack and McLaughlin, 2011; Bamber et al., 2012). This strengthens the water column stratification and restricts both the downward mixing of biomass and the upward nutrient flux into the surface layer (Carmack and McLaughlin, 2011). Low nutrient concentrations in the surface favor small phytoplankton cells (< 2 µm) as it has been observed in the Canadian Arctic (Li et al., 2009; Li et al., 2013). The high surface: volume ratio of these cells gives them a competitive advantage for the nutrient uptake under these conditions. Small cells also tend to have lower sinking velocities than large cells (Richardson and Jackson, 2007), and a shift in the phytoplankton community toward smaller cells may cause a decline in the downward biomass flux.

Zooplankton is a major regulating factor of the downward biomass flux (Turner, 2002; Turner, 2015). In case of a warming Arctic with earlier ice-break up and earlier phytoplankton spring blooms (Kahru et al., 2011; Arrigo and van Dijken, in press), a temporal mismatch of the primary production peak and the maximum abundance of certain life stages of the Arctic copepod *Calanus glacialis* may occur (Søreide et al., 2010). Sinking of ungrazed autotrophic biomass could enhance the downward biomass flux, but the impact of northwards moving

species, such as temperate zooplankton and fish species (Slagstad et al., 2011; Dalpadado et al., 2012; Fossheim et al., 2015), is still rather unclear.

Glacial run-off from land increases in some parts of the Arctic (Bamber et al., 2012). It has been suggested that entrained nutrients locally stimulated primary production in a Greenlandic fjord (Jensen et al., 1999). In the case that the produced biomass is not utilized by grazers, it may enhance the downward biomass flux. Lithogenic material, entrained with the glacial run-off, has a high density and a high sinking velocity (De La Rocha and Passow, 2007) and it may ballast sinking of organic aggregates and enhance the downward biomass flux.

These examples illustrate that predicting the downward biomass flux in a future (warmer) Arctic is challenging due to a variety of influencing factors as well as the high temporal and spatial variability in the Arctic (Wassmann et al., 2004). Studies covering different seasons, hydrographic situations and contrasting Arctic marine ecosystems are therefore needed to further develop the mechanistic understanding and improve predictions of the (future) downward biomass flux.

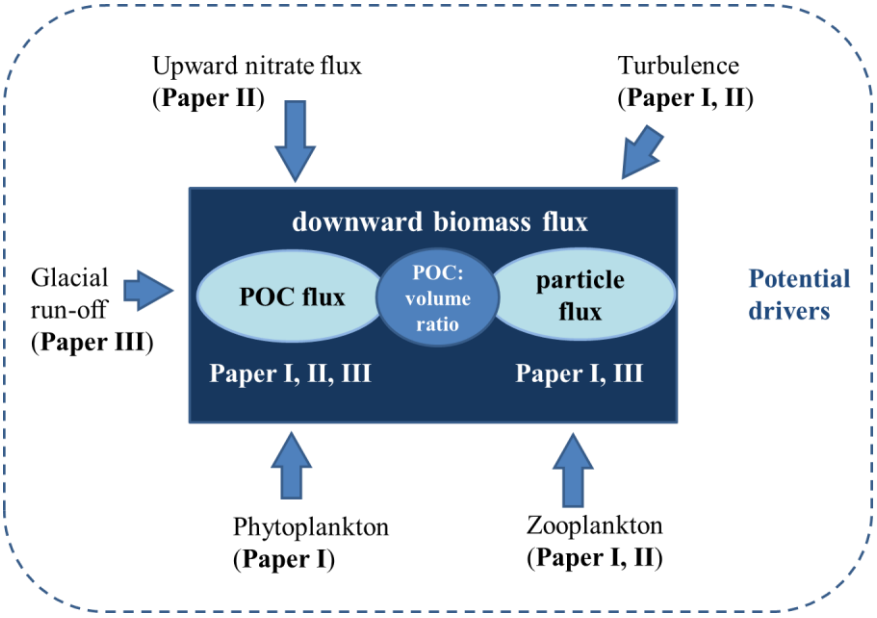

Figure 1: Schematic overview illustrating the structure of the present study. Downward biomass flux was here studied as POC flux and particle flux (interlinked via the POC: volume ratio) and different potential drivers of the fluxes were examined. Detailed information on the downward POC and particle flux and its potential drivers can be found in **Paper I-III** (see List of papers).

In the present study, I focus on the downward biomass flux and its potential drivers during contrasting scenarios of stratification, season and biological setting (bloom/ not-bloom) in an Arctic shelf sea (Barents Sea) and an Arctic fjord (Adventfjorden, western Svalbard). The downward flux was quantified as (1) flux of particulate organic carbon (POC > 0.7 µm, Figure 1) and (2) particle flux (particles ≥ 50 µm equivalent spherical diameter, ESD_{image}, collected in "gel traps" and quantified in an image analysis, Figure 1). Both fluxes could be interlinked by the POC: volume ratio of the particles (**Paper I, III**). Small-scale turbulence (**Paper I**), upward nitrate flux (**Paper II**), phyto-/ zooplankton abundance (**Paper I, III**) and glacial run-off (**Paper III**) were examined as potential drivers of the downward flux.

2 BACKGROUND

2.1 SEASONALITY OF THE DOWNWARD POC FLUX IN ARCTIC MARINE ECOSYSTEMS

Sun light penetrates the surface ocean and stimulates autotrophic biomass production in the euphotic zone (> 1% surface irradiance). Buesseler and Boyd (2009) described this surface layer as the zone, "where the 'strength' of the biological pump is set". The abundance and composition of the autotrophs in this layer determine how much biomass is produced by photosynthetic processes.

Heterotrophic grazers utilize the produced biomass and can often be found associated with a subsurface Chl *a* maximum or somewhat below it in the upper twilight zone (< 1 % surface irradiance) (Longhurst and Glen Harrison, 1989; Checkley Jr. et al., 2008), causing a strong biomass attenuation (Olli et al., 2002; Reigstad et al., 2008; Olli, 2015). In other words, the ecological interactions of primary producers and consumers in the upper twilight zone define "the 'efficiency' of the biological pump" (Wassmann et al., 2003; Buesseler and Boyd, 2009).

The downward POC flux in Arctic marine ecosystems is affected by the alternation between the polar night during winter (e.g. 78°N: from mid-November to end of January) and the period of midnight sun during the summer (e.g. 78°N: from mid-April to late August). This causes strong seasonal changes in light, temperature and environmental conditions, which, in turn, influence hydrography, phyto-/ zooplankton abundance and composition. The ecological interaction of these parameters then determines the downward POC flux.

A compilation of POC fluxes (200 m) from both long-term and short-term deployed sediment traps in Arctic regions with and without seasonal ice-cover illustrates a high spatial variability, especially depending on the ice break-up. Nevertheless, it also shows that there is a seasonal cycle in the downward POC flux, and that more POC tends to sink out during the productive summer period than in winter (January to April, Figure 2).

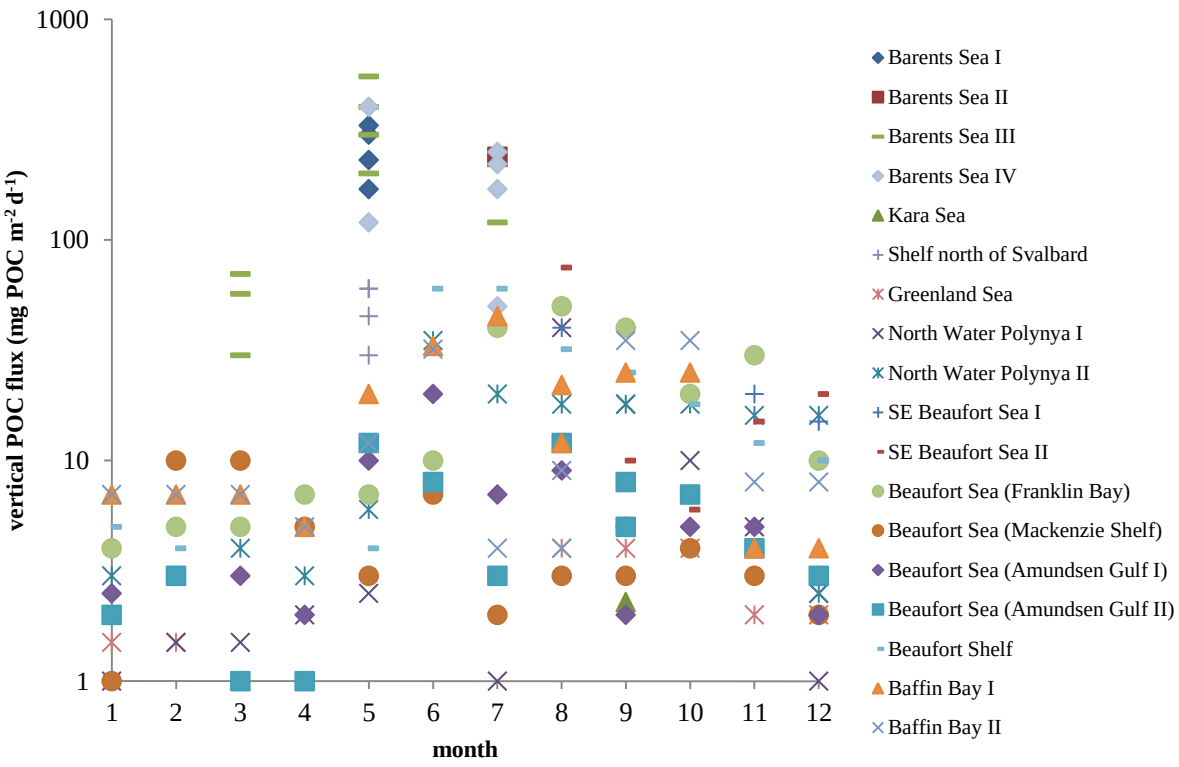

Figure 2: Compilation of downward POC flux measurements at 200 m from the Barents Sea (Barents Sea I: Andreassen and Wassmann, 1998; Barents Sea II: Coppola et al., 2002; Barents Sea III: Olli et al., 2002; Barents Sea IV: Reigstad et al., 2008), the Kara Sea (Wassmann et al., 2004), the shelf north of Svalbard (Andreassen et al., 1996), the Greenland Sea (Noji et al., 1999), the North Water Polynya (Hargrave et al., 2002), the Beaufort Sea (Beaufort Shelf: O'Brien et al., 2006; Beaufort Sea (Franklin Bay): Forest et al., 2008; Beaufort Sea (Mackenzie Shelf, Amundsen Gulf I+II): Lalande et al., 2009; SE Beaufort Sea I+II: Forest et al., 2013), and Baffin Bay (Lalande et al., 2009). Please note the log scale on the y-axis.

The seasonal changes in the hydrography, ice cover and plankton dynamics cause variations of the downward POC flux throughout the year. Convection, brine formation and wind cause deep-mixing in Arctic seas during winter (Yang et al., 2004; Ingvaldsen and Loeng, 2009). Nitrate, the primary limiting nutrient in the Arctic (Tremblay and Gagnon, 2009) is replenished in the euphotic zone, if these mixing processes penetrate below the nitracline. Since microalgae are light-limited during the winter and deep convectional mixing counteracts the biomass build-up (Behrenfeld, 2014), their concentrations remain low (Eilertsen and Degerlund, 2010; Vader et al., 2014).

Ice algae blooms are observed under the sea ice cover in April and May (Ji et al., 2013). When the ice breaks up, the algal cells are released into the water column. They form an

important food source for pelagic grazers, but also contribute to the downward POC flux (Tremblay et al., 1989; Tamelander et al., 2009).

In seasonally ice-covered regions, the phytoplankton spring bloom takes place dependent on latitude and ice break-up between May and August (Leu et al., 2011 and citations therein). In contrast, it can already be observed in April/ May in ice-free high latitude regions. The bloom is commonly dominated by diatoms and the prymnesiophyte *Phaeocystis pouchetii* in northern Norway, the Barents Sea, and waters around Svalbard (Degerlund and Eilertsen, 2010). Senescent diatom cells and resting stages are frequently observed after the peak bloom stage (Eilertsen et al., 1981; Hegseth and Sundfjord, 2008). They have a high sinking velocity (Eppley et al., 1967; Sugie and Kuma, 2008) and commonly cause a substantial POC sedimentation associated with the bloom (Thompson et al., 2008; Rynearson et al., 2013).

The strong nitrate drawdown during the first part of the bloom (Dugdale and Goering, 1967; Kristiansen et al., 1994) causes a decline in the nitrate concentrations in the euphotic zone. This induces a gradual shift from the nitrate based new production to a regenerative production, based on ammonium, urea or other biogenic nitrogen compounds (Kristiansen et al., 1994). Small autotrophic cells (< 10 µm, Hodal and Kristiansen, 2008) become abundant, which are better adapted to take up nutrients at low concentrations due to their higher surface to volume ratio.

While mesozooplankton species like *Metridia longa* and some small omnivorous/ detritivorous taxa (e.g. *Oithona* spp., *Pseudocalanus* spp.) actively graze throughout the year (Hirche and Kosobokova, 2011; Tommasi et al., 2013; Darnis and Fortier, 2014), the life cycle of e.g. *Calanus* spp. is adapted to the timing of the microalgae bloom (Søreide et al., 2010; Melle et al., 2014). This taxon goes into diapause during winter, but the timing of different life cycle stages is adjusted to the peak bloom of ice algae and phytoplankton. Accordingly, *Calanus* spp. may exert a strong grazing pressure and reduce the downward POC flux, but this repackaging of organic material into fast-sinking fecal pellets may also increase the sinking velocity of the sedimenting biomass (Thompson et al., 2008; Wexels Riser et al., 2008).

Wassmann et al. (1991) proposed a conceptual model of nutrient concentration and phyto-/ zooplankton biomass throughout the year. It describes a major POC sedimentation linked to the weak temporal coupling of the phytoplankton peak bloom and the zooplankton maximum abundance during summer (Figure 3). Throughout the last 15 years, some more details of the

Arctic marine ecosystem were revealed, such as weak downward POC flux during winter (Forest et al., 2008) and the contribution of ice algae to the POC sedimentation (Tamelander et al., 2009; Søreide et al., 2013). These aspects are included in a new version of the conceptual model of the Arctic pelagic ecosystem and the downward POC flux (Wassmann and Reigstad, 2011), but the basic pattern is still the same with the highest downward POC flux taking place linked to the phytoplankton spring bloom.

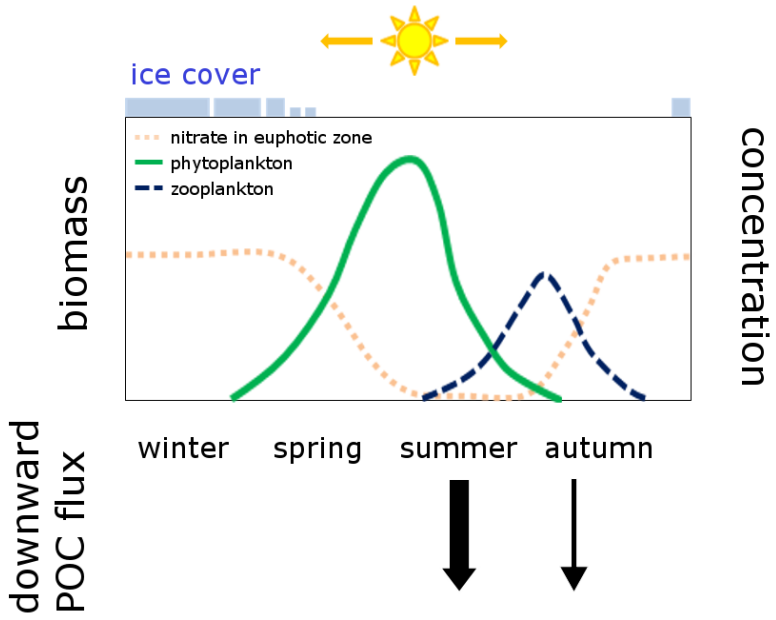

Figure 3: Conceptual understanding of the Arctic pelagic ecosystem with seasonal ice cover (with nitrate concentration, phyto-/ and zooplankton biomass) and the associated downward POC flux throughout the year (modified from Wassmann et al., 1991; Wassmann and Reigstad, 2011).

2.2 Formation, Modification and Characteristics of Sinking Particles

The intensity of the downward POC flux has been determined by (1) in-situ pumps and a settling model (Bishop and Edmond, 1976; Liu et al., 2009), (2) deployment of sediment traps (Zeitschel et al., 1978), filtration of the collected material and analysis of the filters (Ehrhardt, 1983)(**Paper I-III**), as well as (3) using disequilibria of particle-reactive tracers like ^{234}Th, ^{210}Po, or ^{210}Pb with their soluble parent element in the water column (Moran, 2004; Stewart et al., 2007; Gustafsson and Andersson, 2012).

All of these methods determine a downward bulk flux, but POC is not a "single amorphous category […] of undefined behavior and uniform property" (De La Rocha and Passow, 2007). The particles of organic carbon have distinct characteristics like shape, composition, density,

and sinking velocity, which crucially determine the downward POC flux (De La Rocha and Passow, 2007; Passow et al., 2014; Durkin et al., in press).

An increasing number of "particle studies" has been conducted during the last years (Lundsgaard et al., 1999; Waite et al., 2000; Ebersbach and Trull, 2008; Ebersbach et al., 2011; Laurenceau-Cornec et al., 2015; Durkin et al., in press; Nowald et al., in press). All these investigations used short-term sediment traps modified with gel-containing jars, which allowed collecting sinking particles with a largely conserved three dimensional structure. Despite the increasing number of studies, the terminology of the term "particle" is still challenging and strongly dependent on the research discipline (Box 1).
In the present work, a "particle" is used as an umbrella definition for particulate material $\geq$ 50 µm ESD_{image} and includes algal and detrital aggregates, fecal pellets, and conglomerates of these units.

Stokes' Law tightly connects particles size and sinking velocity (Mann and Lazier, 2006) and suggests that small particles sink slowly and large particles sink fast. Following this argumentation, aggregation of small particles into larger ones increases the sinking velocity and the downward biomass flux. Two mechanistic concepts of aggregation were described by Kiørboe (2001): aggregation via physical coagulation (Figure 4a) and a zooplankton mediated pathway (Figure 4b).

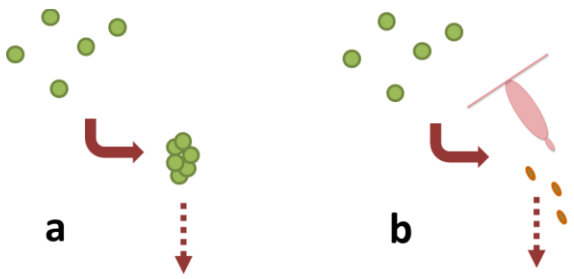

Figure 4: Aggregate formation by a) physical coagulation (collision and adhesion of particles) and b) zooplankton mediated (modified from Kiørboe, 2001).

Box 1: What is a "particle"?

Hill (1998) describes various important roles for particles in the sea and states that the "understanding of particles is a keystone of overall understanding of the seas". However, he leaves us without a clear definition of the term "particle". A short and certainly incomplete compilation of literature indicates that it is frequently used in different fields of marine geology and marine biology. The upper size limit for a particle is not defined (even jellyfish may be regarded as particles in a Lagrangian tracking model, Lee et al., 2013), and also the lower limit is somewhat blurry, but set at the transition stage of particulate and dissolved material (Azam and Malfatti, 2007).

In a geological framework, "particle" is used as an umbrella term for "sand and silt grains, clay casts, mineral-bearing fecal pellets, flocculates, and agglomerates" (Syvitski and Murray, 1981). The sub-categories "aggregates", "agglomerates" and "flocculates" are then defined by the type of compound material (inorganic or organic) as well as the force holding the units together (surface tension, electrostatic, cohesive forces).

In the field of marine biology, less focus is put on the combining forces, but particles are defined by size and origin.

In biogeochemical work, "particle flux" is often used synonymously with the downward flux of particulate organic material (POM) or particulate organic carbon (POC) (e.g. Andreassen et al., 1996). Particulate material is here defined in contrast to dissolved material, which passes through standard filters with a pore size of e.g. 0.7 µm (GF/F Whatmann Filters). In contrast, studies determining the POC flux based on the ^{234}Th method often use 53 µm or 70 µm to distinguish between suspended material and sedimenting particles (Le Moigne et al., 2013). Studies using optical plankton or particle counters (e.g. LOPC: Herman et al., 2004; UVP: Stemmann et al., 2008), define "particle" in a somewhat different way, and so do groups working with short-term sediment traps modified with gel-jars ("gel traps"). Particles here often range "from individual cells through chains to assemblages of highly degraded detritus forming aggregates; they can be formed by biological processes such as cell division and fecal pellet production or indirectly by coagulation of particles due to differential settling and turbulence" (Stemmann and Boss, 2012). Dependent on the applied instruments and sampling/ analysis technique different particle size ranges are included (> 11 µm, Durkin et al., in press; ≥ 50 µm, **Paper I, III**; > 73 µm, McDonnell and Buesseler, 2010; > 150 µm, Ebersbach and Trull, 2008).

The coagulation theory describes physical coagulation as a two-step process: Particles collide in the water column, and the collision rate primarily depends on the particle abundance (Jackson, 1990), differential sinking velocities (Alldredge, 2001) and turbulent mixing (McCave, 1984; Kiørboe et al., 1990). As a second step, some 'natural glue' ensures coagulation after collision. This can either be sticky phytoplankton cells or adhesive extracellular polymeric substances, which are excreted by microalgae or bacteria associated with them (Kiørboe and Hansen, 1993; Thornton, 2002; Gärdes et al., 2011). As particles

stick together after collision, larger aggregates are formed. The coagulation theory has also been verified by experiments in beakers (Kiørboe et al., 1990), roller tanks (compiled in Jackson, 2015) and mesocosm experiments (Kiørboe et al., 1994). Therefore, it is a common way to explain an enhanced POC export e.g. during the phytoplankton spring bloom, when the number of particles in the water column is high.

Algal aggregates are a special type of aggregate, because they mainly consist of one type of original particles. Alldredge and Silver (1988) coined in contrast the term 'marine snow' for conglomerates (> 0.5 mm diameter) of algal cells and other units, such as detritus, bacteria, and fecal pellets. Particles observed in the present work (**Paper I, III**) sometimes resembled the composition of marine snow, but they were smaller. To prevent confusion, these particles were not labelled "marine snow", but termed "aggregates" (**Paper III** Table 3) or "other" (**Paper I** Table 5), whereas the latter implys that they were not classified as fecal pellets or phytoplankton aggregates.

The sinking velocity and the downward POC flux can alternatively be increased, when "ballast" material with high specific weight (e.g., lithogenic matter, coccolithophores) is incorporated into (algal) aggregates and marine snow (reviewed in De La Rocha and Passow, 2007; Engel et al., 2009; Iversen et al., 2010). This is described by the "ballasting hypothesis" (De La Rocha et al., 2008), but the concept is still under discussion. A high contribution of lithogenic material has for example been shown to enhance the sinking velocity of the aggregate, but also it also increased aggregate break-up, which, in turn, reduces the sinking velocity due to the smaller particles size (Hamm, 2002; Passow et al., 2014).

Large, fast-sinking particles, which enhance the downward POC flux, are alternatively formed by zooplankton-mediated aggregation (Kiørboe, 2001, Figure 4b). Pteropods and larvaceans mediate particle formation by collecting bacteria and algal cells in their mucus feeding webs or houses, which are regularly lost or rejected and sink out as marine snow (Kiørboe, 2001). Crustacean plankton, such as copepods or krill, feed on small particles (e.g. algal cells) and re-package them into dense fecal pellets, which sink few tens to several hundreds of meters per day (Turner, 2002).

At the same time, copepods and krill also fragment fecal pellets (coprohexy) when rejecting them (Dilling and Alldredge, 2000; Iversen and Poulsen, 2007). The fragments, smaller in size, have a lower sinking velocity and are more exposed to microbial degradation processes

(Svensen et al., 2012; Giering et al., 2014). Accordingly, the “retention filter” in the upper twilight zone contributes both to the biomass attenuation in the upper twilight zone (Wexels Riser et al., 2001), but also enhances the downward POC flux by producing fast-sinking fecal pellets.

This chapter only describes the most basic lines of particle formation and modification, but it still illustrates that the term “sinking particles” integrates a variety of different types of particles and that these particles are formed and modified in size, shape and composition in numerous ways.

3 OBJECTIVES

In this thesis two different Arctic marine ecosystems, an Arctic fjord (Adventfjorden, western Svalbard) and an Arctic shelf sea (Barents Sea) were studied under contrasting hydrographical and ecological settings (i.e., bloom vs. non-bloom phase) to investigate the following questions:

(1) Is the highest downward flux of POC and particles (collected by deployment of gel traps and $\geq$ 50 µm ESD_{image}) associated with the phytoplankton spring bloom? (**Paper I, III**)

(2) Are turbulence (**Paper I**), upward nitrate flux (**Paper II**), phytoplankton composition and abundance (**Paper I, III**), zooplankton composition and abundance (**Paper I, III**), and the influence of glacial run-off (**Paper III**) potential drivers of the downward POC flux in these regions?

4 SAMPLING AREA AND METHODS

The present work was part of the "Conflux" project in the central Barents Sea (**Paper I, II**) and the Isfjorden-Adventfjorden (IsA) field campaign in Adventfjorden, western Svalbard (**Paper III**).

4.1 BARENTS SEA

The Barents Sea is with 1.5 x 10^6 km^2 the largest Arctic shelf sea (Jakobsson et al., 2004). It has a mean depth of 200 m and is bordered by the Svalbard Archipelago, Franz Josef Land, Novaya Zemlya and the Norwegian mainland (Figure 5). Fresh and cold Arctic derived water (salinity S = 34.3-34.8, temperature T < 0.0 °C, Loeng, 1991) enters the Barents Sea from the north (eastern) edge and a seasonal ice-cover is found in the region. Saline and relatively warm Atlantic water (S > 35.0, T > 3.0 °C, Loeng, 1991) flows into the Barents Sea through the Barents Sea Opening between the Norwegian mainland and the Bear Island. This water is the oceanic main heat source for the region (Årthun et al., 2012), causing a permanently ice-free southern Barents Sea. Arctic and Atlantic derived water masses meet in the topographically steered Polar Front in the central Barents Sea. Lighter Arctic derived water covers here warmer and more saline Atlantic water.

Data presented in this thesis (**Paper I, II**) followed a stratification, turbulent mixing and bloom gradient along the 30°E longitude from the northernmost station M1 (78°N) in stratified ice-covered Artic derived waters (Figure 5) through the Polar Front (M2, 77°N) to the southernmost station M4, located in the deep-mixed ice-free Atlantic derived waters (75°N).

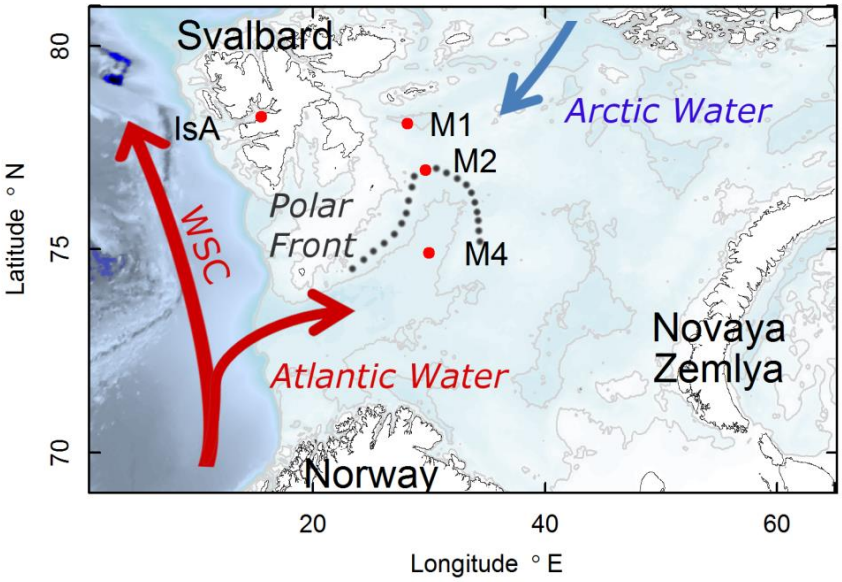

Figure 5: Map indicating the sampling stations in the Barents Sea (M1, M2, M4, **Paper I**, **II**) and in Adventfjorden, Svalbard (IsA, **Paper III**). Warm and saline derived Atlantic water meets Arctic derived water in the Polar Front in the Central Barents Sea. The West Spitsbergen Current (WSC) brings warm and saline Atlantic derived water to the western coast of Svalbard.

4.2 ADVENTFJORDEN

The sampling station IsA (Figure 6) was located in the mouth of the high Arctic Adventfjorden, which is a small side branch in the Isfjorden system. Since neither Adventfjorden nor Isfjorden has a sill, both fjords are strongly influenced by warm and saline water derived from the West Spitsbergen Current. The IsA station (~80 m) was permanently ice-free during our nine-month study between December 2011 and September 2012 (Table 1). During summer and autumn Adventfjorden is affected by sediment-loaded glacial melt water run-off (Advent River, Longyear River, Węsławski et al., 1999), which also influenced the present work during September 2012. Data presented here were collected during field periods covering three seasons. The field period in mid-December, mid-January and late January, was denoted as Winter I, II, III, respectively. The field sampling in late April, mid-May and late May are termed Spring I, II, III, respectively, and the mid-September investigation is denoted as Autumn I (Table 1).

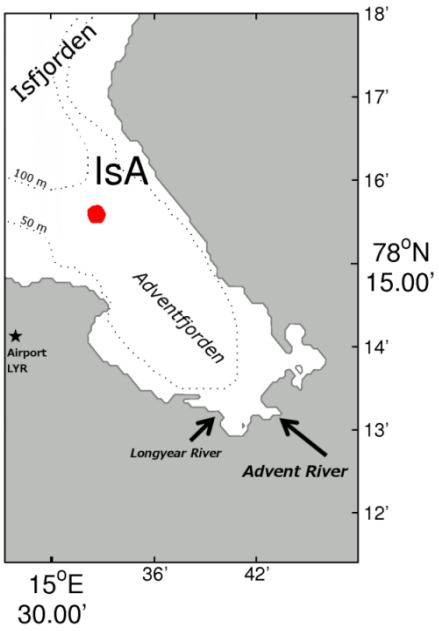

Figure 6: Detailed map of the sampling station IsA in the mouth of Adventfjorden, a side fjord of the Isfjorden system at the western coast of Svalbard (see Figure 5). Modified from **Paper III** Figure 1. Depth lines following Zajączkowski et al. (2010).

4.3 METHODS

Hydrographical data on temperature, salinity and density were measured by CTD casts and data were processed following standard procedures. Hydrography microstructure (small-scale current shear) was quantified in the Barents Sea with a loosely tethered turbulence drop sonde (**Paper I, II**). These data were used to determine the mixing layer, which is defined as the actively mixed surface layer with a vertical diffusivity > 10^{-4} m^2 s^{-1} during the time of data acquisition (Brainerd and Gregg, 1995; background vertical diffusivity of 10^{-4} m^2 s^{-1} defined following **Paper I** Figure 4b and Sundfjord et al., 2007). In contrast, the "mixed layer" describes the weakly stratified water layer above the pycnocline (Brainerd and Gregg, 1995). Suspended chlorophyll *a* (Chl *a*), POC and the atomic carbon to nitrogen ratio (C/N) were determined from sea water collected with Niskin bottles and analyzed according to standard procedures (**Paper I-III**). Zooplankton abundance in the Barents Sea was estimated using a Laser Optical Plankton Counter (LOPC, **Paper I**). In addition, zooplankton was identified and quantified in microscopic studies (Barents Sea: Svensen et al., in prep., C. Svensen, pers. comm., **Paper I**; Adventfjorden: Stübner et al., in rev., E.I. Stübner, pers. comm., **Paper III**). Short-term sediment trap arrays (**Paper I, II**: free floating or anchored on an ice floe, **Paper III**: anchored at the bottom) were deployed for ~ 24 h to study the biogeochemical flux of Chl

a and POC as well as the C/N ratio of sinking material. Deployment depths were chosen to cover the transition from the lower euphotic zone (1% surface irradiance) to the upper twilight zone. This depth interval has been described to be the zone of the highest POC attenuation (Martin et al., 1987; Olli, 2015). Sediment traps were deployed between 20 m and 200 m in the Barents Sea (**Paper I, II**; 20 m and 30 m only included in the present summary to allow comparison between the fjord and shelf sea data, but not included in the papers) and between 20 m and 60 m in Adventfjorden (**Paper III**). To limit collection of resuspended bottom material, the lowest trap was deployed approximately 20 m above the seafloor. Downward particle flux (**Paper I, III**) was examined by deploying sediment trap cylinders modified with gel containing glass jars, denoted as "gel traps" in the following (conceptual idea of gel traps, Lundsgaard, 1995; Lundsgaard et al., 1999; image analysis following Ebersbach and Trull, 2008; modification from acrylamidegels to commercially available gels, Thiele et al., 2015; Wiedmann et al., 2014). Gel traps were deployed at 30, 40, 60, and 90 m in the Barents Sea (**Paper I**) and at 20, 30, 40 and 60 m in Adventfjorden (**Paper III**). Gels were photographed and an image analysis was conducted. Only particles ≥ 50 µm ESD_{image} were included in the analysis, because a very low light reflection of smaller particles at the used magnification (15 x) would have caused underestimation of the number of particles < 50 µm ESD_{image} (Jackson et al., 2005). The image analysis gave information on the size composition, origin and structure of the sinking particles, which cannot be grasped in an estimation of the downward biomass bulk flux. However, some challenging steps are linked to the image analysis (Box 2).

Box 2: Challenges in Particle Image Analysis

Extracting particles from images requires a threshold level, which sets the border between the background and the particle (Figure 7). A good estimation of this threshold is necessary, because it keeps over- or underestimation of the (two-dimensional) particle size to a minimum. In the present work, I used two different approaches to determine the threshold. In **Paper I**, I determined the threshold using the "plot profile function" of the program ImageJ (**Paper I** Figure 2). The intermediate grey value between the background and the particle was chosen by eyeballing and then used for all images of one gel. This worked well for the gels deployed in the Barents Sea, because most particles had a compact form (**Paper I** Figure 7). They could even be distinguished from the background under not absolute optimal illumination, such as at the edges of the glass, where some reflection occurred. For the fine, detrital particulate material in Adventfjorden (**Paper III** Figure 6a, b), the AutoThresholding function of ImageJ was the better choice. This automatically set an optimal threshold for the analysis of each image, which was accepted or manually adjusted after visual inspection. Among the AutoThresholding functions, the Otsu clustering algorithm gave the best result and was therefore applied in **Paper III**.

The second challenging step in the image analysis is the conversion from the two-dimensional particle area to the three-dimensional particle volume. I presumed here an ellipsoidal volume for the particles and chose the third dimension being equal to the minor axis, which reflected the elongated form of most particles.

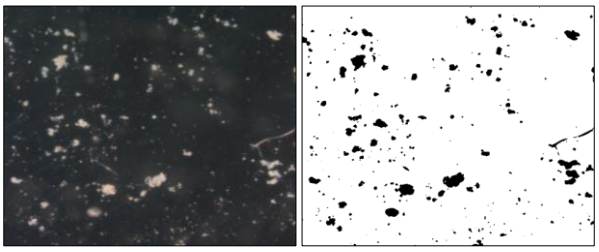

Figure 7: Original image of particles in the gel (left, black background, white particles) and after applying a thresholding process to the image (right, white background, black particles.

5 Results and Discussion

5.1 Suspended and Sedimented Biomass in a Seasonal Context

Investigations along a north-south transect in the Barents Sea and during a nine months seasonal study in Adventfjorden resulted in contrasting snap-shot pictures of the situation in the water column, defined by hydrography, nutrient concentrations, suspended biomass (Chl *a*, POC, phytoplankton) and downward POC flux. Here, these snap-shots are put in a seasonal context with the help of parallel conducted zooplankton studies (Svensen et al., in prep.; Stübner et al., in rev.; E.I. Stübner pers. comm.) and literature.

During winter, high nitrate surface concentrations were found in Adventfjorden, accompanied by low Chl *a* concentrations in the whole water column (Table 1, **Paper III** Figure 3). It is assumed that nitrate was replenished by convective mixing and wind mixing previous to mid-December (Winter I), which resulted in the high nitrate surface concentrations. Low Chl *a* concentrations during winter (Table 1, **Paper III** Figure 3) have previously been reported from other high-latitude regions (Węsławski et al., 1991; Eilertsen and Degerlund, 2010; Iversen and Seuthe, 2011; Vader et al., 2014). In Adventfjorden they were rather caused by limited primary production (negligible irradiance levels during the polar night) than by top-down regulation, because zooplankton abundance was low during winter (approx. 100 ind. m^{-3}, Stübner et al., in rev.). Based on the high nitrate concentrations, the low Chl *a* concentrations and the low zooplankton abundance, the situations observed during mid-December, mid-January and late January (Winter I, Winter II and Winter III, respectively) was regarded to reflect a typical Arctic winter conditions.

Low downward POC fluxes have been reported from Arctic shelf seas during winter or the pre-bloom phase (Olli et al., 2002; Forest et al., 2008), but studies in an Arctic fjord show that moderate downward POC fluxes may occur in these embayments during winter (25-750 mg POC m^{-2} d^{-1}; Wassmann, 1984; Noji et al., 1993; Zajączkowski et al., 2010). Moderate fluxes were also observed in Adventfjorden during the polar night (Winter II, 195-410 mg POC m^{-2} d^{-1}, Figure 8), potentially caused by resuspension of bottom material, lateral advection to the middle of the fjord and subsequent sedimentation (Noji et al., 1993).

Table 1: Concentrations of suspended nitrate, chlorophyll *a* (Chl *a*) and particulate organic carbon (POC) as well as the depth of the sub-surface Chl *a* maximum (SCM) and the classification of the field periods in the Barents Sea (**Paper I-II**) and Adventfjorden (**Paper III**).

	Date	Nitrate concen-tration (µM) [(1)]	Chl *a* concentration (mg Chl *a* m^{-3}) [(2)] and depth of SCM (m)	Range of suspended POC (mg m^{-3}) [(2)]	Season/ ecological category
Barents Sea (BS)					
M1 (northern BS)	22.06.11	2.8	0.2-4.3 (40 m)	160-390	late peak bloom
M2 (Polar Front)	24.06.11	1.9	0.06-1.4 (44 m)	130-320	late bloom
M4 (southern BS)	27.06.11	0.8	0.03-1.6 (45 m)	130-360	post bloom
Adventfjorden					
Winter I	14.12.11	2.8	0.04 (60 m)	43-50	winter
Winter II	18.01.12	-	0.06 (60 m)	92-144	winter
Winter III	28.01.12	7.2	0.0-0.1 (15 m)	65-73	winter
Spring I	27.04.12	4.5	0.6-2.1 (5 m)	238-324	early bloom
Spring II	10.05.12	1.5	3.2-4.2 (25 m)	235-400	peak bloom
Spring III	30.05.12	0	0.6-1.6 (60 m)	246-635	late bloom
Autumn I	19.09.12	2.6	0.3-0.4 (5 m)	94-137	autumn

[(1)] Nitrate concentration at 30 m in the Barents Sea, at 25 m in Adventfjorden
[(2)] Chl *a* and POC concentrations measured between sub-surface and 60 m

Spring bloom scenarios were investigated at three stations in the Barents Sea and during three sampling episodes in Adventfjorden.

In the Barents Sea, the stations were located along a north-south transect. Drift ice cover decreased from the northernmost station M1 (30 % sea ice) to station M2 in the Polar Front (20 % sea ice) and station M4, which was located in ice-free waters. The different stages in sea ice melt resulted in a moderately and strongly halocline driven water column stratification at the two northernmost stations, respectively. A weak, thermocline driven stratification was found in the deep-mixed waters at the southernmost station (**Paper I** Figure 3).

Associated with the north-south transect, a conceptual model of the spring bloom development has been established (Sakshaug et al., 1991; Wassmann et al., 2006; Sakshaug et al., 2009). It suggests an earlier bloom stage in the north and a later one in the south.

This bloom gradient was also observed during the present study. The integrated nitrate concentration declined from north to south (integrated to 40 m, M1: 7.04 mmol nitrate m^{-2}, M2: 5.43 mmol nitrate m^{-2}, M4: 2.31 mmol nitrate m^{-2}) and implied a minor nitrate drawdown, and thus an earlier phytoplankton bloom stage, at M1 in the north than at M4 in the south. The change in the phytoplankton composition, from a diatom dominated ice edge bloom (cells > 10 µm) in the north to a prevailing *Phaeocystis* community (cells ~5 µm,

Paper I Table 3) in the south, pinpoints the same, because it has been proposed that the peak bloom stage in the Barents Sea is dominated by large cells, while small cells prevail during the early and late bloom (Hodal and Kristiansen, 2008). Taking into account these findings, M1 in the north was classified as a typical late peak bloom situation and M2 in the Polar Front as a late bloom situation (Table 1). Classification of M4 was challenging. The deep mixing layer (25 m, **Paper I** Table 3) and the comparable higher Chl *a* concentrations at 5 m (M4: 0.6 mg Chl *a* m^{-3} versus M1: 0.4 mg Chl *a* m^{-3} and M2: 0.2 mg Chl *a* m^{-3}, **Paper I** Figure 5) contradicted previously reported traits of a post bloom stage, such as a strongly stratified water column and negligible Chl *a* surface concentration (Leu et al., 2006; Hodal et al., 2012). Nevertheless, M4 was here classified as a post bloom situation, because of the deep nitracline and the more advanced late spring to summer zooplankton composition, dominated by microzooplankton, small mesozooplankton species, and high abundances of mesozooplankton eggs and nauplii (Svensen et al., in prep.).

A conceptual model described by Sakshaug et al. (1991) proposes a major biomass sedimentation along the ice edge of the Barents Sea and a prevailing top-down regulation in the ice-free waters further south, channeling the produced biomass rather into the food web than contributing to export. In this study, we deployed short-term sediment traps in the marginal ice zone of the Barents Sea (M1, M2) and they indicated a downward POC flux of 150-370 mg POC m^{-2} d^{-1} (Figure 8). This met previous spring and summer data on downward fluxes observed in the region (Andreassen and Wassmann, 1998; Olli et al., 2002; Reigstad et al., 2008).

Contrasting the conceptual model of Sakshaug and co-workers (1991), the highest downward POC flux was not found along at the ice edge, but observed in the ice-free southern Barents Sea (M4: 261-600 mg POC m^{-2} d^{-1}, Figure 8). This has occasionally been reported before during spring and summer (Olli et al., 2002; Reigstad et al., 2008), but mechanisms causing the high flux during the post bloom situation remained poorly understood.

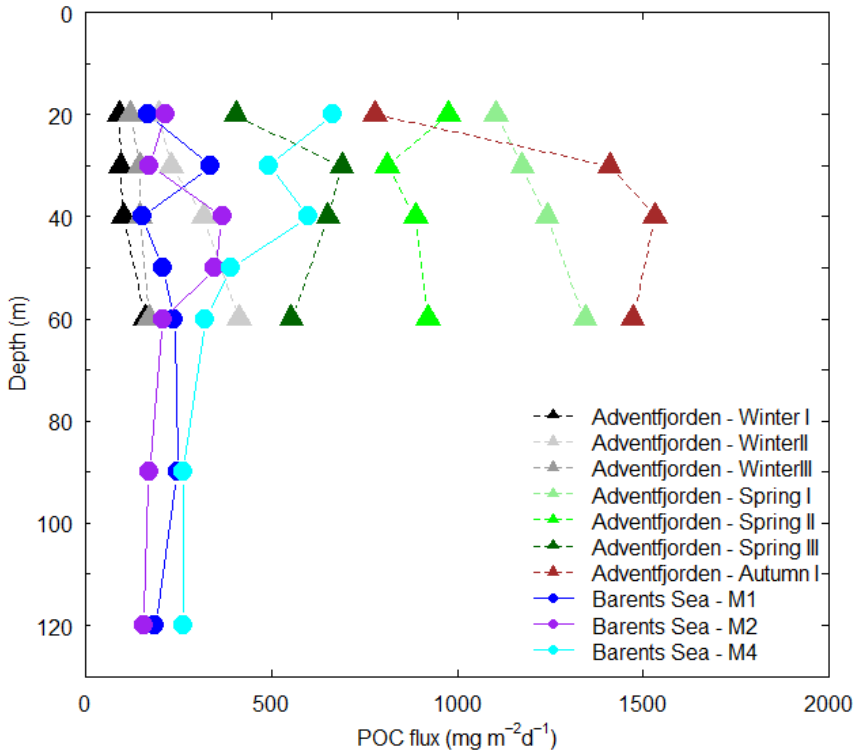

Figure 8: Downward POC flux estimated by deployment of short-term sediment traps (for ~24 h) in the Barents Sea (**Paper II**) and Adventfjorden (IsA, **Paper III**).

As observed in the Barents Sea, a decline of the suspended nitrate concentrations (25 m) was also found in Adventfjorden throughout spring (Table 1). The Chl *a* concentrations peaked during Spring II in mid-May and the maximum concentrations were similar to those observed during the late peak bloom in the Barents Sea (Spring II: 4.2 mg Chl *a* m^{-3}, M1: 4.3 mg Chl *a* m^{-3}, Table 1). Nitrate and Chl *a* concentrations in Adventfjorden were also comparable to previously measured spring bloom concentrations in Adventfjorden (Zajączkowski et al., 2010) and the ice-free Kongsfjorden, Svalbard (Iversen and Seuthe, 2011). Due to the highest Chl *a* concentration, Spring II was identified as peak bloom stage, while Spring I and Spring III were classified as early bloom and late bloom, respectively.

In Adventfjorden, the early bloom stage was associated with a high downward POC flux, and the intensity of the flux declined toward the peak bloom and late bloom stage (Figure 8). The downward POC flux exceeded the present spring bloom observations from the Barents Sea (Figure 8) and literature data from ice-free fjords in northern Norway (Keck and Wassmann, 1996; Reigstad and Wassmann, 1996; Reigstad et al., 2000; Zajączkowski et al., 2010), and Conception Bay, Canada (Thompson et al., 2008), but was comparable to fluxes found in a

study in the Barents Sea (Olli et al., 2002). Along these lines, the high downward POC flux associated with the spring bloom in Adventfjorden matched the situation described by the conceptual model of an Arctic marine ecosystem (Figure 3).

The autumn situation in Adventfjorden was characterized by replenished nitrate concentrations (Table 1), which was used as an indicator that water column stratification broke down previous to Autumn I. However, the Chl *a* concentrations remained low (5-60 m: 0.2-0.4 mg Chl *a* m^{-3}, **Paper III** Figure 3) and no autumn bloom was observed, such as it has been reported from the autumn situation in Kongsfjorden (Iversen and Seuthe, 2011) and the Barents Sea (Hegseth, 1997). Due to lacking data on primary production, it was not possible to evaluate if the low Chl *a* concentrations were caused by low primary production or high loss rates by the moderately abundant zooplankton community (7 x 10^3 ind. m^{-3}, Stübner et al., in rev.). Based on the nitrate and Chl *a* concentrations, Autumn I was classified as a typical Arctic autumn situation, though the downward POC flux in Adventfjorden (Figure 8) exceeded previous studies in the same fjord in October (Zajączkowski et al., 2010) as well as autumn studies conducted in north/ western Norwegian fjords (Wassmann, 1984; Keck and Wassmann, 1996) and Hudson Bay, Canada (Lapoussière et al., 2013).

The concentration of suspended biomass (Chl a, POC) and downward POC fluxes observed in the Barents Sea and Adventfjorden were largely comparable to literature data. The snap-shot sampling episodes conducted here are therefore regarded to represent typical Arctic winter, spring and autumn situations. The peak bloom and late bloom situation was investigated both in the Barents Sea and Adventfjorden. Though comparable concentrations of suspended biomass were found, the downward POC flux was higher in Adventfjorden.
The conceptual understanding of the Arctic sedimentation pattern (Figure 3) suggests that the major sedimentation event is associated with the phytoplankton spring bloom. This was observed during the early bloom situation in Adventfjorden. However, the highest downward POC flux in the Barents Sea was found during the post bloom situation in deep mixed, ice-free waters (M4) and the highest POC flux in Adventfjorden occurred during autumn (Autumn I, Figure 8).

5.2 Seasonal and Spatial Variation in Sinking Particles' Characteristics (Size Composition and POC: Volume Ratio)

The deployment of short-term sediment traps modified with gel-containing jars allows investigating characteristics of sinking particles such as the microbial community associated with sedimenting marine snow (Thiele et al., 2015), the sinking velocity of particles (McDonnell and Buesseler, 2010), or the contribution of different particle types to the downward flux (Ebersbach et al., 2011). In the present work, I focused on the size distribution of sinking particles, the volume flux (Figure 9) and the link between the downward particle flux and the POC flux (Figure 9).

Following Stokes' Law, very low sinking velocities have been estimated for small particles (few µm, McCave, 1975) and these particles have often been regarded as "non-sinking". In the present image analysis (**Paper I, III**), particles < 50 µm ESD_{image} were not included. Their light reflection was very low at the used magnification (15 x), most likely causing an underestimation of the particle number (Jackson et al., 2005). Nevertheless, particles < 50 µm ESD_{image} were very abundant in the gels deployed in the Barents Sea and Adventfjorden, which matches the results of other field and model studies (≥ 11 µm, Durkin et al., in press; ≥ 2 µm ESD, Richardson and Jackson, 2007; ≥ 43 µm, McDonnell and Buesseler, 2010). However, a comparison with literature also shows that abundance of small sinking particles varies spatially. Ebersbach and Trull (2008) deployed gel traps around the Kerguelen Plateau and chose to exclude particles < 150 µm ESD from their image analysis because of the low abundance and statistical challenges.

The particle coverage in gels is determined by the particle abundance and the size of the particles. Both factors vary with location and season. Gel trap deployment for ~24 h during mid-December (Winter I) resulted in densely covered, but not overloaded, gels. In contrast, the deployment time had to be shortened during spring and autumn (Barents Sea: 4-5 h, Adventfjorden: 2 h) to prevent particle overload in the gels, which would have made them unusable in the image analyses.

In this context, a comparison with literature is remarkable: Gel traps were deployed in the southern Ocean (Austral spring and summer) (Ebersbach and Trull, 2008; McDonnell and Buesseler, 2010; Ebersbach et al., 2011; Laurenceau-Cornec et al., 2015; Durkin et al., in press). They were deployed at greater depth than in the present study (100-500 m vs. 20-90 m). A lower particle abundance must be assumed for greater depth, and thus a longer

deployment time is possible. Nevertheless, it is remarkable that the gels could be deployed for up to three days in the Southern Ocean without particle overload, while a 4-5 h deployment time was appropriate in the Barents Sea. This pinpoints in my opinion a certain difference between the system in the southern Ocean and an Arctic shelf sea, which may be subject to future investigations.

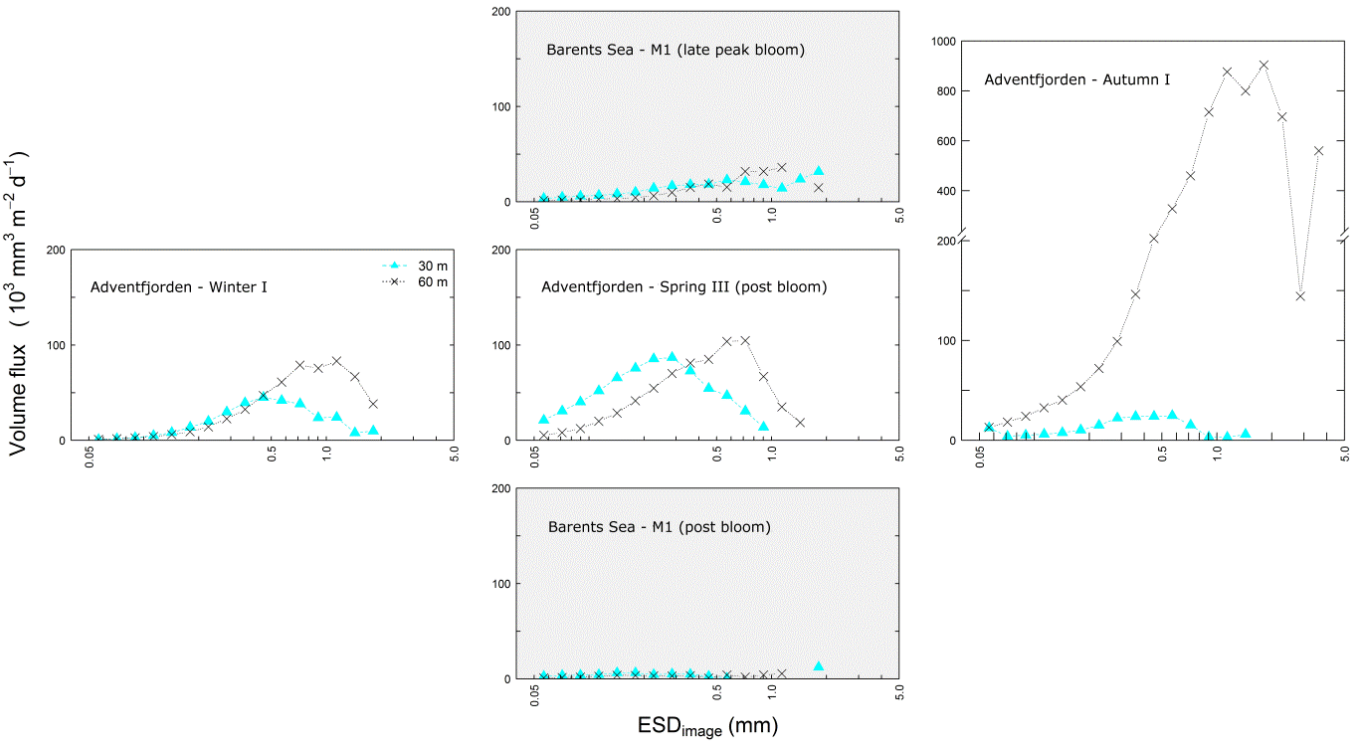

Figure 9: Particle volume flux in the Barents Sea (grey shaded; top: M1; bottom: M4, **Paper I**) and Adventfjorden (left: Winter I; middle: Spring III; right: Autumn I; **Paper III)**. The area under the curve corresponds to the total volume of sinking particles. Data from M2 (late bloom, Barents Sea) and Spring II (peak bloom in Adventfjorden) were not included, because the volume flux spectra were very similar to M1 and Spring III, respectively.

In volume flux spectra, the area under the curve corresponds to the total sinking volume, which is the sum of the volume of all sinking particles at a certain depth. In addition, the spectra give an indication on the contribution of different sized particles to the downward volume flux. Comparing the two regions investigated here (Barents Sea, Adventfjorden) indicates that the downward volume flux generally was lower in the Barents Sea (Figure 9). The spectra further show that the volume flux tended to be higher at 60 m than at 30 m. This meets predictions of the coagulation theory (Jackson, 1990; Kiørboe et al., 1990), which suggests that larger particles could be expected at greater depth.

The highest downward POC flux in the Barents Sea (M4, Figure 8) was associated with the lowest particle volume flux of the present study (40-130 x 10^3 mm^3 m^{-2} d^{-1} Figure 9). In contrast, the highest POC flux in Adventfjorden occurred during Autumn I at 40 m and 60 m in form of the highest particle volume found during the present study (2150-6190 x 10^3 mm^3 m^{-2} d^{-1}, Figure 9). Interlinking the downward particle volume flux with the POC flux showed substantially different POC: volume ratios. They ranged over almost three orders of magnitude (Figure 10, note log scale on x-axis).

The POC: volume ratios found in Adventfjorden and the Barents Sea corresponded well with ratios established for diatom aggregates (Alldredge, 1998) and fecal pellets of the copepod species *C. finmarchicus* and *C. glacialis* (Reigstad et al., 2005; Wexels Riser et al., 2007). Also, the POC: volume ratio matched the visual inspection. The gels deployed in the southern Barents Sea and the Polar Front contained predominantly fecal pellets (**Paper I** Table 5), and had the highest POC: volume ratio in the present study (Figure 10). In Adventfjorden, fine detrital material prevailed in the gels during Winter I and the two deepest sampling depths of Autumn I (Figure 10), and it must be assumed that it had a low POC: volume ratio.

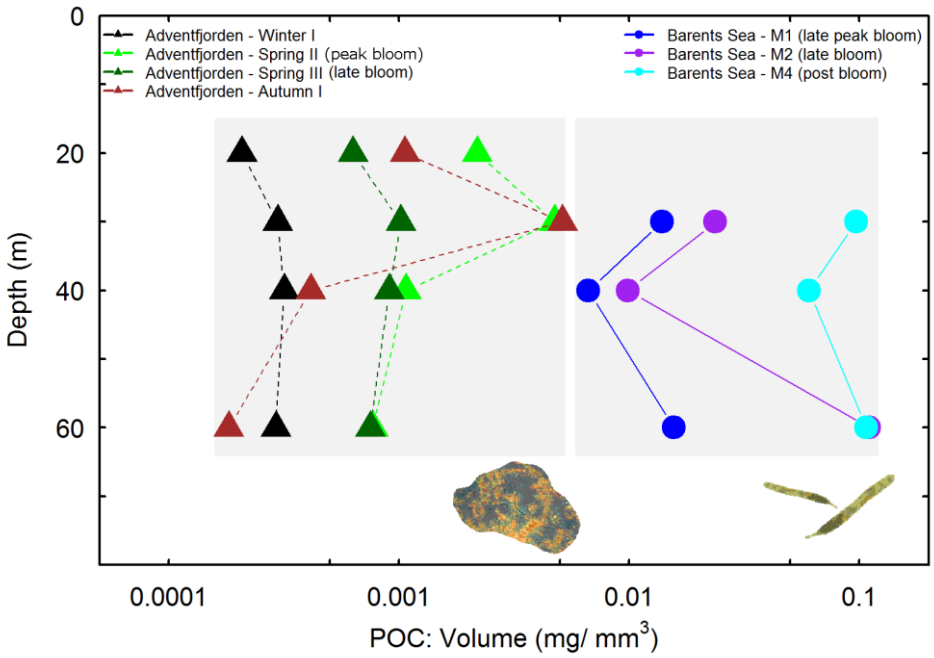

Figure 10: POC: volume ratio for sinking particles (≥ 50 µm ESD_{image}) collected in the gel traps, which were deployed in the Barents Sea (filled circles, **Paper I**) and Adventfjorden (triangles, **Paper III**).The algae aggregate and fecal pellets close to the x-axis indicate literature values of the respective particles type (Alldredge, 1998; Reigstad et al., 2005; Wexels Riser et al., 2007).

The differences in the POC: volume ratio between the Barents Sea and Adventfjorden were remarkable. To my knowledge, these ratios have not been determined from gel traps. However, several studies aimed to estimate the downward POC flux from size spectra of suspended particles, which were determined with different types of optical instruments (e.g. underwater video profiler, UVP, Guidi et al., 2008; particle camera, ParCam, Iversen et al., 2010; video plankton recorder, VPR, McDonnell and Buesseler, 2010). Guidi et al. (2008) presented a global equation to link optically determined particle spectra to the downward POC flux, but later studies indicated that temporal and spatial calibration of this equation is necessary to achieve a good estimate of the downward flux (Iversen et al., 2010; McDonnell and Buesseler, 2010; Nowald et al., in press). Despite the different approach in the present work, the results here point in the same direction. Sinking particles have distinctly different POC: volume ratios, dependent on location, season and depth (e.g. Figure 10, Autumn I), and the downward POC flux may only be determined from the particle flux if the predominant particle type and/ or composition of particles is known and taken account.

Deployment of gel traps and a subsequent image analysis revealed that the particle size composition in the Barents Sea and Adventfjorden differed with location and season. It was remarkable, that the low particle volume flux in the deep-mixed southern Barents Sea and the high particle volume flux in Adventfjorden during September (40 m, 60 m) were both associated with a high downward POC flux. This indicates that the POC: volume ratio of different types of particles (e.g. fecal pellets, algal aggregates, detritus) varied considerably.

5.3 Potential Drivers of the Downward Particle and POC Flux

The downward POC flux and sinking particles characteristics, such as size composition and the POC: volume ratio, varied between locations, seasons and depths in the present study. In the following, potential drivers of the downward POC and particle flux are examined to improve the understanding of the downward flux regulation.

5.3.1 Vertical Turbulent Mixing

Shear rate is a measure of turbulent mixing and it affects particle size. An enhanced shear rate increases the collision rate of particles and thus promotes formation of larger particles, but a too high shear rate also fragments large particles into smaller ones. The shear rate accordingly

impacts the downward POC flux, because larger/ smaller particles are assumed to have a higher/ lower sinking velocity and enhance/ reduce the downward POC flux.

During the present study, shear rates of 0.02-13.11 s^{-1} were observed in the Barents Sea (**Paper I**, Figure 5), which generally matches previous observations (Sundfjord et al., 2007). Shear rates > 2.8 s^{-1} appear to fragment larger particles (Alldredge et al., 1990), but these intensities were only observed in the upper 11-12 m of M2 and M4.

Assuming that the background shear rate in the Barents Sea was ca. 0.03 s^{-1} (found at the deep layers of all three stations), the depth layer of enhanced shear rate (background shear: 0.03 s^{-1} < enhanced shear rate < threshold for fragmentation: 2.8 s^{-1}) was located between 0-28 m at M1, 11-78 m at M2 and 13-38 m at M4. Because the depth distribution of high Chl *a* concentrations coincided with the depth interval of enhanced shear rates, particle aggregation was most likely stimulated at all three stations

The promoted aggregate formation raises the question if the observed particle maximum size in the Barents Sea data matched the theoretical maximum size. Jackson (1990) suggested that the Kolmogorov length scale, calculated based on the kinematic viscosity υ of seawater (10^{-2} cm^2 s^{-1}, Moum and Lueck, 1985, cited in Jackson, 1990) and the shear rate γ by the equation

$$\text{Kolmogorov length scale} = \sqrt{\frac{\upsilon}{\gamma}} \qquad (1),$$

could give a coarse indication of the theoretical maximum particle diameter. Using this shear rates from the Barents Sea indicates a theoretical particles maximum size of 5 mm ESD. All particles found in the deployed gels were ≤ 3.2 mm ESD_{image} and thus well below this crude upper size limit.

Apart from promoting aggregate formation, vertical turbulent mixing may have also enhanced the downward POC flux by active down-mixing of organic biomass. The upper mixing layer (vertical diffusivity > 10^{-4} m^{-2} s^{-1}) reached down to 13 m, 17 m and 25 m at M1, M2 and M4, respectively (Figure 11). Stronger stratification and the partial ice-cover at M1 and M2 probably dampened the effect of wind mixing (7-13 m), while the weakly stratified water column at M4 (pycnocline at 35-40 m) was more prone to deep wind-induced mixing.

Indications of an enhanced down-mixing of biomass were found at M4 in the southern Barents Sea. The sedimenting biomass at 60 m had a C/N ratio of 7.5, which suggested that little degraded biomass was sinking out. *P. pouchetii* dominated the phytoplankton community, and this phytoplankton taxon has been reported to sink slowly (approx. 1 m d^{-1}, Osinga et al., 1996; Reigstad and Wassmann, 2007) in comparison to for example diatoms, which may sink up to several meters per day (Smayda and Boleyn, 1966a; Smayda and Boleyn, 1966b). Thus, the vertical transport of recently produced *P. pouchetii* cells was potentially driven by wind-induced downward mixing.

Deep vertical mixing probably enhanced the downward POC flux in the weakly stratified southern Barents Sea in two ways: (1) Enhanced shear rate (higher than the background shear, but lower than the threshold of fragmentation) may have stimulated aggregate formation in the depth layer of the high particle abundance (~15-30 m depth), resulting in larger, faster sinking particles. (2) Vertical deep mixing most likely caused an active downwards transport of otherwise slowly sinking P. pouchetii *cells.*

5.3.2 Upward Nitrate Flux

Vertical turbulent mixing (section 5.3.1) as well as phytoplankton composition (section 5.3.3) have a direct effect on the downward particle and POC flux. Enhanced shear rate or the amount of excreted transparent exopolymer particles by diatoms, for example, promotes particle coagulation, increases the abundance of large particles with a higher sinking velocity and, in turn, increases the downward POC flux. In contrast, the upward nitrate flux has an indirect effect on the downward POC flux, because it stimulates the whole ecosystem and may only potentially, via a multistep process explained in the following, enhance the downward particle and POC flux.

Due to the weakly stratified water column in the southern Barents Sea, M4 was more prone to wind effects and had a deeper mixing layer with vertical diffusivity > 10^{-4} m^{-2} s^{-1} than M1 and M2 (Figure 11). This affected also the upward nitrate flux, which is determined by the vertical diffusivity and the depth gradient of the nitrate concentration (**Paper II** equation 2).

The upward nitrate flux into the base of the mixing layer at M4 (25 m: 5.39 mmol nitrate m^{-2} d^{-1}) was one order of magnitude higher than the flux at M2 (base of

mixing layer 17 m: 0.35 mmol nitrate m^{-2} d^{-1}) and two orders higher than the flux at M1 (base of mixing layer 13 m: 0.04 mmol nitrate m^{-2} d^{-1}, Figure 11). The three investigated stations illustrate thus a gradual change in water column stratification and upward nitrate flux along the north-south transect in the central Barents Sea. In the following, however, I will focus on upward nitrate flux as a driver of the downward POC flux under the most "extreme" situations, i.e. M1 and M4, because also the nitrate uptake rate was determined there.

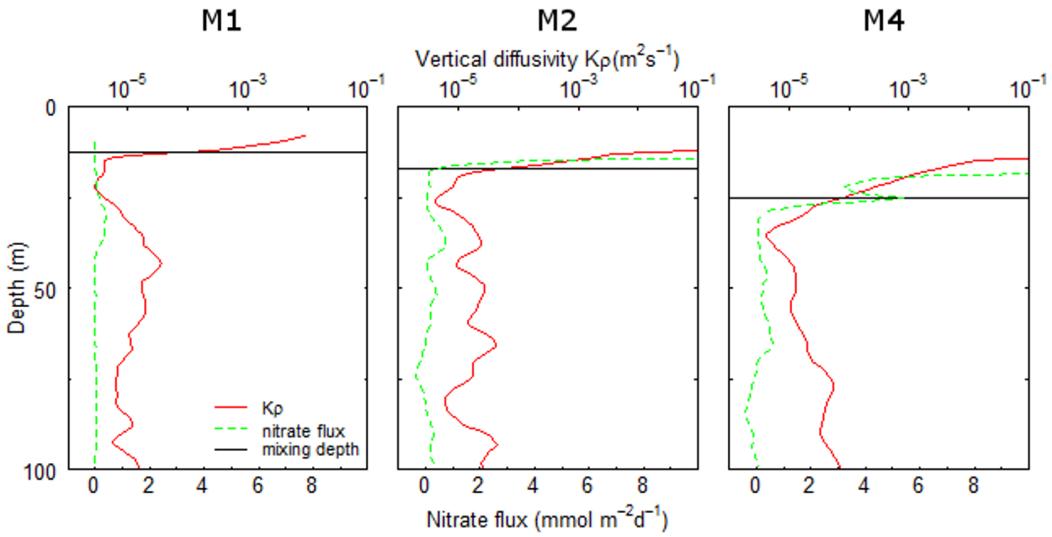

Figure 11: Vertical diffusivity and nitrate flux (upward: positive values, downward: negative values) in the upper 100 m of station M1 (left), M2 (middle) and M4 (right) in the central Barents Sea.

At M1, the low upward nitrate flux negligibly contributed to the nitrate stock in the mixing layer (ca. < 0.5 % d^{-1}). Similar observations were reported from the subpolar North Atlantic during summer (Painter et al., 2014). Model calculations were set up to investigate the development of the nitrate stock in the mixing layer over several days. They were based on he observed upward nitrate flux and the nitrate uptake rate measured in this depth interval (**Paper II**). This model indicated that the nitrate stock continuously decreased in the mixing layer, because the nitrate uptake rate always exceeded the upward nitrate flux into the layer.

Sakshaug and Slagstad (1992) suggested, based on observed wind patterns, that strong wind events occur roughly every ten days in the southern Barents Sea. This was used as a basis for the model simulations for M4. Model runs were set up in a way that a period of 1-3 days of enhanced upward nitrate flux into the base of the mixing layer (5.29 mmol nitrate m^{-2} d^{-1}) was followed by a 7-9 days relaxation period (upward nitrate flux: 0.3 mmol nitrate m^{-2} d^{-1},

equaling the average upward nitrate flux in the layer 50-70 m at M4, **Paper II** Table 4). The upward nitrate flux before the assumed relaxation period considerably exceeded the nitrate uptake rate (> 3 fold, **Paper II** Figure 3d, h), causing almost a doubling of the nitrate concentration in the mixing layer after three days. Thus, repetitive strong wind events (Sakshaug and Slagstad, 1992) potentially replenish the nitrate stock in the surface layer also during the productive early summer.

Svensen et al. (2002) conducted a mesocosm experiment under boreal summer conditions and found that a pulsed nutrient repletion (every nine days) enhanced the downward biomass flux. Despite this indication, it is challenging to link the upward nitrate flux to the downward POC flux in this study due to the time lag between the upward and the potential downward flux. A conceptual model from the Fram Strait suggested a lag of up to 60 days between primary production and vertical export in the upper 200 m (Forest et al., 2010), and a somewhat longer time window must be assumed between the upward nitrate flux, a stimulating factor of the primary production, and the downward POC flux. Station work here was conducted within ~27 h, and a mechanistic link between the upward nitrate flux and downward POC flux can therefore only be inferred. In the upper 26 m, the nitrate uptake rate was slightly higher during the post bloom situation at M4 than during the late peak bloom at M1 (**Paper II** 3c, d). Using the nitrate uptake rate as a proxy for nitrate based new primary production (Dugdale and Goering, 1967), it is suggested that new production was stimulated at M4. No particularly high Chl *a* concentrations were however observed and it is assumed that some produced phytoplankton biomass was down-mixed by the enhanced vertical mixing (section 5.3.1). In addition, the biomass was probably utilized by the abundant zooplankton community (Svensen et al., in prep.), which, in turn, enhanced the downward POC flux by production of fast-sinking fecal pellets (detailed discussion in section 3.5.4).

The upward nitrate flux into the base of the mixing layer of M4 was one order of magnitude higher than into the corresponding depth at M2 and even two orders of magnitude higher than at M1. Model calculations suggest that the strong upward nitrate flux replenished the nitrate stock in the mixing layer at M4, while it contributed negligible to the replenishment of the nitrate stock at M1. It is assumed that the enhanced upward nitrate flux stimulated new production at M4. The produced biomass was probably down-mixed by the vertical mixing processes or repackaged into fast-sinking fecal pellets. In both instances it increased the downward POC flux.

5.3.3 PHYTOPLANKTON

Phytoplankton composition potentially drives the downward POC flux by the sinking velocity of the cells or the potential to form aggregates. Both factors vary with the prevailing taxon and the physiological stage (Smayda, 1970, Kiørboe and Hansen, 1993).

Diatoms potential increase the downward POC flux in two ways: Their cells have been described to sink fast, especially as senescent cells or resting stages (Smayda and Boleyn, 1966a; Smayda and Boleyn, 1966b; Eppley et al., 1967; Bienfang, 1981). Also, some diatom genera, such as *Chaetoceros* and *Thalassiosira*, have been reported to produce sticky cells, excrete adhesive substances or occur associated with bacteria, which excrete these sticky substances (Kiørboe and Hansen, 1993; Hansen and Kiørboe, 1997; Thornton, 2002; Gärdes et al., 2011). The production of this "natural" glue promotes aggregate formation, and enhances the downward flux.

Chaetoceros spp. and *Thalassiosira* spp. were abundant during the spring bloom in the Barents Sea and in Adventfjorden (SCM, M1: ~421 x 10^3 cells L^{-1}, **Paper I** Table 3; SCM, Spring I: 270 x 10^3 cells L^{-1}, Kubiszyn et al., in prep.) and aggregates were frequently found in the gels deployed at M1 (**Paper I** Table 5). No gel trap data were available from Spring I, because the gels were completely covered after a too long deployment time and unsuitable for particle enumeration and characterization. A molecular biological analysis (18S rDNA) of the water in the sediment traps however indicates that diatoms contributed substantially to the downward flux (M. Marquardt, pers. comm.). Thus, it is inferred that diatoms enhanced the downward POC flux at both locations.

The prymnesiophyte *P. pouchetii* is another common spring bloom species in high latitudes (Degerlund and Eilertsen, 2010). It dominated during the post bloom scenario (M4) and toward the end of the bloom in Adventfjorden (SCM, M4: 1,810 x 10^3 cells L^{-1}, **Paper I** Table 3; SCM 24.5.2012: 1,340 x 10^3 cells L^{-1}, no data available during Spring III, Kubiszyn et al., in prep.). *P. pouchetii* cells have a low stickiness (Passow and Wassmann, 1994), tend to sink slowly (with 2.7-5.0 m d^{-1}, Reigstad and Wassmann, 2007) and may thus not substantially contribute to the downward POC flux. Its colonies were not observed in the gels deployed at the two sampling sites, and its single cells were too small to be included in the analysis. Neither was *P. pouchetii* identified by the 18S rDNA analysis as a dominant

contributor to the downward flux in Adventfjorden (Spring III). It is therefore presumed that *P. pouchetii* was not a driver of the downward POC flux.

Diatoms dominated the phytoplankton late peak bloom at the ice edge in the Barents Sea and the early bloom situation in Adventfjorden. Diatom aggregates were frequently observed in the gel deployed at the ice edge and diatom DNA dominated in the sediment traps in Adventfjorden during the early bloom (18S rDNA analysis, M. Marquardt, pers. comm.). The prymnesiophyte Phaeocystis pouchetii *was in contrast most abundant in the ice-free waters of the southern Barents Sea (M4) and probably during the late spring bloom in Adventfjorden. Its cells were not observed in the gels at M4, presumably because of their small size. The 18S rDNA analysis suggested that they neither contributed substantially to the downward flux in Adventfjorden (M. Marquardt, pers. comm.). It is accordingly suggested that a high diatom abundance enhanced the downward POC flux, while high numbers of* P. pouchetii *did not promote it.*

5.3.4 ZOOPLANKTON

Zooplankton attenuates POC in the upper water column, but dependent on the dominant species (e.g. copepods, meroplankton, pteropods) the downward POC flux is affected in different ways. Preferred prey size of zooplankton varies (Hansen et al., 1994; Wirtz, 2012) as well as timing of the peak abundance (Stübner et al., in rev.; Arashkevich et al., 2002; Arendt et al., 2013; Kwasniewski et al., 2013), and sinking velocity of fecal pellets (Turner, 2015).

Calanoid copepods, such as *C. finmarchicus* and *C. glacialis,* were abundant in the Barents Sea (Svensen et al., in prep.). They were characterized to be mainly suspension feeders (Wexels Riser, 2007), and it was therefore examined here if the grazers' depth distribution was associated with the SCM. Phytoplankton depth distribution was determined by vertical fluorescence profiles and the *Calanus* spp. depth allocation was quantified by LOPC profiles, a non-invasive optical technique. This revealed that the vertical zooplankton distribution was highly variable in the upper 100 m in the Barents Sea and that *Calanus* spp. was not associated with the SCM (**Paper I** Figure 6). Instead, reduction and modification of sinking biomass appeared to take place over a wide vertical range, as it has also been reported by Norrbin et al. (2009) for the waters around Svalbard.

Zooplankton biomass increased along the north-south transect in the Barents Sea (Svensen et al., in prep.). At station M4 in the southern Barents Sea, the highest *Calanus* spp. biomass was found (Svensen et al., in prep.) and also the abundance of fecal pellets was highest in the gel traps (**Paper I** Table 5). Enhanced upward nitrate flux at M4 probably stimulated primary production (section 5.3.2) and increased copepod feeding rates (Turner and Ferrante, 1979). Wexels Riser et al. (2007) observed in experiments with older stages of *C. finmachicus, C. glacialis* and *C. hyperboreus* that rather the production of larger fecal pellets sizes was promoted than the production of a higher number of pellets. According to Stokes' Law, these larger fecal pellets would have higher sinking velocities and potentially enhanced the downward POC flux at M4.

The gels deployed at M4 (40 m, 60 m, 90 m) also contained substantial amounts of unidentifiable material. Due to the high POC: volume ratio of the sinking material, it is assumed the unidentifiable material partly consisted of fragmented fecal pellets. Handling, rejection or swimming activities by crustacean zooplankton can cause fecal pellet breakage (Dilling and Alldredge, 2000; Iversen and Poulsen, 2007). This will reduce the sinking velocity of the fragmented pellets compared to unbroken ones. The slower sinking prolongs the period in the pelagic zone and exposes the pellet fragments for a longer time to zooplankton grazing and other degradation processes by dinoflagellates or bacteria (Svensen et al., 2012; Svensen et al., 2014). These processes probably caused the high POC attenuation at M4 (**Paper II** Figure 4), but the high POC: volume ratio of fecal pellets and their fragments still caused a high downward POC flux.

During spring, the zooplankton community in Adventfjorden was dominated (40-70 %) by meroplankton nauplii and larvae (approx. 16 x 10^3 ind. m^{-3}, Stübner et al., in rev.). Their high abundances probably caused a major grazing pressure especially of small cells (Sommer et al., 2000) though the ingestion rate of meroplankton has been estimated to be lower than e.g. for copepods (Hansen et al., 1997). Thus, it is here assumed, that meroplankton mainly contributed to POC attenuation in the water column by their grazing and decreased the downward POC flux. The active downward migration during meroplankton settling at the seafloor probably has an effect on the downward POC flux, but this was not investigated here.

During Autumn I, a substantial number of pteropods (*Limacina* sp.) was found in the gels deployed in Adventfjorden. It could not be determined if the animals were actively swimming

down and trapped in the gels, passively sinking or if they were dead when reaching the gel. Accordingly, they were not included in the image analysis, though major sedimentation events of this suspension feeder have been reported from the Fram Strait (Meinecke and Wefer, 1990; Bauerfeind et al., 2009) and the Norwegian Sea (Bathmann et al., 1991). Lost or rejected mucous feeding nets of pteropods have been described to promote aggregate formation (Bathmann et al., 1991; Noji et al., 1997), and they may potentially explain the high abundance of the large particles found in the gels deployed in Adventfjorden during September (Autumn I, Figure 8, **Paper III** Figure 6).

In the Barents Sea, no direct correlation was found between the SCM or the zone of the strongest POC attenuation and the zooplankton depth distribution. However, the highest zooplankton abundance coincided with the highest number of fecal pellets in the gel traps in the southern Barents Sea (M4). Apart from fecal pellets, also unidentified material was found here below 30 m, probably fragmented fecal pellets with a lower sinking velocity compared to unbroken ones. Due to their high POC: volume ratio, it is suggested that they nevertheless enhanced to the downwards POC flux.
The role of zooplankton taxa as drivers of the downward POC flux in Adventfjorden is more unclear. High meroplankton abundances during spring potentially attenuated POC in the water column, while lost or rejected feeding webs of pteropods may have promoted formation of large particles, which were found during autumn.

5.3.5 Glacial Run-Off

Adventfjorden is affected by glacial run-off between June and September (Węsławski et al., 1999), and entrained sediment-loaded meltwater could be a potential driver of the high downward POC flux (780-1530 mg POC m^{-2} d^{-1}, Figure 8) found during mid-September (Autumn I).

Hood et al. (2015) proposed that entrained glacial run-off is generally high in terrestrial dissolved and particulate organic carbon. Sedimenting material collected in the short-term sediment traps in Adventfjorden during Autumn I had a high C/N ratio of 13-15 (**Paper III** Table 3). This suggests sinking of either very degraded marine material or a mixture of marine and entrained terrestrial material (Bianchi, 2006), which was brought to the sampling location in the middle of Adventfjorden by the meandering melt water plume.

A second sediment trap deployment was not affected by the plume and indicated C/N ratios of 7-9 of the sinking material (**Paper III**). It is inferred that the first deployment was affected by the melt water plume and a mixture of marine and terrestrial material was collected in the trap cylinders.

The particle size spectra showed that large detrital particles were sinking out at 40 m and 60 m (Figure 10). Their low POC: volume ratio resembled the probably resuspended particles observed during winter. The major glacial run-off probably induced estuarine circulation in Adventfjorden, and a strong current at the bottom potentially resuspended detrital material from the seafloor and enhanced the downward POC flux at the deeper sampling depths during Autumn I.

Sinking inorganic material was not analyzed during the present study, but a downward flux of ~80 g particulate inorganic material (PIM) m^{-2} d^{-1} has been previously found during summer in Adventfjorden (Zajączkowski and Włodarska-Kowalczuk, 2007). The inorganic material may flocculate when entrained into sea water and enhance the downward flux by formation of large, faster sinking flocs, such as observed in laboratory experiments and field studies in fjords and estuaries (Kranck, 1973; Syvitski and Murray, 1981; Papenmeier et al., 2014; Sutherland et al., 2015). Entrained lithogenic material has a high specific weight and sinking velocity. In case it is incorporated into organic aggregates and fecal pellets, the lithogenic material may also enhance the sinking velocity of these particles (Syvitski and Murray, 1981; Passow and De La Rocha, 2006; Ploug et al., 2008; Iversen et al., 2010). Though these processes have not been addressed here, the present study indicated roughly 3 fold higher POC bulk sinking velocities during autumn (12-15 m d^{-1}) than during winter and spring (2-4 m d^{-1} and 2-6 m d^{-1}, respectively, **Paper III** Table 2). This may not only have been an effect of the high POC: volume ratio of the particles at the shallower sampling depths (Figure 10) or the large size of the particles at the deeper sampling depths (Figure 9), but also a ballasting effect.

A high downward POC flux was observed in Adventfjorden during September, while a major glacial run-off from land occurred. Entrained terrestrial POC apparently enhanced the downward POC flux in Adventfjorden. Increasing effects on the downward POC flux by inorganic flocculation and ballasting of organic particles (by lithogenic material) are likely, but definite conclusions cannot be drawn from the data collected here. Glacial run-off probably induced estuarine circulation and caused re-suspension of large, detrital material with low POC: volume ratio from the seafloor, which enhanced the downward POC flux at the deepest sampling depths.

6 CONCLUSION: DRIVERS OF HIGH POC FLUX EVENTS IN THE BARENTS SEA AND ADVENTFJORDEN

In this study, the downward POC and particle (≥ 50 µm ESD_{image}) flux and their potential drivers were examined in Arctic marine ecosystems. The application of a space-for-time substitution by a north-south transect in the Barents Sea, an Arctic shelf sea, allowed the investigation of contrasting bloom scenarios. In addition, a seasonal study was conducted in the ice-free, but glacially impacted, Arctic fjord Adventfjorden, western Svalbard, to study the fluxes and their drivers during winter, spring and autumn.

The highest downward POC flux was observed during (1) a post bloom situation in the deeply mixed Barents Sea, (2) an early bloom situation in Adventfjorden, and (3) an autumn situation in Adventfjorden (Figure 8). The high downward POC flux took place in form of a minor particle volume flux (post bloom situation, Barents Sea), an intermediate particle volume flux (early bloom situation, Adventfjorden) and an intermediate (20 m, 30 m) to high (40 m, 60 m) particle volume flux (autumn, Adventfjorden, Figure 9), respectively. This pinpoints that different mechanisms drove the high downward POC flux in the Barents Sea and Adventfjorden.

High downward POC flux associated with vertical mixing and high zooplankton abundance

The post bloom situation in the southern Barents Sea (M4) occurred in a weakly stratified and deeply mixed water column. Strong winds, which are re-occurring in the region (Sakshaug and Slagstad, 1992), apparently induced the high upward nitrate flux into the mixing layer (5.39 mmol nitrate m^{-2} d^{-1}). It is assumed that this stimulated the new primary production. The prymnesiophyte *P. pouchetii* was the dominant phytoplankton taxon and its small cells tend to sink slowly (Reigstad and Wassmann, 2007). Vertical mixing most likely enhanced the downward transport, because the low C/N ratio sedimenting material at 60 m (**Paper II** Figure 4) suggests sinking of recently produced biomass.

The abundant zooplankton community at M4 (Svensen et al., in prep.) utilized the produced biomass and repackaged it into fast-sinking fecal pellets, which were frequently found in the gel traps. Zooplankton however also formed a "retention filter" (Wexels Riser et al., 2001), and caused POC attenuation in the water column by for example fragmenting sinking material such as fecal pellets. Due to the high POC: volume ratio of the sinking material (Figure 10), also sinking of pellet fragments apparently enhanced the downward POC flux.

High downward POC flux associated with a diatom spring bloom

The second highest downward POC flux in the present study was found in Adventfjorden during an early bloom situation. It was the only scenario which was associated with the phytoplankton bloom, such as suggested by the conceptual model for the Arctic pelagic ecosystem (Figure 3). Diatoms were the dominating phytoplankton taxon in the water column during the early bloom, and 18S rDNA analyses (M. Marquardt, pers. comm.) indicated that they also prevailed in the sediment traps. Because the deployed gels from this sampling episode were not useable, it can only be speculated if diatom cells were sinking out in form of aggregates, which would enhance their sinking velocity (Iversen and Ploug, 2013). Alternatively, also the physiological state (e.g. senescent cells, nitrate limitation) of the cells may have caused a fast sinking of single cells, short chains or resting stages (Eppley et al., 1967; Smayda, 1970; Bienfang et al., 1982). The latter appears rather unlikely due to the previously defined situation of an early bloom stage, but cannot be disproven. This context illustrates well how gel traps can improve the understanding of an ecosystem, because an image analysis of the sinking material would show if single cells or aggregates were sinking out. Apart from the high diatom concentrations, also the low zooplankton abundance (4×10^3 ind. m^{-3}, E.I. Stübner, pers. comm.) contributed to the downward POC flux intensity, because the weak top-down regulation allowed biomass export rather than channeling biomass into the pelagic food web.

High downward POC flux associated with glacial run-off

The highest downward POC flux was observed in Adventfjorden during mid-September (Autumn I). During this time, Adventfjorden was affected by glacial run-off. It is indicated here, that a combination of factors related to the run-off enhanced the downward POC flux during this situation.

The present data imply that entrained terrestrial POC contributed to the downward POC flux. In addition, the bulk sinking velocity of POC was high (12-15 m d^{-1}, **Paper III** Table 3). Large particles with a low POC: volume ratio were found at 40 m and 60 m (Figure 10). It is assumed that these particles, potentially resuspended detrital material or marine snow formed from pteropod feeding nets, had a high sinking velocity due to their large size. At the shallower sampling depths, the POC sinking velocity was however also high. Here, mesozooplankton fecal pellets and aggregates with a comparable high POC: volume ratio (Figure 10) prevailed and probably contributed to the downward POC flux by their high POC content. In addition, ballasting of organic aggregates by entrained lithogenic material (with a

high specific weight and sinking velocity) or flocculation of entrained inorganic material is likely, but cannot be verified by data collected during the present study.

These three instances illustrate that different factors drove the downward POC flux in the ice-free Arctic Adventfjorden and the partially ice-covered Arctic shelf sea Barents Sea.
The conceptual model of the downward POC flux should therefore be extended (Figures 3 & 12). In this way it would point out that a high downward POC flux in Arctic marine ecosystem not only occurs coupled to a phytoplankton spring bloom. Instead, periods of high downward POC flux may also take place

(1) during a post bloom situation in weakly stratified, deep-mixed waters, where pulsed upward nitrate flux stimulates new production, which, in turn, is utilized by an abundant zooplankton community and repackaged into fast-sinking pellets, or
(2) in a coastal Arctic region (e.g., fjord, embayment), where high pteropod abundances coincide with glacial run-off, which entrains terrestrial POC and sediment-loaded melt water, whereas the latter may have an ballasting effect on organic aggregates.

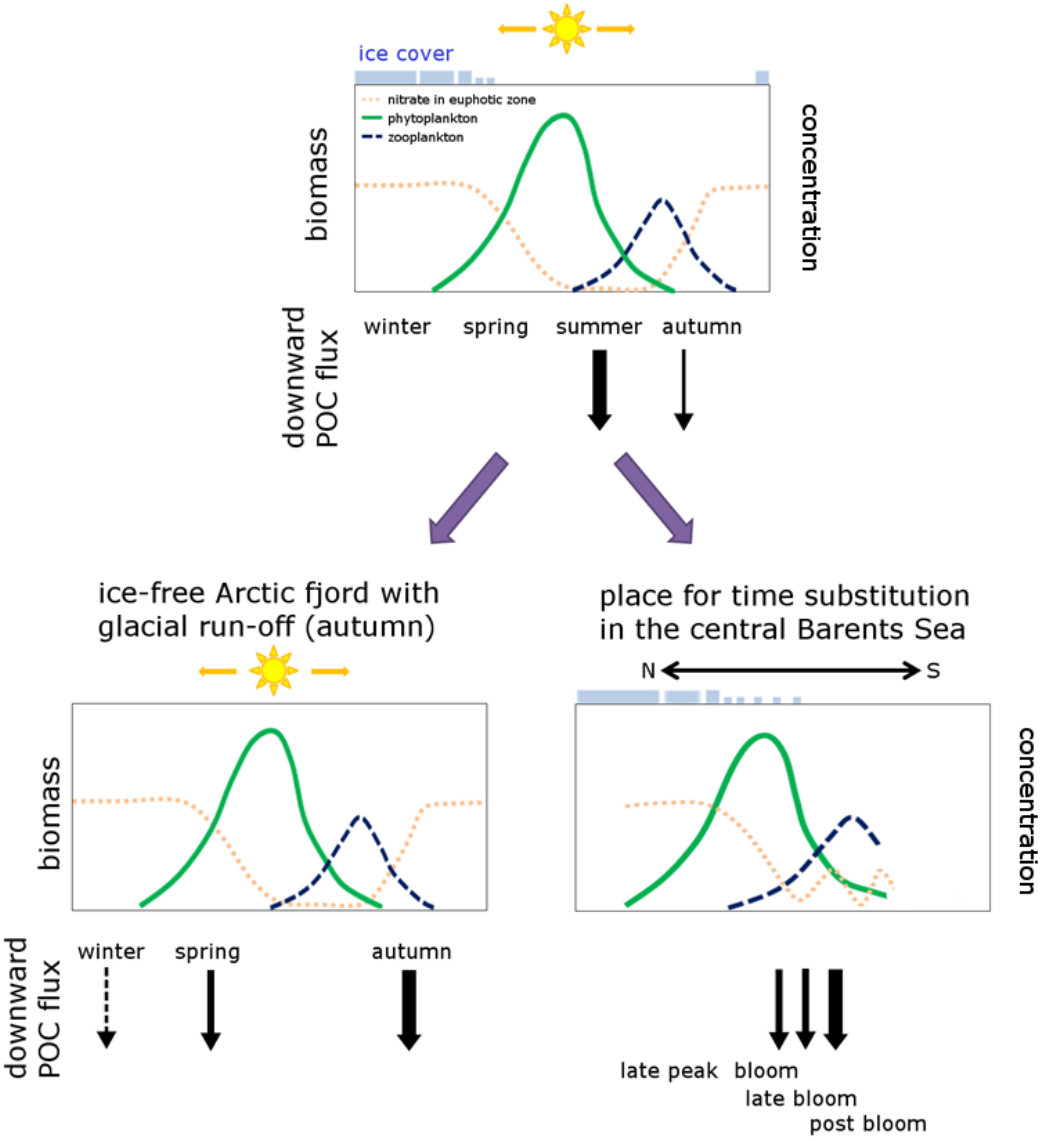

Figure 12: Conceptual understanding of the Arctic marine ecosystem with the major sedimentation event during late spring/ summer (top figure) and expansion of the conceptual model. Bottom left: Situation in the ice-free Arctic Adventfjorden with glacial run-off during autumn, which was associated with a high downward POC flux. Bottom right: Situation in the central Barents Sea, where a space for time substitution allowed investigation of different hydrographical and ecological situations (spring bloom scenarios) and the high downward POC flux in the weakly stratified southern Barents Sea, where wind mixing caused a pulsed upward nitrate flux.

7 OUTLOOK

The downward POC flux in a future seasonally ice-covered Arctic is challenging to predict due to the strong spatial variability and the simultaneous changes of sea ice cover, water temperature, salinity, water column stratification, upward nitrate flux, phyto-/ zooplankton composition and other factors (e.g., Slagstad et al., 2011; Dalpadado et al., 2012; Coupel et al., 2015; Arrigo and van Dijken, in press).

Summer data from the last 30 years in the southern, ice-free Barents Sea show a weakly increasing salinity and declining stratification, as well as a slight increase in wind speed (Peralta-Ferriz and Woodgate, 2015). Thus, a high downward POC flux as found in the present study in the southern Barents Sea may also occur in the future. However, climatic warming in the Arctic will most likely strengthen the thermal stratification of the surface layers (Wassmann and Reigstad, 2011), limit the upward nitrate flux and favor smaller phytoplankton species with a lower sinking velocity. A decline has already been reported for the large ice-associated copepods *C. glacialis* and *C. hyperboreus* in the Barents Sea (Dalpadado et al., 2012), and thus a predominant regenerative system with minor POC export during summer is likely.

Though fjords make up a small part of Arctic ecosystems, they appear to be highly important for carbon burial (Smith et al., 2015). In a future, warmer Arctic glacial run-off will probably increase and thus also enhance the downward POC flux in the marine ecosystem. However, more run-off, potentially during a longer time of the year, will also enhance the turbidity of the water and reduce the irradiance level, which may decline the pelagic production.

The high uncertainty of these predictions leaves me with the conclusion that it is important to continue research on downward POC and particle flux in the Arctic, because this will improve our mechanistic understanding of the system and processes as well as it will provide a basis for more trustworthy predictions of the future Arctic marine ecosystem.

REFERENCES

Alldredge, A., 1998. The carbon, nitrogen and mass content of marine snow as a function of aggregate size. *Deep-Sea Res. I* 45, 529-541. doi: 10.1016/S0967-0637(97)00048-4

Alldredge, A., 2001. Particle Aggregation Dynamics, in: Steele, J.H., Thorpe, S.A., Turekian, K.K. (Eds.), Encyclopedia of Ocean Sciences. Academic Press, San Diego, USA, pp. 2090-2097. doi: 10.1006/rwos.2001.0468.

Alldredge, A.L., Silver, M.W., 1988. Characteristics, dynamics and significance of marine snow. *Prog. Oceanogr.* 20, 41-82. doi: 10.1016/0079-6611(88)90053-5

Alldredge, A.L., Granata, T.C., Gotschalk, T.D., Dickey, T.D., 1990. The physical strength of marine snow and its implications for particle disaggregation in the ocean. *Limnol. Oceanogr.* 35, 1415-1428. doi: 10.4319/lo.1990.35.7.1415

Andreassen, I., Nöthig, E., Wassmann, P., 1996. Vertical particle flux on the shelf off northern Spitsbergen, Norway. *Mar. Ecol. Prog. Ser.* 137, 215-228. doi: 10.3354/meps137215

Andreassen, I.J., Wassmann, P., 1998. Vertical flux of phytoplankton and particulate biogenic matter in the marginal ice zone of the Barents Sea in May 1993. *Mar. Ecol. Prog. Ser.* 170, 1-14.

Arashkevich, E., Wassmann, P., Pasternak, A., Wexels Riser, C., 2002. Seasonal and spatial changes in biomass, structure, and development progress of the zooplankton community in the Barents Sea. *J. Mar. Sys.* 38, 125-145.

Arendt, A.A., Echelmeyer, K.A., Harrison, W.D., Lingle, C.S., Valentine, V.B., 2002. Rapid Wastage of Alaska Glaciers and Their Contribution to Rising Sea Level. *Science* 297, 382-386. doi: 10.1126/science.1072497

Arendt, K.E., Juul-Pedersen, T., Mortensen, J., Blicher, M.E., Rysgaard, S., 2013. A 5-year study of seasonal patterns in mesozooplankton community structure in a sub-Arctic fjord reveals dominance of *Microsetella norvegica* (Crustacea, Copepoda). *J. Plankton Res.* 35, 105-120. doi: 10.1093/plankt/fbs087

Arrigo, K.R., van Dijken, G.L., Continued increases in Arctic Ocean primary production. *Prog. Oceanogr.* doi: 10.1016/j.pocean.2015.05.002 (in press)

Azam, F., Malfatti, F., 2007. Microbial structuring of marine ecosystems. *Nat. Rev. Micorbiol.* 5, 782-791.

Bamber, J., van den Broeke, M., Ettema, J., Lenaerts, J., Rignot, E., 2012. Recent large increases in freshwater fluxes from Greenland into the North Atlantic. *Geophys. Res. Lett.* 39, L19501. doi: 10.1029/2012GL052552

Bathmann, U.V., Noji, T.T., von Bodungen, B., 1991. Sedimentation of pteropods in the Norwegian Sea in autumn. *Deep-Sea Res. I* 38, 1341-1360. doi: 10.1016/0198-0149(91)90031-A

Bauerfeind, E., Nöthig, E.-M., Beszczynska, A., Fahl, K., Kaleschke, L., Kreker, K., Klages, M., Soltwedel, T., Lorenzen, C., Wegner, J., 2009. Particle sedimentation patterns in the eastern Fram Strait during 2000–2005: Results from the Arctic long-term observatory HAUSGARTEN. *Deep-Sea Res. I* 56, 1471-1487. doi: 10.1016/j.dsr.2009.04.011

Behrenfeld, M.J., 2014. Climate-mediated dance of the plankton. *Nature Clim. Change* 4, 880-887. doi: 10.1038/nclimate2349

Bianchi, T.S., 2006. *Biochemistry of Estuaries*. Oxford University Press, Cary, USA 720 pp.

Bienfang, P.K., 1981. Sinking rates of heterogeneous, temperate phytoplankton populations. *J. Plankton Res.* 3, 235-253. doi: 10.1093/plankt/3.2.235

Bienfang, P.K., Harrison, P.J., Quarmby, L.M., 1982. Sinking rate response to depletion of nitrate, phosphate and silicate in four marine diatoms. *Mar. Biol.* 67, 295-302.
Bishop, J.K.B., Edmond, J.M., 1976. A new large volume filtration system for the sampling of oceanic particulate matter. *J. Mar. Res.* 34, 181-198.
Brainerd, K.E., Gregg, M.C., 1995. Surface mixed and mixing layer depths. *Deep-Sea Res. I* 42, 1521-1543. doi: 10.1016/0967-0637(95)00068-H
Buesseler, K.O., Boyd, P.W., 2009. Shedding light on processes that control particle export and flux attenuation in the twilight zone of the open ocean. *Limnol. Oceanogr.* 54, 1210-1232. doi: 10.4319/lo.2009.54.4.1210
Carmack, E., McLaughlin, F., 2011. Towards recognition of physical and geochemical change in Subarctic and Arctic Seas. *Prog. Oceanogr.* 90, 90-104. doi: 10.1016/j.pocean.2011.02.007
Carmack, E.C., Macdonald, R.W., Jasper, S., 2004. Phytoplankton productivity on the Canadian Shelf of the Beaufort Sea. *Mar. Ecol. Prog. Ser.* 277, 37-50. doi: 10.3354/meps277037
Checkley Jr., D.M., Davis, R.E., Herman, A.W., Jackson, G.A., Beanlands, B., Regier, L.A., 2008. Assessing plankton and other particles in situ with the SOLOPC. *Limnol. Oceanogr.* 53, 2123–2136. doi: 10.4319/lo.2008.53.5_part_2.2123
Coppola, L., Roy-Barman, M., Wassmann, P., Mulsow, S., Jeandel, C., 2002. Calibration of sediment traps and particulate organic carbon export using ^{234}Th in the Barents Sea. *Mar. Chem.* 80, 11-26. doi: 10.1016/S0304-4203(02)00071-3
Coupel, P., Ruiz-Pino, D., Sicre, M.A., Chen, J.F., Lee, S.H., Schiffrine, N., Li, H.L., Gascard, J.C., 2015. The impact of freshening on phytoplankton production in the Pacific Arctic Ocean. *Prog. Oceanogr.* 131, 113-125. doi: 10.1016/j.pocean.2014.12.003
Dalpadado, P., Ingvaldsen, R.B., Stige, L.C., Bogstad, B., Knutsen, T., Ottersen, G., Ellertsen, B., 2012. Climate effects on Barents Sea ecosystem dynamics. *ICES J. Mar. Sci.* 69, 1303-1316. doi: 10.1093/icesjms/fss063
Darnis, G., Fortier, L., 2014. Temperature, food and the seasonal vertical migration of key arctic copepods in the thermally stratified Amundsen Gulf (Beaufort Sea, Arctic Ocean). *J. Plankton Res.* 36, 1092-1108. doi: 10.1093/plankt/fbu035
De La Rocha, C.L., Nowald, N., Passow, U., 2008. Interactions between diatom aggregates, minerals, particulate organic carbon, and dissolved organic matter: Further implications for the ballast hypothesis. *Global Biogeochem. Cy.* 22, GB4005. doi: 10.1029/2007GB003156
De La Rocha, C.L., Passow, U., 2007. Factors influencing the sinking of POC and the efficiency of the biological carbon pump. *Deep-Sea Res. II* 54, 639-658. doi: 10.1016/j.dsr2.2007.01.004
Degerlund, M., Eilertsen, H.C., 2010. Main Species Characteristics of Phytoplankton Spring Blooms in NE Atlantic and Arctic Waters (68-80°N). *Estuar. Coasts* 33, 242-269. doi: 10.1007/s12237-009-9167-7
Dilling, L., Alldredge, A.L., 2000. Fragmentation of marine snow by swimming macrozooplankton: A new process impacting carbon cycling in the sea. *Deep-Sea Res. I* 47, 1227-1245. doi: 10.1016/S0967-0637(99)00105-3
Dugdale, R.C., Goering, J.J., 1967. Uptake of new and regenerated forms of nitrogen in primary productivity. *Limnol. Oceanogr.* 12, 196-206. doi: 10.4319/lo.1967.12.2.0196
Durkin, C.A., Estapa, M.L., Buesseler, K.O., Observations of carbon export by small sinking particles in the upper mesopelagic. *Mar. Chem.* doi: 10.1016/j.marchem.2015.02.011 (in press)

Ebersbach, F., Trull, T.W., 2008. Sinking particle properties from polyacrylamide gels during the Kerguelen Ocean and Plateau compared Study (KEOPS): Zooplankton control of carbon export in an area of persistent natural iron inputs in the Southern Ocean. *Limnol. Oceanogr.* 53, 212-224. doi: 10.2307/40006162

Ebersbach, F., Trull, T.W., Davies, D.M., Bray, S.G., 2011. Controls on mesopelagic particle fluxes in the Sub-Antarctic and Polar Frontal Zones in the Southern Ocean south of Australia in summer - Perspectives from free-drifting sediment traps. *Deep-Sea Res. II* 58, 2260-2276. doi: 10.1016/j.dsr2.2011.05.025

Ehrhardt, M., 1983. Determination of organic constituents, in: Grasshoff, K., Ehrhardt, M., Kremling, K. (Eds.), *Methods of Seawater Analysis. Second, Revised and Extended Edition*. Verlag Chemie, Weinheim, pp. 269-346.

Eilertsen, H.C., Degerlund, M., 2010. Phytoplankton and light during the northern high-latitude winter. *J. Plankton Res.* 32, 899-912. doi: 10.1093/plankt/fbq017

Eilertsen, H.C., Schei, B., Taasen, J.P., 1981. Investigations on the plankton community of Balsfjorden, Northern Norway. The phytoplankton 1976 - 1978. Abundance, species composition, and succession. *Sarsia* 66, 129-141.

Engel, A., Szlosek, J., Abramson, L., Liu, Z., Lee, C., 2009. Investigating the effect of ballasting by $CaCO_3$ in *Emiliania huxleyi*: I. Formation, settling velocities and physical properties of aggregates. *Deep-Sea Res. II* 56, 1396-1407. doi: 10.1016/j.dsr2.2008.11.027

Eppley, R.W., Holmes, R.W., Strickland, J.D.H., 1967. Sinking rates of marine phytoplankton measured with a fluorometer. *J. Exp. Mar. Biol. Ecol.* 1, 191-208. doi: 10.1016/0022-0981(67)90014-7

Forest, A., Babin, M., Stemmann, L., Picheral, M., Sampei, M., Fortier, L., Gratton, Y., Bélanger, S., Devred, E., Sahlin, J., Doxaran, D., Joux, F., Ortega-Retuerta, E., Martín, J., Jeffrey, W.H., Gasser, B., Carlos Miquel, J., 2013. Ecosystem function and particle flux dynamics across the Mackenzie Shelf (Beaufort Sea, Arctic Ocean): an integrative analysis of spatial variability and biophysical forcings. *Biogeosciences* 10, 2833-2866. doi: 10.5194/bg-10-2833-2013

Forest, A., Sampei, M., Makabe, R., Sasaki, H., Barber, D.G., Gratton, Y., Wassmann, P., Fortier, L., 2008. The annual cycle of particulate organic carbon export in Franklin Bay (Canadian Arctic): Environmental control and food web implications. *J. Geophys. Res.-Oceans* 113, C03S05. doi: 10.1029/2007JC004262

Forest, A., Wassmann, P., Slagstad, D., Bauerfeind, E., Nöthig, E.-M., Klages, M., 2010. Relationships between primary production and vertical particle export at the Atlantic-Arctic boundary (Fram Strait, HAUSGARTEN). *Polar Biol.* 33, 1733-1746. doi: 10.1007/s00300-010-0855-3

Fossheim, M., Primicerio, R., Johannesen, E., Ingvaldsen, R.B., Aschan, M.M., Dolgov, A.V., 2015. Recent warming leads to a rapid borealization of fish communities in the Arctic. *Nature Clim. Change* 5, 673-677. doi: 10.1038/nclimate2647

Giering, S.L.C., Sanders, R., Lampitt, R.S., Anderson, T.R., Tamburini, C., Boutrif, M., Zubkov, M.V., Marsay, C.M., Henson, S.A., Saw, K., Cook, K., Mayor, D.J., 2014. Reconciliation of the carbon budget in the ocean's twilight zone. *Nature* 507, 480-483. doi: 10.1038/nature13123

Guidi, L., Jackson, G.A., Stemmann, L., Miquel, J.C., Picheral, M., Gorsky, G., 2008. Relationship between particle size distribution and flux in the mesopelagic zone. *Deep-Sea Res. I* 55, 1364-1374. doi: 10.1016/j.dsr.2008.05.014

Gustafsson, Ö., Andersson, P.S., 2012. ^{234}Th-derived surface export fluxes of POC from the Northern Barents Sea and the Eurasian sector of the Central Arctic Ocean. *Deep-Sea Res I* 68, 1-11. doi: 10.1016/j.dsr.2012.05.014

Gärdes, A., Iversen, M.H., Grossart, H.-P., Passow, U., Ullrich, M.S., 2011. Diatom-associated bacteria are required for aggregation of *Thalassiosira weissflogii*. *ISME J.* 5, 436-445. doi: 10.1038/ismej.2010.145

Hamm, C.E., 2002. Interactive aggregation and sedimentation of diatoms and clay-sized lithogenic material. *Limnol. Oceanogr* 47, 1790-1795.

Hansen, B., Bjornsen, P.K., Hansen, P.J., 1994. The Size Ratio Between Planktonic Predators and Their Prey. *Limnol. Oceanogr.* 39, 395-403. doi: 10.2307/2838340

Hansen, J.L.S., Kiørboe, T., 1997. Quantifying interspecific coagulation efficiency of phytoplankton. *Mar. Ecol. Prog. Ser.* 159, 75-79. doi: 10.3354/meps159075

Hansen, P.J., Bjørnsen, P.K., Hansen, B.W., 1997. Zooplankton grazing and growth: Scaling within the 2–2,000 µm body size range. *Limnol. Oceanogr.* 42, 687-704.

Hargrave, B.T., Walsh, I.D., Murray, D.W., 2002. Seasonal and spatial patterns in mass and organic matter sedimentation in the North Water. *Deep-Sea Res. II* 49, 5227-5244. doi: 10.1016/S0967-0645(02)00187-X

Hegseth, E.N., 1997. Phytoplankton of the Barents Sea - the end of a growth season. *Polar Biol.* 17, 235-241. doi: 10.1007/s003000050127

Hegseth, E.N., Sundfjord, A., 2008. Intrusion and blooming of Atlantic phytoplankton species in the high Arctic. *J. Mar. Syst.* 74, 108-119. doi: 10.1016/j.jmarsys.2007.11.011

Herman, A.W., Beanlands, B., Phillips, E.F., 2004. The next generation of Optical Plankton Counter: the Laser-OPC. *J. Plankton Res.* 26, 1135-1145. doi: 10.1093/plankt/fbh095

Hill, P.S., 1998. Controls on floc size in the sea. *Oceanography* 11, 13-18. doi: 10.5670/oceanog.1998.03

Hirche, H.J., Kosobokova, K.N., 2011. Winter studies on zooplankton in Arctic seas: the Storfjord (Svalbard) and adjacent ice-covered Barents Sea. *Mar. Biol.* 158, 2359-2376. doi: 10.1007/s00227-011-1740-5

Hodal, H., Falk-Petersen, S., Hop, H., Kristiansen, S., Reigstad, M., 2012. Spring bloom dynamics in Kongsfjorden, Svalbard: nutrients, phytoplankton, protozoans and primary production. *Polar Biol.* 35, 191-203. doi: 10.1007/s00300-011-1053-7

Hodal, H., Kristiansen, S., 2008. The importance of small-celled phytoplankton in spring blooms at the marginal ice zone in the northern Barents Sea. *Deep-Sea Res. II* 55, 2176-2185. doi: 10.1016/j.dsr2.2008.05.012

Hood, E., Battin, T.J., Fellman, J., O'Neel, S., Spencer, R.G.M., 2015. Storage and release of organic carbon from glaciers and ice sheets. *Nature Geosci.* 8, 91-96. doi: 10.1038/ngeo2331

Ingvaldsen, R., Loeng, H., 2009. Chapter 2: Physical Oceanography, in: Sakshaug, E., Johnsen, G.H., Kovacs, K.M. (Eds.), *Ecosystem Barents Sea*. Tapir Academic Press, Trondheim, Norway, pp. 33-64.

IPCC, 2013. Climate Change 2013: The Physical Science Basis. Contribution of Working Group I to the Fifth Assessment Report of the Intergovernmental Panel on Climate Change, in: Stocker, T.F., Qin, D., Plattner, G.-K., Tignor, M., Allen, S.K., Boschung, J., Nauels, A., Xia, Y., Bex, V., Midgley, P.M. (Eds.). Cambridge University Press, Cambridge, United Kingdom and New York, NY, USA, p. 1535. doi: 10.1017/CBO9781107415324.

Iversen, K.R., Seuthe, L., 2011. Seasonal microbial processes in a high-latitude fjord (Kongsfjorden, Svalbard): I. Heterotrophic bacteria, picoplankton and nanoflagellates. *Polar Biol.* 34, 731-749. doi: 10.1007/s00300-010-0929-2

Iversen, M.H., Nowald, N., Ploug, H., Jackson, G.A., Fischer, G., 2010. High resolution profiles of vertical particulate organic matter export off Cape Blanc, Mauritania: Degradation processes and ballasting effects. *Deep-Sea Res. I* 57, 771-784. doi: 10.1016/j.dsr.2010.03.007

Iversen, M.H., Ploug, H., 2013. Temperature effects on carbon-specific respiration rate and sinking velocity of diatom aggregates - potential implications for deep ocean export processes. *Biogeosciences* 10, 4073-4085. doi: 10.5194/bg-10-4073-2013

Iversen, M.H., Poulsen, L.K., 2007. Coprorhexy, coprophagy, and coprochaly in the copepods *Calanus helgolandicus*, *Pseudocalanus elongatus*, and *Oithona similis*. *Mar. Ecol. Prog. Ser.* 350, 79-89. doi: 10.3354/meps07095

Jackson, G.A., 1990. A model of the formation of marine algal flocs by physical coagulation processes. *Deep-Sea Res. Oceanogr., A* 37, 1197-1211. doi: 10.1016/0198-0149(90)90038-W

Jackson, G.A., 2015. Coagulation in a rotating cylinder. *Limnol. Oceanogr.-Meth.* 13, 194-201. doi: 10.1002/lom3.10018

Jackson, G.A., Waite, A.M., Boyd, P.W., 2005. Role of algal aggregation in vertical carbon export during SOIREE and in other low biomass environments. *Geophys. Res. Lett.* 32, L13607. doi: 10.1029/2005gl023180

Jakobsson, M., Grantz, A., Kristoffersen, Y., Macnab, R., 2004. The Arctic Ocean: Boundary Conditions and Background Information, in: Stein, R., Macdonald, R.W. (Eds.), *The Organic Carbon Cycle in the Arctic Ocean*. Springer, Berlin, pp. 1-32.

Jensen, H.M., Pedersen, L., Burmeister, A., Winding Hansen, B., 1999. Pelagic primary production during summer along 65 to 72°N off West Greenland. *Polar Biol.* 21, 269-278. doi: 10.1007/s003000050362

Ji, R., Jin, M., Varpe, Ø., 2013. Sea ice phenology and timing of primary production pulses in the Arctic Ocean. *Glob. Change Biol.* 19, 734-741. doi: 10.1111/gcb.12074

Kahru, M., Brotas, V., Manzano-Sarabia, M., Mitchell, B.G., 2011. Are phytoplankton blooms occurring earlier in the Arctic? *Glob. Change Biol.* 17, 1733-1739. doi: 10.1111/j.1365-2486.2010.02312.x

Keck, A., Wassmann, P., 1996. Temporal and spatial patterns of sedimentation in the subarctic fjord Malangen, Northern Norway. *Sarsia* 80, 259-276.

Kiørboe, T., 2001. Formation and fate of marine snow: small-scale processes with large-scale implications. *Sci. Mar.* 65, 57-71.

Kiørboe, T., Andersen, K.P., Dam, H.G., 1990. Coagulation efficiency and aggregate formation in marine phytoplankton. *Mar. Biol.* 107, 235-245. doi: 10.1007/BF01319822

Kiørboe, T., Hansen, J.L.S., 1993. Phytoplankton aggregate formation: observations of patterns and mechanisms of cell sticking and the significance of exopolymeric material. *J. Plankton Res.* 15, 993-1018. doi: 10.1093/plankt/15.9.993

Kiørboe, T., Lundsgaard, C., Olesen, M., Hansen, J.L.S., 1994. Aggregation and sedimentation processes during a spring phytoplankton bloom: A field experiment to test coagulation theory. *J. Mar. Res.* 52, 297-323. doi: 10.1357/0022240943077145

Kranck, K., 1973. Flocculation of Suspended Sediment in the Sea. *Nature* 246, 348-350. doi: 10.1038/246348a0

Kristiansen, S., Farbrot, T., Wheeler, P.A., 1994. Nitrogen cycling in the Barents Sea–Seasonal dynamics of new and regenerated production in the marginal ice zone. *Limnol. Oceanogr* 39, 1630-1642. doi: 10.4319/lo.1994.39.7.1630

Kubiszyn, A.M., Wiktor, J.M., Wiktor, J.M.J., Griffiths, C., Kristiansen, S., Gabrielsen, T.M., The annual planktonic protist community structure in an ice-free high Arctic fjord (Adventfjorden, West Spitsbergen). (in prep.)

Kwasniewski, S., Walkusz, W., Cottier, F.R., Leu, E., 2013. Mesozooplankton dynamics in relation to food availability during spring and early summer in a high latitude glaciated fjord (Kongsfjorden), with focus on *Calanus*. *J. Mar. Syst.* 111–112, 83-96. doi: 10.1016/j.jmarsys.2012.09.012

Lalande, C., Forest, A., Barber, D.G., Gratton, Y., Fortier, L., 2009. Variability in the annual cycle of vertical particulate organic carbon export on Arctic shelves: Contrasting the Laptev Sea, Northern Baffin Bay and the Beaufort Sea. *Cont. Shelf Res.* 29, 2157-2165. doi: 10.1016/j.csr.2009.08.009

Lapoussière, A., Michel, C., Gosselin, M., Poulin, M., Martin, J., Tremblay, J.-É., 2013. Primary production and sinking export during fall in the Hudson Bay system, Canada. *Cont. Shelf Res.* 52, 62-72. doi: 10.1016/j.csr.2012.10.013

Laurenceau-Cornec, E.C., Trull, T.W., Davies, D.M., Bray, S.G., Doran, J., Planchon, F., Carlotti, F., Jouandet, M.P., Cavagna, A.J., Waite, A.M., Blain, S., 2015. The relative importance of phytoplankton aggregates and zooplankton fecal pellets to carbon export: insights from free-drifting sediment trap deployments in naturally iron-fertilised waters near the Kerguelen Plateau. *Biogeosciences* 12, 1007-1027. doi: 10.5194/bg-12-1007-2015

Le Moigne, F.A.C., Henson, S.A., Sanders, R.J., Madsen, E., 2013. Global database of surface ocean particulate organic carbon export fluxes diagnosed from the ^{234}Th technique. *Earth Syst. Sci. Data* 5, 295-304. doi: 10.5194/essd-5-295-2013

Lee, P.L.M., Dawson, M.N., Neill, S.P., Robins, P.E., Houghton, J.D.R., Doyle, T.K., Hays, G.C., 2013. Identification of genetically and oceanographically distinct blooms of jellyfish. *J. Roy. Soc. Interface* 10, 20120920. doi: 10.1098/rsif.2012.0920

Leu, E., Falk-Petersen, S., Kwaśniewski, S., Wulff, A., Edvardsen, K., Hessen, D.O., 2006. Fatty acid dynamics during the spring bloom in a High Arctic fjord: importance of abiotic factors versus community changes. *Can. J. Fish. Aquat. Sci.* 63, 2760-2779. doi: 10.1139/f06-159

Leu, E., Søreide, J.E., Hessen, D.O., Falk-Petersen, S., Berge, J., 2011. Consequences of changing sea-ice cover for primary and secondary producers in the European Arctic shelf seas: Timing, quantity, and quality. *Progr. Oceanogr.* 90, 18-32. doi: 10.1016/j.pocean.2011.02.004

Li, W.K.W., Carmack, E.C., McLaughlin, F.A., Nelson, R.J., Williams, W.J., 2013. Space-for-time substitution in predicting the state of picoplankton and nanoplankton in a changing Arctic Ocean. *J. Geophys. Res.-Oceans* 118, 5750-5759. doi: 10.1002/jgrc.20417

Li, W.K.W., McLaughlin, F.A., Lovejoy, C., Carmack, E.C., 2009. Smallest Algae Thrive As the Arctic Ocean Freshens. *Science* 326, 539. doi: 10.1126/science.1179798

Lique, C., 2015. Ocean science: Arctic sea ice heated from below. *Nature Geosci.* 8, 172-173. doi: 10.1038/ngeo2357

Liu, Z., Cochran, J.K., Lee, C., Gasser, B., Miquel, J.C., Wakeham, S.G., 2009. Further investigations on why POC concentrations differ in samples collected by Niskin bottle and in situ pump. *Deep-Sea Res. II* 56, 1558-1567. doi: 10.1016/j.dsr2.2008.12.019

Loeng, H., 1991. Features of the physical oceanographic conditions of the Barents Sea. *Polar Res.* 10, 5-18. doi: 10.1111/j.1751-8369.1991.tb00630.x

Longhurst, A.R., Glen Harrison, W., 1989. The biological pump: Profiles of plankton production and consumption in the upper ocean. *Prog. Oceanogr.* 22, 47-123. doi: 10.1016/0079-6611(89)90010-4

Lundsgaard, C., 1995. Use of a high viscosity medium in studies of aggregates, in: Floderus, S., Heisakanen, A.-S., Oleson, M., Wassmann, P. (Eds.), *Sediment trap studies in the Nordic countries. 3. Proceedings of the Symposium: Seasonal Dynamics of Planktonic Ecosystems and Sedimentation in Coastal Nordic Waters*. Finnish Environment Agency.

Lundsgaard, C., M., O., Reigstad, M., Olli, K., 1999. Sources of settling material: aggregation and zooplankton mediated fluxes in the Gulf of Riga. *J. Mar. Syst.* 23, 197–210. doi: 10.1016/S0924-7963(99)00058-5

Mann, K., Lazier, J., 2006. *Dynamics of Marine Ecosystems: Biological-Physical Interactions in the Oceans, Third Edition*. Blackwell Publishing 496 pp.

Martin, J.H., Knauer, G.A., Karl, D.M., Broenkow, W.W., 1987. VERTEX: carbon cycling in the northeast Pacific. *Deep-Sea Res. Oceanogr., A* 34, 267-285. doi: 10.1016/0198-0149(87)90086-0

Martin, T., Steele, M., Zhang, J., 2014. Seasonality and long-term trend of Arctic Ocean surface stress in a model. *J. Geophys. Res.-Oceans* 119, 1723-1738. doi: 10.1002/2013JC009425

McCave, I.N., 1975. Vertical flux of particles in the ocean. *Deep-Sea Res. Oceanogr., A* 22, 491-502. doi: 10.1016/0011-7471(75)90022-4

McCave, I.N., 1984. Size spectra and aggregation of suspended particles in the deep ocean. *Deep-Sea Res. Oceanogr., A* 31, 329-352. doi: 10.1016/0198-0149(84)90088-8

McDonnell, A.M.P., Buesseler, K.O., 2010. Variability in the average sinking velocity of marine particles. *Limnol. Oceanogr.* 55, 2085-2096. doi: 10.4319/lo.2010.55.5.2085

Meinecke, G., Wefer, G., 1990. Seasonal pteropod sedimentation in the Norwegian Sea. *Palaeogeogr. Palaeocl.* 79, 129-147. doi: 10.1016/0031-0182(90)90109-K

Melle, W., Runge, J., Head, E., Plourde, S., Castellani, C., Licandro, P., Pierson, J., Jonasdottir, S., Johnson, C., Broms, C., Debes, H., Falkenhaug, T., Gaard, E., Gislason, A., Heath, M., Niehoff, B., Nielsen, T.G., Pepin, P., Stenevik, E.K., Chust, G., 2014. The North Atlantic Ocean as habitat for *Calanus finmarchicus*: Environmental factors and life history traits. *Prog. Oceanogr.* 129, Part B, 244-284. doi: 10.1016/j.pocean.2014.04.026

Moran, B., 2004. Regional Variability in POC Export Flux in the Arctic Ocean Determined Using ^{234}Th as a Tracer, in: Stein, R., Macdonald, R.W. (Eds.), *The Organic Carbon Cycle in the Arctic Ocean*. Springer, Berlin, Heidelberg, pp. 126-130.

Noji, T.T., Bathmann, U.V., Bodungen, B.v., Voss, M., Antia, A., Krumbholz, M., Klein, B., Peeken, I., Noji, C.I.-M., Rey, F., 1997. Clearance of picoplankton-sized particles and formation of rapidly sinking aggregates by the pteropod, *Limacina retroversa*. *J. Plankton Res.* 19, 863-875. doi: 10.1093/plankt/19.7.863

Noji, T.T., Noji, C.I.-M., Barthel, K.-G., 1993. Pelagic-benthic coupling during the onset of winter in a northern Norwegian fjord. Carbon flow and fate of suspended particulate matter. *Mar. Ecol. Prog. Ser.* 93, 89-99.

Noji, T.T., Rey, F., Miller, L.A., Børsheim, K.Y., Urban-Rich, J., 1999. Fate of biogenic carbon in the upper 200 m of the central Greenland Sea. *Deep-Sea Res. II* 46, 1497-1509. doi: 10.1016/S0967-0645(99)00032-6

Norrbin, F., Eilertsen, H.C., Degerlund, M., 2009. Vertical distribution of primary producers and zooplankton grazers during different phases of the Arctic spring bloom. *Deep-Sea Res.* II 56, 1945-1958. doi: 10.1016/j.dsr2.2008.11.006

Nowald, N., Iversen, M.H., Fischer, G., Ratmeyer, V., Wefer, G., Time series of in-situ particle properties and sediment trap fluxes in the coastal upwelling filament off Cape Blanc, Mauritania. *Prog. Oceanogr.* doi: 10.1016/j.pocean.2014.12.015 (in press)

O'Brien, M.C., Macdonald, R.W., Melling, H., Iseki, K., 2006. Particle fluxes and geochemistry on the Canadian Beaufort Shelf: Implications for sediment transport and deposition. *Cont. Shelf Res.* 26, 41-81. doi: 10.1016/j.csr.2005.09.007

Olli, K., 2015. Unraveling the uncertainty and error propagation in the vertical flux Martin curve. *Prog. Oceanogr.* 135, 146-155. doi: 10.1016/j.pocean.2015.05.016

Olli, K., Rieser, C.W., Wassmann, P., Ratkova, T., Arashkevich, E., Pasternak, A., 2002. Seasonal variation in vertical flux of biogenic matter in the marginal ice zone and the central Barents Sea. *J. Mar. Syst.* 38, 189-204. doi: 10.1016/S0924-7963(02)00177-X

Osinga, R., Kwint, R.L.J., Lewis, W.E., Kraay, G.W., Lont, J.D., Lindeboom, H.J., van Duyl, F.C., 1996. Production and fate of dimethylsulfide and dimethylsulfoniopropionate in pelagic mesocosms: the role of sedimentation. *Mar. Ecol. Prog. Ser.* 131, 275-286. doi: 10.3354/meps131275

Painter, S.C., Henson, S.A., Forryan, A., Steigenberger, S., Klar, J., Stinchcombe, M.C., Rogan, N., Baker, A.R., Achterberg, E.P., Moore, C.M., 2014. An assessment of the vertical diffusive flux of iron and other nutrients to the surface waters of the subpolar North Atlantic Ocean. *Biogeosciences* 11, 2113-2130. doi: 10.5194/bg-11-2113-2014

Papenmeier, S., Schrottke, K., Bartholomä, A., 2014. Over time and space changing characteristics of estuarine suspended particles in the German Weser and Elbe estuaries. *J. Sea Res.* 85, 104-115. doi: 10.1016/j.seares.2013.03.010

Passow, U., De La Rocha, C.L., 2006. Accumulation of mineral ballast on organic aggregates. *Global Biogeochem. Cy.* 20, GB1013. doi: 10.1029/2005GB002579

Passow, U., De La Rocha, C.L., Fairfield, C., Schmidt, K., 2014. Aggregation as a function of P_{CO2} and mineral particles. *Limnol. Oceanogr* 59, 532-547.

Passow, U., Wassmann, P., 1994. On the trophic fate of *Phaeocystis pouchetii* (Hariot): IV. The formation of marine snow by *P. pouchetii*. *Mar. Ecol. Prog. Ser.* 104, 153-161. doi:

Peralta-Ferriz, C., Woodgate, R.A., 2015. Seasonal and interannual variability of pan-Arctic surface mixed layer properties from 1979 to 2012 from hydrographic data, and the dominance of stratification for multiyear mixed layer depth shoaling. *Prog. Oceanogr.* 134, 19-53. doi: 10.1016/j.pocean.2014.12.005

Ploug, H., Iversen, M.H., Fischer, G., 2008. Ballast, sinking velocity, and apparent diffusivity within marine snow and zooplankton fecal pellets: Implications for substrate turnover by attached bacteria. *Limnol. Oceanogr.* 53, 1878-1886. doi: 10.4319/lo.2008.53.5.1878

Rainville, L., Lee, C.M., Woodgate, R.A., 2011. Impact of wind-driven mixing in the Arctic Ocean. *Oceanography* 24, 136. doi: 10.5670/oceanog.2011.65

Reigstad, M., Riser, C.W., Svensen, C., 2005. Fate of copepod faecal pellets and the role of *Oithona* spp. *Mar. Ecol. Prog. Ser.* 304, 265-270. doi: 10.3354/meps304265

Reigstad, M., Riser, C.W., Wassmann, P., Ratkova, T., 2008. Vertical export of particulate organic carbon: Attenuation, composition and loss rates in the northern Barents Sea. *Deep-Sea Res. II* 55, 2308-2319. doi: 10.1016/j.dsr2.2008.05.007

Reigstad, M., Wassmann, P., 1996. Importance of advection for pelagic-benthic coupling in north Norwegian fjords. *Sarsia* 80, 245-257. doi: 10.1080/00364827.1996.10413599

Reigstad, M., Wassmann, P., 2007. Does *Phaeocystis* spp. contribute significantly to vertical export of organic carbon? *Biogeochemistry* 83, 217-234. doi: 10.1007/s10533-007-9093-3

Reigstad, M., Wassmann, P., Ratkova, T., Arashkevich, E., Pasternak, A., Øygarden, S., 2000. Comparison of the springtime vertical export of biogenic matter in three northern Norwegian fjords. *Mar. Ecol. Prog. Ser.* 201, 73-80. doi: 10.3354/meps201073

Reigstad, M., Wassmann, P., Wexels Riser, C., Øygarden, S., Rey, F., 2002. Variations in hydrography, nutrients and chlorophyll a in the marginal ice-zone and the central Barents Sea. *J. Mar. Syst.* 38, 9-29. doi: 10.1016/S0924-7963(02)00167-7

Richardson, T.L., Jackson, G.A., 2007. Small Phytoplankton and Carbon Export from the Surface Ocean. *Science* 315, 838-840. doi: 10.1126/science.1133471

Rynearson, T.A., Richardson, K., Lampitt, R.S., Sieracki, M.E., Poulton, A.J., Lyngsgaard, M.M., Perry, M.J., 2013. Major contribution of diatom resting spores to vertical flux in the sub-polar North Atlantic. *Deep-Sea Res. I* 82, 60-71. doi: 10.1016/j.dsr.2013.07.013

Sakshaug, E., Johnsen, G., Kristiansen, S., von Quillfeldt, C., Rey, F., Slagstad, D., Thingstad, F., 2009. Phytoplankton and primary production, in: Sakshaug, E., Johnsen, G., Kovacs, K. (Eds.), *Ecosystem Barents Sea*. Tapir Academic Press, Trondheim, Norway, pp. 167-208.

Sakshaug, E., Kristiansen, S., Syvertsen, E., 1991. Planktonalger, in: Sakshaug, E., Bjørge, A., Gulliksen, F., Loeng, H., Melhum, F. (Eds.), *Økosystem Barentshav*. Universitetsforlaget, Oslo.

Sakshaug, E., Slagstad, D., 1992. Sea ice and wind: Effects on primary productivity in the Barents Sea. *Atmos. Ocean* 30, 579-591.

Slagstad, D., Ellingsen, I.H., Wassmann, P., 2011. Evaluating primary and secondary production in an Arctic Ocean void of summer sea ice: An experimental simulation approach. *Prog. Oceanogr.* 90, 117-131. doi: 10.1016/j.pocean.2011.02.009

Smayda, T.J., 1970. The suspension and sinking of phytoplankton in the sea. *Oceanogr. Mar. Biol. Ann. Rev.* 8, 353-414.

Smayda, T.J., Boleyn, B.J., 1966a. Experimental Observations on the Flotation of Marine Diatoms. II. *Skeletonema costatum* and *Rhizosolenia setigera*. *Limnol. Oceanogr.* 11, 18-34. doi: 10.2307/2833219

Smayda, T.J., Boleyn, B.J., 1966b. Experimental observations on the Flotation of marine diatoms. III. *Bacteriastrum hyalinum* and *Chaetoceros lauderi*. *Limnol. Oceanogr.* 11, 35-43. doi:

Smith, R.W., Bianchi, T.S., Allison, M., Savage, C., Galy, V., 2015. High rates of organic carbon burial in fjord sediments globally. *Nat. Geosci.* 8, 450-453. doi: 10.1038/ngeo2421

Sommer, F., Stibor, H., Sommer, U., Velimirov, B., 2000. Grazing by mesozooplankton from Kiel Bright, Baltic Sea, on different sized algae and natural seston size fractions. *Mar. Ecol. Prog. Ser.* 199, 43-53.

Spall, M.A., Pickart, R.S., Brugler, E.T., Moore, G.W.K., Thomas, L., Arrigo, K.R., 2014. Role of shelfbreak upwelling in the formation of a massive under-ice bloom in the Chukchi Sea. *Deep-Sea Res. II* 105, 17-29. doi: 10.1016/j.dsr2.2014.03.017

Stemmann, L., Boss, E., 2012. Plankton and Particle Size and Packaging: From Determining Optical Properties to Driving the Biological Pump. *Annu. Rev. Mar. Sci.* 4, 263-290. doi: 10.1146/annurev-marine-120710-100853

Stemmann, L., Eloire, D., Sciandra, A., Jackson, G.A., Guidi, L., Picheral, M., Gorsky, G., 2008. Volume distribution for particles between 3.5 to 2000 μm in the upper 200 m region of the South Pacific Gyre. *Biogeosciences* 5, 299-310. doi: 10.5194/bg-5-299-2008

Stewart, G., Kirk Cochran, J., Xue, J., Lee, C., Wakeham, S.G., Armstrong, R.A., Masqué, P., Carlos Miquel, J., 2007. Exploring the connection between ^{210}Po and organic matter in the northwestern Mediterranean. *Deep-Sea Res. I* 54, 415-427. doi: 10.1016/j.dsr.2006.12.006

Stübner, E.I., Søreide, J.E., Reigstad, M., Marquardt, M., Blachowiak-Samolyk, K., 2015. Common strangers – seasonal meroplankton dynamics at high latitudes in Adventfjorden, Svalbard. (In revision in *J. Plankton Res.*)

Sugie, K., Kuma, K., 2008. Resting spore formation in the marine diatom *Thalassiosira nordenskioeldii* under iron- and nitrogen-limited conditions. *J. Plankton Res.* 30, 1245-1255. doi: 10.1093/plankt/fbn080

Sundfjord, A., Fer, I., Kasajima, Y., Svendsen, H., 2007. Observations of turbulent mixing and hydrography in the marginal ice zone of the Barents Sea. *J. Geophys. Res.-Oceans* 112, C05008. doi: 10.1029/2006JC003524

Sutherland, B.R., Barrett, K.J., Gingras, M.K., 2015. Clay settling in fresh and salt water. *Environ. Fluid. Mech.* 15, 147-160. doi: 10.1007/s10652-014-9365-0

Svensen, C., Sundfjord, A., Lavrentyev, P., Zooplankton dynamics and plankton productivity across the Barents Sea polar front in June: High contribution of small-sized copepods and protozooplankton revealed by water bottle sampling. (in prep.)

Svensen, C., Morata, N., Reigstad, M., 2014. Increased degradation of copepod faecal pellets by co-acting dinoflagellates and *Centropages hamatus*. *Mar. Ecol. Prog. Ser.* 516, 61-70. doi: 10.3354/meps10976

Svensen, C., Nejstgaard, J.C., Egge, J.K., Wassmann, P., 2002. Pulsing versus constant supply of nutrients (N, P and Si): effect on phytoplankton, mesozooplankton and vertical flux of biogenic matter. *Sci. Mar.* 66, 189-203.

Svensen, C., Wexels Riser, C., Reigstad, M., Seuthe, L., 2012. Degradation of copepod faecal pellets in the upper layer: role of microbial community and *Calanus finmarchicus*. *Mar. Ecol. Prog. Ser.* 462, 39-49. doi: 10.3354/meps09808

Syvitski, J.P.M., Murray, J.W., 1981. Particle interaction in fjord suspended sediment. *Mar. Geol.* 39, 215-242. doi: 10.1016/0025-3227(81)90073-6

Søreide, J.E., Carroll, M.L., Hop, H., Ambrose, W.G., Hegseth, E.N., Falk-Petersen, S., 2013. Sympagic-pelagic-benthic coupling in Arctic and Atlantic waters around Svalbard revealed by stable isotopic and fatty acid tracers. *Mar. Biol. Res.* 9, 831-850. doi: 10.1080/17451000.2013.775457

Søreide, J.E., Leu, E., Berge, J., Graeve, M., Falk-Petersen, S., 2010. Timing of blooms, algal food quality and *Calanus glacialis* reproduction and growth in a changing Arctic. *Glob. Change Biol.* 16, 3154-3163. doi: 10.1111/j.1365-2486.2010.02175.x

Tamelander, T., Reigstad, M., Hop, H., Ratkova, T., 2009. Ice algal assemblages and vertical export of organic matter from sea ice in the Barents Sea and Nansen Basin (Arctic Ocean). *Polar Biol.* 32, 1261-1273. doi: 10.1007/s00300-009-0622-5

Thiele, S., Fuchs, B.M., Amann, R., Iversen, M.H., 2015. Colonization in the photic zone and subsequent changes during sinking determines bacterial community composition in marine snow. *Appl. Environ. Microbiol.* 81, 1463-1471. doi: 10.1128/aem.02570-14

Thompson, R.J., Deibel, D., Redden, A.M., McKenzie, C.H., 2008. Vertical flux and fate of particulate matter in a Newfoundland fjord at sub-zero water temperatures during spring. *Mar. Ecol. Prog. Ser.* 357, 33-49. doi: 10.3354/meps07277

Thornton, D., 2002. Diatom aggregation in the sea: mechanisms and ecological implications. *Eur. J. Phycol.* 37, 149-161. doi: 10.1017/S0967026202003657

Tommasi, D., Hunt, B.P.V., Pakhomov, E.A., Mackas, D.L., 2013. Mesozooplankton community seasonal succession and its drivers: Insights from a British Columbia, Canada, fjord. *J. Mar. Sys.* 115–116, 10-32. doi: 10.1016/j.jmarsys.2013.01.005

Tremblay, C., Runge, J., Legendre, L., 1989. Grazing and sedimentation of ice algae during and immediately after a bloom at the ice-water interface. *Mar. Ecol. Prog. Ser.* 56, 291-300.

Tremblay, J.-É., Gagnon, J., 2009. The effects of irradiance and nutrient supply on the productivity of Arctic waters: a perspective on climate change, in: Nihoul, J.C.J., Kostianoy, A.G. (Eds.), *Influence of Climate Change on the Changing Arctic and Sub-Arctic Conditions*. Springer Netherlands, pp. 73-93.

Turner, J.T., 2002. Zooplankton fecal pellets, marine snow and sinking phytoplankton blooms. *Aquat. Microb. Ecol.* 27, 57-102. doi: 10.3354/ame027057

Turner, J.T., 2015. Zooplankton fecal pellets, marine snow, phytodetritus and the ocean's biological pump. *Prog. Oceanogr.* 130, 205-248. doi: 10.1016/j.pocean.2014.08.005

Turner, J.T., Ferrante, J.G., 1979. Zooplankton Fecal Pellets in Aquatic Ecosystems. *Bioscience* 29, 670-677. doi: 10.2307/1307591

Vader, A., Marquardt, M., Meshram, A.R., Gabrielsen, T.M., 2014. Key Arctic phototrophs are widespread in the polar night. *Polar Biol.*, 1-9. doi: 10.1007/s00300-014-1570-2

Waite, A.M., Safi, K.A., Hall, J.A., Nodder, S.D., 2000. Mass sedimentation of picoplankton embedded in organic aggregates. *Limnol. Oceanogr* 45, 87-97. doi: 10.4319/lo.2000.45.1.0087

Wassmann, P., 1984. Sedimentation and benthic mineralization of organic detritus in a Norwegian fjord. *Mar. Biol.* 83, 83-94. doi: 10.1007/BF00393088

Wassmann, P., Bauerfeind, E., Fortier, M., Fukuchi, M., Hargrave, B., Moran, B., Noji, T., Nöthig, E.-M., Olli, K., Peinert, R., Sasaki, H., Shevchenko, V., 2004. Particulate Organic Carbon Flux to the Arctic Ocean Sea Floor, in: Stein, R., Macdonald, R.W. (Eds.), *The Organic Carbon Cycle in the Arctic Ocean*. Springer, Berlin, Heidelberg, pp. 101-138.

Wassmann, P., Duarte, C.M., Agustí, S., Sejr, M.K., 2011. Footprints of climate change in the Arctic marine ecosystem. *Glob. Change Biol.* 17, 1235-1249. doi: 10.1111/j.1365-2486.2010.02311.x

Wassmann, P., Olli, K., Riser, C.W., Svensen, C., 2003. Ecosystem Function, Biodiversity and Vertical Flux Regulation in the Twilight Zone, in: Wefer, G., Lamy, F., Mantoura, F. (Eds.), *Marine Science Frontiers for Europe*. Springer Berlin Heidelberg, pp. 279-287.

Wassmann, P., Peinert, R., Smetacek, V., 1991. Patterns of production and sedimentation in the boreal and polar Northeast Atlantic. *Polar Res.* 10, 209-228. doi: 10.1111/j.1751-8369.1991.tb00647.x

Wassmann, P., Reigstad, M., 2011. Future Arctic Ocean seasonal ice zones and implications for pelagic-benthic coupling. *Oceanography* 24, 220-231. doi: 10.6570/oceanog.2011.74

Wassmann, P., Reigstad, M., Haug, T., Rudels, B., Carroll, M.L., Hop, H., Gabrielsen, G.W., Falk-Petersen, S., Denisenko, S.G., Arashkevich, E., Slagstad, D., Pavlova, O., 2006. Food webs and carbon flux in the Barents Sea. *Prog. Oceanogr.* 71, 232-287. doi: 10.1016/j.pocean.2006.10.003

Węsławski, J.M., Kwasniewski, S., Wiktor, J., 1991. Winter in a Svalbard fjord ecosystem. *Arctic* 44, 115-123. doi: 10.14430/arctic1527115-123

Węsławski, J.M., Szymelfenig, M., Zajączkowski, M., Keck, A., 1999. Influence of salinity and suspended matter of benthos of an Arctic tidal flat. *ICES J. Mar. Sci.* 56 Supplement, 194-202. doi:

Wexels Riser, C., 2007. Fate of zooplankton fecal pellets in marine ecosystems: export or retention?, Department of Aquatic BioSciences. Norwegian College of Fishery Science, University of Tromsø, Norway.

Wexels Riser, C., Reigstad, M., Wassmann, P., Arashkevich, E., Falk-Petersen, S., 2007. Export or retention? Copepod abundance, faecal pellet production and vertical flux in the marginal ice zone through snap shots from the northern Barents Sea. *Polar Biol.* 30, 719-730. doi: 10.1007/s00300-006-0229-z

Wexels Riser, C., Wassmann, P., Olli, K., Arashkevich, E., 2001. Production, retention and export of zooplankton faecal pellets on and off the Iberian shelf, north-west Spain. *Prog. Oceanogr.* 51, 423-441. doi: 10.1016/S0079-6611(01)00078-7

Wexels Riser, C., Wassmann, P., Reigstad, M., Seuthe, L., 2008. Vertical flux regulation by zooplankton in the northern Barents Sea during Arctic spring. *Deep-Sea Res. II* 55, 2320-2329. doi: 10.1016/j.dsr2.2008.05.006

Wiedmann, I., Reigstad, M., Sundfjord, A., Basedow, S., 2014. Potential drivers of sinking particle's size spectra and vertical flux of particulate organic carbon (POC): Turbulence, phytoplankton, and zooplankton. *J. Geophys. Res.-Oceans* 119, 6900-6917. doi: 10.1002/2013JC009754

Wirtz, K.W., 2012. Who is eating whom? Morphology and feeding type determine the size relation between planktonic predators and their ideal prey. *Mar. Ecol. Prog. Ser.* 445, 1-12. doi: 10.3354/meps09502

Yang, J., Comiso, J., Walsh, D., Krishfield, R., Honjo, S., 2004. Storm-driven mixing and potential impact on the Arctic Ocean. *J. Geophys. Res.-Oceans* 109, C04008. doi: 10.1029/2001JC001248

Zajączkowski, M., Nygård, H., Hegseth, E.N., Berge, J., 2010. Vertical flux of particulate matter in an Arctic fjord: the case of lack of the sea-ice cover in Adventfjorden 2006-2007. *Polar Biol.* 33, 223-239. doi: 10.1007/s00300-009-0699-x

Zajączkowski, M., Włodarska-Kowalczuk, M., 2007. Dynamic sedimentary environments of an Arctic glacier-fed river estuary (Adventfjorden, Svalbard). I. Flux, deposition, and sediment dynamics. *Estuar. Coastal Shelf S.* 74, 285-296. doi: 10.1016/j.ecss.2007.04.015

Zeitschel, B., Diekmann, P., Uhlmann, L., 1978. A New Multisample Sediment Trap. *Mar. Biol.* 45, 285-288. doi:

Årthun, M., Eldevik, T., Smedsrud, L.H., Skagseth, Ø., Ingvaldsen, R.B., 2012. Quantifying the Influence of Atlantic Heat on Barents Sea Ice Variability and Retreat. *J. Clim.* 25, 4736-4743. doi: 10.1175/JCLI-D-11-00466.1

Paper I

Wiedmann I, Reigstad M, Sundfjord A, Basedow S

Potential drivers of sinking particle's size spectra and vertical flux of particulate organic carbon (POC): Turbulence, phytoplankton and zooplankton.

Journal of Geophysical Research: Oceans, 2014, 119: 6900-6917

AGU PUBLICATIONS

JGR

Journal of Geophysical Research: Oceans

RESEARCH ARTICLE

10.1002/2013JC009754

Key Points:
- Postbloom scenario can provide a high export of particulate organic carbon
- Enhanced carbon export can be driven by flux of particles <1.0 mm
- Fecal pellet fragments can be important for the downward carbon flux

Correspondence to:
I. Wiedmann,
Ingrid.wiedmann@uit.no

Citation:
Wiedmann, I., M. Reigstad, A. Sundfjord, and S. Basedow (2014), Potential drivers of sinking particle's size spectra and vertical flux of particulate organic carbon (POC): Turbulence, phytoplankton, and zooplankton, *J. Geophys. Res. Oceans*, *119*, doi:10.1002/2013JC009754.

Received 20 DEC 2013
Accepted 18 SEP 2014
Accepted article online 22 SEP 2014

This is an open access article under the terms of the Creative Commons Attribution-NonCommercial-NoDerivatives License, which permits use and distribution in any medium, provided the original work is properly cited, the use is non-commercial and no modifications or adaptations are made.

Potential drivers of sinking particle's size spectra and vertical flux of particulate organic carbon (POC): Turbulence, phytoplankton, and zooplankton

Ingrid Wiedmann[1], Marit Reigstad[1], Arild Sundfjord[2], and Sünnje Basedow[3]

[1]Department of Arctic and Marine Biology, UiT The Arctic University of Norway, Breivika, Tromsø, Norway, [2]Norwegian Polar Institute, Framsenteret, Tromsø, Norway, [3]University of Nordland, Bodø, Norway

Abstract Phytoplankton spring blooms in temperate and high-latitude shelf seas are commonly associated with an enhanced particulate organic carbon (POC) export of aggregates from the euphotic zone. In contrast, a postbloom situation is usually linked to a predominant POC retention, where small cells (<10 μm) and strong grazing pressure prevail. This study aimed to examine impacts of turbulence, phytoplankton, bloom stage, and zooplankton abundance on the sinking particles' size spectra and POC flux to improve the understanding of the downward flux mechanisms in the upper 100 m. We deployed sediment traps, partly modified with gel jars, at four depths along a stratification and phytoplankton bloom gradient in the Barents Sea, an Arctic shelf sea. The highest POC export (60 m: 923 mg C m^{-2} d^{-1}) was found in deep-mixed, postbloom Atlantic influenced waters, despite the high grazer abundance (12,000 individuals m^{-3}). Particle size spectra indicated that this flux was dominated by particles of 0.05–1.00 mm equivalent spherical diameter (ESD_{image}) with a POC:volume ratio matching copepod fecal pellets. Large particles (0.5–2.8 mm ESD_{image}) dominated the flux at a stratified, late peak bloom station in Arctic Waters and a stratified, late bloom situation at the Polar Front, but with lower POC:volume ratio and POC flux (60 m: <823 mg C m^{-2} d^{-1}). Accordingly, a high POC flux at the base of the euphotic zone is not necessarily driven by large phytoplankton aggregates, but can also occur during a postbloom situation in form of small fecal pellet fragments with high POC content.

1. Introduction

The export of particulate organic carbon (POC) in temperate and high-latitude shelf seas tends to fluctuate between (1) a strong carbon export, often associated with e.g., diatom blooms, and (2) a prevailing POC retention with small cells (<10 μm) and a major carbon recycling through the microbial loop [*Wassmann*, 1998; *Tamigneaux et al*., 1999]. Several studies indicate that a future warming and freshening of these seas will increase the importance of picoplankton [*Li et al*., 2009; *Morán et al*., 2010]. These investigations further propose that a change in community size structure may also alter the export and retention of POC in the water column. It is therefore important to focus on mechanisms and regulation of the vertical particle flux in contrasting phases, as this forms the basis for understanding consequences for the biological carbon pump in a future ocean.

An enhanced POC export is typically observed during a phytoplankton bloom [*Wassmann*, 1998]. A mismatch of intensely growing autotrophic algae and grazing by herbivore zooplankton causes first an accumulation of biomass in the euphotic zone, followed by an enhanced vertical POC flux to deeper layers. Phytoplankton can either sink in form of single cells (e.g., diatom resting spores) or as aggregates, formed by coagulation of sticky cells [*McCave*, 1984; *Smetacek*, 1985; *Alldredge*, 2001]. Zooplankton like copepods and krill contribute to the enhanced POC flux by grazing on small organic particles and producing large, fast-sinking fecal pellets [*McCave*, 1984; *Hamm et al*., 2001]. In contrast, a retention dominated system is usually linked to a postbloom situation [*Wassmann*, 1998]. Small primary producers and microzooplankton have been identified as central actors in this system [*Gifford et al*., 1995; *Møller et al*., 2006; *Hodal and Kristiansen*, 2008]. Due to the high carbon overturn, POC is here rather recycled in the pelagic food web than exported to depth.

Though the concept of a fluctuation between an export and retention dominated system is largely accepted, recent studies indicate that the link "large particles—export" (respectively, "small particles—retention") may not be representative for all pelagic systems at all times.

© 2014. The Authors.

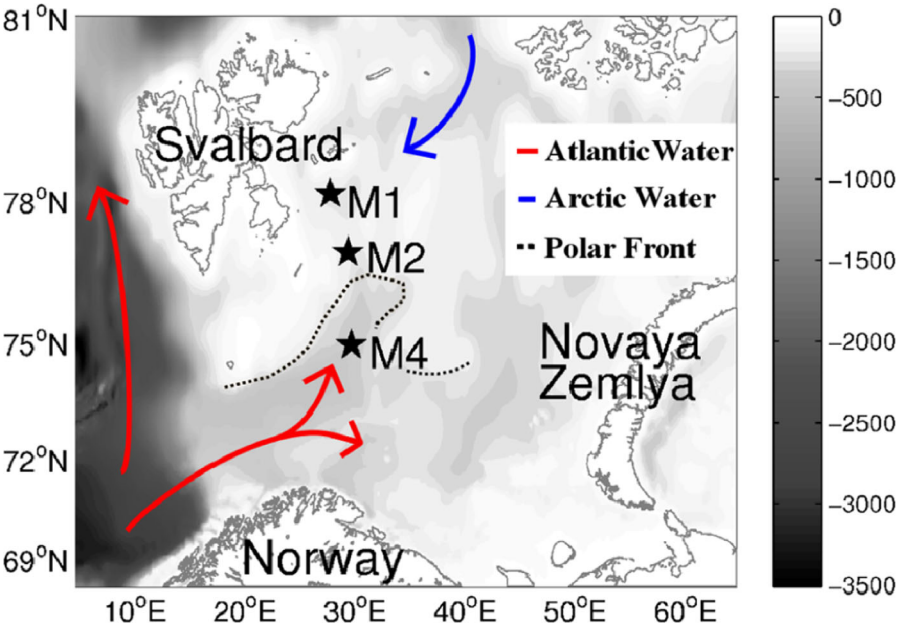

Figure 1. Sampling localities in the Barents Sea (bathymetry is given in gray shades, see color bar for depths in meters).

McDonnell and Buesseler [2010] suggested, for example, that small particles (equivalent spherical diameter, ESD: ~0.07–0.12 mm) can have a high sinking velocity, while medium-sized ones (ESD: ~0.12–0.50 mm) can sink slower. Ballasting effects have been suggested to play a major role for the downward flux [e.g., *Iversen et al*., 2010]. Further, it has also been put forward that cells of all sizes (even picoplankton) might contribute to the vertical carbon flux [*Richardson and Jackson*, 2007]. The present study was therefore designed to reconsider the link between particles sizes and intensity of the POC flux in the upper 100 m (zone of the strongest attenuation of sinking organic material) under contrasting hydrographical scenarios, spring bloom stages and grazer abundances by conducting sampling along a north-south transect in the Barents Sea (BS).

This Arctic shelf sea is surrounded by Norway, Svalbard, Franz Josef Land, and Novaya Zemlya (70–80°N; 15–60°E, Figure 1). It has a mean depth of 230 m and is a well-suited model area with contrasting water masses. Cold Arctic Water (<0°C, 34.3–34.8 salinity) enters the BS from the northeast, while the inflow of comparably warm and saline Atlantic Water (>3°C, >35.0 salinity) takes place at the southwestern opening, resulting in the formation of the Polar Front [*Loeng*, 1991; *Loeng et al*., 1997]. Sea ice is locally formed north of the Polar Front during winter and reaches its maximum extension in March to May. As ice-melting sets in, the marginal ice zone (MIZ) gradually retreats north and eastward, and the ice-free areas become stratified by a strong halocline. The resulting shallow mixed layer, the increased irradiance level, and the high nutrient concentrations facilitate phytoplankton blooms in the MIZ, resulting in an enhanced vertical carbon export before planktonic grazers become abundant [*Olli et al*., 2002]. Waters in the southwestern BS are permanently ice-free. Episodic strong winds from passing Polar Lows cause deep mixing (>30 m) until early summer [*Slagstad and Støle-Hansen*, 1991; *Ingvaldsen and Loeng*, 2009]. This partly counteracts the development of the spring bloom, but compared to the MIZ, the ice-free, Atlantic influenced waters have higher irradiance levels, promoting an early start of the primary production in the southwestern BS [*Wassmann et al*., 1991]. A peak bloom situation may thus still facilitate an enhanced POC export in the northern, Arctic influenced part of the BS, while a retention dominated, postbloom situation with an effective carbon grazing and recycling may already prevail in the southern, Atlantic part.

Sampling along a north-south transect in the BS thus gives insight into contrasting hydrographical situations and bloom scenarios within a short distance (late peak bloom in stratified waters versus postbloom in deep-mixed waters). We collected samples at representative stations in the Arctic part, the Polar Front, and the Atlantic part of the BS to quantify the hydrographical conditions, small-scale water shear, vertical diffusivity, and suspended biomass in the upper 100 m. Also, we determined the particle size spectra of sinking particles (>0.05 mm equivalent spherical diameter, ESD_{image}) collected by short-term sediment traps

© 2014. The Authors.

Table 1. Station Identity (Incl. Ice Cover) and Sampling Schedule for Suspended Material[a]

Station	Position	Date	Depth (m)	Ice Cover	Water Sampling (UTC)	Depth of Water Samples (m)
M1	78.0973°N, 28.1258°E	22 Jun 2011	278	Very open drift ice (30%)	16:15	1, 5, 10, 20, 30, 31, 40, 50, 60, 90, 120, 200
M2	76.9493°N, 29.7117°E	24 Jun 2011	235	Very open drift ice (20%)	07:46	1, 5, 10, 20, 30, 40, 44, 50, 60, 90, 120, 200
M4	74.9107°N, 30.0033°E	27 Jun 2011	371	Open water	09:11	1, 5, 10, 20, 30, 40, 45, 50, 60, 90, 120, 200

[a]Water samples analyzed for particulate organic carbon (POC), total chlorophyll *a* >0.7 μm (Chl *a*) and Chl *a* >10 μm.

modified with gel jars (30, 40, 60, and 90 m). Based on these results, we addressed the questions (1) how do turbulence, prevailing phytoplankton taxa, and zooplankton abundance (used as approximation for the grazing pressure) influence the size spectra of the sinking particles and the vertical POC flux, and (2) if a high POC flux of material >0.7 μm is always associated with a bloom scenario characterized by large sinking particles (>0.5 mm) like diatom aggregates, marine snow, or fecal pellets.

2. Materials and Methods

Sampling was conducted on board the ice-enforced R/V "Helmer Hanssen" between 22 and 27 June 2011. We followed the 30°E longitude in the Barents Sea from north to south and sampled at three drift stations referred to as M1 (78°N), M2 (77°N), and M4 (75°N) (Figure 1 and Table 1). The stations were chosen as representative locations for well-stratified Arctic Water masses (M1), the Polar Front (M2), and deep-mixed Atlantic waters (M4) based on a northward high resolution CTD transect prior to station work (S. Basedow et al., unpublished data, 2012).

2.1. Hydrography, Small-Scale Current Shear, and Diffusivity

A standard sampling program on the hydrography was conducted at each of the three stations. Vertical profiles of temperature and salinity from surface to bottom were measured using a CTD-F (Sea-Bird 911*plus*). The CTD data were processed and bin averaged to 0.5 m using Sea-Bird's standard software package. Sea ice conditions were visually estimated using the scale of the Norwegian Meteorological Institute (11 categories from ice-free to fast ice) and recorded in the ship log.

Profiles of small-scale current shear and hydrography microstructure were measured with a loosely tethered turbulence dropsonde MSS-90L, equipped with a pair of PNS06 shear probes [*Prandke and Stips*, 1998]. The sets of three profiles were collected approximately every 4 h during each drift station. After processing of each set, mean profiles cover the depth range from 8 to >100 m. In this paper, the sets of microstructure profiles, which were taken closest in time to the deployment of each of the sediment traps with gel jars, are presented (Table 2). The microstructure data were processed as described in *Sundfjord et al.* [2007], but had a lower dissipation noise threshold due to use of a longer-bodied profiler and more optimal fall speed. Dissipation ε (W kg^{-1}), vertical shear rate S (s^{-1}), and diffusivity K (m^2 s^{-1}) were calculated and bin averaged to 0.5 m:

$$\varepsilon = 7.5\nu \left(\partial u'/\partial z\right)^2 \quad (1)$$

Table 2. Sampling Schedule of the Sediment Traps (Partly Modified With Gel Jars, Denoted as "Gel Trap")[a] and the LOPC Profiles[b]

Station	Deployment Trap Array (Start Time in UTC)	Deployment Time Trap Array (d^{-1})	Gel Trap Sampling Depths (m)	Exported POC Analyzed (m)	Exported Chl *a* Analyzed (m)	Deployment Turbulence Dropsonde (Start in UTC)	Deployment LOPC (Start Time in UTC)	Number of LOPC Profiles
M1	22 Jun 2011, 15:40	0.22	30, 40, 60, 90	30, 40, 60	30, 40, 60	18:52	14:23	5
M2	24 Jun 2011, 09:00	0.19	30, 40, 60, 90	30, 40, 60	30, 40, 60	10:44	18:19	10
M4	27 Jun 2011, 10:40	0.17	30, 40, 60, 90	30, 40, 60		13:37	13:09	10

[a]Chlorophyll *a* (Chl *a*) samples from M4 were lost.
[b]For zooplankton biomass determination.

© 2014. The Authors.

[*Yamazaki and Osborn*, 1990], where v is the temperature dependent viscosity of seawater and $\partial u'/\partial z$ is shear resolved at cm scales (with u' representing horizontal velocity variation and z depth)

$$S=\sqrt{\varepsilon/v} \tag{2}$$

[*Hebert and de Bruyn Kops*, 2006], and

$$K=\Gamma\varepsilon/N^2 \tag{3}$$

[*Osborn*, 1980], where N is the Brunt-Väisälä buoyancy frequency and Γ is the dissipation ratio, which is set to a typical value of 0.2 [*Moum*, 1996].

2.2. Suspended Biomass (Chlorophyll *a*, Dominant Phytoplankton Taxa, POC, PON)

A vertical profile of suspended biomass was collected at each sampling station at 12 depths between surface and 200 m by Niskin bottles attached to a sampling rosette (Table 1). On board the ship, the sampled water was gently transferred into carboys and stored cool and dark until filtration within few hours. Size-fractionated suspended chlorophyll *a* (Chl *a*) concentrations were determined from subsamples. Triplicates (50–200 mL) from each sampling depth were vacuum-filtered on (1) Whatman GF/F filters for the total Chl *a* ($>$0.7 μm) concentration and on (2) Whatman Nucleopore membrane filters (10 μm) for the Chl *a* size fraction $>$10 μm. Extraction of Chl *a* was subsequently conducted in 5 mL methanol for 12 h at room temperature in darkness before measuring the Chl *a* concentration using a Turner Design 10-AU fluorometer (calibrated with Chl *a*, Sigma C6144) before and after adding two drops of 5% HCl [*Holm-Hansen and Riemann*, 1978]. A 100 mL subsample of the suspended water sample was fixated with 2% glutaraldehyde lugol for phytoplankton cell counts. From the Chl *a* maximum, the most dominant species were determined by counting at least 400 cells in a 50 mL sedimentation chamber after 25 h of sedimentation [*Utermöhl*, 1931].

Triplicate subsamples (200 mL) were filtered on precombusted Whatman GF/F filters to determine the concentration of suspended particulate organic carbon (POC) and nitrogen (PON). We removed larger organisms such as copepods before freezing the filters at -20°C. Within 6 months after the cruise the filters were exposed to fumes of concentrated HCl for 24 h (removal of inorganic carbon) prior to analysis on a Leeman Lab CHN Elemental Analyzer [for details see *Reigstad et al*., 2008].

2.3. Zooplankton Abundance

Distribution and abundance of zooplankton grazers in the water column were assessed by a laser optical plankton counter (LOPC; Rolls Royce Canada Ltd.) that was mounted on a frame together with a second CTD-F (CTD: SBE19plusV2, Seabird Inc., F: Wetlabs ECO FL fluorescence sensor). The LOPC was deployed several times at each station, and here we present data from the sampling closest in time to the deployment of the sediment traps (Table 2). At M1 and M4, the LOPC was deployed in close temporal proximity, but at M2 9 h lay between both deployments (Table 2).

During the LOPC samplings, 5–10 vertical profiles from bottom to surface were obtained at each station (Table 2). The LOPC counts particles flowing through its channel and registers their size and transparency twice per second [*Herman et al*., 2004]. Based on the LOPC data, zooplankton abundance was calculated and binned into 15 m depth intervals as described in *Gaardsted et al*. [2010] and *Basedow et al*. [2013]. To exclude transparent, carnivorous zooplankton such as hydrozoans and chaetognaths, and all possible aggregates, we limited our analyses to single element particles (SEPs) and more opaque multiple element particles (MEPs) (attenuation index $>$0.4) [see *Checkley et al*., 2008; *Basedow et al*., 2013] in the size range of 0.63–2.00 mm ESD (equivalent spherical diameter).

At the Polar Front in the Barents Sea, these plankton particles typically consist of *Calanus* spp. CI-CVI, older stages of *Pseudocalanus* spp. and some individuals of *Metridia* sp. [*Basedow et al*., 2014, and references therein].

2.4. Vertical Flux of Chlorophyll *a*, POC and Particles (0.050–1.139 mm)

A semi-Lagrangian drifting sediment trap array was deployed at the three sampling stations for 4–5 h (Table 2). It was anchored to a free-drifting ice floe at M1 and M2, while it was drifting in the open waters at M4. Paired sediment traps (outer diameter 72 mm, length 450 mm, KC Denmark) were arranged at sampling depths of 30, 40, 60, and 90 m to measure the vertical POC and particle flux in the vertical zone of the highest attenuation in POC export (below the euphotic zone, Table 3). Following the conceptual idea of

© 2014. The Authors.

Table 3. Hydrophysical and Biological Characterization of the Sampling Stations M1, M2, and M4[a]

Station ID	M1	M2	M4
Water mass	Arctic	Polar Front	Atlantic
PC type	Halocline	Halocline	Thermocline
PC interval (m)	7–23	14–21	35–38
Density across PC (kg m^{-3})	0.96	1.19	0.15
Maximal Brunt-Väisälä frequency N (s^{-1})	0.034	0.054	0.025
Mixing depth (diffusivity $>10^{-4}$ m^2 s^{-1})	13.0 m	17.0 m	25.5 m
Euphotic zone (1% light, 430 nm)	65 m	54 m	45 m
Nutricline ($\leq$1 μM Nitrat + Nitrit)	<20 m	<30 m	<30 m
Chl *a* max depth (m)	40	44	45
Chl *a* max concentration (μg L^{-1})	4.38	1.42	1.6
Dominant suspended phytoplankton taxa at Chl *a* max (cells L^{-1})			
Thalassiosira spp.	265,000	3700	
Chaetoceros spp.	156,800	30,500	4050
Phaeocystis pouchetii	107,280	274,000[b]	1,810,090[c]
Bloom stage	Late peak bloom	Late bloom	Postbloom

[a]PC, pycnocline and Chl *a* max, chlorophyll *a* maximum.
[b]Average colony size 1.3 cells.
[c]Almost exclusively single cells.

Lundsgaard et al. [1999] and *Ebersbach and Trull* [2008], one of the two sediment cylinders at each sampling trap was used to determine POC and Chl *a* flux (in the following called "sediment trap"). The content of these traps was transferred into carboys right after recovery and subsampled for Chl *a* >0.7 μm, Chl *a* >10 μm, and POC. Samples were treated and analyzed as described above for the suspended water samples. The other trap cylinder at each sampling depth was equipped with a gel jar, allowing for sampling and analysis of particle size composition of sinking material (in the following called "gel trap").

Previous to deployment of the trap array in the lower euphotic zone and below it, the gel traps with Tissue-Tec® gel (Sakura Finetek Europe B.V., Netherlands) were prepared according to procedures developed by Iversen (M. H. Iversen, personal communication, 2010). Duran glass cups without spout (ø 70 mm) were filled with ca. 5 mm gel and frozen (−20°C). These cups, exactly fitting into the trap cylinder, were placed in the traps right before deployment and covered with GF/F filtered bottom water from the deployment area to allow gentle defrosting of the water soluble gel. Prefiltered (GF/F) bottom water (without fixation) was also added to the sediment traps to balance the weight of the water filled gel trap. Deployment time of 4–5 h was chosen to prevent an overload of particles in the gel traps. After recovery, the gel traps were stored dark and cold for 0.5–2 h to allow particles to sink into the gel. The overstanding water in the trap cylinder was then gently siphoned out with a silicone hose (ø 3 mm) and a 3 mL plastic pipette, but the last millimeter of water was left on the gel to prevent unintentional removal of particles. Gel jars were immediately frozen (−20°C) for later photography and image analysis ashore. Between January 2012 and June 2012, the 12 gel jars were defrosted one by one at room temperature and stored in the fridge until handling within 7 days. A preliminary test showed that storage in the fridge for a few days caused no significant decay in particle abundance and size (data not shown). The complete surface of each gel sample was photographed using a stereo microscope (15X magnification, Zeiss Discovery.V20) with an AxioCam ERc 5s digital camera (5 megapixels). Due to small changes in gel thickness and different light reflections, not all images were taken under the exact same light conditions, but a similar illumination was assured. The resulting 150–200 images (resolution 0.431 pixels/ μm) were combined into 20–25 mosaic image using the plugin MosaicJ [*Thévenaz and Unser*, 2007] in Fiji [*Schindelin et al.*, 2012]. Images were manually inspected and particles that were included in two mosaics, light reflections, bubbles in the gel, and copepods were removed. In this way, major errors were eliminated, but the amount of particles (1000–13,000 particles per glass jar) made it impossible to inspect every particle for, e.g., overlays with other particles. A minor bias must therefore be assumed. Image analysis was conducted using 8-bit gray values converted pictures. The threshold to distinguish particles from the background was determined manually for each gel jar to correct for the slight differences in the pictures' brightness. Applying the "plot profile" function of ImageJ (Figure 2), we determined an intermediate value between the maximum gray value in particles and the average of the background value by eyeballing and tested then the chosen values on several images for its ability to distinguish between particle and background noise. Threshold values for all images

© 2014. The Authors.

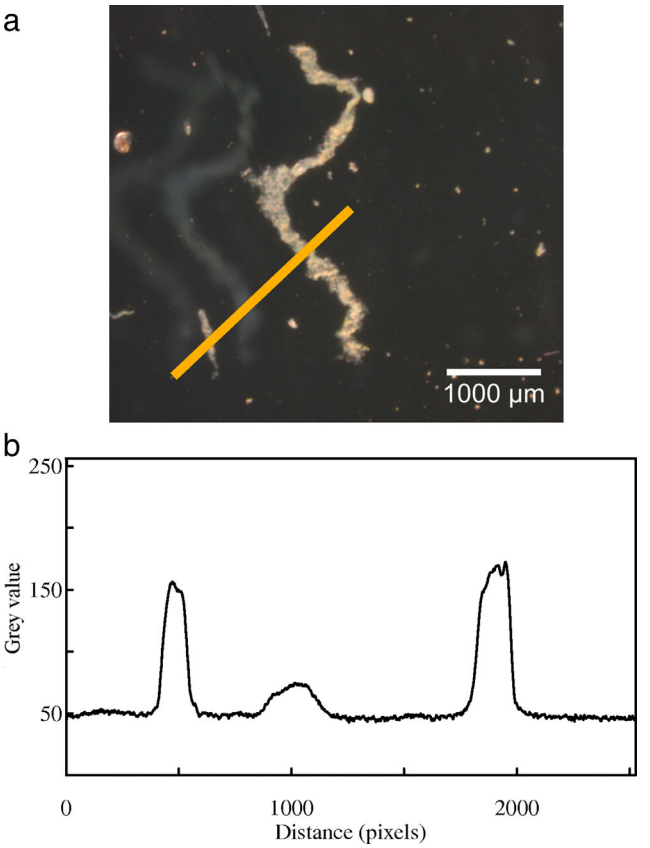

Figure 2. Binary pictures were produced after determining the gray value threshold between particle and background by the plot profile function of ImageJ. (a) Detail image from one gel jar with a krill fecal pellet. (b) Gray values along the yellow line (image (a)), starting at the lower left side, ending at the upper right side.

were between a gray value of 75 and 100. Based on the threshold value, the pictures were converted into binary images and the 2-D area of all particles extracted. The estimated spherical diameter was then calculated from the area of each particle. However, the ESD of particles extracted from images differs from the ESD that is estimated by the LOPC (based on light absorbance), and is more similar to the occluded diameter that can be computed for particles counted by the LOPC [*Checkley et al*., 2008]. To stress the difference between the two estimates, in the following we call the ESD estimated from images for ESD_{image}, in contrast to the ESD estimated by the LOPC. Since the abundance of the smallest particles in the images is underestimated due to their low spectral reflectance, the lower limit of included particles was set to 0.05 mm ESD_{image} following the methods described in *Jackson et al*. [1997, 2005]. Particles within the accepted size limit were logarithmically binned according to their ESD_{image} (Table 4) [following *Jackson and Checkley*, 2011]. An upper limit of the bins was chosen to be $\sqrt[3]{2} \approx 1.26$ times of the lower bin limit. We included all particles in the following analysis, since very large particles can—despite being very rare—contribute considerably to the volume flux. Particle spectra were calculated following *Jackson and Burd* [1998] to allow a comparison with other data. The volume of sinking particles was, however, computed using an ellipsoidal volume calculation, since most of the particles had this form. The third axis was here chosen to be equal with the minor axis of an ellipsis fitted to the 2-D image the fitting function of ImageJ. Volume flux was then calculated as the sum of the ellipsoidal particle volume in each bin, normalized with the sampling time, the trap cylinder opening and the bin width (to make the results comparable with other studies) and then multiplied by the bin mean (Table 4) to make the area under the curve (Figure 8) proportional to the total flux.

Table 4. Particle Bin Sizes Used in the Analyses and Particle Size Classification

Bin	Bin Mean ESD_{image}[a]	Classification
1	0.057	Small Particles
2	0.071	
3	0.090	
4	0.113	Medium-Sized Particles
5	0.142	
6	0.180	
7	0.226	
8	0.285	
9	0.359	
10	0.452	
11	0.570	Large Particles
12	0.718	
13	0.904	
14	1.139	
15	1.435	Very Large (Rare) Particles
16	1.808	
17	2.279	
18	2.870	

[a]ESD, equivalent spherical diameter in millimeter.

© 2014. The Authors.

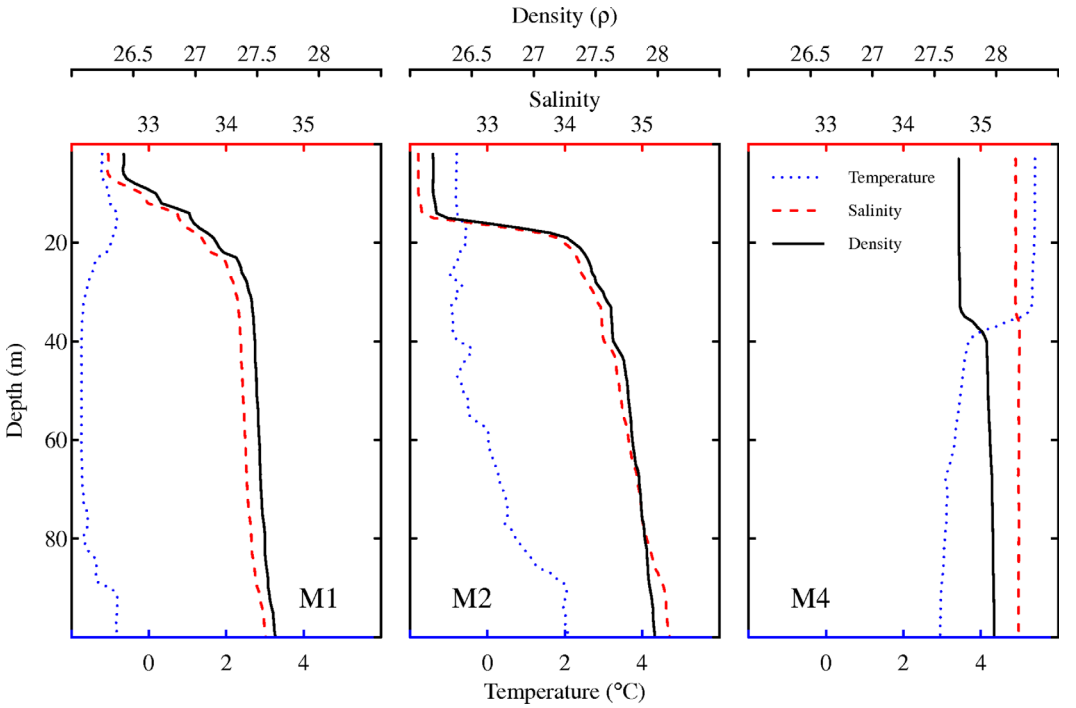

Figure 3. Hydrographical situation at the sampling station at (left) M1, (center) M2, and (right) M4.

Volume flux (used in the POC flux: volume flux ratio, Figure 9) was in contrast computed as the total ellipsoidal volume per bin, normalized for deployment time and sediment trap cylinder opening.

3. Results

3.1. Hydrography, Small-Scale Shear Rate, and Diffusivity Profiles

The three sampling stations in the Barents Sea (BS) differed in terms of hydrography, shear rate distribution, and vertical mixing. Very open drift ice (around 30% coverage, Table 1) was encountered at M1, the northernmost station. Water temperature was $<0^{\circ}$C throughout the upper 100 m (Figure 3), and the well-mixed surface meltwater layer (upper 5 m, salinity $\sim$32.9) was separated by a staircase-like halocline (7–23 m) from intermediate salinity water of Arctic origin (salinity 34.0–34.4 between 25 and 100 m, Figure 3). We will therefore refer to the subsurface water masses at M1 as "Arctic Water." Shear rate at 8–100 m was $<2.8\ s^{-1}$ (Figure 4a), which has been described to be the threshold fragmenting the majority of diatom aggregates [*Alldredge et al*., 1990]. Vertical diffusivity (K) was enhanced in the uppermost 13.0 m compared to the typical background values in deeper layers (for station intercomparison we delimited the "background diffusivity" to $<10^{-4}\ m^2\ s^{-1}$) (Figure 4b and Table 3). In the following, this zone is referred to as mixing layer, since it is actively mixed by turbulence [*Brainerd and Gregg*, 1995].

Station M2 was located in the central BS and also characterized by very open drift ice (20% coverage, Table 1). Water temperature was below 0°C in the uppermost 60 m, but increasing to 2°C at 90 m (Figure 3). A melt water layer (salinity 32.6) in the upper 15 m was separated by a strong halocline between 15 and 20 m (Table 3) from the deeper slightly warmer, intermediate saline water of Atlantic origin (salinity 35.0 at 100 m). This layering is typically observed in the Polar Front, and this station will be referred to accordingly in the following. Shear rate exceeded $2.8\ s^{-1}$ above 11 m (Figure 4a), the mixing layer depth was found in the uppermost 17.0 m characterized by a $K > 10^{-4}\ m^2\ s^{-1}$ (Figure 4b and Table 3).

At the southernmost station, M4 no seasonal sea ice was found. Water temperature was 5.4°C in the uppermost 35 m, but decreased to $\sim$3.0°C below. Salinity was very stable (35.1) down to 100 m and the station was therefore only weakly stratified, primarily by a thermocline at 35–40 m (Figure 3 and Table 3). This station was strongly influenced by Atlantic Water throughout the water column and showed a beginning summer

© 2014. The Authors.

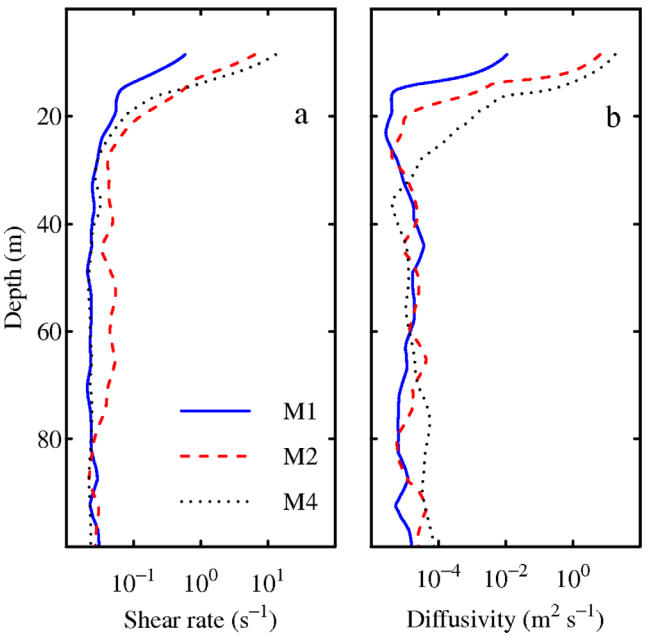

Figure 4. (a) Shear rate and (b) diffusivity in the upper 100 m at station M1 (blue, line), M2 (red, dashed), and M4 (black, stippled).

stratification due to warming of the upper water layers. It is therefore referred to as "Atlantic station" [*Loeng*, 1991]. Shear rate was >2.8 s^{-1} in the 12 m top layer (Figure 4a), while the actively mixing layer with $K > 10^{-4}$ m^2 s^{-1} reached down to 25.5 m (Figure 4b and Table 3).

3.2. Suspended Chlorophyll *a*, Phytoplankton Community, POC, and POC:PON Ratio

Different stages of the phytoplankton spring bloom were encountered at the three stations.

At M1 in Arctic Water, we found a distinct chlorophyll *a* maximum (Chl *a* max, 4.38 μg Chl *a* L^{-1}, Figure 5) at 40 m. It was dominated by large phytoplankton cells (>10 μm, mainly diatom genera *Thalassiosira* and *Chaetoceros*, Table 3). Single cells or small colonies (4–5 cells) of the flagellate *Phaeocystis pouchetii* ($\sim$5 μm diameter) were, however, also present (Table 3). The suspended particulate organic carbon (POC) followed the depth distribution of Chl *a* and peaked at 40 m (494 mg C m^{-3}, Figure 5). This suggests that the POC consisted to a great extent of autotrophic cells. The POC:PON ratio of 8.2 (atomic ratio, a:a, average of the upper 40 m) is higher than the Redfield ratio of 6.6 and points toward partly regenerated organic material above the Chl *a* max. Values of >17 at 90 m are too high to indicate degraded marine material [*Andreassen et al.*, 1996]. Instead, resuspended or terrestrial material from ice

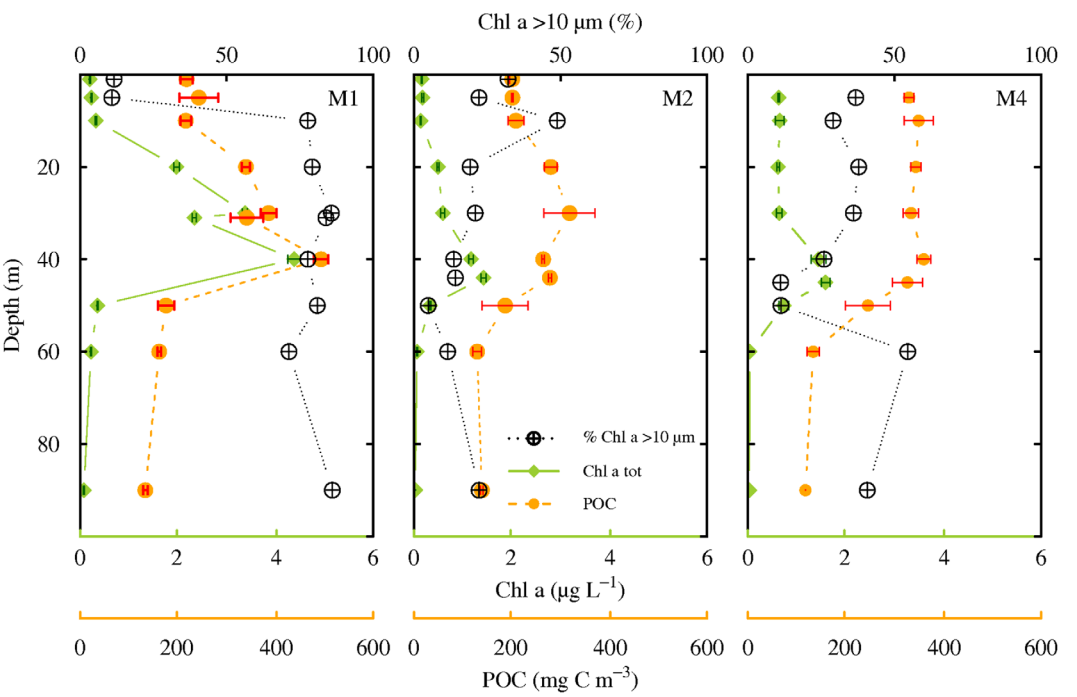

Figure 5. Suspended particulate organic carbon (POC, orange), suspended chlorophyll *a* (Chl *a*, green) and abundance of larger phytoplankton cells (Chl *a* >10 μm in % of total Chl *a*, black) in the upper 90 m at the sampling stations (left) M1, (center) M2, and (right) M4.

© 2014. The Authors.

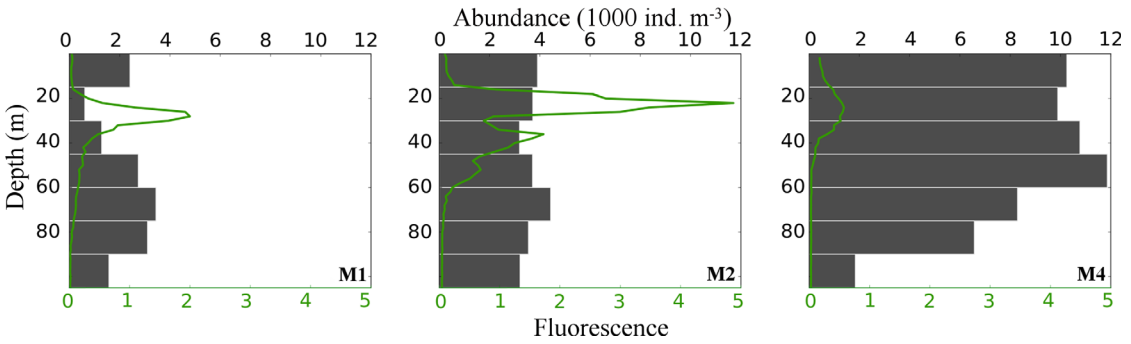

Figure 6. Zooplankton abundance (0.63–2.00 mm ESD, gray bars) in the upper 100 m at (left) M1, (center) M2, and (right) M4, obtained from 5 to 10 profiles of a laser optical plankton counter, and fluorescence depth profile (green line) from a CTD-F, vertically deployed together.

melting or vertical advection must be assumed. Taking into account the nutricline at <20 m (Table 3), the depth of the subsurface Chl *a* max and its concentration as well as the dominance of large diatoms, we classified this station to be in a late peak bloom stage (Table 3).

At station M2 in the Polar Front, the Chl *a* max was located slightly deeper and less distinct than at M2 (44 m: 1.42 μg L^{-1}, Figure 5). Single cells and few small colonies (up to eight cells) of *P. pouchetii* dominated and large cells made up only 20–50% of the autotrophic biomass. The concentration of suspended POC peaked at 30 m (318 mg C m^{-3}, Figure 5). A POC:PON ratio of 8.6 (a:a average of the uppermost 44 m) indicated a similar degradation of organic material down to the Chl *a* maximum at M2 compared to M1. Due to the deeper nutricline (<30 m), a subsurface Chl *a* max at 44 m with lower concentration and a higher abundance of small cells, M2 was suggested to be in a later bloom stage than M1. Since spring bloom diatoms were still present (Table 3), M2 was categorized as "late bloom", though the situation in the Polar Front was highly patchy and dynamic as indicated by variability of the Chl *a* depth distribution and the fluorescence measurements taken with the CTD-F, mounted on the same frame as the LOPC (S. Basedow, unpublished data, 2012).

The Chl *a* concentration at M4 was similar to M2, and peaked at 45 m (1.59 μg L^{-1}, Figure 5). The phytoplankton community however consisted almost exclusively of *P. pouchetii* single cells (Table 3). The suspended POC showed a relatively constant concentration of ~300 mg C m^{-3} down to 45 m, before dropping to 120–130 mg C m^{-3}. An POC:PON a:a ratio of 7.7 (average down to 45 m) indicates less degraded organic material above the Chl *a* max, than at deeper layers (POC:PON >11.7 at ≥60 m) and the other sampling stations. M4 was in terms of nutricline depth (above 30 m), Chl *a* max depth, POC concentration, and POC:PON rather similar to M2, but the observed deep-mixing made a biological characterization difficult. Since, however, very few diatoms were observed, the dominant species *P. pouchetii* was accompanied by unidentified flagellates, lower fluorescence values were found, and the zooplankton community was at a later stage (C. Svensen, personal communication, 2012) compared to M1 and M2 (Figure 6), we considered M4 to be in a postbloom stage.

3.3. Zooplankton Abundance and Vertical Distribution

Throughout the LOPC sampling at the three stations, we observed a large temporal variability in the vertical zooplankton distribution (S. Basedow, unpublished data, 2012). Here we present data from the LOPC profiles carried out closest in time to the deployment of the sediment traps (Table 2). We limited the profiles to the upper 105 m, to convey the situation in zooplankton abundance and distribution that could have influenced the POC and particle flux into the sediment traps by grazing. Lowest abundances of zooplankton were observed at the Arctic station M1, intermediate abundances at the M2 in the Polar Front, and very high abundances of up to 12,000 individuals m^{-3} at the Atlantic station M4 (Figure 6). At all stations, grazing zooplankton (0.63–2 mm ESD) was distributed relatively evenly in the upper 105 m. No relationship between the depth of the Chl *a* maximum (Figure 5) or the fluorescence maximum (Figure 6) and the vertical distribution of zooplankton could be observed.

3.4. Vertical Flux of Chlorophyll *a*, POC, and the POC:PON Ratio of Sinking Material

The Chl *a* and POC flux as well as the atomic (a:a) ratio POC:PON of sinking material was determined from the sediment traps. At M1, we measured a downward flux of ~3.4 mg Chl *a* m^{-2} d^{-1} at both 30 and 40 m, and a lower flux at 60 m (1.99 mg Chl *a* m^{-2} d^{-1}, Table 5). Similarly to the Chl *a* flux, more POC was sinking

© 2014. The Authors.

Table 5. Downward Fluxes of Chl *a* and POC[a], the POC:PON (Atomic Ratio) of the Exported Material, Average Particle Size of Sinking Particles, and Semiquantitative Abundance of the Most Abundant Particles Types Found in Gel Jars Deployed at M1, M2, and M4[b]

	Depth (m)	Chl *a* (mg m^{-2} d^{-1})	POC ± SD (mg C m^{-2} d^{-1})	POC:PON ± SD	Average Size (ESD_{image}, mm)	Diatom Colonies	FP (Krill) (10^3 m^{-2} d^{-1})	FP (Copepod)	Other	Copepods
M1	30	3.36	856.2 ± 67.5	9.2 ± 0.4	0.094	++	7	*	+	*
	40	3.39	813.8 ± 29.9	9.5 ± 0.1	0.113	++	23	+		*
	60	1.99	628.7 ± 24.9	9.1 ± 0.6	0.107	+	**28**	+		*
	90				0.104	+	**17**	++		
M2	30	0.98	748.6 ± 37.5	8.7 ± 0.4	0.111	*	9	*	+	*
	40	1.89	832.2 ± 32.5	9.1 ± 0.4	0.114	+	**21**	+		*
	60	1.36	823.8 ± 54.7	9.5 ± 0.2	0.117	*	**19**	+	+	+
	90				0.119	*	**26**	+	+	*
M4	30		1431.0 ± 108.7	7.0 ± 0.3	0.083		*	*	+	+
	40		1847.4 ± 169.7	6.2 ± 0.3	0.086	*	0	++	++	++
	60		927.2 ± 99.6	7.5 ± 0.6	0.091		*	++	++	++
	90				0.104	+	**36**	*	++	*

[a]POC and PON concentration at 90 m are lacking.

[b]ESD, equivalent spherical diameter in millimeter; FP, fecal pellets; ++, many; +, few; *, present; dominant particle group for each depth in bold. The category "other" holds sinking particles which could not be clearly classified (detritus, different phytoplankton and zooplankton). The category "copepods" gives the number of copepods found per gel jar (maximum 60 individuals per gel jar in M4, 40 m).

out at 30 and 40 m (856.2 and 813.8 mg C m^{-2} d^{-1}, respectively) compared to 60 m (628.7 mg C m^{-2} d^{-1}, Table 5) at M1. The POC:PON ratio was comparable at all three depths (9.1–9.5, Table 5), indicating the outsinking of degraded marine material. At M2 less Chl *a* sank out compared to M1 (0.98–1.89 mg Chl *a* m^{-2} d^{-1}, Table 5), though the downward POC flux with a peak at 40 m (832.2 mg C m^{-2} d^{-1}, Table 5) was similar at both stations. Also, the POC:PON ratio was in the same range (8.7–9.5) at M1 and M2. In contrast, a much higher POC flux was observed at the deep-mixed Atlantic station M4. The POC flux for M4 at 30 and 40 m was more than twice as high as at the other stations (1431 and 1847 mg C m^{-2} d^{-1}, Table 5). The flux at 60 m was, however, <30% greater at M4 than at M1 and M2. The POC:PON ratio of 6.2–7.5 was consistent with the Redfield ratio of 6.6, suggesting a downward flux of relatively fresh and high quality organic material relative to the more northern stations.

3.5. Numbers and Size-Spectra of Exported Particles

A qualitative assessment of the gel jars indicates that composition of sinking particles differed at M1, M2, and M4 (exemplified by mosaic images from 60 m, Figure 7). Based on the image analyses, we conclude small particles were most important for the vertical flux at the Atlantic station (average over all depths 0.091 mm ESD_{image}, Table 5). At M2 in the Polar Front the size of sinking particles was on average largest (ESD 0.115 mm, Table 5). At both stations, the size increased with depth. Particles from the Arctic station were of intermediate size (ESD 0.104 mm, Table 5), and though they became larger between 30 and 40 m, size decreased down to 90 m. Adding all depth, the number of exported particles was lowest at M2 (167×10^6 particles), intermediate at M4 (450×10^6 particles), and highest at M1 (533×10^6 particles). Also, small particles (0.05–0.1 mm ESD_{image}, Table 4) were at all sampling depths more abundant than large ones (0.50–1.14 mm ESD_{image}, Figure 8).

The highest number of particles per sampling depth was found in the gel jar deployed at 40 m at station M4 (2.61×10^6 particles m^{-2} d^{-1}). Small and medium-sized particles were more abundant at 40 m than 30 m at this station, but their numbers decreased again at 60 m. Large and extralarge particles were rare (1–4 particles per gel jar) at these three depths, but large particles were more frequently observed at 90 m (Figure 8e). In the gel jar deployed at 30 m at M1, we found the second highest number of particles (2.25×10^6 particles m^{-2} d^{-1}). At this station, small and medium-sized particles (0.05–0.50 mm ESD_{image}, Table 4) became less abundant with depth (Figure 8a), while large particles (0.50–1.14 mm ESD_{image}, Table 4) were most abundant at 40 and 60 m (Figure 8a). At M2, we found fewest particles at 30 m while most were observed at 40 m (Figure 8c).

The volume of exported particles is reflected by the area under the curve in the volume flux spectra (Figures 8b, 8d, and 8f). All spectra demonstrate that small particles contributed little to the volume export at the three sampling stations, despite their high abundance. In contrast, large and extralarge particles explained most of the downward volume flux. The highest volume fluxes were found at 40 m at M1 and M2 (Figures 8b and 8d). Due to the low magnification (15X) in the image analysis, only a semiquantitative particle identification was achievable, but a higher magnification would have enhanced the problem of choosing the level of

© 2014. The Authors.

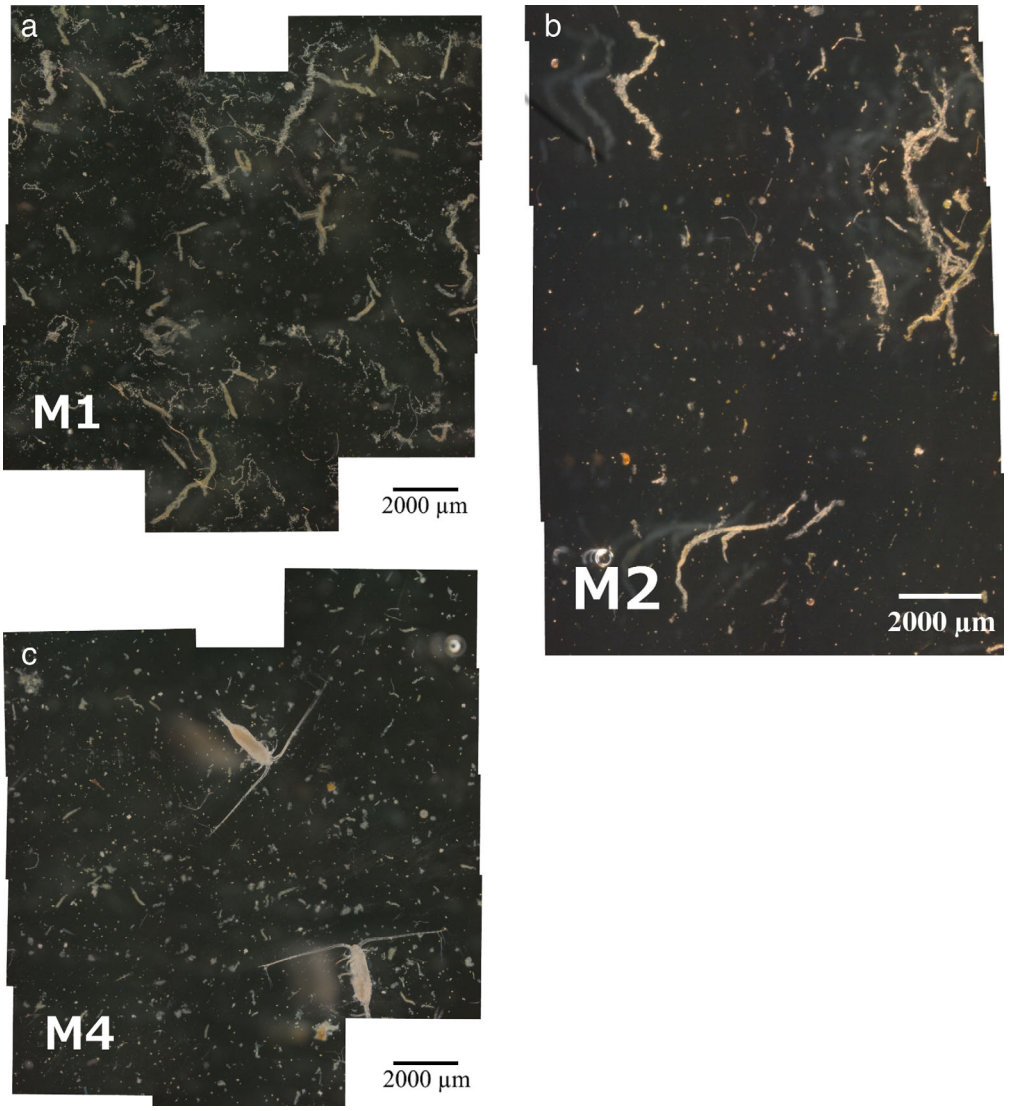

Figure 7. Qualitative support for the observations at station (a) M1, (b) M2, and (c) M4. Note that copepods and nauplii (in M4) were removed before the image analysis was conducted.

focus in the gel. Accordingly, we can state that mainly diatom colonies were exported at 30 and 40 m at station M1, while krill and copepod fecal pellets dominated at 60 and 90 m (Table 5). Krill pellets fragments were enumerated (23–93 per gel jar, corresponding with up to 7–27 $\times$ 10^3 pellet fragments m^{-2} d^{-1}, Table 5). Since krill pellets are filiform, without defined tips and easily break apart [*Wexels Riser et al*., 2007], the fragments vary in size. They can therefore not be used as defined fecal pellet units corresponding to a defined volume flux.

The low particle abundance at 30 m at M2 resulted also in a low volume flux. It was difficult to identify the small and medium-sized particles exported here, consisting mainly of fecal pellets and fine detritus (Table 5). At the other sampling depths at M2 large krill fecal pellets and diatom colonies dominated.

Gel jars deployed at M4 (30, 40, and 60 m) contained mainly small unidentifiable particles, assumingly detritus, as well as several benthic larvae. In addition, we found a remarkably high number of copepods (up to 60 individuals) in the 40 and 60 m gel jar (Table 5). Since only 1–2 individuals were found per glass jar at most other sampling depths, and individuals fallen into the gel were not able to continue grazing due to the high gel viscosity, we do not regard the short-term sediment traps with gel jar we used as generally more attractive to copepods. Small unidentified particles and krill fecal pellets dominated in the 90 m jar at M4 (36 $\times$ 10^3 pellets m^{-2} d^{-1}, Table 5).

© 2014. The Authors.

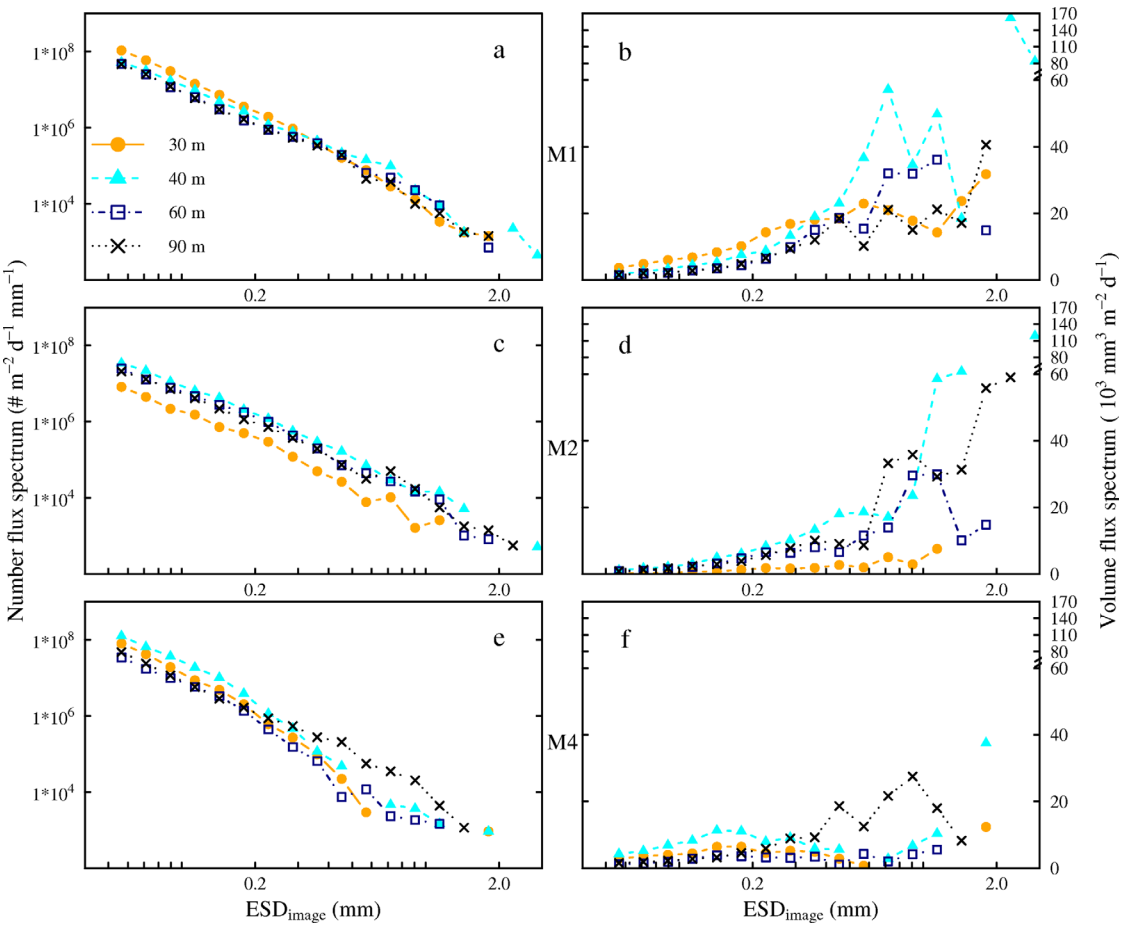

Figure 8. (Left) Number size spectra and (right) computed volume flux spectrum of particles collected in the gel traps at 30, 40, 60, and 90 m (top: M1, middle: M2, bottom: M4). Note that the broken *y* axis in the right column.

4. Discussion

In the present study, we investigated the vertical fluxes and characteristics of sinking particles in the central Barents Sea (BS) along a north-south transect from Arctic Water, crossing the Polar Front, to Atlantic Water. Along this track, we expected to meet contrasting situations with respect to hydrography, small-scale turbulence, vertical mixing, phytoplankton spring bloom stage, zooplankton abundance, and vertical export rates of particulate organic carbon (POC). We anticipated that there would be a (late) peak spring bloom and a high POC flux at station M1 in the stratified Arctic Water, an "intermediate stage" spring bloom and POC flux at M2 in the Polar Front, and strong POC retention in the Atlantic deep-mixed, postbloom waters at M4. Surprisingly, the POC export at 60 m was ~30% higher at M4 in Atlantic Water compared to the flux at station M1 in Arctic Water (930 versus 630 mg C m^{-2} d^{-1}) even if large and extralarge sinking particles (0.5–2.8 mm equivalent spherical diameter, ESD_{image}, Table 4) were extremely rare down to 60 m at M4.

To explore the impact of physical and biological processes on the size spectra of sinking particles and the POC flux, we evaluate the role of small-scale turbulence, phytoplankton and zooplankton abundance on the particle size spectra and then discuss if a high POC flux is always associated with large sinking particles (>0.5 mm ESD_{image}) like diatom aggregates, marine snow, and krill fecal pellets.

4.1. Influence of Small-Scale Shear Rate and Diffusivity on the Particle Size Spectra and the POC Flux

Small-scale shear rates in the range of 0.02–13.11 s^{-1} were calculated for the upper 100 m at the three sampling stations (Figure 4a) and the maximum rates computed in our study somewhat exceeded previously reported shear rates for the inner ocean and estuaries (10^{-7}–10 s^{-1}) [*Kiørboe et al.*, 1990, and citations therein].

An enhanced shear rate is commonly assumed to facilitate the coagulation of particles into larger, usually faster sinking aggregates by increasing the collision rate of suspended particles [*McCave*, 1984; *Jackson*, 1990].

© 2014. The Authors.

However, the shear rate in the uppermost 11–12 m of station M2 and M4 was $>2.8\ s^{-1}$ (corresponding to an energy dissipation rate $>0.001\ m^2\ s^{-3}$) exceeded a threshold, which has been suggested to fragment the majority of diatom aggregates [*Alldredge et al*., 1990]. This indicates that particle aggregation was not promoted in the surface layer at M2 and M4. At the deeper chlorophyll *a* maximum (Chl *a* max) depths, the shear rates were however $\leq 0.035\ s^{-1}$ at all three sampling stations, resulting in a theoretical particle maximum size of $\leq$5 mm ESD_{image} [*Jackson*, 1990]. Particles in all deployed gel traps had ESD_{image} <3.2 mm, and were well below this upper theoretical size limit.

We conclude that shear rates at station M1 at all depths were in a range facilitating formation of larger particles. Diatoms, which are known to excrete a natural "glue" for particle formation [*Alldredge*, 2001], were also abundant here (Table 3) and may have promoted particle aggregation further. In contrast, the formation of larger particles may have been limited by the high shear rate in the uppermost 10 m at M2 and M4. This is however not assumed to have a strong effect on particle aggregation, since the Chl *a* max, the zone of highest biomass, particle abundance and accordingly particle aggregation, was located well below this layer of high shear rate (Figure 4a and Table 3).

The vertical diffusivity (*K*) indicates a mixing layer of 13.0, 17.0 m, and 25.5 m at M1, M2, and M4, respectively. This means that enhanced, surface-driven vertical mixing reached considerably deeper (>10 m) at the sampling station in Atlantic Water compared to the stations in Arctic Water or the Polar Front. A deeper mixing at M4 may enhance the sinking speed, with consequently reduced exposure time for degradation processes to take place [*Svensen et al*., 2012], and can help explain the high POC flux and the presence of rather fresh material down to 60 m at this station (Table 5, POC:PON ratio of exported material of 6.2–7.5 compared to the Redfield ratio of 6.6).

4.2. Flux of Autotrophic Biomass in Form of Small and Large Particles

The concentrations of suspended Chl *a* at the deep chlorophyll maximum were highest in the late peak bloom situation at M1 and lowest during the late bloom station at M2 (Figure 5 and Table 3). This may contradict our bloom classification into M1 "late peak bloom," M2 "late bloom," M4 "postbloom" at the first sight, but frequent LOPC deployments at M2 indicated a high short-time variability in the relative pigment distribution fluorescence measurements especially in the Polar Front. During six deployments at station M2 (within 30 h), the fluorescence peak changed from >500 to <100 (relative units) (S. Basedow, unpublished data, 2012). A direct comparison between Niskin-bottle based Chl *a* concentrations and the closest in time fluorescence from LOPC profiling was therefore not feasible (Figures 5 and 6, linear regression, $R^2 = 0.2–0.3$). Instead, this reflects the previously reported strong spatial variability in the Polar Front [*Våge*, 2010], and indicates the importance of including not only Chl *a* concentrations, but also hydrography, euphotic depth, nutricline, and the zooplankton composition in the bloom stage characterization as it was done in the present study.

At the Arctic Water station M1, we found a high number of particles <0.05 mm ESD_{image} in the 30 m gel trap. These particles were not included in the image analysis due to underestimation concerns for particles this small (see section 2) and we could not identify them visually in the jars. The high Chl *a* export at this sampling depth at M1 (Table 5) however suggests the export of autotrophs. *Thalassiosira* single cells (10–50 μm diameter) [*Hasle and Syvertsen*, 1997] or short chains were highly abundant in the sediment traps deployed for 24 h during the present cruise (M. Reigstad et al., unpublished data, 2012) and it is likely that this genus was also abundant in the gel jars. Diatoms and their resting spores have previously been described to sink with velocities of $>10\ m\ d^{-1}$ [*Smayda*, 1970] and they represented one of the most abundant particle groups in gel traps deployed along the Antarctic Peninsula [*McDonnell and Buesseler*, 2010]. Despite the unquestionable importance of large particles in the downward mass transport, we argue accordingly that it is important to keep in mind that also particles <0.05 mm ESD_{image} do sink and can contribute to the vertical export, especially if their density is high enough or if the particles are ballasted [*Iversen et al*., 2010].

In terms of mass flux, sinking diatom aggregates are much more important than single cells. They form an important vehicle of POC export and they were highly abundant in the gel jar deployed at 40 m at M1 (Table 5). The genera *Chaetoceros* and *Thalassiosira* dominated the suspended phytoplankton sample taken at this station (Table 3) and were also found in the 24 h deployed sediment traps (M. Reigstad et al., unpublished data, 2012). We suggest accordingly that they contributed to aggregate formation at M1, especially since some species in these genera are known to have potentially sticky cells or produce adhesive extracellular substances [*Kiørboe*

© 2014. The Authors.

and Hansen, 1993; *Hansen and Kiørboe*, 1997], the natural "glue" in aggregate formation [*Alldredge*, 2001]. However, even if the particle spectra from M1 indicate a shift from many small particles at 30 m (0.05–0.1 mm ESD_{image}) to a majority of particles >0.9 mm ESD_{image} at 40 m, our data cannot confirm that this was solely due to aggregate formation. Also cell growth and increasing length of chains may have contributed to enhanced particle size.

Phaeocystis pouchetii single cells (5 μm) and small colonies clearly dominated the Chl *a* max at station M4 (45 m: $>1.8 \times 10^6$ suspended cells L^{-1}). This cell number exceeded the total phytoplankton cell abundance at the other stations by more than one order of magnitude. Based on the high cell number, a substantial cell collision rate and a potentially high aggregate formation may have been anticipated. Conversely, *P. pouchetii* has been shown to have low stickiness [*Passow and Wassmann*, 1994] and cell counts from the sediment traps deployed for 24 h during the present cruise (M. Reigstad et al., unpublished data, 2012), indicate that mainly single cells or small colonies were sinking out at 60 m. This may contradict previous results that cells <5 μm ESD are too small to sink [*Legendre and Rivkin*, 2002]. However, at M4, we also observed vertical mixing down to 35–38 m (Table 3), and assumed that this mixing enhanced the vertical transport of *P. pouchetii* cells down to the mixed depth. As phytoplankton grows mainly in the illuminated upper water layers, deep mixing can contribute to the distribution of biomass also deeper layers (with initially lower cell concentrations) and may then result in a greater contribution of phytoplankton cells to the higher carbon flux. *Olli et al.* [2002] and *Reigstad and Wassmann* [2007] described this previously, when *P. pouchetii* single cells were exported in substantial amounts (60–200 mg C m^{-2} d^{-1}) to >90 m.

4.3. Potential Impact of Zooplankton on the Particle Size Spectrum

Zooplankton can influence the size spectrum of sinking particles and the vertical POC flux in various ways: They can (1) generally reduce the number of particles due to grazing, (2) contribute to the formation of larger particles (fecal pellets) by repackaging small food particles into fecal pellets, and (3) modify the particle size spectra toward smaller particles due to fragmentation of both fecal pellets and aggregates [*Wexels Riser et al.*, 2007]. Data from the LOPC indicate that abundances of grazers in the size range of 0.63–2.00 mm ESD (different stages of *Calanus* spp.) reached up to 12,000 individuals m^{-3} at M4 in Atlantic Water (Figure 6). We can therefore assume that the effect of zooplankton was strongest at M4.

The combined approach of particle size spectra (Figure 8) and the semiquantitative analysis of the material in the gel jars (Table 5) also showed that copepod fecal pellets (FP) were frequently sinking out at 40 and 60 m at M4 (Table 5 and Figure 8f: particles 0.10–0.35 mm ESD_{image} in the volume flux spectra match *Calanus* spp. FP sizes [*Wexels Riser et al.*, 2002]). This indicates that the comparable low Chl *a* concentrations at M4 with a prevailing phytoplankton community of <10 μm (Figure 5) could sustain a considerable zooplankton population with a high FP production that provided an important vehicle for vertical carbon flux in this postbloom situation. The great amount of unidentifiable detritus at M4 may also origin from FP, but being modified to smaller particles through fragmentation. The copepod species, *Calanus finmarchicus*, abundant at M4 (C. Svensen, personal communication, 2012) has been shown to impact the particle size spectra through unintended fragmentation of FP while feeding [*Svensen et al.*, 2012].

In addition, krill pellets fragments were abundant at most sampling depths at M1 and M2, as well as 90 m at M4 (Table 5), matching previous findings from the region [*Wexels Riser et al.*, 2002] and confirming, that krill pellets form, besides diatom aggregates and copepod pellets, an important pathway of downward carbon flux. Since krill pellets however easily break apart when being produced, the number of pellets and pellet fragments does not give a good approximation to the actual biomass sinking out.

Grazing has been described to take place associated with thin layers of enhanced particle abundance [*Möller et al.*, 2012], often formed at strong density gradients [*Alldredge et al.*, 2002; *Prairie et al.*, 2013]. Prior to the sampling, we therefore assumed that a strong vertical gradient in particle size spectra resulting from thin layer distribution of grazers, modifying the particle composition, would be detected by the high vertical resolution of sediment traps. Our LOPC data did however indicate a rather even zooplankton distribution in the upper 90 m at all three stations, neither associated with a density gradient or layers of high autotrophic biomass, which could serve as preferred feeding sites (Figure 6). Neither did we see a strong vertical shift in particle size spectra. Furthermore, no evidence for a synchronized diurnal vertical migration (DVM) could be identified during the sampling period (S. Basedow, unpublished data, 2012), supporting previous observations from the Arctic summer with 24 h of day light [*Blachowiak-Samolyk et al.*, 2006; *Wexels Riser et al.*, 2007]. The particle modification by zooplankton therefore seemed to take place over a wide vertical zone, and this distribution could be

© 2014. The Authors.

expected to increase the attenuation and reduce vertical flux. Still, the POC flux was high at 60 m on the M4 station.

4.4. Linking the Downward Flux of POC and Particles >0.05 mm ESD_{image}

The POC fluxes measured during the present study (30–90 m: 630–1850 mg C m^{-2} d^{-1}) match previously reported values from the upper 200 m of the central BS during spring (<2000 mg C m^{-2} d^{-1}) [*Olli et al*., 2002; *Reigstad et al*., 2008]. It was however unexpected that the POC flux in the 4–5 h deployed traps of the present study (60 m: 628–927 mg C m^{-2} d^{-1}) exceeded the export measured in the subsequently deployed 24 h sediment traps (60 m: 208–322 mg C m^{-2} d^{-1}) (M. Reigstad et al., unpublished data, 2012). *Lampitt et al*. [1993] reported a strong diurnal variability in the marine snow abundance, and suggested variation in the diel production and export to cause it. An analogous reason may have contributed to the variability in the POC flux in our results. Despite no DVM was observed, there may be diurnal variability in feeding activity influencing the flux. *Juul-Pedersen et al*. [2006] stated that a deployment time of 6 or 24 h did not change the results of the measured carbon flux significantly in a Greenlandic fjord. Since the 24 h deployments of the traps used in the present study have previously been calibrated through comparison with thorium-based flux measurements in the Barents Sea and found good [*Coppola et al*., 2002], we suggest further investigation of the potential diurnal flux variability.

The deployment of the gel jars revealed that a high particle number flux (up to 10^9 particles m^{-2} d^{-1} mm^{-1}) takes place in the Arctic, Polar Front, and Atlantic part of the BS. These fluxes exceed the number of particles found in studies conducted in the Southern Ocean by up to 3 orders of magnitude [*Ebersbach and Trull*, 2008; *McDonnell and Buesseler*, 2010; *Ebersbach et al*., 2011]. In addition particles <0.05 mm ESD_{image} were highly abundant in our gel traps deployed in the BS, while *Ebersbach and Trull* [2008] excluded particles <0.15 mm ESD since they were infrequently observed. These results may hint toward major differences in particle flux in the two ecosystems [present study: uppermost 90 m on productive Arctic shelf, *Ebersbach and Trull*, 2008; *Ebersbach et al*., 2011: 100–439 m in the open Southern Ocean off Kerguelen Island and Tasmania], the sampling period [present study: early European summer, *Ebersbach and Trull*, 2008; *Ebersbach et al*., 2011: late Austral summer] methodological differences like gel type [present study: Tissue tec gel®, *Ebersbach and Trull*, 2008; *Ebersbach et al*., 2011: acrylamide], trap aspect ratio [present study: 6.4, *Ebersbach and Trull*, 2008; *Ebersbach et al*., 2011: 5], or a combination of different factors.

Previous to our study, we anticipated a higher POC export at the late peak bloom station M1 in Arctic Water compared to the late bloom at M2 in the Polar Front and the postbloom at M4 in Atlantic Water. A high suspended biomass of diatoms during the (late) peak bloom (M1) was expected to result in an enhanced export of large aggregates, while the postbloom scenario (M4) was supposed to have a high carbon turn over and a prevailing POC retention [*Wassmann*, 1998]. However, our results indicate a higher POC flux in the well-mixed Atlantic part compared to the Arctic part or the Polar Front. High flux combined with weak stratification has previously been described from this area during spring and summer [*Olli et al*., 2002; *Reigstad et al*., 2008]. It was surprising to find this high POC export combined with the, on average, smallest particles at M4 (Table 5). Large and extralarge particles were here very rare compared to M1 and M2. However, when a POC: volume ratio is calculated from all sampling depths (Figure 9), it becomes obvious, that sinking particles at M4 had a higher POC: volume content than particles at M1 and at most depths at M2. The ratios calculated for M4 are

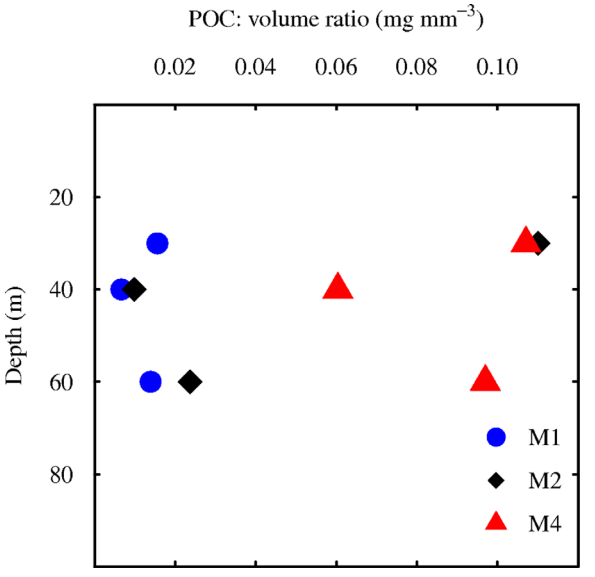

Figure 9. Average POC:volume ratio of the particles found in the gel traps. Note: No POC samples were available for 90 m and sample M2, 30 m contained very few particles, which makes the result probably biased.

© 2014. The Authors.

Table 6. Literature Values on the Carbon Conversion Factor (mg C mm^{-3}) of Diatom Aggregates and Different Fecal Pellet Types

Reference	Carbon Conversion Factor (mg C mm^{-3})	Particle Type
Alldredge [1998]	0.0001–0.003	Diatom aggregates
Wexels Riser et al. [2007]	0.045	Euphausiid fecal pellets
Riebesell et al. [1995]	0.0694	Copepod fecal pellets
Reigstad et al. [2005]	0.0803	*Calanus finmarchicus* fecal pellet
Wexels Riser et al. [2007]	0.0943	*Calanus glacialis* fecal pellet

comparable with fecal pellet carbon: volume ratios, and suggest the downward flux was of copepod fecal pellet origin (Table 6). Those from M1 and 40 and 60 m samples from M2 correspond in contrast to the carbon:volume ratios described for diatom aggregates [*Alldredge*, 1998].

Since these signals are also in agreement with the semiquantitative observations from the gel jars, we suggest that the high abundance of copepods and their repackaging of material into fecal pellets played a major role in enhancing the flux at station M4 compared to M1 and M2, despite that the fecal material was partly fragmented, probably resulting in reduced sinking rates.

5. Conclusion

Enhanced POC export is often linked to a late (peak) bloom situation and strong downward flux of large, fast-sinking particles like phytoplankton aggregates, marine snow, and zooplankton fecal pellets [*Riebesell*, 1991; *Alldredge*, 2001]. The results from the sediment traps (partly modified with gel jars) deployed in the Arctic influenced part of the Barents Sea (BS) confirm this (POC, 60 m: 629 mg C m^{-2} d^{-1}). However, our study also indicate that an even higher vertical POC export (60 m: 927 mg C m^{-2} d^{-1}) took place in at the deep-mixed, postbloom sampling station in the Atlantic influenced part of the BS. Here many small and medium-sized particles (0.05–0.5 mm ESD_{image}) were observed down to 60 m, while larger ones were rare. Coagulation into larger particles appeared to play a minor role in this case, due to the low stickiness of the most abundant phytoplankton taxon *Phaeocystis pouchetii*, but the producing fast-sinking fecal pellets obviously enhanced the vertical transport substantially, despite a high degree of fragmentation, resulting in a small average particle size.

We argue accordingly that the general concept of associating large, fast-sinking particles of phytoplankton origin with an export dominated system during the late peak bloom or late bloom phase contrasting small, slow-sinking particles with a postbloom retention dominated system, is not valid at all instances: we observed that an enhanced POC export can not only take place in form of diatom aggregates during the late bloom, but also in a deeper mixed, postbloom situation dominated by *Phaeocystis pouchetii*. This scenario co-occurred with a substantial zooplankton community. The flux was mainly characterized by small and medium-sized particles (0.05–0.5 mm ESD_{image}), and the POC:volume ratio matched fecal pellets. Zooplankton modification is therefore a likely driver of this high flux.

By including not only the POC flux, but also the size of sinking particles, the obtained, highly variable POC:-volume ratio may help identifying the source and mechanisms driving the downward flux of organic material. Understanding the mechanisms and attenuation of flux better, and including this into ecosystem- and carbon flux models, will improve predictions of future vertical carbon flux resulting from changing climate and the resulting pelagic ecosystem, where both the phytoplankton and zooplankton communities may change.

Acknowledgments
The authors would like to thank the captain and the crew of the R/V "Helmer Hanssen" for practical assistance during the fieldwork and C. Svensen, C. Wexels Riser, and S. Øygaarden for a helping hand during the filtration aboard and the CHN analysis. The detailed comments of two anonymous reviewers were highly appreciated and improved the paper substantially. The conducted work was part of the CONFLUX project, funded by Tromsø Forskningsstiftelse and Sundfjord's participation was also funded by the Centre for Ice, Climate, and Ecosystems (ICE) at the Norwegian Polar Institute.

References

Alldredge, A. (1998), The carbon, nitrogen and mass content of marine snow as a function of aggregate size, *Deep Sea Res., Part I*, *45*(4–5), 529–541, doi:10.1016/S0967-0637(97)00048-4.

Alldredge, A. (2001), Particle aggregation dynamics, in *Encyclopedia of Ocean Sciences*, edited by J. H. Steele, S. A. Thorpe, and K. K. Turekian, pp. 2090–2097, Academic, San Diego, Calif., doi:10.1006/rwos.2001.0468.

Alldredge, A. L., T. C. Granata, T. D. Gotschalk, and T. D. Dickey (1990), The physical strength of marine snow and its implications for particle disaggregation in the ocean, *Limnol. Oceanogr.*, *35*(7), 1415–1428, doi:10.4319/lo.1990.35.7.1415.

Alldredge, A. L., T. J. Cowles, S. MacIntyre, J. E. B. Rines, P. L. Donaghey, Ch. F. Greenlaw, D. V. Holliday, M. M. Dekshenieks, J. M. Sullivan, and J. R. V. Zaneveld (2002), Occurrence and mechanisms of formation of a dramatic thin layer of marine snow in a shallow Pacific fjord, *Mar. Ecol. Prog. Ser.*, *233*, 1–12, doi:10.3354/meps233001.

Andreassen, I., E. Nöthig, and P. Wassmann (1996), Vertical particle flux on the shelf off northern Spitsbergen, Norway, *Mar. Ecol. Prog. Ser.*, *137*, 215–228, doi:10.3354/meps137215.

Basedow, S. L., K. S. Tande, M. F. Norrbin, and S. A. Kristiansen (2013), Capturing quantitative zooplankton information in the sea: Performance test of laser optical plankton counter and video plankton recorder in a *Calanus finmarchicus* dominated summer situation, *Prog. Oceanogr.*, *108*, 72–80, doi:10.1016/j.pocean.2012.10.005.

© 2014. The Authors.

Basedow, S. L., M. Zhou, and K. S. Tande (2014), Secondary production at the Polar Front, Barents Sea, August 2007, *J. Mar. Syst.*, *130*, 147–159, doi:10.1016/j.jmarsys.2013.07.015.

Blachowiak-Samolyk, K., S. Kwasniewski, K. Richardson, K. Dmoch, E. Hansen, H. Hop, S. Falk-Petersen, and L. T. Mouritsen (2006), Arctic zooplankton do not perform diel vertical migration (DVM) during periods of midnight sun, *Mar. Ecol. Prog. Ser.*, *308*, 101–116, doi:10.3354/meps308101.

Brainerd, K. E., and M. C. Gregg (1995), Surface mixed and mixing layer depths, *Deep Sea Res., Part I*, *42*(9), 1521–1543, doi:10.1016/0967-0637(95)00068-H.

Checkley, D. M., Jr., R. E. Davis, A. W. Herman, G. A. Jackson, B. Beanlands, and L. A. Regier (2008), Assessing plankton and other particles in situ with the SOLOPC, *Limnol. Oceanogr.*, *53*(5, part 2), 2123–2136, doi:10.4319/lo.2008.53.5_part_2.2123.

Coppola, L., M. Roy-Barman, P. Wassmann, S. Mulsow, and C. Jeandel (2002), Calibration of sediment traps and particulate organic carbon export using 234Th in the Barents Sea, *Mar. Chem.*, *80*(1), 11–26, doi:10.1016/S0304-4203(02)00071-3.

Ebersbach, F., and T. W. Trull (2008), Sinking particle properties from polyacrylamide gels during the Kerguelen Ocean and Plateau compared Study (KEOPS): Zooplankton control of carbon export in an area of persistent natural iron inputs in the Southern Ocean, *Limnol. Oceanogr.*, *53*(1), 212–224, doi:10.2307/40006162.

Ebersbach, F., T. W. Trull, D. M. Davies, and S. G. Bray (2011), Controls on mesopelagic particle fluxes in the Sub-Antarctic and Polar Frontal Zones in the Southern Ocean south of Australia in summer—Perspectives from free-drifting sediment traps, *Deep Sea Res., Part II*, *58*(21–22), 2260–2276, doi:10.1016/j.dsr2.2011.05.025.

Gaardsted, F., K. S. Tande, and S. L. Basedow (2010), Measuring copepod abundance in deep-water winter habitats in the NE Norwegian Sea: Intercomparison of results from laser optical plankton counter and multinet, *Fish. Oceanogr.*, *19*(6), 480–492, doi:10.1111/j.1365-2419.2010.00558.x.

Gifford, D. J., L. M. Fessenden, P. R. Garrahan, and E. Martin (1995), Grazing by microzooplankton and mesozooplankton in the high-latitude North Atlantic Ocean: Spring versus summer dynamics, *J. Geophys. Res.*, *100*(C4), 6665–6675, doi:10.1029/94JC00983.

Hamm, C., M. Reigstad, C. W. Riser, A. Mühlebach, and P. Wassmann (2001), On the trophic fate of *Phaeocystis pouchetii*. VII. Sterols and fatty acids reveal sedimentation of *P. pouchetii*-derived organic matter via krill fecal strings, *Mar. Ecol. Prog. Ser.*, *209*, 55–69, doi:10.3354/meps209055.

Hansen, J. L. S., and T. Kiørboe (1997), Quantifying interspecific coagulation efficiency of phytoplankton, *Mar. Ecol. Prog. Ser.*, *159*, 75–79, doi:10.3354/meps159075.

Hasle, G. R., and E. E. Syvertsen (1997), Marine diatoms, in *Identifying Marine Phytoplankton*, edited by C. R. Tomas, pp. 5–385, Academic, San Diego, Calif.

Hebert, D. A., and S. M. de Bruyn Kops (2006), Relationship between vertical shear rate and kinetic energy dissipation rate in stably stratified flows, *Geophys. Res. Lett.*, *33*, L06602, doi:10.1029/2005GL025071.

Herman, A. W., B. Beanlands, and E. F. Phillips (2004), The next generation of optical Plankton counter: The laser-OPC, *J. Plankton Res.*, *26*(10), 1135–1145, doi:10.1093/plankt/fbh095.

Hodal, H., and S. Kristiansen (2008), The importance of small-celled phytoplankton in spring blooms at the marginal ice zone in the northern Barents Sea, *Deep Sea Res., Part II*, *55*(20–21), 2176–2185, doi:10.1016/j.dsr2.2008.05.012.

Holm-Hansen, O., and B. Riemann (1978), Chlorophyll *a* determination: Improvements in methodology, *Oikos*, *30*(3), 438–447, doi:10.2307/3543338.

Ingvaldsen, R., and H. Loeng (2009), Chapter 2: Physical oceanography, in *Ecosystem Barents Sea*, edited by E. Sakshaug, G. H. Johnsen and K. M. Kovacs, pp. 33–64, Tapir, Trondheim, Norway.

Iversen, M. H., N. Nowald, H. Ploug, G. A. Jackson, and G. Fischer (2010), High resolution profiles of vertical particulate organic matter export off Cape Blanc, Mauritania: Degradation processes and ballasting effects, *Deep Sea Res., Part I*, *57*(6), 771–784, doi:10.1016/j.dsr.2010.03.007.

Jackson, G. A. (1990), A model of the formation of marine algal flocs by physical coagulation processes, *Deep Sea Res., Part A*, *37*(8), 1197–1211, doi:10.1016/0198-0149(90)90038-W.

Jackson, G. A., and A. B. Burd (1998), Aggregation in the marine environment, *Environ. Sci. Technol.*, *32*(19), 2805–2814, doi:10.1021/es980251w.

Jackson, G. A., and D. M. Checkley (2011), Particle size distributions in the upper 100 m water column and their implications for animal feeding in the plankton, *Deep Sea Res., Part I*, *58*(3), 283–297, doi:10.1016/j.dsr.2010.12.008.

Jackson, G. A., R. Maffione, D. K. Costello, A. L. Alldredge, B. E. Logan, and H. G. Dam (1997), Particle size spectra between 1 μm and 1 cm at Monterey Bay determined using multiple instruments, *Deep Sea Res., Part I*, *44*(11), 1739–1767, doi:10.1016/S0967-0637(97)00029-0.

Jackson, G. A., A. M. Waite, and P. W. Boyd (2005), Role of algal aggregation in vertical carbon export during SOIREE and in other low biomass environments, *Geophys. Res. Lett.*, *32*, L13607, doi:10.1029/2005GL023180.

Juul-Pedersen, T., T. G. Nielsen, C. Michel, E. F. Møller, P. Tiselius, P. Thor, M. Olesen, E. Selander, and S. Gooding (2006), Sedimentation following the spring bloom in Disko Bay, West Greenland, with special emphasis on the role of copepods, *Mar. Ecol. Prog. Ser.*, *314*, 239–255, doi:10.3354/meps314239.

Kiørboe, T., and J. L. S. Hansen (1993), Phytoplankton aggregate formation: Observations of patterns and mechanisms of cell sticking and the significance of exopolymeric material, *J. Plankton Res.*, *15*(9), 993–1018, doi:10.1093/plankt/15.9.993.

Kiørboe, T., K. P. Andersen, and H. G. Dam (1990), Coagulation efficiency and aggregate formation in marine phytoplankton, *Mar. Biol.*, *107*(2), 235–245, doi:10.1007/BF01319822.

Lampitt, R. S., W. R. Hillier, and P. G. Challenor (1993), Seasonal and diel variation in the open ocean concentration of marine snow aggregates, *Nature*, *362*(6422), 737–739, doi:10.1038/362737a0.

Legendre, L., and R. B. Rivkin (2002), Fluxes of carbon in the upper ocean: Regulation by food-web control nodes, *Mar. Ecol. Prog. Ser.*, *242*, 95–109, doi:10.3354/meps242095.

Li, W. K. W., F. A. McLaughlin, C. Lovejoy, and E. C. Carmack (2009), Smallest algae thrive As the Arctic Ocean Freshens, *Science*, *326*(5952), 539, doi:10.1126/science.1179798.

Loeng, H. (1991), Features of the physical oceanographic conditions of the Barents Sea, *Polar Res.*, *10*(1), 5–18, doi:10.1111/j.1751-8369.1991.tb00630.x.

Loeng, H., V. Ozhigin, and B. Ådlandsvik (1997), Water fluxes through the Barents Sea, *ICES J. Mar. Sci.*, *54*, 310–317, doi:10.1006/jmsc.1996.0165.

Lundsgaard, C., M. Olesena, M. Reigstad, and K. Olli (1999), Sources of settling material: Aggregation and zooplankton mediated fluxes in the Gulf of Riga, *J. Mar. Syst.*, *23*, 197–210, doi:10.1016/S0924-7963(99)00058-5.

© 2014. The Authors.

McCave, I. N. (1984), Size spectra and aggregation of suspended particles in the deep ocean, *Deep Sea Res., Part A*, *31*(4), 329–352, doi:10.1016/0198-0149(84)90088-8.
McDonnell, A. M. P., and K. O. Buesseler (2010), Variability in the average sinking velocity of marine particles, *Limnol. Oceanogr.*, *55*(5), 2085–2096, doi:10.4319/lo.2010.55.5.2085.
Møller, E. F., T. G. Nielsen, and K. Richardson (2006), The zooplankton community in the Greenland Sea: Composition and role in carbon turnover, *Deep Sea Res., Part I*, *53*(1), 76–93, doi:10.1016/j.dsr.2005.09.007.
Möller, K. O., M. St John, A. Temming, J. Floeter, A. F. Sell, J. P. Herrmann, and C. Möllmann (2012), Marine snow, zooplankton and thin layers: Indications of a trophic link from small-scale sampling with the Video Plankton Recorder, *Mar. Ecol. Prog. Ser.*, *468*, 57–69, doi:10.3354/meps09984.
Morán, X. A. G., Á. López-Urrutia, A. Calvo-Díaz, and W. K. W. Li (2010), Increasing importance of small phytoplankton in a warmer ocean, *Global Change Biol.*, *16*(3), 1137–1144, doi:10.1111/j.1365-2486.2009.01960.x.
Moum, J. N. (1996), Efficiency of mixing in the main thermocline, *J. Geophys. Res.*, *101*(C5), 12,057–12,069, doi:10.1029/96JC00508.
Olli, K., C. W. Rieser, P. Wassmann, T. Ratkova, E. Arashkevich, and A. Pasternak (2002), Seasonal variation in vertical flux of biogenic matter in the marginal ice zone and the central Barents Sea, *J. Mar. Syst.*, *38*, 189–204, doi:10.1016/S0924-7963(02)00177-X.
Osborn, T. R. (1980), Estimates of the local rate of vertical diffusion from dissipation measurements, *J. Phys. Oceanogr.*, *10*(1), 83–89, doi:10.1175/1520-0485(1980)010<0083:EOTLRO>2.0.CO;2.
Passow, U., and P. Wassmann (1994), On the trophic fate of *Phaeocystis pouchetii* (Hariot): IV. The formation of marine snow by *P. pouchetii*, *Mar. Ecol. Prog. Ser.*, *104*, 153–161.
Prairie, J. C., K. Ziervogel, C. Arnosti, R. Camassa, C. Falcon, S. Khatri, R. M. McLaughlin, B. L. White, and S. Yu (2013), Delayed settling of marine snow at sharp density transitions driven by fluid entrainment and diffusion-limited retention, *Mar. Ecol. Prog. Ser.*, *487*, 185–200, doi:10.3354/meps10387.
Prandke, H., and A. Stips (1998), Test measurements with an operational microstructure-turbulence profiler: Detection limit of dissipation rates, *Aquat. Sci.*, *60*(3), 191–209, doi:10.1007/s000270050036.
Reigstad, M., and P. Wassmann (2007), Does *Phaeocystis* spp. contribute significantly to vertical export of organic carbon?, *Biogeochemistry*, *83*(1–3), 217–234, doi:10.1007/s10533-007-9093-3.
Reigstad, M., C. Wexels Riser, and C. Svensen (2005), Fate of copepod faecal pellets and the role of *Oithona* spp., *Mar. Ecol. Prog. Ser.*, *304*, 265–270, doi:10.3354/meps304265.
Reigstad, M., C. W. Riser, P. Wassmann, and T. Ratkova (2008), Vertical export of particulate organic carbon: Attenuation, composition and loss rates in the northern Barents Sea, *Deep Sea Res., Part II*, *55*, 2308–2319, doi:10.1016/j.dsr2.2008.05.007.
Richardson, T. L., and G. A. Jackson (2007), Small phytoplankton and carbon export from the surface ocean, *Science*, *315*(5813), 838–840, doi:10.1126/science.1133471.
Riebesell, U. (1991), Particle aggregation during a diatom bloom. 2. Biological aspects, *Mar. Ecol. Prog. Ser.*, *69*(3), 281–291, doi:10.3354/meps069281.
Riebesell, U., M. Reigstad, P. Wassmann, T. Noji, and U. Passow (1995), On the trophic fate of *Phaeocystis pouchetii* (Harlot): VI. Significance of *Phaeocystis*-derived mucus for vertical flux, *Neth. J. Sea Res.*, *33*(2), 193–203, doi:10.1016/0077-7579(95)90006-3.
Schindelin, J., et al. (2012), Fiji: An open-source platform for biological-image analysis, *Nat. Methods*, *9*(7), 676–682, doi:10.1038/nmeth.2019.
Slagstad, D., and K. Støle-Hansen (1991), Dynamics of plankton growth in the Barents Sea: Model studies, *Polar Res.*, *10*(1), 173–186, doi:10.1111/j.1751-8369.1991.tb00643.x.
Smayda, T. J. (1970), The suspension and sinking of phytoplankton in the sea, *Oceanogr. Mar. Biol.*, *8*, 353–414.
Smetacek, V. S. (1985), Role of sinking in diatom life-history cycles—Ecological, evolutionary and geological significance, *Mar. Biol.*, *84*(3), 239–251, doi:10.1007/bf00392493.
Sundfjord, A., I. Fer, Y. Kasajima, and H. Svendsen (2007), Observations of turbulent mixing and hydrography in the marginal ice zone of the Barents Sea, *J. Geophys. Res.*, *112*, C05008, doi:10.1029/2006JC003524.
Svensen, C., C. Wexels Riser, M. Reigstad, and L. Seuthe (2012), Degradation of copepod faecal pellets in the upper layer: Role of microbial community and *Calanus finmarchicus*, *Mar. Ecol. Prog. Ser.*, *462*, 39–49, doi:10.3354/meps09808.
Tamigneaux, E., L. Legendre, B. Klein, and M. Mingelbier (1999), Seasonal dynamics and potential fate of size-fractionated phytoplankton in a temperate nearshore environment (Western Gulf of St Lawrence, Canada), *Estuarine Coastal Shelf Sci.*, *48*(2), 253–269, doi:10.1006/ecss.1999.0416.
Thévenaz, P., and M. Unser (2007), User-friendly semiautomated assembly of accurate image mosaics in microscopy, *Microsc. Res. Technol.*, *70*(2), 135–146, doi:10.1002/jemt.20393.
Utermöhl, v. H. (1931), Neue Wege in der quantitativen Erfassung des Planktons. (Mit besondere Berücksichtigung des Ultraplanktons), *Verh. Int. Verein. Theor. Angew. Limnol.*, *5*, 567–595.
Våge, S. (2010), Structure and dynamics of the Barents Sea Polar Front near the Great Bank and associated plankton distribution in August 2007, MS thesis, Dep. of Arctic and Mar. Biol., Univ. of Tromsø, Tromsø, Norway.
Wassmann, P. (1998), Retention versus export food chains: Processes controlling sinking loss from marine pelagic ecosystems, *Hydrobiologia*, *363*, 29–57, doi:10.1023/A:1003113403096.
Wassmann, P., R. Peinert, and V. Smetacek (1991), Patterns of production and sedimentation in the boreal and polar Northeast Atlantic, *Polar Res.*, *10*(1), 209–228, doi:10.1111/j.1751-8369.1991.tb00647.x.
Wexels Riser, C., P. Wassmann, K. Olli, A. Pasternak, and E. Arashkevich (2002), Seasonal variation in production, retention and export of zooplankton faecal pellets in the marginal ice zone and central Barents Sea, *J. Mar. Syst.*, *38*, 175–188, doi:10.1016/s0924-7963(02)00176-8.
Wexels Riser, C., M. Reigstad, P. Wassmann, E. Arashkevich, and S. Falk-Petersen (2007), Export or retention? Copepod abundance, faecal pellet production and vertical flux in the marginal ice zone through snap shots from the northern Barents Sea, *Polar Biol.*, *30*(6), 719–730, doi:10.1007/s00300-006-0229-z.
Yamazaki, H., and T. Osborn (1990), Dissipation estimates for stratified turbulence, *J. Geophys. Res.*, *95*(C6), 9739–9744, doi:10.1029/JC095iC06p09739.

© 2014. The Authors.

Paper II

Wiedmann I, Tremblay JE, Sundfjord A, Reigstad M

Upward nitrate flux and downward particulate organic carbon (POC) flux along a stratification gradient in the Arctic shelf sea, Barents Sea.

Manuscript formatted to the standards of *Journal of Geophysical Research: Oceans*

Upward nitrate flux and downward particulate organic carbon (POC) flux along a gradient of stratification and turbulent mixing in an Arctic shelf sea (Barents Sea)

Ingrid Wiedmann (1)
Jean-Éric Tremblay (2)
Arild Sundfjord (3)
Marit Reigstad (1)

(1) UiT The Arctic University of Norway, Breivika, Tromsø, Norway
(2) Université Laval, 3058 Québec, Canada
(3) Norwegian Polar Institute, Tromsø, Norway

Abstract

Declining sea ice cover impacts Arctic pelagic ecosystems by strengthening the stratification due to sea ice melt and exposing previously ice-covered regions to wind mixing. Here, we used the Barents Sea (BS), an Arctic shelf sea, as a model area to examine effects of wind mixing and stratification on Arctic ecosystems upward nitrate flux and the downward particulate organic carbon (POC) flux. In the northern, Arctic influenced BS, we found open drift ice and a moderate halocline stratification. This apparently hindered wind-induced deep-mixing, because the upward nitrate flux was negligible (flux into mixing layer, 13 m: 0.004 mmol nitrate m^{-2} d^{-1}) and the downward POC flux was moderate (40-200 m: 150-250 mg POC m^{-2} d^{-1}) during the ice edge diatom bloom. The Atlantic influenced, weakly stratified, ice-free southern BS was more prone to wind mixing, and we observed a high upward nitrate flux (into the mixing layer, 25 m: 5.395 mmol nitrate m^{-2} d^{-1}) and a high downward POC flux (40-120 m: 260-600 mg POC m^{-2} d^{-1}) in a post bloom situation. We suggest that the downward POC flux in a future Arctic may decline if the nitrate replenishment weakens due to halocline strengthening. However, the downward POC flux may also increase when strong winds, weak stratification and a shallow nitracline allow a pulsed nitrate replenishment in the surface layers and stimulate primary production during a summer post bloom. Enhanced downward POC flux may then either result from active down-mixing or re-packaging of biomass into fast-sinking fecal pellets by mesozooplankon.

(250 words)

1 Introduction

Arctic seas are affected by the declining sea ice cover [*Arrigo and van Dijken,* in press; *IPCC,* 2013]. Sea ice melt freshens surface waters, strengthens column stratification [*Rainville et al.,* 2011], and exposes previously ice-covered areas to wind mixing, causing shelf break upwelling and deep wind-induced mixing [*Tremblay et al.*, 2011; *Martin et al.,* 2014; *Falk-Petersen et al.,* 2015]. These changes impact Arctic pelagic ecosystems, because the intensity of the nutrient replenishment in the euphotic zone and the sedimentation of organic biomass is affected, but regulating mechanisms are still debated [*Carmack and Wassmann*, 2006; *Tremblay and Gagnon*, 2009; *Tremblay et al.*, 2011; *Wassmann and Reigstad*, 2011; *Falk-Petersen et al.*, 2015].

The Barents Sea, an Arctic shelf sea, is here used as model area to investigate the upward nitrate flux and the downward flux of particulate organic carbon (POC) in a field study under contrasting situations of hydrography and turbulent mixing (Figure 1). Arctic derived water masses [temperature $T < 0$ °C, salinity $S = 34.4\text{-}34.8$, *Loeng*, 1991] influence the northern Barents Sea, and contributes to the seasonal sea ice cover, which reaches its annual maximum extension in March/April [*Kvingedal*, 2005].When the sea ice retracts northwards during late spring and summer, sea ice melt water freshens surface waters. This strengthens the halocline and, in combination with the open drift ice, hampers wind-induced deep-mixing [*Rainville et al.*, 2011]. Surface nitrate concentrations are usually high subsequent to ice break-up, and give rise to an ice-edge related diatom bloom [*Hegseth and Sundfjord*, 2008]. This phytoplankton taxon potentially cause a major downward POC flux, such as described in the conceptual model of the northwards propagating ice edge bloom in the Barents Sea [*Sakshaug et al.,* 1991; *Sakshaug et al.*, 2009] due to the high sinking velocity of senescent stages, resting stages or aggregates [*Eppley et al.*, 1967; *Bienfang*, 1981; *Iversen and Ploug*, 2013].

Atlantic derived waters [$T > 3$ °C, $S > 35.0$, *Loeng*, 1991] influence the southern Barents Sea, where a weak stratification has been observed during the late spring and early summer [*Andreassen and Wassmann,* 1998; *Reigstad et al.*, 2002]. Accordingly, this region is more prone to wind mixing compared to the marginal ice zone. As phytoplankton growth is not light limited by sea ice in the southern Barents Sea. The onset of the bloom occurs earlier [*Leu et al.*, 2011], and, while a peak bloom still occurs at the ice edge, a post bloom stage with low nitrate concentrations may already be found in the southern Barents Sea in late June

[*Wassmann et al.*, 1999]. The low nitrate concentrations favor small cells (< 10 µm) with a high surface to volume ratio. These cells have low sinking velocities, and probably contribute little to the downward POC flux [*Mann and Lazier*, 2006]. Further, also the estimated ingestion of mesozooplankton is higher during the post bloom situation compared to the early bloom [*Wexels Riser et al.*, 2008], which enhances the POC attenuation in the water column and reduces the downward POC.

A lower downward POC flux may accordingly be presumed for the weakly stratified southern Barents Sea during a post bloom situation. However, model results for the southern Barents Sea suggested that strong winds (> 12 m s^{-1}), associated with low pressure belts, could induce deep-mixing entrain nutrients every ten days and stimulate primary production [*Sakshaug and Slagstad*, 1992]. These results were in line with measurements of wind driven turbulent mixing in the same area in summer [*Sundfjord et al.*, 2007], and potential effects on the whole pelagic ecosystem may be assumed: *Svensen et al.* [2002] observed in mesocosm studies that pulsed nitrate injections into the euphotic zone resulted in an enhanced downward POC flux, and this matches observations from the weakly stratified Barents Sea [*Olli et al.*, 2002; *Reigstad et al.*, 2008].

During the present field study, we used the Barents Sea as a model area and focused on the upward nitrate flux and downward POC flux under contrasting conditions of stratification, turbulent mixing and phytoplankton bloom along a north-south gradient from the marginal ice zone in the north to the ice-free region in the south. In this way, we aimed to (1) examine the intensity of the upward nitrate flux, (2) investigate if the upward nitrate flux considerably contributes to the nitrate stock in the upper water column, and (3) describe possible mechanisms regulating the downward POC flux under these contrasting conditions of stratification and vertical mixing.

2 Materials and Methods

Field work was carried out with the ice-enforced R/V "Helmer Hanssen" (22 – 27 June 2011) as part of the CONFLUX project. Based on a high-resolution northward CTD-F transect along the 30°E longitude (S. Basedow, pers. com.), three stations were chosen in the central Barents Sea for more detailed process studies. The north-south transect provided a gradient in

hydrography and bloom stage from the marginal ice zone in Arctic influenced waters (M1), through the Polar Front (M2) into deep-mixed, Atlantic influenced waters (M4).

2.1 Hydrography, sea ice and light conditions

Hydrography data (temperature, salinity, conductivity) and fluorescence were obtained at each station from surface to bottom (CTD-F, SeaBird 911*plus*). Data were processed with the SeaBird standard software package (bin average 0.5 m). Following *Brainerd and Gregg* [1995], we use here the term 'mixed layer' for a weakly stratified surface layer, which was not necessarily actively mixed during the time of data collection. In contrast, 'mixing layer' denotes the surface depth interval, which was actively mixed with a diffusivity > 10^{-4} m^2 s^{-1} during data collection [*Wiedmann et al.*, 2014]. Due to our focus on upward and downward transport of nitrate and organic matter, we use the term 'mixing layer' instead of the recently suggested term 'turbulent layer' [*Franks*, 2014]. The sea ice conditions were visually estimated, based on the scale of the Norwegian Meteorological Institute (11 categories from ice-free to fast ice). Underwater irradiance was measured with a GMBDH TRIOS light scanner (190-575 nm, 2.15 nm wavelength resolution) at each process station between subsurface and 20 m during local noon. The base of the euphotic zone (1 % sub-surface irradiance) was estimated for the wavelength of chlorophyll *a* (Chl *a*) [430 nm, *South and Whittick*, 1987] using the equation

$$I_D = I_0 * \exp(-k * z) \quad (1)$$

where I_D was the irradiance at depth z, I_0 the sub-surface irradiance, and k the diffuse attenuation coefficient. A minor error must be assumed, since the attenuation coefficient did not take into account the shading effects by phytoplankton at the Chl *a* maximum (located below 20 m).

2.2 Turbulence, nitrate concentrations and nitrate flux

A loosely tethered microstructure drop sonde (MSS-90L) with a pair of PNS06 shear probes [*Prandke and Stips*, 1998] was used to collect sets of 2-3 profiles roughly every four hours during station work. Only the profiles taken closest in time to the CTD and the nitrate profiles are included here. The sets of shear profiles were processed as described in *Fer* [2006], with data from above 8 m depth being discarded to avoid influence from the ship's keel. We

calculated the diffusivity K (m^2 s^{-1}) as described in [*Wiedmann et al.*, 2014]. The data were averaged over four meter moving intervals before they were used to calculate the nitrate flux.

Continuous depth profiles of nitrate were measured with a Satlantic ISUS V3 ultra-violet spectrophotometer. The accuracy of individual measurements can be up to +/- 2 mmol m^{-3} [*Johnson and Coletti*, 2002] but when several data points are averaged in vertical bins, as done here, we expect accuracy around 0.5 mmol m^{-3} [*Randelhoff et al.*, 2015]. The instrument was integrated with the ship-borne CTD system in order to get simultaneous depth data from the CTD's pressure sensor. Individual nitrate sensor spectra were processed using software provided by the manufacturer. The vertical profiles were objectively adjusted to match near-surface (10 m) nitrate concentration achieved from chemical sea water analysis [procedure following *Martin et al.*, 2010b] and smoothed using a 10 m moving average before gradients were obtained for nitrate flux calculations.

Computation of nitrate flux F_N was based on the gradient of nitrate (N) concentration with depth z and the diffusivity (K):

$$F_N = K * (dN / dz) \quad (2)$$

2.3 Nitrate uptake rates

Nitrate uptake rates are strongly dependent in the available PAR. To assess this relationship, water from the surface and the subsurface Chl *a* maximum (SCM) was collected at station M1 and M4, split in ten 500 mL tissue culture flasks each and spiked with a trace amount of ^{15}N-potassium nitrate (0.1 mM). Each set of ten flasks was placed in a separate ten-position, linear light-gradient incubator designed to minimize spectral shift [*Marcel et al.*, 1994]. Both incubators were illuminated by a single full-spectrum 400 W Optimarc metal-halide lamp mimicing solar irradiance. Optically-neutral filters (Lee Filters) were placed in front of the incubator with the surface samples to yield measured irradiances ranging from 5 to 630 µmol quanta m^{-2} s^{-1}. For the incubator with SCM samples, one layer of a blue filter (118 Light Blue Lee Filters Ltd.) was combined with optically-neutral filters (Lee Filters) to provide irradiances ranging from 3 to 365 µmol quanta m^{-2} s^{-1}. Temperature was maintained at in-situ levels with a chilling circulator. In order to minimize isotopic dilution and photo-acclimation to experimental conditions, the incubations were kept as short as possible (5-6 h) to ensure detection. Incubations were terminated by filtration onto 24 mm pre-combusted Whatman

GF/F filters. All filters were desiccated at 60 °C and stored dry for analysis ashore. An elemental analyzer (ECS 4010, Costech Analytical Technologies Inc.) coupled to a mass spectrometer (Delta V Advantage, Thermo-Finnigan) was used to determine isotopic enrichment and particulate organic nitrogen (PON) using a modified Dumas method [for details see *Blais et al.*, 2012].

Specific nitrate uptake (N) was calculated using Equation 3 of *Collos* [1987] and Uptake-irradiance parameters (and standard errors on these parameters) were calculated on specific uptake data using the double exponential model of *Platt et al.* [1980]:

$$N = N_d + N_s [1\text{-}\exp(\text{-}\alpha E / N_s)] [\exp(\text{-}\beta E / N_s)] \quad (3)$$

and

$$N_m = N_s [\alpha / (\alpha+\beta)] [\beta / (\alpha+\beta)]^{\beta/\alpha} \quad (4)$$

where N_d is the dark uptake (h^{-1}), N_s is the theoretical maximum uptake in the absence of photoinhibition (h^{-1}), N_m is the maximum observed uptake (h^{-1}), E is the incubation irradiance (PAR, µmol quanta m^{-2} s^{-1}), and α and β [h^{-1} (µmol quanta m^{-2} s^{-1})$^{-1}$] are the photosynthetic efficiency at low irradiance (initial slope of the relationship) and the photoinhibition parameter, respectively. In order to use the parameters directly in the model determining the nitrate uptake rates (calculations not shown), values were multiplied by the mean concentration of PON for the ten subsamples and divided by the concentration of Chl *a* at the depth of collection.

The continuous record of PAR on deck was combined with the vertical attenuation coefficient of underwater irradiances (k), measured at local noon, to estimate instantaneous PAR at each 1-m depth bin throughout the day. Chl *a* concentration for each depth bin was estimated by using post-calibrated in vivo fluorescence data from the CTD. For each depth bin and time of day, absolute nitrate uptake rates (µmol N L^{-1} h^{-1}) were estimated from equation (3) by substituting instantaneous PAR for E and multiplying by Chl *a*. Parameters established with the surface sample were assigned to all depths in the upper mixed layer, whereas parameters established for the SCM were used at the SCM and below it. Between the base of the mixed layer and the SCM, parameters were interpolated according to the vertical gradient of nitrate concentration for N_d and N_m, and according to depth for α and β. This procedure is justified by

the fact the nitrate concentration and depth were robust predictors of N_m and α, respectively, for the set of eight curves obtained for stations M1, M2, M3 (located between M2 and M4, not shown on Figure 1) and M4 at the surface and the SCM.

Nitrate uptake simulations in the model were run using a five days averaged record during occupation at M1 and M4 to prevent giving too much importance to short-term conditions at the time of sampling. Since running the simulation with the darkest and clearest days resulted in a variation of the depth-integrated uptake by a small variation around the mean (8-10 %), we chose to neglect this here.

2.4 Suspended and sedimented biomass (Chl *a*, POC, PON, C/N ratio)

Suspended biomass was collected with Niskin bottles attached to the CTD rosette at 12 sampling depths between subsurface and 200 m (Table 1) to construct depth profiles of Chl *a*, POC, PON and the atomic C/N ratio. A C/N ratio of 6.6 represents the Redfield ratio [*Redfield*, 1934; 1958], indicating fresh phytoplankton material. Higher ratios reflect more degraded material, or material from terrestrial origin [*Bianchi*, 2006]. Collected water was gently transferred from Niskin bottles and stored cool and dark until filtration within few hours. Triplicates (50-200 mL) of each depth were vacuum-filtered onto Whatman GF/F filters (pore size 0.7 µm) and Whatman Nucleopore membrane filters (pore size 10 µm) to achieve a size-fractionation of the Chl *a* containing material (total and > 10 µm). Chl *a* was extracted in 5 mL methanol (12 h, room temperature, darkness) and the Chl *a* concentration was measured using a Turner Design 10-AU fluorometer (calibrated with Chl *a*, Sigma C6144), applying the acidification method [*Holm-Hansen and Riemann*, 1978]. For POC and PON, triplicates (200 mL) of each sampling depth were filtered on pre-combusted Whatman GF/F filters. Larger organisms such as copepods or chaetognats were removed before the filters were frozen (-20 °C) until analyses (< 6 months). Analyses were carried out using a Leeman Lab CHN Elemental Analyzer [for details see *Reigstad et al.*, 2008].

A neutrally buoyant free-floating sediment trap array was deployed for ~20-24 h at M1, M2 and M4 (Table 1). Semi-Lagrangian drifting was ensured, by anchoring the trap array on an ice-floe at M1 and M2. At M4 the trap array was freely drifting in open waters, but with the buoyancy located below the surface to minimize the wind drift. Paired trap cylinders (KC Denmark, outer diameter 72 mm, length 450 m) were mounted at the sampling depths (40, 50, 60, 90, 120 and 200 m). The content of the cylinders was transferred into carboys after recovery and stored cool and in darkness until filtered in triplicates (200 mL, swimmers were

removed as far as possible) and analyzed as described previously for suspended POC and PON.

2.5 Calculations

Upward nitrate flux and the nitrate uptake of autotrophs affect the nitrate stock in the surface layer. We run a simple model (Table 2) to investigate the interaction of both factors in detail in different biological important depth intervals, such as the layer with a nitrate stock < 1 mmol nitrate m^{-3} (nitrate limitation), the depth interval between the surface and the SCM, the euphotic zone (irradiance > 1 % of the sub-surface irradiance), the mixed layer and the mixing layer (see definition section 2.1). The contribution of the upward nitrate flux to the stock (% input from below, Table 2) was calculated as the ratio of the upward nitrate flux to the integrated nitrate concentration in each layer. The time to nitrate exhaustion without upward nitrate flux equals the ratio of the integrated nitrate stock to the integrated nitrate uptake above the base of the respective layer. For the time to nitrate exhaustion with upward nitrate flux, we put up a model calculation, which starts with the integrated nitrate stock in a certain depth layer (e.g. mixing layer) and assumed for each consecutive day a constant nitrate uptake and a certain upward nitrate flux (see Table 2 for the chosen conditions).

3 Results

3.1 Hydrography, euphotic zone and wind

Station M1 in the northern Barents Sea was covered with very open drift ice (Table 1, Figure 1). A staircase-like halocline (7-23 m) structured the water column in a well-mixed meltwater affected layer in the upper 7 m (temperature T = -1.2 °C, salinity S = 32.9) and a water layer of Arctic origin gradually mixed with some Atlantic water at depth (25-200 m: T < 0 °C, S = 34.0-34.7, Figure 2a). The base of the euphotic zone with 1 % irradiance (430 nm) was located at 65 m (Figure 2d). M2 was located in very open drift ice in the Polar Front (Table 1). In this area, colder and fresher Arctic derived water masses tend to cover warmer and more saline Atlantic derived water [*Loeng*, 1991]. This was also observed during our study (Figure 2b): A well-mixed meltwater layer (0-15 m: T < 0.0 °C, S = 32.6) was separated by a strong halocline (15-20 m) from the lower part of the water column, which was, increasingly with depth, influenced by Atlantic water (200 m: T = 0.9 °C, S = 35.0). The euphotic zone reached down to 54 m (Figure 2e). The southernmost station M4 in the ice-free, Atlantic

influenced, southern part of the Barents Sea (Figure 1), was weakly stratified by a mainly temperature driven pycnocline at 35-40 m (Figure 2c). Above 35 m, we found water masses characterized by T > 5.0 °C and a salinity of 35.09, while a gradually decreasing temperature (40 m: T = 3.5 °C, 200 m: T = 2.3 °C) and a fairly constant salinity (S = 35.10 -35.13) was observed below. The base of the euphotic zone was situated to 45 m (Figure 2f). We observed strong winds during station work at M1 (9.5-13.3 m s^{-1}) and previous to station work at M4 (6.7-13.5 m s^{-1}).

3.2 Nitrate concentration, vertical diffusivity, and nitrate flux

At M1, nitrate was nearly depleted in the upper 20 m (Figure 3a). Surface-enhanced mixing (diffusivity > 10^{-4} m^2 d^{-1}) protruded to 13 m, but due to the negligible nitrate concentrations in this depth interval, the high diffusivity resulted in a low nitrate flux (Figure 3g). The nitracline, here defined as the depth interval of the sharp increase in nitrate concentration, was located between 20 and ~40 m (Figure 3a). Diffusivity was low in the 15-25 m interval, because of the staircase like halocline in this depth interval. Between ca. 25 and nearly 40 m, stratification was weaker than in the 15-25 m depth interval and the nitrate concentration increased with depth, resulting in a nitrate flux of ~0.4 mmol m^{-2} d^{-1}. Below 40 m, nitrate fluxes were estimated to be < 0.1 mmol m^{-2} d^{-1} (Figure 3g). The upward nitrate flux into the biological significant depth intervals was calculated and found to be negligible when compared to the integrated nitrate stock (< 0.4 % d^{-1}, Table 2).

At M4, nitrate concentrations increased from the (near-)surface (1 m: < 0.1 mmol nitrate m^{-3}) down to ~73 m (7.54 mmol nitrate m^{-3}, Figure 3b) and an enhanced diffusivity (> 10^{-4} m^2 d^{-1}) was found in the uppermost 25 m (Figure 3h). The upward nitrate flux into the euphotic zone (0-45 m, Table 2), the mixed layer (0-38 m) as well as layer above the SCM (0-45 m) was small compared to the nitrate stock in these layers (< 1 % d^{-1}, Table 2). However, the upward nitrate flux added 12 % d^{-1} and 38 % d^{-1} to the nitrate stock in the zone of < 1 mmol nitrate m^{-3} (0-27 m) and the mixing layer (0-25 m, Table 2), respectively.
The minor decline in concentration below the maximum values (~70 m, Figure 3a, b) likely reflects differences in advection history at the different subsurface depths or may be a small artifact related to the accuracy of the nitrate sensor.

3.3 Suspended biological parameters (size fractionated Chl *a*, POC, C/N ratio)

At station M1, the most pronounced sub-surface Chl *a* maximum (40 m: 4.4 mg Chl *a* m^{-3}) was observed, dominated by large cells (> 10 µm, Figure 2d). The suspended POC also showed a distinct sub-surface peak at 40 m, but the Chl *a* and POC depth distribution was strongly linked (R^2 = 0.91). A C/N ratio of 7.5-9.5 (1-50 m) indicated little to moderately degraded biomass in this depth interval (Figure 2g).

A subsurface Chl *a* peak was also found at M2 (44 m: 1.5 mg Chl *a* m^{-3}), but it was weaker when compared to M1 and dominated by small cells (50-80 %, Figure 2e). The POC maximum at 40 m (Figure 2h) was only weakly correlated to Chl *a* (R^2 = 0.56). A C/N ratio of 8.1-9.2 was observed in the uppermost 50 m (Figure 2h).

Also at M4 we found a sub-surface Chl *a* maximum (45 m: 1.6 mg m^{-3}, dominated by small cells, Figure 2f). The suspended POC was here evenly distributed in the uppermost 40 m (330-360 mg POC m^{-3}, Figure 2i), before abruptly declining to "background" concentrations of ~120-130 mg m^{-3} (60-200 m). This pattern was also observed at M1 and M2. Chl *a* and POC concentration were weakly correlated at M4 (R^2 = 0.60), and the vertical distribution of C/N ratio was comparable to M1 and M2 (Figure 2i).

Based on the integrated nitrate concentrations, which were highest at M1 and lowest at M4 (Figure 3a, b), as well as the phyto-/ zooplankton composition and abundance [*Wiedmann et al.*, 2014], the three stations M1, M2 and M4 were classified as a late peak bloom stage, late bloom stage and post bloom stage, respectively.

3.4 Nitrate uptake rates and time to nitrate exhaustion

The nitrate uptake rate at M1 peaked at 32 m (2.5 mmol nitrate m^{-3} $d^{-1,}$ Figure 3c), and the estimated time to nitrate exhaustion reached its minimum of 5.3 days in the depth layer 0-35 m (Figure 3e). At M4 the maximum nitrate uptake rate was found at 37 m (0.4 mmol nitrate m^{-3} d^{-1}, Figure 3d). Our nitrate model indicates that the time to nitrate exhaustion was shortest in the layers 0-38 m and 0-42 m (~9.4 d, Figure 3f).

According to our model, nitrate concentrations in the mixing layer of M1 (13 m) were exhausted after 15 days if the upward nitrate flux was set to zero (Table 2). When including the upward nitrate flux of 0.004 nitrate m^{-2} d^{-1}, the time to exhaustion was prolonged to 16 days (Table 2).

The model suggested for M4, that nitrate concentrations would become exhausted in the mixing layer (0-25 m) after 10 days if the upward nitrate flux was set to zero. The observed

upward nitrate flux rate at M4 was however high at 25 m (5.39 mmol nitrate m^{-2} d^{-1}). We presume that this was linked to the strong winds for 1-3 days during the passage of low pressure fronts, but that a relaxation would take place after this period (assumed flux: 0.30 mmol nitrate m^{-2} d^{-1}, equaling the average flux between 50 and 70 m, which was a depth interval not influenced by surface mixing processes). Depending on the number of days with strong mixing (1-3 days), our model suggested that nitrate would be exhausted in the mixing layer after 16, 21 or 25 days, respectively (Table 2).

3.4 Characterization of the vertical flux (POC, C/N ratio)

The intensity of the vertical POC flux and the C/N ratio of the sedimenting material varied between the stations.

The POC flux (at 120 m) was highest at M4 (261 mg POC m^{-2}) compared to the other stations (156-187 mg POC m^{-2} d^{-1}). The attenuation of the flux, calculated from the depth of the highest flux (M1: 90 m, M2 and M4: 40 m) to 120 m, was weakest at M1 (~20 %) and higher at the other stations (56 and 65 % at M2 and M4, respectively).

Along the stratification gradient from the north to the south, we found a declining trend of the C/N ratio (Figure 4), implying that sinking material was more degraded at M1 and M2 than at M4.

4 Discussion

In our field study, we used the Barents Sea as a model area to investigate the upward nitrate flux, the impacts on the nitrate stock in the upper water column and the downward POC flux under contrasting hydrographical and phytoplankton bloom situations along the north-south gradient. We found a negligible upward nitrate flux and a moderate downward POC flux in Arctic influenced waters at the ice edge in the north, and high upward nitrate and downward POC fluxes in the Atlantic influenced waters and discuss in the following if water column stratification and vertical mixing were drivers of these fluxes.

4.1 Impact of water column stratification and vertical turbulent mixing on the upward nitrate flux

The vertical nitrate flux (Equation 1) in the water column is linked to the diffusivity in the water column [*Osborn*, 1980; *Moum*, 1996] and the vertical gradient of the nitrate

concentration. Diffusivity is low in strongly stratified waters and thus restrains the vertical nitrate flux. In contrast, tide and wind mixed waters have a high diffusivity, which drives the nitrate flux together. The nitrate concentration determines the nitrate flux intensity by the steepness of its slope with depth, and governs the flux direction, because the nitrate flux follows Fick's Law of diffusion from high to low concentrations. An upward nitrate flux is commonly observed in marine ecosystems, because primary production in the euphotic zone mainly depletes nitrate close to the surface while high concentrations are found at depth [Figure 3g, h; *Mann and Lazier*, 2006].

At our northernmost station, the combination of a moderately strong halocline, following the ice break-up and melting, and the partial sea ice cover hampered deep turbulent mixing [*Le Fouest et al.*, 2011; *Rainville et al.*, 2011], resulting in a negligible upward nitrate flux (< 0.04 mmol nitrate m^{-2} d^{-1}) into biologically interesting layers (Table 2). The low fluxes were comparable to previous studies from a stratified, partly ice-covered location in the northern Barents Sea [upward nitrate flux into the upper mixed layer during a summer ice edge bloom: 0.14 mmol nitrate m^{-2} d^{-1}, *Sundfjord et al*., 2007], the ice-free northeast Atlantic subpolar gyre [upward nitrate flux in the upper mixed layer during summer: 0.02-0.60 mmol nitrate m^{-2} d^{-1}, *Painter et al*., 2014] and the Porcupine Abyssal Plain, NE Atlantic [upward nitrate flux into the euphotic zone during a weakly stratified summer situation: 0.09 mmol N m^{-2} d^{-1}, *Martin et al.*, 2010a].

The ice-free, weakly stratified waters at M4 were more prone to surface forced wind mixing, resulting in a considerable upward nitrate flux (> 5 mmol m^{-2} d^{-1}, Table 2) into the base of the mixing layer (Figure 3 g, h). This nitrate flux was up to two orders of magnitude higher than observed flux at the respective depth at M1 (Table 2), but comparable intensities of upward nitrate fluxes were observed in other deep-mixed locations, such as the southern Barents Sea during late July [nitrate flux into the base of the upper mixed layer: 2.4 mmol nitrate m^{-2} d^{-1}, *Sundfjord et al.*, 2007] and the tidally mixed Celtic Sea during summer [nitrate flux into the base of the SCM: 1.3-9 mmol nitrate m^{-2} d^{-1}, *Sharples et al*., 2007].

The upward nitrate flux at the Polar Front (data not shown) had an intermediate strength when compared to M1 and M2 and our data accordingly suggest a gradual change in terms of upward nitrate flux from marginal ice zone to ice-free waters in the Barents Sea.

The restricted nitrate replenishment in the euphotic zone at the ice edge region matches previous suggestions for the subpolar North Atlantic. In this area, convective winter mixing

was pointed out to be a period of major upward nutrient flux [*Louanchi and Najjar*, 2001], because thermal stratification tends to hamper deep vertical wind mixing during the summer [e.g., NE Atlantic, *Martin et al.*, 2010a; *Painter et al.*, 2014]. Nitrate replenishment during early summer, such as observed here, was also reported from the southeast Bering Shelf [*Sambrotto et al.*, 1986]. We suggest it may be a phenomenon restricted to high latitude seas [*Townsend et al.*, 1992; *Eilertsen*, 1993], where phytoplankton blooms take place in unstratified waters and warming of the surface and thermocline stratification occurs during summer.

4.2 Impact of water column stratification and turbulent mixing on the nitrate stock of the upper water column

The nitrate concentrations during our field study were low at the surface, but enhanced at depth (> 6 mmol m^{-3} at 100 m, Figure 3a, b), which corresponded to previously observed spring bloom scenarios in the region [*Reigstad et al.*, 2002; *Hodal and Kristiansen*, 2008]. When modelling the effect of the upward nitrate flux and the nitrate uptake rates on the nitrate stock in different layers (Table 2), our data show that time until nitrate exhaustion was shorter at M4 than at M1 if the upward nitrate flux is not taken into account. We anticipated that this was due to the combination of a higher nitrate uptake rate (< 24 m) and a lower integrated nitrate concentration at M4 than at M1 (Table 2).

In the model runs with upward nitrate flux, the time to nitrate exhaustion in the mixing layer was only prolonged by one day at M1, because of the generally low upward nitrate flux and the minor contribution of the upward nitrate flux to the stock (0.0-0.4 % d^{-1}, Table 2) at this station. A correspondingly low daily injection into the upper mixed layer (< 0.5 % of the nitrate stock d^{-1}) was found in the subpolar Atlantic Ocean gyre [*Painter et al.*, 2014], but we wondered if the low upward nitrate flux (0.035 mmol nitrate m^{-2} d^{-1}) resembled the reality at M1. The marginal ice zone moved northward subsequent to our station work and the location was ice-free by 27 June 2011 (ice map from the Norwegian Meteorological Institute, http://157.249.32.242/archive/). Ice melt probably strengthened the halocline stratification [*Sundfjord et al.*, 2008], and created a strong stratified system such as the one found at M2. We chose in the set-up of our model therefore to use an upward nitrate flux of 0.035 mmol nitrate m^{-2} d^{-1} (such as observed at M1) for 5 days, followed by an upward flux equaling the one into the base of the mixing zone at M2 (~0.35 mmol nitrate m^{-2} d^{-1}). This enhanced upward nitrate flux prolonged the time to nitrate exhaustion in the mixing layer to 45 days at

M1. Nevertheless, a constant decline of the nitrate concentrations is suggested by the model run, because the nitrate uptake rates always exceeded the upward nitrate flux. We assume that this situation would have triggered a gradual transition from system based on nitrate production to a regenerative, post bloom system, such as described for the spring-summer transition e.g. in the Arctic Kongsfjorden, Svalbard [*Iversen and Seuthe*, 2011].
Alternatively, it would be possible that strong wind mixing after disappearance of all sea ice caused a break down the stratification and induce mixing. Model results of this scenario by *Sundfjord et al.* [2008] suggest a mixing in the uppermost 10-20 m, but not deeper. This pinpoints that no considerable deepening of the mixing layer occurred, and we consider our model assumptions as reliable.

Deep-mixing and the observed high upward nitrate flux in the ice-free waters at M4 were assumed to be rather linked to a passing low pressure front than to be a constant trait of the system in the southern Barents Sea. In the model, we used therefore a 1-3 days of deep-mixing followed by relaxation (Table 2). The calculations still indicate that one day of high upward nitrate flux could prolong the time to nitrate exhaustion in the mixing layer by six days (Table 2). A two day deep-mixing doubled the time to nitrate exhaustion and a three-day deep-mixing replenished the nitrate concentration so much, that the initial nitrate concentration would be reached after seven consecutive days of low upward flux and constant nitrate uptake. This matches well with the rhythmic pattern of wind peaks occurring every 10 days [*Sakshaug and Slagstad*, 1992].
Accordingly, we suggest, that a weak stratified water column and strong wind mixing below the nitracline could replenished nitrate concentrations in the mixing layer of the ice-free Barents Sea, because the intensity of the upward nitrate flux exceeded the nitrate uptake rate more than 3-fold. Enhanced nitrate concentrations in the surface could however not be observed in this field study. Our short stay at the station (ca. 24 h) could be considered as one reason, but we rather suggest that no build-up in nitrate concentration took place, but that nitrate was immediately been taken up by the abundant cells of the phytoplankton taxon *Phaeocystis pouchetii* (ca. 1.8 x 10^6 cells L^{-1}) [*Wiedmann et al.*, 2014].

4.3 Impact of water column stratification and turbulent mixing on the downward POC flux

The intensity of the downward POC flux reflects the hydrographical situation and the planktonic ecological interactions in the water column above. High biomass sedimentation

events tend to occur, when a weak temporal coupling of primary production and maximum grazer activity allows for sinking of biomass, such as suggested for the northward propagating ice edge in the Barents Sea [*Sakshaug et al.*, 1991; *Sakshaug et al.*, 2009; *Wassmann and Reigstad*, 2011].

POC flux rates of 150-1000 mg POC m^{-2} d^{-1} ($\geq$ 40 m) have been observed in this region during the present study and match previous measurements in this region during the same season [*Andreassen and Wassmann*, 1998; *Coppola et al.*, 2002; *Olli et al.*, 2002; *Reigstad et al.*, 2008]. We propose that a combination of factors promoted the downward POC flux at the ice edge during the present study. The high Chl *a*: POC ratio at M1 suggests that suspended autotrophs were the prevailing form of particulate organic carbon in the water column, and aggregates of large diatoms (> 10 µm) have been identified as the prevailing vehicle of vertically exported biomass to ≤60 m [*Wiedmann et al.*, 2014]. These aggregates can sink with few meters to few hundred meters per day, depending on species and physiological stage [*Bienfang et al.*, 1982; *Iversen and Ploug*, 2013]. Also, mesozooplankton abundances were low at M1 when compared to M2 and M4 [*Wiedmann et al.*, 2014, *Svensen et al*., in prep.], and caused a low attenuation of the sinking biomass at this northernmost station.

The downward POC flux at the weakly stratified station M4 exceeded the one observed at M1. Similarly high downward fluxes have previously been observed the deep-mixed, Atlantic influenced part of the southern Barents Sea [*Reigstad et al*., 2008: early bloom 400-750 mg POC m^{-2} d^{-1} at 30-200 m], though a post bloom situation is often associated with a minor POC sedimentation [*Wassmann and Reigstad*, 2011]. We suggest that the wind-induced deep-mixing stimulated the downward POC flux in different ways. The abundant prymnesiophyte *Phaeocystis pouchetii* [*Wiedmann et al.*, 2014] has a low sinking velocity, but its cells may contribute to the downward POC flux when down-mixing occurs such as at M4 [*Reigstad and Wassmann*, 2007]. This line of argumentation is bolstered by the low C/N ratio of the sedimenting material (C/N = 6.4-7.7, Figure 4), suggesting a fast downwards transport of recently produced biomass.

Along our north-south transect, the mesozooplankton abundance increased toward south [*Svensen et al*., in prep.]. We assume that these grazers executed an intense top-down control especially at M4 and caused the strong POC attenuation. Pulsed nitrate supply stimulates primary production, such as described from the southeastern Bering Sea [*Sambrotto et al.*, 1986]. In situations of high zooplankton abundance, the increased primary production may cause enhanced feeding rates of copepods and the production of larger fecal pellets [*Turner*

503 *and Ferrante,* 1979, and references therein; *Wexels Riser et al.*, 2007]. Following Stokes'
504 Law, a higher sinking velocity must be assumed for these larger pellets, and they obviously
505 enhanced the downward POC flux, because they were frequently observed in the sediment
506 traps at M4 [*Wiedmann et al.*, 2014].
507 In summary, we suggest that deep-mixing enhanced the downward POC flux in the weakly
508 stratified water column at M4 in two ways: pulsed upward nitrate flux events stimulated
509 primary production and the produced biomass was both actively down-mixed and repackaged
510 into large mesozooplankton fecal pellets with high sinking velocity.
511
512

513 # 5. Conclusion

514 This field study was conducted along a north-south located transect in the central Barents Sea,
515 an Arctic shelf sea. We used it as a model area to study upward nitrate and downward POC
516 flux along a gradient of turbulent surface mixing, water column stratification and bloom stage.
517 At the northernmost, moderately stratified, station at the ice edge, a negligible upward nitrate
518 flux and a moderate downward POC flux was found during a late peak bloom dominated by
519 planktonic diatoms. The situation largely resembled the conceptual model of a northward
520 propagating ice edge phytoplankton bloom (Figure 5) [*Sakshaug et al.*, 1991; *Sakshaug et al.*,
521 2009].
522 In the weakly stratified, Atlantic influenced waters of our southernmost station we found a
523 contrasting situation. Wind-induced deep-mixing reached here down to 35-40 m, and
524 enhanced the upward nitrate flux considerably. This apparently stimulated the primary
525 production and the produced biomass was (1) actively down-mixed and (2) utilized by the
526 abundant zooplankton community and repackaged into fast-sinking fecal pellets, which
527 enhanced the downward POC flux. Accordingly, we recommend extending the conceptual
528 model of a northward propagating ice edge phytoplankton bloom by a deep-mixed, post
529 bloom situation with high downward POC flux towards the south (Figure 5).
530 The present study shows that there are two possible mechanisms of a considerable downward
531 POC flux in Arctic pelagic ecosystems; one coupled to the ice edge phytoplankton bloom and
532 another one, which is linked to an ice-free, weakly stratified water column. Re-occurring
533 strong winds may here induce deep-mixing below the nitracline during the productive
534 summer season, stimulate primary production and enhance the biomass sedimentation. In a
535 perspective of climate warming, these results indicate that the downward POC flux not

necessarily ceases if sea ice declines and ice edge phytoplankton blooms are restricted to smaller areas, because an enhanced downward POC flux may also take place in weakly stratified ice-free Arctic regions, where strong winds induce an upward nitrate flux. However, a warming Arctic climate will most likely also strengthens thermal warming of the surface layers during summer [*Wassmann and Reigstad*, 2011] and impact stratification in the water column. This factor has not been regarded in the present study, but needs further attention in the future.

Acknowledgements

We thank the captain and the crew of the R/V "Helmer Hanssen" for practical support during the field work. Sigrid Øygaarden, Christian Wexels Riser and Camilla Svensen helped with field and laboratory work and this was highly appreciated. The present work is a part of the Conflux project, funded by Tromsø Forskningsstiftelse, but also financially supported by the CarbonBridge project (Norwegian Research Council, no. 226415). A. Sundfjords's participation was partially funded by the Center of Ice, Climate and Ecosystem (ICE) at the Norwegian Polar Institute.

Literature

Andreassen, I. J., and P. Wassmann (1998), Vertical flux of phytoplankton and particulate biogenic matter in the marginal ice zone of the Barents Sea in May 1993, *Mar. Ecol. Prog. Ser.*, *170*, 1-14.

Arrigo, K. R., and G. L. van Dijken (in press), Continued increases in Arctic Ocean primary production, *Prog. Oceanogr.*, doi:10.1016/j.pocean.2015.05.002.

Bianchi, T. S. (2006), *Biochemistry of Estuaries*, Oxford University Press, Cary, USA.

Bienfang, P. K. (1981), Sinking rates of heterogeneous, temperate phytoplankton populations, *J. Plankton Res.*, *3*(2), 235-253, doi:10.1093/plankt/3.2.235.

Bienfang, P. K., P. J. Harrison, and L. M. Quarmby (1982), Sinking rate response to depletion of nitrate, phosphate and silicate in four marine diatoms, *Mar. Biol.*, *67*(3), 295-302.

Blais, M., J.-É. Tremblay, A. D. Jungblut, J. Gagnon, J. Martin, M. Thaler, and C. Lovejoy (2012), Nitrogen fixation and identification of potential diazotrophs in the Canadian Arctic, *Global Biogeochem. Cy.*, *26*(3), GB3022, doi:10.1029/2011GB004096.

Brainerd, K. E., and M. C. Gregg (1995), Surface mixed and mixing layer depths, *Deep-Sea Res. I*, *42*(9), 1521-1543, doi:10.1016/0967-0637(95)00068-H.

Carmack, E., and P. Wassmann (2006), Food webs and physical–biological coupling on pan-Arctic shelves: Unifying concepts and comprehensive perspectives, *Prog. Oceanogr.*, *71*(2–4), 446-477, doi:10.1016/j.pocean.2006.10.004.

Collos, Y. (1987), Calculations of ^{15}N uptake rates by phytoplankton assimilating one or several nitrogen sources, *Int. J. Radiat. Appl. Instrum. Part A.*, *38*(4), 275-282, doi:10.1016/0883-2889(87)90038-4.

Coppola, L., M. Roy-Barman, P. Wassmann, S. Mulsow, and C. Jeandel (2002), Calibration of sediment traps and particulate organic carbon export using ^{234}Th in the Barents Sea, *Mar. Chem.*, *80*(1), 11-26, doi:10.1016/S0304-4203(02)00071-3.

Eilertsen, H. C. (1993), Spring blooms and stratification, *Nature*, *363*(6424), 24-24, doi:10.1038/363024a0.

Eppley, R. W., R. W. Holmes, and J. D. H. Strickland (1967), Sinking rates of marine phytoplankton measured with a fluorometer, *J. Exp. Mar. Biol. Ecol.*, *1*(2), 191-208, doi:10.1016/0022-0981(67)90014-7.

Falk-Petersen, S., V. Pavlov, J. Berge, F. Cottier, K. Kovacs, and C. Lydersen (2015), At the rainbow's end: high productivity fueled by winter upwelling along an Arctic shelf, *Polar Biol.*, *38*(1), 5-11, doi:10.1007/s00300-014-1482-1.

Fer, I. (2006), Scaling turbulent dissipation in an Arctic fjord, *Deep-Sea Res. I*, *53*(1–2), 77-95, doi:10.1016/j.dsr2.2006.01.003.

Franks, P. J. S. (2014), Has Sverdrup's critical depth hypothesis been tested? Mixed layers vs. turbulent layers, *ICES J. Mar. Sci.*, 1-11, doi:10.1093/icesjms/fsu175.

Hegseth, E. N., and A. Sundfjord (2008), Intrusion and blooming of Atlantic phytoplankton species in the high Arctic, *J. Mar. Syst.*, *74*(1–2), 108-119, doi:10.1016/j.jmarsys.2007.11.011.

Hodal, H., and S. Kristiansen (2008), The importance of small-celled phytoplankton in spring blooms at the marginal ice zone in the northern Barents Sea, *Deep-Sea Res. II*, *55*(20–21), 2176-2185, doi:10.1016/j.dsr2.2008.05.012.

Holm-Hansen, O., and B. Riemann (1978), Chlorophyll *a* Determination: Improvements in Methodology, *Oikos*, *30*(3), 438-447, doi:10.2307/3543338.

IPCC (Ed.) (2013), *Climate Change 2013: The Physical Science Basis. Contribution of Working Group I to the Fifth Assessment Report of the Intergovernmental Panel on Climate Change*, 1535 pp., Cambridge University Press, Cambridge, United Kingdom and New York, NY, USA, doi:10.1017/CBO9781107415324.

Iversen, K. R., and L. Seuthe (2011), Seasonal microbial processes in a high-latitude fjord (Kongsfjorden, Svalbard): I. Heterotrophic bacteria, picoplankton and nanoflagellates, *Polar Biol.*, *34*(5), 731-749, doi:10.1007/s00300-010-0929-2.

Iversen, M. H., and H. Ploug (2013), Temperature effects on carbon-specific respiration rate and sinking velocity of diatom aggregates - potential implications for deep ocean export processes, *Biogeosciences*, *10*(6), 4073-4085, doi:10.5194/bg-10-4073-2013.

Johnson, K. S., and L. J. Coletti (2002), In situ ultraviolet spectrophotometry for high resolution and long-term monitoring of nitrate, bromide and bisulfide in the ocean, *Deep-Sea Res. I*, *49*(7), 1291-1305, doi:10.1016/S0967-0637(02)00020-1.

Kvingedal, B. (2005), Sea-Ice Extent and Variability in the Nordic Seas, 1967—2002, in *The Nordic Seas: An Integrated Perspective*, edited by H. Drange, T. Dokken, T. Furevik, R. Gerdes and W. Berger, pp. 39-49, American Geophysical Union, Washington, D. C.. doi:10.1029/158GM04.

Le Fouest, V., C. Postlethwaite, M. A. Morales Maqueda, S. Bélanger, and M. Babin (2011), On the role of tides and strong wind events in promoting summer primary production in the Barents Sea, *Cont. Shelf Res.*, *31*(17), 1869-1879, doi:10.1016/j.csr.2011.08.013.

Leu, E., J. E. Søreide, D. O. Hessen, S. Falk-Petersen, and J. Berge (2011), Consequences of changing sea-ice cover for primary and secondary producers in the European Arctic shelf seas: Timing, quantity, and quality, *Progr. Oceanogr.*, *90*(1–4), 18-32, doi:10.1016/j.pocean.2011.02.004.

Loeng, H. (1991), Features of the physical oceanographic conditions of the Barents Sea, *Polar Res.*, *10*(1), 5-18, doi:10.1111/j.1751-8369.1991.tb00630.x.

Louanchi, F., and R. G. Najjar (2001), Annual cycles of nutrients and oxygen in the upper layers of the North Atlantic Ocean, *Deep-Sea Res. II*, *48*(10), 2155-2171, doi:10.1016/S0967-0645(00)00185-5.

Mann, K., and J. Lazier (2006), *Dynamics of Marine Ecosystems: Biological-Physical Interactions in the Oceans, Third Edition*, Blackwell Publishing.

Marcel, B., A. Morel, and R. Gagnon (1994), An incubator designed for extensive and sensitive measurements of phytoplankton photosynthetic parameters, *Limnol. Oceanogr.*, *39*(3), 694-702, doi:10.4319/lo.1994.39.3.0694.

Martin, A. P., M. I. Lucas, S. C. Painter, R. Pidcock, H. Prandke, H. Prandke, and M. C. Stinchcombe (2010a), The supply of nutrients due to vertical turbulent mixing: A study at the Porcupine Abyssal Plain study site in the northeast Atlantic, *Deep-Sea Res. II*, *57*(15), 1293-1302, doi:10.1016/j.dsr2.2010.01.006.

Martin, J., J.-É. Tremblay, J. Gagnon, G. Tremblay, A. Lapoussiére, C. Jose, M. Poulin, M. Gosselin, Y. Gratton, and C. Michel (2010b), Prevalence, structure and properties of subsurface chlorophyll maxima in Canadian Arctic waters, *Mar. Ecol. Prog. Ser.*, *412*, 69-84, doi:10.3354/meps08666.

Martin, T., M. Steele, and J. Zhang (2014), Seasonality and long-term trend of Arctic Ocean surface stress in a model, *J. Geophys. Res.-Oceans*, *119*(3), 1723-1738, doi:10.1002/2013JC009425.

Moum, J. N. (1996), Efficiency of mixing in the main thermocline, *J. Geophys. Res.*, *101*(C5), 12057-12069, doi:10.1029/96JC00508.

Olli, K., C. W. Rieser, P. Wassmann, T. Ratkova, E. Arashkevich, and A. Pasternak (2002), Seasonal variation in vertical flux of biogenic matter in the marginal ice zone and the central Barents Sea, *J. Mar. Syst.*, *38*, 189-204, doi:10.1016/S0924-7963(02)00177-X

Osborn, T. R. (1980), Estimates of the Local Rate of Vertical Diffusion from Dissipation Measurements, *J. Phys. Oceanogr.*, *10*(1), 83-89, doi:10.1175/1520-0485(1980)010<0083:EOTLRO>2.0.CO;2.

683 Painter, S. C., S. A. Henson, A. Forryan, S. Steigenberger, J. Klar, M. C. Stinchcombe, N. Rogan, A.
684 R. Baker, E. P. Achterberg, and C. M. Moore (2014), An assessment of the vertical diffusive flux of
685 iron and other nutrients to the surface waters of the subpolar North Atlantic Ocean, *Biogeosciences*,
686 *11*(8), 2113-2130, doi:10.5194/bg-11-2113-2014.
687
688 Platt, T., C. L. Gallegos, and W. G. Harrison (1980), Photoinhibition of photosynthesis in natural
689 assemblages of marine phytoplankton, *J. Mar. Res.*, *38*, 687-701.
690
691 Prandke, H., and A. Stips (1998), Test measurements with an operational microstructure-turbulence
692 profiler: Detection limit of dissipation rates, *Aquat. Sci.*, *60*(3), 191-209, doi:10.1007/s000270050036.
693
694 Rainville, L., C. M. Lee, and R. A. Woodgate (2011), Impact of wind-driven mixing in the Arctic
695 Ocean, *Oceanography*, *24*(3), 136, doi:10.5670/oceanog.2011.65.
696
697 Randelhoff, A., A. Sundfjord, and M. Reigstad (2015), Seasonal variability and fluxes of nitrate in the
698 surface waters over the Arctic shelf slope, *Geophys. Res. Lett.*, *42*(9), 3442-3449,
699 doi:10.1002/2015GL063655.
700
701 Redfield, A. C. (1934), On the proportion of organic derivates in sea water and their relation to the
702 composition of plankton, in *James Johnstone Memorial Volume*, edited, pp. 177-192, Liverpool
703 University Press, Liverpool.
704
705 Redfield, A. C. (1958), The biological control of chemical factors in the environment, *Am. Sci.*, *46*(3),
706 205-221.
707
708 Reigstad, M., and P. Wassmann (2007), Does *Phaeocystis* spp. contribute significantly to vertical
709 export of organic carbon?, *Biogeochemistry*, *83*(1-3), 217-234, doi:10.1007/s10533-007-9093-3.
710
711 Reigstad, M., C. W. Riser, P. Wassmann, and T. Ratkova (2008), Vertical export of particulate organic
712 carbon: Attenuation, composition and loss rates in the northern Barents Sea, *Deep-Sea Res. II*, *55*,
713 2308-2319, doi:10.1016/j.dsr2.2008.05.007.
714
715 Reigstad, M., P. Wassmann, C. Wexels Riser, S. Øygarden, and F. Rey (2002), Variations in
716 hydrography, nutrients and chlorophyll a in the marginal ice-zone and the central Barents Sea, *J. Mar.*
717 *Syst.*, *38*(1–2), 9-29, doi:10.1016/S0924-7963(02)00167-7.
718
719 Sakshaug, E., and D. Slagstad (1992), Sea ice and wind: Effects on primary productivity in the Barents
720 Sea, *Atmos. Ocean*, *30*(4), 579-591.
721
722 Sakshaug, E., S. Kristiansen, and E. Syvertsen (1991), Planktonalger, in *Økosystem Barentshav*, edited
723 by E. Sakshaug, A. Bjørge, F. Gulliksen, H. Loeng and F. Melhum, Universitetsforlaget, Oslo.
724
725 Sakshaug, E., G. Johnsen, S. Kristiansen, C. von Quillfeldt, F. Rey, D. Slagstad, and F. Thingstad
726 (2009), Phytoplankton and primary production, in *Ecosystem Barents Sea*, edited by E. Sakshaug, G.
727 Johnsen and K. Kovacs, pp. 167-208, Tapir Academic Press, Trondheim, Norway.
728
729 Sambrotto, R. N., H. J. Niebauer, J. J. Goering, and R. L. Iverson (1986), Relationships among vertical
730 mixing, nitrate uptake, and phytoplankton growth during the spring bloom in the southeast Bering Sea
731 middle shelf, *Cont. Shelf Res.*, *5*(1–2), 161-198, doi:10.1016/0278-4343(86)90014-2.
732
733 Sharples, J., J. F. Tweddle, J. Mattias Green, M. R. Palmer, Y.-N. Kim, A. E. Hickman, P. M.
734 Holligan, C. M. Moore, T. P. Rippeth, and J. H. Simpson (2007), Spring-neap modulation of internal
735 tide mixing and vertical nitrate fluxes at a shelf edge in summer, *Limnol. Oceanogr*, *52*(5), 1735-1747.
736

South, G. R., and A. Whittick (1987), *An Introduction to Phycology*, Wiley-Blackwell.

Sundfjord, A., I. Fer, Y. Kasajima, and H. Svendsen (2007), Observations of turbulent mixing and hydrography in the marginal ice zone of the Barents Sea, *J. Geophys. Res.-Oceans*, *112*, C05008, doi:10.1029/2006JC003524.

Sundfjord, A., I. Ellingsen, D. Slagstad, and H. Svendsen (2008), Vertical mixing in the marginal ice zone of the northern Barents Sea—Results from numerical model experiments, *Deep-Sea Res. II*, *55*(20–21), 2154-2168, doi:10.1016/j.dsr2.2008.05.027.

Svensen, C., J. C. Nejstgaard, J. K. Egge, and P. Wassmann (2002), Pulsing versus constant supply of nutrients (N, P and Si): effect on phytoplankton, mesozooplankton and vertical flux of biogenic matter, *Sci. Mar.*, *66*(3), 189-203.

Townsend, D. W., M. D. Keller, M. E. Sieracki, and S. G. Ackleson (1992), Spring phytoplankton blooms in the absence of vertical water column stratification, *Nature*, *360*(6399), 59-62, doi:10.1038/360059a0.

Tremblay, J.-É., and J. Gagnon (2009), The effects of irradiance and nutrient supply on the productivity of Arctic waters: a perspective on climate change, in *Influence of Climate Change on the Changing Arctic and Sub-Arctic Conditions*, edited by J. C. J. Nihoul and A. G. Kostianoy, pp. 73-93, Springer Netherlands, doi:10.1007/978-1-4020-9460-6_7.

Tremblay, J. É., S. Bélanger, D. G. Barber, M. Asplin, J. Martin, G. Darnis, L. Fortier, Y. Gratton, H. Link, P. Archambault, A. Sallon, C. Michel, W. J. Williams, B. Philippe, and M. Gosselin (2011), Climate forcing multiplies biological productivity in the coastal Arctic Ocean, *Geophys. Res. Lett.*, *38*(18), L18604, doi:10.1029/2011GL048825.

Turner, J. T., and J. G. Ferrante (1979), Zooplankton Fecal Pellets in Aquatic Ecosystems, *Bioscience*, *29*(11), 670-677, doi:10.2307/1307591.

Wassmann, P., and M. Reigstad (2011), Future Arctic Ocean seasonal ice zones and implications for pelagic-benthic coupling, *Oceanography*, *24*(3), 220-231, doi:10.6570/oceanog.2011.74.

Wassmann, P., T. Ratkova, I. Andreassen, M. Vernet, G. Pedersen, and F. Rey (1999), Spring Bloom Development in the Marginal Ice Zone and the Central Barents Sea, *Mar. Ecol. , 20*(3-4), 321-346, doi:10.1046/j.1439-0485.1999.2034081.x.

Wexels Riser, C., P. Wassmann, M. Reigstad, and L. Seuthe (2008), Vertical flux regulation by zooplankton in the northern Barents Sea during Arctic spring, *Deep-Sea Res. II*, *55*(20–21), 2320-2329, doi:10.1016/j.dsr2.2008.05.006.

Wexels Riser, C., M. Reigstad, P. Wassmann, E. Arashkevich, and S. Falk-Petersen (2007), Export or retention? Copepod abundance, faecal pellet production and vertical flux in the marginal ice zone through snap shots from the northern Barents Sea, *Polar Biol.*, *30*(6), 719-730, doi:10.1007/s00300-006-0229-z.

Wiedmann, I., M. Reigstad, A. Sundfjord, and S. Basedow (2014), Potential drivers of sinking particle's size spectra and vertical flux of particulate organic carbon (POC): Turbulence, phytoplankton, and zooplankton, *J. Geophys. Res.-Oceans*, *119*(10), 6900-6917, doi:10.1002/2013JC009754.

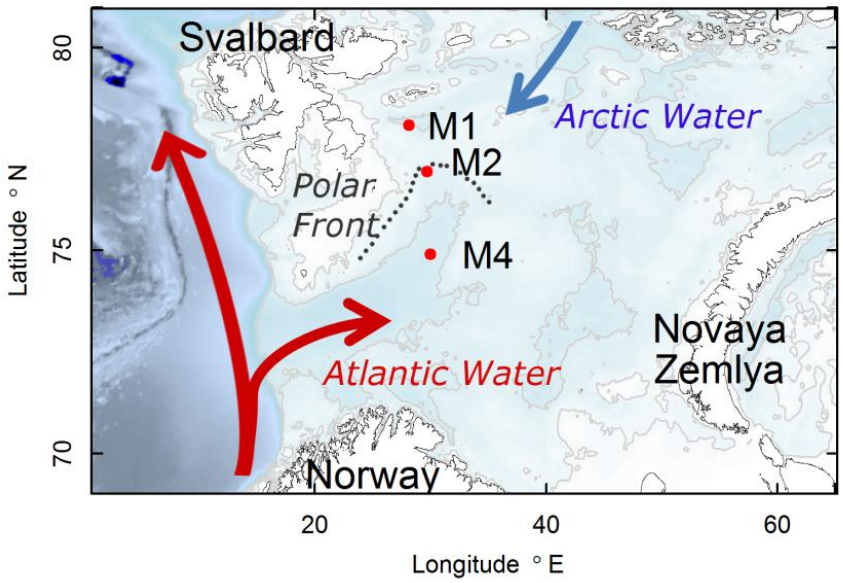

Figure 1: Map showing the Barents Sea with the three sampling stations (M1, M2, M4). Hydrography in the Barents Sea is influenced by Atlantic derived water (entering from the southwest) and Arctic derived water (entering from the northeast).

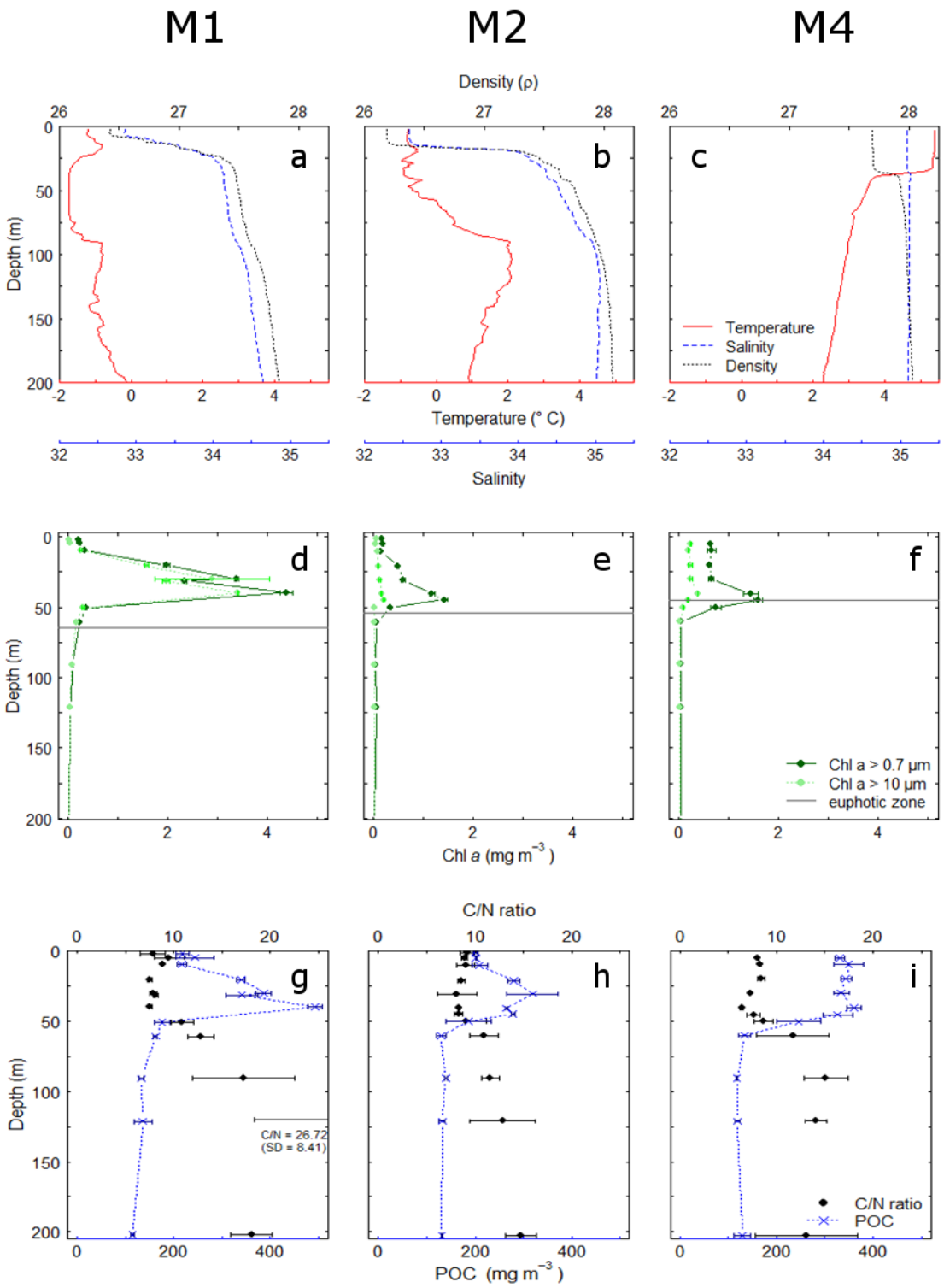

Figure 2: Hydrography with temperature (red line), salinity (blue stippled) and density black dotted) in upper panel (a, b, c), irradiance (grey line) and suspended chlorophyll *a* (Chl *a*, dark green: total Chl *a*, light green: > 10 µm) in middle panel (d, e, f) as well as suspended particulate organic carbon (POC) and atomic C/N ratio in the lower panel (g, h, i) of the upper 200 m at M1 (left column), M2 (middle column) and M4 (right column).

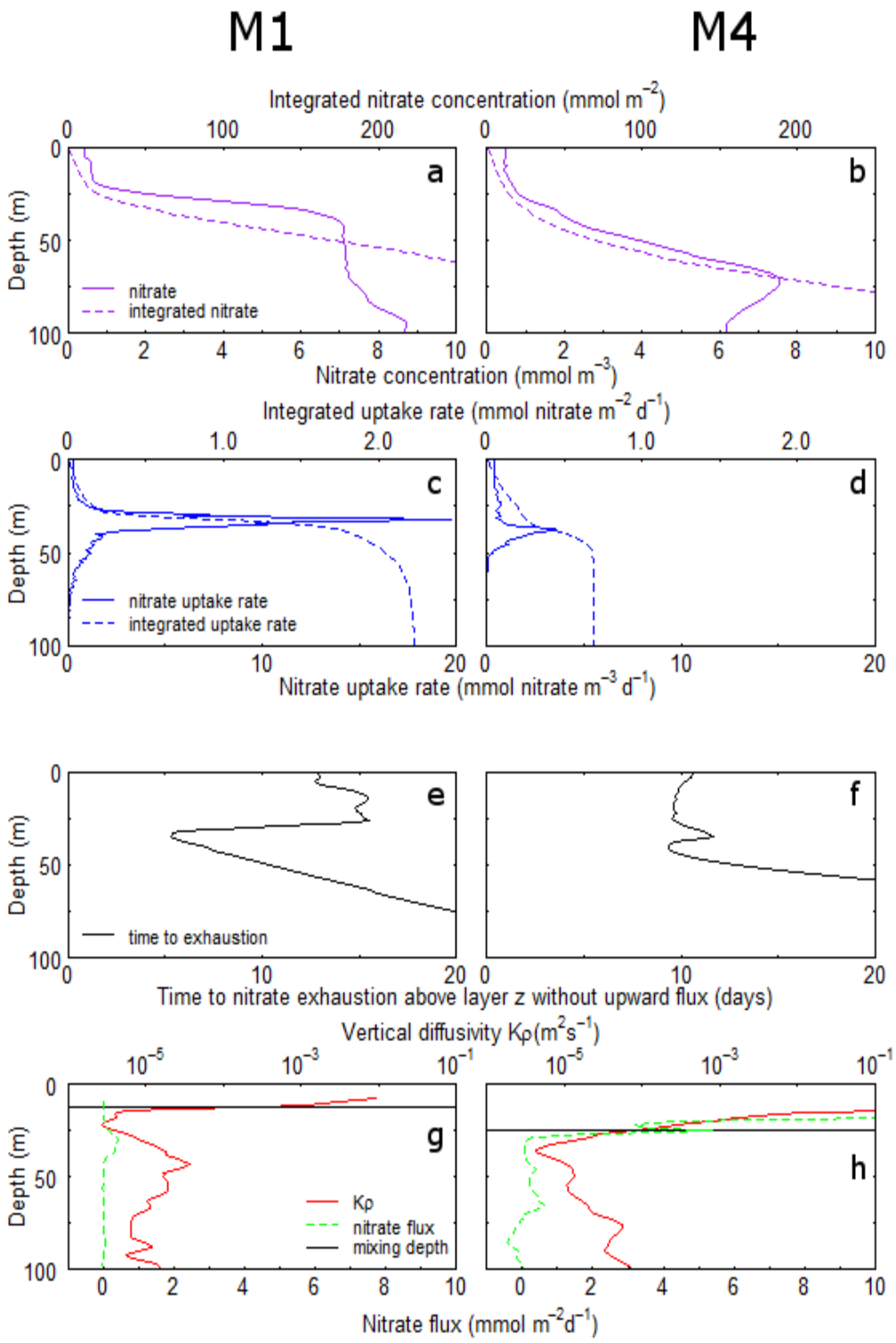

Figure 3: Nitrate concentrations (a, b; line: concentration, dotted: integrated concentration), nitrate uptake rate (c, d; line: uptake rate, dotted: integrated uptake rate), time to nitrate exhaustion (e, f) and vertical diffusivity (g, h, red line) and the upward nitrate flux (g, h, green dotted) in the upper 100 m of the water column at M1 (left column) and M4 (right column).

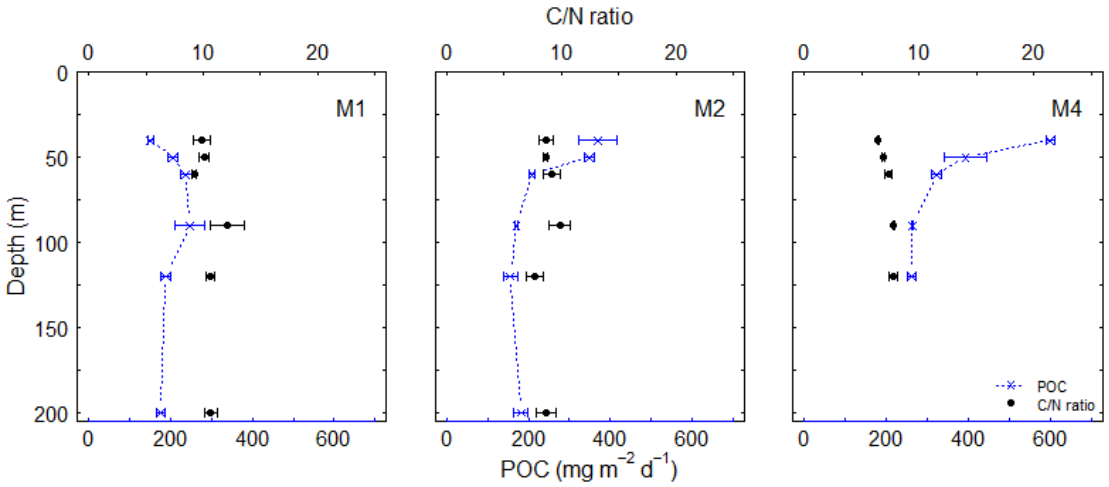

Figure 4: Vertical flux of particulate organic carbon (POC, blue crosses, bars indicating the standard deviation) and the C:N ratio of the sedimenting material (black dots, bars indicating the standard deviation) atM1 (left), M2 (middle) and M4 (right). The 200 m sample was not available for M4.

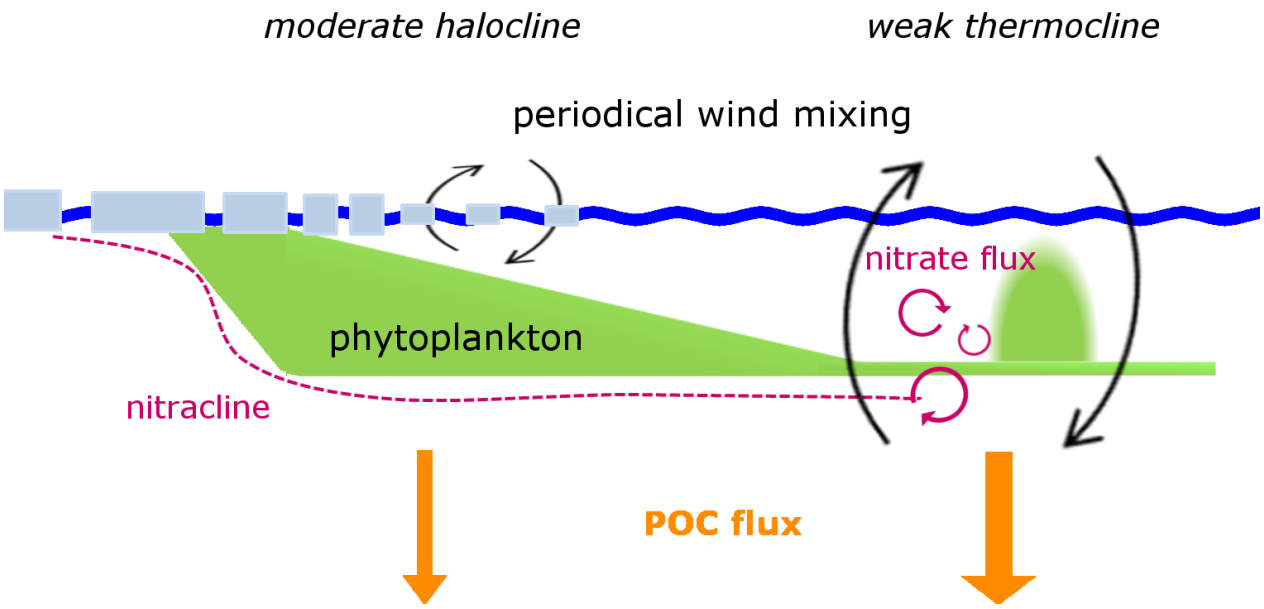

Figure 5: Conceptual model of the phytoplankton bloom in the marginal ice zone and the associated downward flux of particulate organic carbon (POC). Figure modified from a model developed by *Sakshaug et al*., [1991] and *Sakshaug et al*., [2009] for the Barents Sea. Model was extended to include upward nitrate flux and downward POC flux events associated with the periodical wind-induced deep-mixing.

Table 1: Station identity and sampling schedule.

	Position	Date	Depth (m)	Ice cover	Chl *a* max (m)	Suspended sampling (UTC)[1]	Deployment trap array (UTC)[2]	Deploy-ment time (d)
M1	78.0973°N, 28.1258°E	22 June 2011	278	Very Open Drift Ice (30%)	31	16:45	23:30	0.85
M2	76.9493°N, 29.7117°E	24 June 2011	235	Very Open Drift Ice (20%)	44	07:46	16:15	0.94
M4	74.9107°N, 30.0033°E	27 June 2011	371	Open Water	45	09:11	16:55	0.98

[1]sampled parameters: chlorophyll *a* (Chl *a*), particulate organic carbon (POC) and nitrogen (PON); 1, 5, 10, 20, 30, 40, 50, 60, 90, 120, 200 m and Chl *a* maximum

[2]sampled parameters: POC and PON: 40, 50, 60, 90, 120, 200 m

Table 2: Compilation of the integrated nitrate stock in different biological interesting layers and the upward nitrate flux into these layers. See section 2.4 for an explanation of the calculations. SCM: subsurface chlorophyll *a* maximum.

	Depth interval	Nitrate stock in the layer (mmol m^{-2})	Upward nitrate flux into the base of the layer (mmol m^{-2} d^{-1})	% input from below (d^{-1})	Time to nitrate exhaustion (no upward nitrate flux) (d)	Time to nitrate exhaustion (with upward nitrate flux) (d)
M1						
Nitrate < 1 mmol m^{-3}	0-21 m	13.1	0.046	0.4	15	
Above SCM	0-40 m	99.8	0.068	0.1	16	
Euphotic zone	0-65 m	277.9	0.008	0.0	9	
Mixed layer	0-23 m	15.7	0.063	0.4	15	
Mixing layer	0-13 m	7.3	0.004	0.0	15	16[1], 45[2]
M4						
Nitrate < 1 mmol m^{-3}	0-27 m	16.3	1.948	12.0	10	
Above SCM	0-45 m	52.1	0.340	0.7	10	
Euphotic zone	0-45 m	52.1	0.340	0.7	10	
Mixed layer	0-38 m	34.2	0.108	0.3	10	
Mixing layer	0-25 m	14.4	5.395	37.4	10	16[3], 21[4], 25[5]

(1) constant upward nitrate flux 0.004 mmol m^{-2} d^{-1}
(2) nitrate upward flux 0.004 mmol m^{-2} d^{-1} for 5 days, then constant upward nitrate flux of 0.350 mmol m^{-2} d^{-1}
(3) nitrate upward flux of 5.395 mmol m^{-2} d^{-1} for 1 day, then constant upward nitrate flux of 0.300 mmol m^{-2} d^{-1}
(4) nitrate upward flux of 5.395 mmol m^{-2} d^{-1} for 2 days, then constant upward nitrate flux of 0.300 mmol m^{-2} d^{-1}
(5) nitrate upward flux of 5.395 mmol m^{-2} d^{-1} for 3 days, then constant upward nitrate flux of 0.300 mmol m^{-2} d^{-1}

Paper III

Wiedmann I, Reigstad M, Marquardt M, Vader A, Gabrielsen T M

Seasonality of vertical flux and sinking particle characteristics in an ice-free high Arctic fjord – different from sub-Arctic fjords?

Submitted after revision to *Journal of Marine Systems*.

Seasonality of vertical flux and sinking particle characteristics in an ice-free high Arctic fjord – different from sub-Arctic fjords?

Ingrid Wiedmann (1)
Marit Reigstad (1)
Miriam Marquardt (1, 2)
Anna Vader (2)
Tove M. Gabrielsen (2)

(1) UiT The Arctic University of Norway, Breivika, 9037 Tromsø, Norway
(2) The University Centre in Svalbard (UNIS), 9171 Longyearbyen, Norway

Corresponding author:
Ingrid Wiedmann
UiT The Arctic University of Norway
9037 Tromsø
Norway
Email: Ingrid.Wiedmann@uit.no
Tel.: 0047 776 44214

Abstract

Seasonality in plankton dynamics is strongly affected by sea ice cover and light regime in the Arctic. The Arctic Adventfjorden (78 °N, 15 °E, western Svalbard) was previously seasonally ice-covered, but has tended to be ice-free since 2007. It may accordingly serve as a model area to study the vertical flux in a year-round ice-free Arctic fjord. We investigated (1) how the vertical flux of organic matter follows the seasonal pattern of suspended material, (2) how sinking particles' characteristics change with seasons and are linked to the vertical flux, and (3) if the vertical flux in an Arctic but ice-free fjord with a major glacial run-off during autumn is comparable to boreal and sub-Arctic ice-free fjords. We conducted seven field samplings between December 2011 and September 2012, measuring the suspended biomass (chlorophyll *a*, particulate organic carbon) at 5, 15, 25 and 60 m and the vertical biomass flux (short-term sediment traps for 24 h; 20, 30, 40, 60 m). Sediment traps modified with gel-filled jars were deployed to study sinking particles' characteristics (size and frequency distribution, particle type). The resuspension from the seafloor by winter wind mixing and thermal convection resulted in large, detrital sinking particles. Intense biomass sedimentation (fresh to little degraded biomass) was found during the early spring bloom but diminished toward the late bloom phase. The highest flux of particulate organic carbon (POC) was found during autumn (770-1530 mg POC m^{-2} d^{-1}), when sediment loaded glacial run-off and high pteropod abundances were observed. The vertical carbon flux in the Arctic Adventfjorden appears to resemble sub-Arctic fjords during winter and spring, but during autumn, a pulsed major POC flux may be induced by glacial run-off.

(277 words)

Keywords

- Gel trap
- Particulate organic carbon (POC)
- Particle size spectra
- Aggregate
- Detritus
- Glacial run-off

Highlights

- Ice-free Adventfjorden resembled sub-Arctic fjords during winter and spring
- Two major annual sedimentation events in ice-free Adventfjorden, Svalbard
- Highly variable POC: volume ratio due to different particle types and seasons
- High autumn POC flux associated with glacial run-off

1 Introduction

Strong seasonality in high latitude marine ecosystems generates an oscillating annual pattern of nutrient concentrations as well as phytoplankton and zooplankton abundance throughout the year (Leu et al., 2011; Rat'kova and Wassmann, 2002; Węsławski et al., 1991). This, in turn, is presumed to determine the quality and intensity of the vertical biomass flux (De La Rocha and Passow, 2007; Peinert et al., 1989; Wassmann et al., 1991), but few field studies thus far have examined how sinking particles' characteristics change with seasons and how they may be linked to the vertical carbon flux during different seasons (e.g., Mackenzie Shelf, Forest et al., 2013).

It has been postulated that fjords are areas of enhanced organic carbon sequestration (Smith et al., 2015). The major vehicle of the vertical carbon flux are algal aggregates, fecal pellets detritus and marine snow, i.e. conglomerates (> 0.5 mm) of diverse composition and structure (Alldredge and Silver, 1988).

Ice algae tend to form blooms in seasonally ice-covered fjords in April-May (Ji et al., 2013; Leu et al., 2011). Heterotrophs, such as the copepod *Calanus glacialis*, utilize these blooms (Søreide et al., 2010; Weydmann et al., 2013), but ice algal biomass also contributes to the vertical export, when the cells are released into the water column during ice break-up (Arrigo, 2014; Tremblay et al., 1989).

Phytoplankton spring blooms occur in ice-free fjords in April and May and in seasonally ice-covered fjords subsequent to the ice break-up (Eilertsen and Frantzen, 2007; Leu et al., 2011). Diatoms, a prominent spring bloom taxon in high latitudes, can cause major biomass sedimentation (Thompson et al., 2008; Wassmann et al., 1991). Their senescent cells and resting stages have high sinking velocities (Rynearson et al., 2013; Smayda, 1971), and some taxa release sticky exopolymeric substances, which contribute to the formation of algal aggregates (Kiørboe et al., 1994; Thornton, 2002) and marine snow (Alldredge and Silver, 1988; Lampitt, 2001). Coagulation of single cells into aggregates or marine snow increases the particle size, which, in turn, enhances the sinking velocity and the vertical export of organic carbon.

However, the prymnesiophyte *Phaeocystis pouchetii* can also dominate the phytoplankton blooms in the Barents Sea and the waters around Svalbard (Degerlund and Eilertsen, 2010). This small flagellate has a low sinking velocity, and high cell abundances of this species appear to diminish the vertical carbon flux below 60 m (Reigstad and Wassmann, 2007; Reigstad et al., 2000).

Irrespective of the phytoplankton composition, an enhanced vertical carbon flux only occurs, when the zooplankton community in the fjords executes a weak top-down regulation, allowing sinking of ungrazed biomass. Top-down regulation by zooplankton reduces the vertical biomass flux by grazing and some taxa, such as copepods, also fragment sinking particles into smaller, slowly sinking material (Noji et al., 1991; Svensen et al., 2012). Alternatively, copepods and krill also enhance the vertical carbon flux by re-packaging small particles into fast sinking fecal pellets (Turner, 2002; Turner, 2015; Wexels Riser et al., 2008).

Glacial run-off entrains lithogenic material with a high specific weight. When sinking particles 'scavenge' this material, the sinking velocity of the organic material increases and enhances the vertical biomass flux (Passow and De La Rocha, 2006).

In the present study, we conducted a nine-month field study in the Arctic Adventfjorden (78 °N, 15 °E, Fig. 1), western Svalbard. Previously, the fjord was seasonally ice-covered, but it has mostly been ice-free since 2007 (www.met.no). Adventfjorden may therefore serve as a model area to study the mechanisms of vertical flux in an ice-free, but glacially influenced Arctic fjord. Our aim was to investigate: (1) how the vertical flux of organic matter follows the seasonal pattern of suspended material; (2) how sinking particles' characteristics change with season and are linked to the vertical flux, and (3) if the vertical flux in an ice-free Arctic fjord with a major glacial run-off during autumn, is comparable the vertical flux in boreal and sub-Arctic ice-free fjords.

2 Materials and methods

2.1 Study site and sampling program

The present study was conducted at station IsA (Isfjorden-Adventfjorden, 78 ° 15.67' N, 15 ° 32.10' E, Fig. 1) in the mouth of the Arctic Adventfjorden. Adventfjorden is a ~8 km long, 3.5 km wide and < 100 m deep side branch of Isfjorden, a large fjord system on the western coast of Svalbard. Neither Isfjorden nor Adventfjorden has a sill at the fjord-mouth, and they are therefore exposed to advection from the Atlantic-influenced West Spitsbergen Current. Warmer and more saline water from this current reached the study site (~50 km from the open coast) and allowed year-round ship-based sampling in ice-free waters. Glacial run-off (Advent River, Longyear River, Fig. 1) affected IsA during the summer and autumn with substantial

amounts of sediment-loaded melt water (e.g. $9*10^6$ m^{-3} during September, Węsławski et al., 1999).

Field investigations were conducted throughout nine months, starting 14.12.2011 and ending 19.09.2012. We refer to the winter sampling days in December, mid-January and late January as Winter I, Winter II and Winter III, respectively (Table 1). Spring sampling days in late April, mid-May and late May are denoted as Spring I, Spring II and Spring III, respectively, and the mid-September sampling is denoted as Autumn I (Table 1).

2.2 Hydrography, light and wind data

Hydrographical data included temperature and salinity measurements by a CTD (SD204, SAIV A/S, Bergen, Norway) and subsequent computation of the potential density. The seasonal light cycle at 78 °N includes the polar night from mid-November to late January. The sun is below the horizon from early October to early March, and the midnight sun appears between mid-April to late August. The underwater irradiance was quantified using a hand-held LI-1000 Data Logger (Li-COR, Nebraska, USA), and the euphotic zone was defined as the layer of > 1 % surface irradiance. Boat drift due to strong wind events made vertical deployment of the irradiance logger difficult, and an overestimation of the euphotic zone may be assumed. Wind data from Longyearbyen airport (78 ° 14' N, 15 ° 28' E, Fig. 1) is considered to be representative for the IsA station and were downloaded from the Norwegian Meteorological Institute (www.eklima.met.no).

2.3 Suspended biomass (Chl *a*, POC, PON)

Sea water samples were collected at 5, 15, 25 and 60 m with a 10 L Niskin bottle, transferred into carboys, and stored dark and cool until filtration within a few hours (Table 1). Triplicates of 250-400 mL were vacuum-filtered on Whatman GF/F filters for analysis of the Chl *a* concentration. Filters were frozen in liquid nitrogen or at -80 °C until analysis within nine months. Some pigment break-down resulting from the storage period may be assumed (Mantoura et al., 1997). Chl *a* was extracted 20-24 h in 10 mL methanol (darkness, +4 °C) and concentrations were then measured in a Turner Design AU-10 fluorometer (calibrated with Chl *a*, Sigma S6144). For POC and PON analysis, triplicate subsamples (300-500 mL) were filtered on pre-combusted Whatman GF/F filters, stored at -20 °C and analyzed within 2.5 years on a Leeman Lab CHN Analyzer following the procedures described in Reigstad et al. (2008).

2.4 Vertical flux characterization (Chl *a*, POC, particle size spectra)

An anchored short-term sediment trap array was used to study the vertical flux of particulate material at IsA (Table 1). Paired trap cylinders (KC Denmark, d= 7.2 cm, 45 cm high, no bafflers or poison) were mounted at 20, 30, 40 and 60 m and deployed for ca. 24 h (Table 1). In this way, we collected particles sinking out from the lower eutrophic zone and below it (Table 1), and we minimized the sampling of re-suspended material from the seafloor (~80 m).

After the trap array recovery water from one of the paired cylinders per depth was transferred into carboys. Sub-samples were filtered to determine the vertical flux of Chl *a* and POC as described above for the suspended samples (duplicates or triplicates of 150-400 mL for Chl *a*, duplicates or triplicates of 250-500 mL for POC). The second trap cylinder at each depth was modified with a gel-containing glass jar, fitting perfectly inside the trap cylinder (conceptual idea by Lundsgaard et al., 1999; modification from polyacrylamide to commercially available unpoisonous gels by Thiele et al., 2015 and Wiedmann et al., 2014) to study the vertical flux of particles $\geq$ 50 µm ESD_{image} (estimated spherical diameter determined from images) by an image analysis (concept by Ebersbach and Trull, 2008; Wiedmann et al., 2014). The threshold function of ImageJ (AutoThresholding following Otsu clustering algorithm, Otsu, 1979) was applied to establish a border between the particle and background in the 8-bit grey converted images. Particles < 50 µm ESD_{image} were excluded due to abundance underestimation (Jackson et al., 1997; Jackson et al., 2005). The remaining particles were binned in 20 bins from 0.050 mm to 5.080 mm ESD_{image} (Table A.1) and an ellipsoidal particle shape was assumed to estimate the particle volume (Wiedmann et al., 2014). The sediment trap deployment time was adjusted for the season (Table 1). During Winter I-III, we deployed the traps for ~24 h. During spring and autumn, the trap array was first deployed for ~24 h to determine the biogeochemical flux, and then for ~2 h to study the particle flux using gel-modified cylinders (short deployment prevented particle overload in the gels).

2.5 Calculation of the loss rate and sinking velocity

The loss rate can be expressed as the ratio of the vertical flux (POC, Chl *a* at depth z) to the integrated suspended biomass (POC, Chl *a* above depth z). For the calculation of loss rates, the integrated suspended biomass was estimated by trapezoidal integration. Similarly, the average sinking velocity was expressed by the ratio of the vertical flux (mg m^{-2} d^{-1}) to the suspended biomass (mg m^{-3}) at depth z (Kiørboe et al., 1994).

3 Results

3.1 Hydrography, light regime and wind

The hydrographic environment at station IsA (Fig. 2) reflected the seasonal pattern of the region. Cooling of the entire water column took place until mid-January, when warmer, denser and more saline water from the West Spitsbergen Current was advected to the station area. Another cooling period took place in April, and resulted in low water temperatures that persisted throughout May (-0.5 to 1.0 °C). Thermal warming of the surface layers started in June, and maximum surface water temperatures were reached in late August, co-occurring with enhanced glacial melt water run-off and a freshening of the surface water layers (23.8.2012: maximum water temperature 6.4 °C, minimum salinity 31.5). Low air temperatures cooled the surface waters from September onward, while deeper water layers in the fjord were still warm until late October (< 4.1 °C, Fig. 2). As glacial run-off ceased during autumn, the surface salinity increased (Fig. 2). Light was measured from 8.3.2012 onwards, when the sun rose above the horizon. Irradiance measurements indicated an euphotic zone ranging down to 20-40 m (Table 1), with the exception of a very shallow euphotic zone of 8 m on 6.7.2012. Wind data from Longyearbyen airport (Fig. 1) showed a prevailing wind direction "out of Adventfjorden" (6 of 7 sampling periods had a wind direction of E-SSW, data not shown). The opposite wind direction ("into Adventfjorden") was only observed during Spring III.

3.2 Suspended biomass (Chl *a*, POC) and its C/N ratio

The temporal high-frequency sampling of the suspended biomass parameters Chl *a* and POC showed clear seasonal patterns (Fig. 2). The Chl *a* and POC concentrations were both low during winter, increased and peaked during the spring period (late April to end of May) and showed a decreasing trend throughout summer and autumn. These data provided a seasonal framework for our seven sampling events and indicated that Winter I-III, Spring I-III and Autumn I (Fig. 2, blue lines) were typical representatives for seasonal scenarios with low, high and intermediate suspended Chl *a* and POC concentrations, respectively. However, the vertical distribution of the suspended biomass during the sampling events (Fig. 3) indicated that there was also a distinct trend in the suspended biomass during the spring bloom.

A seasonal trend was also observed in the quality of the particulate organic material reflected through (atomic) C/N ratios. Fresh material of algal origin is expected to reflect the Redfield ratio (C/N = 6.6). During Winter II and III, C/N ratios of 8.3-12.1 indicated that the biomass in the water column consisted of partly degraded material or a mixture of fresh marine

material and biomass from terrestrial origin (terrestrial material C/ N > 17, Bianchi, 2006). Fresh organic material prevailed during Spring I-III, as indicated by C/N ratios close to the Redfield ratio. During Autumn I, C/N ratios of 8.5-10.5 indicated again either degraded marine material or a mixture of terrestrial and fresh marine material.

3.3 Vertical biomass flux (Chl *a*, POC) and its C/N ratio

The vertical flux patterns of Chl *a* and POC reflected a seasonality, partly matching the observations for the suspended material. During Winter I-III, vertical Chl *a* and POC flux were relatively low, with 90-140 mg POC m^{-2} d^{-1} and < 0.26 mg Chl *a* m^{-2} d^{-1} (Fig. 4), respectively, but indicated that biomass was sinking out during the polar night. The highest POC fluxes were measured during Winter II in the deepest traps, implying a resuspension event rather than sinking POC from the water column. The highest vertical Chl *a* fluxes were found during Spring I-II, and vertical POC fluxes also were high (>1000 mg POC m^{-2} d^{-1}). The maximum vertical POC flux (< 1500 mg POC m^{-2} d^{-1}) was found during Autumn I (Fig. 4). Generally, the loss rates of Chl *a* and POC were higher at 30 m than at 60 m (exception Winter III, Table 2). The sinking velocities, in contrast, were always higher at 60 m (Table 2). The highest POC loss rate (36 %) and sinking velocity (12 m d^{-1}) was found during Autumn I (Table 2). The C/N ratio of sinking material suggested the sedimentation of degraded material during Winter II-III and Autumn I (C/N ratio: 10-15). During Spring I-III, the sinking material had a C/N ratios similar to the suspended biomass (C/N ratio: 6-8, Table 3), suggesting a vertical flux of recently produced biomass.

3.4 Particle size and volume flux

Volume flux spectra (Fig. 5) provide information on the characteristics of sinking particles in the form of particle size (and volume) distribution and frequency. The area under the curve in the volume flux spectra corresponds to the total particle volume sinking out at a particular sampling date and depth. Our data show that the volume flux tended to be the highest at 60 m and lowest at 30 m (except during Spring III, with minimum at 20 m).

During Winter I, the largest particles were found in the 2.23 mm ESD_{image} size bin (Table A.1), and a total volume flux of 312-545*10^3 mm^{-3} m^{-2} d^{-1} was estimated for the different sediment trap depths (Fig. 5). Due to the ellipsoidal volume calculation (Wiedmann et al., 2014), the median size of the volume flux could not be given, as an ellipsoidal volume could not be converted back to one definite particle ESD_{image}. Thus, we can only state that medium and large sized particles (Fig. 5, Table A.1) contributed most to the volume flux at 30 m and

40 m during Winter I, while large particles were important at 20 m and 60 m. During Spring II, medium sized particles were important contributors to the vertical volume flux down to 40 m, but extra-large particles were also found at 60 m (4.56 mm ESD_{image} size bin). Accordingly, the volume flux spanned from 171 to 1,195*10^3 mm^{-3} m^{-2} d^{-1}. During Spring III, all of the particles were small to medium-sized and found in size bins ≤ 1.81 mm ESD_{image} (apart from one single particle at 20 m with 5.15 mm ESD_{image}), and the total volume flux was moderate with 640-736*10^3 mm^{-3} m^{-2} d^{-1} (Fig. 5). Autumn I was characterized by medium sized sinking particles (bins ≤ 1.44 mm ESD_{image}) at 20 m and 30 m. Extra-large particles (≤ 3.62 mm ESD_{image} size bin) were found at 40 and 60 m, where also the highest volume fluxes of the present study were estimated (2,148 and 6,189 *10^3 mm^{-3} m^{-2} d^{-1}, respectively, Fig. 5).

The semi-quantitative visual inspection of the gels indicated that fine, degraded detritus dominated the vertical flux during Winter I (Fig. 6). The material was accompanied by some individuals of the pteropod *Limacina* sp. (characterized as swimmers and not included in the vertical flux estimates). Detrital material was still observed in the gel deployed during Spring II, but phytoplankton aggregates were also found. Phytoplankton aggregates dominated the observed particles in the gels deployed during Spring III, but they occurred together with detritus and fecal pellets. During Autumn I, a mixture of aggregates (probably phytoplankton), fecal pellets and detritus prevailed in the gels, as well as a substantial number of *Limacina* sp. individuals (up to 138 at 20 m).

4 Discussion

Investigating the seasonality in vertical biomass flux and particle characteristics showed that some of the seasonal drivers, such as phytoplankton blooms, were similar in ice-free Arctic, sub-Arctic and boreal fjords. Glacial run-off impacted sinking particles' characteristics and provided an additional driver for the vertical carbon flux in the open Arctic Adventfjorden during the melting period.

4.1 Seasonal variation of suspended biomass in Adventfjorden – reflecting typical high latitude seasonality?

Adventfjorden, an Arctic fjord influenced by the Atlantic derived West Spitsbergen Current, showed a pronounced seasonal variation during the nine months covered by the present field study. The high frequency sampling program of hydrography and suspended biomass (Fig. 2)

297 placed our field studies within three distinct seasons - winter, spring and autumn. Each of the
298 investigation periods was categorized into one of these seasons, based on environmental and
299 ecological parameters.
300 Low irradiance and deep mixing processes (wind, thermal convection) during the polar night
301 causes light limitation and prevents production and built up of autotrophic biomass in high
302 latitudes. Therefore, our winter data (Fig. 2, 3) were typical for this season and corresponded
303 to previous observations of low biomass concentrations from Svalbard (Iversen and Seuthe,
304 2011; Zajączkowski et al., 2010), the Barents Sea (Olli et al., 2002) and northern Norway
305 (Eilertsen and Degerlund, 2010; Noji et al., 1993) during winter (Table 4).
306 The onset of the phytoplankton spring bloom took place in April in nutrient sufficient (4.5 µM
307 nitrate, Kubiszyn et al., in prep.), cold and non-stratified waters (Fig. 2), with a deep euphotic
308 zone (Table 1). This is a common situation in high latitude regions (Eilertsen, 1993;
309 Townsend et al., 1992). The early spring bloom phase has been associated with a high surface
310 concentration of phytoplankton due to low zooplankton abundances (North Atlantic: Parsons
311 and Lalli, 1988). Because we experienced this situation during Spring I in late April (Fig. 3,
312 low zooplankton abundance: ~$4*10^3$ ind. m^{-3}, E.I. Stübner, pers. comm.), the sampling period
313 was characterized as a typical representation of an early bloom.
314 Spring II in mid-May was classified as a peak bloom situation, based on high Chl *a*
315 concentrations (Fig. 2, 3). Nitrate concentrations were not depleted at 25 m, while silicate was
316 low (1.5 µM nitrate + nitrite, 0.3 µM silicate, Kubiszyn et al., in prep.). A typical spring
317 bloom phytoplankton mixture of the diatoms *Chaetoceros socialis* and *Thalassiosira*
318 *nordenskioeldii* prevailed together with the prymnesiophyte *Phaeocystis pouchetii* (Kubiszyn
319 et al., in prep.). These species represent a typical spring bloom community, as previously
320 described for northern Norway, the waters around Svalbard and the Barents Sea (Degerlund
321 and Eilertsen, 2010).
322 Nitrate is considered to be the primary limiting nutrient for primary production in the Arctic
323 (Tremblay and Gagnon, 2009), and was depleted at 25 m during Spring III in late May.
324 Additionally, silicate concentrations were still low (0.9 µM, Kubiszyn et al., in prep.). The
325 abundant and divers zooplankton community (ca. $20*10^3$ ind. m^{-3}) with 40-70 %
326 meroplanktonic nauplii and larvae (Stübner et al., submitted, E.I. Stübner pers. comm.) most
327 likely exerted a strong grazing pressure and top-down regulation on the phytoplankton,
328 restraining the suspended Chl *a* (Fig. 3). Accordingly, we classified Spring III in late May as a
329 late bloom stage.

Water-mass stratification broke down due to cooling before Autumn I in mid-September. Nutrients were replenished (2.6 µM nitrate, 2.5 µM silicate, Kubiszyn et al., in prep.), but no autumn bloom in the form of biomass build up was observed (Fig. 3). We do not have data on primary production and cannot evaluate if this was a result of low production or of high loss rates (e.g., grazing from moderately abundant zooplankton: ~7*10^3 ind. m^{-3}, Stübner et al., submitted). Autumn I was considered to be a typical representation of an autumn situation.

Zajączkowski et al. (2010) reported higher concentrations of suspended Chl *a* and POC from the innermost, shallow part of Adventfjorden (40 m, ~400 m to Advent River and Longyear River) than we found at IsA. This was probably caused by higher resuspension of previously sedimented allochthonous bottom material in the shallow innermost Adventfjorden (e.g., by thermal convection or tidal mixing, Zajączkowski et al., 2010; Zajączkowski and Włodarska-Kowalczuk, 2007). High C/N ratios (> 16) in their suspended material supports this assumption (Table 4).

Suspended biomass concentrations at IsA corresponded well with previous studies from the central Barents Sea (Olli et al., 2002), western Svalbard (Kongsfjorden, Iversen and Seuthe, 2011), northern Norway (Balsfjorden/ Malangen, Eilertsen and Degerlund, 2010; Ramfjorden, Noji et al., 1993; Balsfjorden, Reigstad and Wassmann, 1996; Malangen, Wassmann et al., 1996), western Norway (Fanafjorden, Wassmann, 1984) and Conception Bay, Canada (Thompson et al., 2008, Table 4). The variability in bloom magnitude reported in the literature (e.g., present study: 0.6-4.2 mg Chl *a* m^{-3}; Kongsfjorden, western Svalbard, Iversen and Seuthe, 2011: 0.2-10 mg Chl *a* m^{-3}) most likely reflected our coarser temporal sampling resolution, which may have missed the bloom maximum.

In conclusion, we assume that the seasonal variation of suspended biomass at IsA reflected the typical high latitude seasonality. The timing of the bloom in April/ May in the fjords seem to be comparable across latitudes from sub-Arctic to Arctic ice-free fjords, while bloom conditions in May were reported for the Barents Sea and Conception Bay, Canada (Olli et al., 2002; Thompson et al., 2008).

4.2 Seasonality of the vertical flux intensity (POC, Chl *a*) in Adventfjorden – congruent with other ice-free high latitude regions?

Vertical flux intensity is determined by the overlaying processes of hydrography, phytoplankton and zooplankton. Short-term sediment traps can be used to estimate the vertical Chl *a* and POC flux and give insight into sinking particles' characteristics and, in combination

with suspended biomass data, into the vertical flux regulation during the time of deployment. However, short-term traps deployed for ~24 h only give a snap-shot picture and cannot provide robust seasonal or annual flux patterns. A comparison with previous published data was conducted to evaluate if the vertical flux seasonality at IsA was comparable to the seasonal flux pattern of other ice-free high latitude regions.

Chl *a* and POC fluxes at IsA during winter were comparable to literature data from the innermost part of Adventfjorden (Zajączkowski et al., 2010), Ramfjorden (northern Norway, Noji et al., 1993), Fanafjorden (western Norway, Wassmann, 1984) and the open Barents Sea (Olli et al., 2002; Table 4). Some differences between the two studies in Adventfjorden (present study: 90-400 mg POC m^{-2} d^{-1}; Zajaczkowski et al., (2010): < 750 mg POC m^{-2} d^{-1}; Table 4) seem to reflect the resuspension of bottom material in the shallow parts of the fjord (as observed for the suspended material), and the C/N ratios of up to 25 in the sinking material clearly reflected terrestrial input (Zajączkowski et al., 2010).

Our strong pulses of vertical Chl *a* and POC flux during the spring exceeded previous measurements from the innermost Adventfjorden (Zajączkowski et al., 2010), Balsfjorden and Malangen (northern Norway, Keck and Wassmann, 1996; Reigstad and Wassmann, 1996; Reigstad et al., 2000), Fanafjorden (western Norway, Wassmann, 1984) and Conception Bay (Canada, Thompson et al., 2008; Table 4), but were comparable with fluxes found in the open Barents Sea (Olli et al., 2002; Table 4). We argue for a two-fold explanation of the decline in vertical biomass flux during the course of the spring bloom (Fig. 4). First, the intensifying top-down regulation by zooplankton probably reduced the vertical flux from Spring I to III (Fig. 4). Second, the observed shift in the phytoplankton bloom composition from diatom-dominated during Spring I to *Phaeocystis*-dominated during Spring III (Kubiszyn et al., in prep.) could impact the vertical flux. Diatoms are known to produce sticky exopolymeric substances, which promote aggregate formation and sinking (Kiørboe et al., 1990; Smetacek, 1985; Thornton, 2002). Because diatoms were also abundant in the sediment traps during Spring I (molecular 454-sequencing analysis, M. Marquardt, pers. com.), we suggest that they contributed to the higher vertical flux rates during early spring. The small celled flagellate *Phaeocystis pouchetii* dominated in the water column during Spring III (> 10^6 cells L^{-1}, Kubiszyn et al., in prep.) and *Phaeocystis pouchetii* was also identified in the IsA sediment traps down to 60 m (454-sequencing, M. Marquardt, pers. com.). However, literature indicates that this species contributes little to the vertical carbon flux at depth > 60 m, despite high suspended concentrations (Reigstad and Wassmann, 2007; Reigstad et al., 2000).

Our estimated bulk sinking velocities (Table 2) further pinpointed a slowing down of the vertical flux during the course of the bloom. This matches the argumentation on a shift from fast-sinking diatoms (Passow, 1991) to slow-sinking detritus, including *Phaeocystis* cells (Reigstad and Wassmann, 2007).

The interpretation of Autumn I data was complex. Glacial run-off occurs in Adventfjorden between June and September when air temperatures (> 0° C) allow snow and glacial melting on land (Węsławski et al., 1999). The tide- and wind-steered meandering glacial plume affected IsA at the surface (seen as reduced surface salinity in Fig. 2, Fig. A.1), but other impacting effects must also be assumed at depths. Our POC flux during Autumn I exceeded reported literature values up to 30-fold (Table 4) and was also higher than the flux observed during Spring I-III (Fig. 4). We suggest that this was linked to the glacial run-off.

Zajaczkowski et al. (2010) described an intense vertical flux of particulate inorganic and organic material (PIM and POM, respectively) in Adventfjorden during the summer melting period. Accordingly, we assume that entrained POM also enhanced the POC flux at IsA. This is bolstered by a high C/N ratio (up to 16, suggesting degraded re-suspended or terrestrial material) in the sinking material in both the present study (Table 3) and Zajączkowski et al. (2010).

Glacial melt water can form "fingers" of high concentration of suspended particulate matter, stretching several kilometers from the Advent River inlet into the fjord (Zajączkowski and Włodarska-Kowalczuk, 2007). We assume that this possibly promoted physical flocculation, a process in which unstable mineral particles, suspended in the entrained melt water, form aggregates with high sinking velocity (Kranck, 1973; Sutherland et al., 2015; Syvitski, 1980). The lithogenic material was probably also incooperated into aggregates and fecal pellets, and ballasted organic biomass due to its high specific sinking velocity (Iversen et al., 2010; Ploug et al., 2008) and increased the vertical POC flux.

The comparison with literature shows that the vertical Chl *a* and POC flux at IsA was congruent with the previously reported fluxes in other ice-free high latitude systems during winter and spring but was higher during autumn.

4.3 Sinking particles' characteristics during different seasons

Drivers of physical and biological particle aggregation (e.g., shear, cell abundance, stickiness, Kiørboe et al., 1994) and modification processes by grazers (Turner, 2002; Turner, 2015) affect sinking particles' characteristics, such as C/N ratio, size, and sinking velocity (De La

Rocha and Passow, 2007). Here, we discuss the characteristics of the sinking material at IsA during the different seasons and possible drivers.

In our study, the C/N ratio of sinking material matched well with the visual analysis (Table 3). Both implied the sedimentation of degenerated material in mid-December (Winter I) and recently produced material during mid-May and late May (Spring II and III, respectively, Table 3). A high C/N ratio, as found during Autumn I (Table 3), usually points toward strongly degraded material or terrestrial material, but the visual inspection (20 m and 30 m gels) suggested sinking of aggregates and fecal pellets (Table 3). We presume that the impact of the meandering glacial plume on IsA was highly variable. When the track of the plume covered IsA, the sinking material had a higher C/N ratio due to more terrestrial material when compared to a situation when the plume followed an alternative route, not hitting IsA. This explanation is supported by the high C/N ratios of the 24 h deployed traps (13.0-15.0, Table 3), but lower ones in the subsequently deployed 2 h gel traps (C/N ratio 6.5-8.8, fresh material observed on the gels, data not shown), as well as the high variability of salinity and density (Fig. A.1).

The average sinking velocity for total POC or Chl *a* biomass (Table 2) at IsA during winter and spring was comparable with the average velocities reported by Kiørboe et al. (1994) in the Danish Isefjorden (10 m), but was somewhat higher than rates at Nordvestbanken (off the Norwegian Shelf, 100 m, Andreassen et al., 1999). A direct comparison with particle sinking velocities estimated by Laurenceau-Cornec et al. (2015) or McDonnell and Buesseler (2010) was difficult, because the calculations were based on different data (our study: integrated biomass and biomass flux; other studies: particle abundance in water column and sediment traps) and differed in the size fraction included in the study (our study: > 0.7 µm, Laurenceau-Cornec et al, 2015: > 150 µm, McDonnell and Buesseler, 2010: > 50 µm).

Following Stokes' Law, which tightly couples particle size and sinking velocity, the highest sinking rates in our study were expected at 60 m, where particles tended to be larger than at shallower depths. Our estimates of the sinking velocity at 30 m and 60 m support this anticipation (Table 2).

In addition, Stokes' Law would suggest higher sinking velocities during Winter I and Autumn I (40, 60 m), where particles tended to be larger than during Spring II, III and Autumn I (20, 30 m, Fig. 5). In case of Autumn I (40, 60 m) the suggestion of Stokes' Law is supported (Table 2): We found here large particles and a high sinking velocity. Particle sizes in the 20 m and 30 m gels during Autumn I however pinpointed that sinking velocity is not merely influenced by size, but a variety of parameters such as sinking particle type, density, and

mineral ballasting (De La Rocha and Passow, 2007; Iversen et al., 2010; Laurenceau-Cornec et al., 2015; McDonnell and Buesseler, 2010). We suggest that incooperation of lithogenic material into organic particles (Iversen et al., 2010) and a higher abundance of fast-sinking fecal pellets (Table 3) overruled the size effect at the shallow sampling depth during Autumn I, and caused the high sinking velocity. During Winter I, the low sinking velocity was apparently a result of prevailing large, fluffy, detrital particles (Table 3) with a low specific weight and the lack of ballasting diatoms (Iversen and Ploug, 2010) or lithogenic material (no run-off during winter).

Precautions must thus be taken when relating particle size or volume to the POC flux. For Winter I we calculated a low POC: volume ratio of ~0.0003 mg POC mm^{-3} (data not shown), which reflects the high contribution of fluffy detritus. The ratios from Spring II were among the highest during the present study (e.g., 30 m: 0.0050 mg POC mm^{-3}) and reflected the higher contribution of aggregates and fecal pellets. However, all POC: volume ratios at IsA were several magnitudes lower when compared to ratios from the central Barents Sea, where sinking material comprised densely packed unidentifiable detritus and fecal material (0.0067-0.1101 mg POC mm^{-3}, Wiedmann et al., 2014). Accordingly, translating particle size or volume into POC flux without considering the prevailing particle type may introduce large errors.

Pteropod sedimentation events were observed during autumn and winter in the North Atlantic, and were also found at IsA (Table 3). The reported abundances range from 24 individuals m^{-2} d^{-1} at 1700-2800 m in the Fram Strait (Meinecke and Wefer, 1990) to ca. $18*10^3$ individuals m^{-2} d^{-1} at 50 m in the Norwegian Sea (Bathmann et al., 1991) and are comparable with our observations at IsA (~$8*10^3$ m^{-2} d^{-1}, Table 3). High pteropod abundances may have enhanced the POC flux during Autumn I, but because our gel trap data did not indicate if these pelagic gastropods were actively swimming or passively sinking into the trap cylinders, we cannot state if the animals also represented a true component of the vertical biomass flux. Nevertheless, they seem to provide an important mechanism for vertical export, because lost or rejected mucous feeding webs of pteropds can promote aggregate formation (Bathmann et al., 1991; Noji et al., 1997) and enhance the sinking velocity of organic matter.

4.4 Ecosystem functioning during different seasons in high Arctic ice-free fjord with a major glacial run-off during autumn

In the context of climate warming, it is likely that seasonally ice-covered Arctic fjords and embayments may become permanently ice-free in the future. To predict the vertical flux

intensity in these areas, an improved understanding is needed. We used Adventfjorden as a model area, because it has been seasonally ice-covered for several months during 2000-2005 (www.met.no, detailed ice maps available for Adventfjorden since 2000), but tended to be ice-free during the last years (2006-2007, 2010, 2012-2014). This was probably a result of strong northerly winds, which enhanced the advection of comparably warm water from the West Spitsbergen Current into the fjords on western Svalbard (Cottier et al., 2007) and higher temperature of the advected water (Onarheim et al., 2014).

Compiling our data, we put forward a conceptual model of the pelagic-benthic coupling in a year-round ice-free Arctic fjord with glacial run-off during autumn (Fig. 7). In terms of suspended POC and Chl *a* concentrations as well as the vertical biomass flux, the winter situation in Adventfjorden was comparable to boreal, sub-Arctic and ice-free Arctic fjords. Enhanced mixing by thermal convection and wind must be assumed when compared to the previous ice-covered situation. We presume that detrital material, previously settled to the bottom, was re-suspended, especially in the shallow areas, and laterally advected to the middle of the fjord as described for the sub-Arctic Ramfjorden (Noji et al., 1993). The vertical flux during the polar night was dominated by large detrital particles with a low density and POC content. In the absence of ballasting materials (e.g., diatom cells or lithogenic material), the sinking velocity and POC flux tended to be lower when compared to the other seasons (Table 2, Fig. 4, Fig. 7).

The spring situation at IsA resembled previous observation from boreal, sub-Arctic and Arctic ice-free fjords in terms of suspended and sedimenting Chl *a* and POC. High vertical flux rates of un-grazed phytoplankton aggregates and detrital material was found during an early bloom phase, but the vertical flux intensity decreased toward the late bloom. We suggest this was caused by a shift from a diatom to a *Phaeocystis* dominated bloom as well as an intensifying top-down control by zooplankton.

During autumn, the ice-free Adventfjorden differed from many investigated fjords e.g., in northern Norway (Table 4), which are rarely affected by major glacial run-off (Fig. 2). We did not observe any phytoplankton autumn blooms and associated POC sedimentation events as described for sub-Arctic regions (Wassmann et al., 1991), but this may be due to low sampling frequency. Instead, the sediment loaded meltwater input was identified as a major driver of the high POC flux during autumn. In addition, high abundances of *Limacina* sp. and rejected or lost mucous nets may be possible drivers of the high POC flux.

We propose that the seasonal vertical flux patterns in an ice-free Arctic fjord with glacial run-off resemble sub-Arctic fjords during winter and spring. During autumn, the systems appear to differ and a major POC sedimentation may be caused by the glacial run-off.

In a scenario of climate warming it must be assumed that previously ice-covered fjords and embayments will turn into permanently open waters in the future. Ice algae blooms associated with the sea ice and their contribution to the vertical carbon flux will no longer occur in these future ice-free fjords. Fjords, affected by glacial run-off, may however still have a high vertical biomass flux because the entrained sediment-loaded melt water can drive the vertical biomass flux in the fjord during the melting season.

Acknowledgements

We would like to thank the captain and the crew of the NorCGV Svalbard, the R/V Helmer Hanssen, R/V Viking and the M/S Farm for great assistance during sampling under the sometimes harsh condition. A helping hand was highly appreciated in the field (E. I. Stübner), during the CHN analyses (S. Øygaarden), and with the hydrographical data (R. Skogseth). We also thank A. M. Kubiszyn and E. I. Stübner for insight in their plankton data and two anonymous reviewers for their comments, which improved this work substantially. The field work was partly funded by the Arctic Field Grant (RIS 5264) and the CONFLUX project (Tromsø Forskningsstiftelse).

Literature

Alldredge, A.L., Silver, M.W., 1988. Characteristics, dynamics and significance of marine snow. Prog. Oceanogr. 20, 41-82. doi: 10.1016/0079-6611(88)90053-5.

Andreassen, I.J., Wassman, P., Ratkova, T.N., 1999. Seasonal variation of vertical flux of phytyoplankton and biogenic matter at Nordvestbanken, north Norwegian shelf in 1994. Sarsia 84, 227-238.

Arendt, K.E., Juul-Pedersen, T., Mortensen, J., Blicher, M.E., Rysgaard, S., 2013. A 5-year study of seasonal patterns in mesozooplankton community structure in a sub-Arctic fjord reveals dominance of *Microsetella norvegica* (Crustacea, Copepoda). J. Plankton Res. 35, 105-120. doi: 10.1093/plankt/fbs087.

Arrigo, K.R., 2014. Sea Ice Ecosystems. Annu. Rev. Mar. Sci. 6, 439-467. doi: 10.1146/annurev-marine-010213-135103.

Bathmann, U.V., Noji, T.T., von Bodungen, B., 1991. Sedimentation of pteropods in the Norwegian Sea in autumn. Deep-Sea Res. I 38, 1341-1360. doi: 10.1016/0198-0149(91)90031-A.

Bianchi, T.S., 2006. Biochemistry of Estuaries. Oxford University Press, Cary, USA 720 pp.

569 Calbet, A., Riisgaard, K., Saiz, E., Zamora, S., Stedmon, C., Nielsen, T.G., 2011. Phytoplankton
570 growth and microzooplankton grazing along a sub-Arctic fjord (Godthåbsfjord, west
571 Greenland). Mar. Ecol. Prog. Ser. 442, 11-22. doi: 10.3354/meps09343.
572 Cottier, F.R., Nilsen, F., Inall, M.E., Gerland, S., Tverberg, V., Svendsen, H., 2007. Wintertime
573 warming of an Arctic shelf in response to large-scale atmospheric circulation. Geophys. Res.
574 Lett. 34, L10607. doi: 10.1029/2007GL029948.
575 De La Rocha, C.L., Passow, U., 2007. Factors influencing the sinking of POC and the efficiency of the
576 biological carbon pump. Deep-Sea Res. II 54, 639-658. doi: 10.1016/j.dsr2.2007.01.004.
577 Degerlund, M., Eilertsen, H.C., 2010. Main Species Characteristics of Phytoplankton Spring Blooms
578 in NE Atlantic and Arctic Waters (68-80° N). Estuar. Coasts 33, 242-269. doi:
579 10.1007/s12237-009-9167-7.
580 Ebersbach, F., Trull, T.W., 2008. Sinking particle properties from polyacrylamide gels during the
581 Kerguelen Ocean and Plateau compared Study (KEOPS): Zooplankton control of carbon
582 export in an area of persistent natural iron inputs in the Southern Ocean. Limnol. Oceanogr.
583 53, 212-224. doi: 10.2307/40006162.
584 Eilertsen, H.C., 1993. Spring blooms and stratification. Nature 363, 24-24. doi: 10.1038/363024a0.
585 Eilertsen, H.C., Degerlund, M., 2010. Phytoplankton and light during the northern high-latitude
586 winter. J. Plankton Res. 32, 899-912. doi: 10.1093/plankt/fbq017.
587 Eilertsen, H.C., Frantzen, S., 2007. Phytoplankton from two sub-Arctic fjords in northern Norway
588 2002–2004: I. Seasonal variations in chlorophyll a and bloom dynamics. Mar. Biol. Res. 3,
589 319-332. doi: 10.1080/17451000701632877.
590 Eilertsen, H.C., Schei, B., Taasen, J.P., 1981. Investigations on the plankton community of
591 Balsfjorden, Northern Norway. The phytoplankton 1976 - 1978. Abundance, species
592 composition, and succession. Sarsia 66, 129-141.
593 Forest, A., Babin, M., Stemmann, L., Picheral, M., Sampei, M., Fortier, L., Gratton, Y., Bélanger, S.,
594 Devred, E., Sahlin, J., Doxaran, D., Joux, F., Ortega-Retuerta, E., Martín, J., Jeffrey, W.H.,
595 Gasser, B., Carlos Miquel, J., 2013. Ecosystem function and particle flux dynamics across the
596 Mackenzie Shelf (Beaufort Sea, Arctic Ocean): an integrative analysis of spatial variability
597 and biophysical forcings. Biogeosciences 10, 2833-2866. doi: 10.5194/bg-10-2833-2013.
598 Iversen, K.R., Seuthe, L., 2011. Seasonal microbial processes in a high-latitude fjord (Kongsfjorden,
599 Svalbard): I. Heterotrophic bacteria, picoplankton and nanoflagellates. Polar Biol. 34, 731-
600 749. doi: 10.1007/s00300-010-0929-2.
601 Iversen, M.H., Nowald, N., Ploug, H., Jackson, G.A., Fischer, G., 2010. High resolution profiles of
602 vertical particulate organic matter export off Cape Blanc, Mauritania: Degradation processes
603 and ballasting effects. Deep-Sea Res. I 57, 771-784. doi:
604 dx.doi.org/10.1016/j.dsr.2010.03.007.
605 Iversen, M.H., Ploug, H., 2010. Ballast minerals and the sinking carbon flux in the ocean: carbon-
606 specific respiration rates and sinking velocity of marine snow aggregates. Biogeosciences 7,
607 2613-2624. doi: 10.5194/bg-7-2613-2010.
608 Jackson, G.A., Maffione, R., Costello, D.K., Alldredge, A.L., Logan, B.E., Dam, H.G., 1997. Particle
609 size spectra between 1 μm and 1 cm at Monterey Bay determined using multiple instruments.
610 Deep-Sea Res. I 44, 1739-1767. doi: 10.1016/S0967-0637(97)00029-0.
611 Jackson, G.A., Waite, A.M., Boyd, P.W., 2005. Role of algal aggregation in vertical carbon export
612 during SOIREE and in other low biomass environments. Geophys. Res. Lett. 32, L13607. doi:
613 10.1029/2005gl023180.
614 Ji, R., Jin, M., Varpe, Ø., 2013. Sea ice phenology and timing of primary production pulses in the
615 Arctic Ocean. Glob. Change Biol. 19, 734-741. doi: 10.1111/gcb.12074.
616 Keck, A., Wassmann, P., 1996. Temporal and spatial patterns of sedimentation in the subarctic fjord
617 Malangen, Northern Norway. Sarsia 80, 259-276.
618 Kiørboe, T., Andersen, K.P., Dam, H.G., 1990. Coagulation efficiency and aggregate formation in
619 marine phytoplankton. Mar. Biol. 107, 235-245. doi: 10.1007/BF01319822.
620 Kiørboe, T., Lundsgaard, C., Olesen, M., Hansen, J.L.S., 1994. Aggregation and sedimentation
621 processes during a spring phytoplankton bloom: A field experiment to test coagulation theory.
622 J. Mar. Res. 52, 297-323. doi: 10.1357/0022240943077145.

623 Kranck, K., 1973. Flocculation of Suspended Sediment in the Sea. Nature 246, 348-350. doi:
624 10.1038/246348a0.
625 Kubiszyn, A.M., Wiktor, J.M., Wiktor, J.M.J., Griffiths, C., Kristiansen, S., T.M., G., The annual
626 planktonic protist community structure in an ice-free high Arctic fjord (Adventfjorden, West
627 Spitsbergen). Prepared for submission to J. Plankton Res.
628 Lampitt, R.S., 2001. Marine Snow, in: Steele, J.H., Thorpe, S.A., Turekian, K.K. (Eds.), Encyclopedia
629 of Ocean Sciences. Academic Press, San Diego, USA, pp. 1667-1675. doi:
630 10.1006/rwos.2001.0218.
631 Laurenceau-Cornec, E.C., Trull, T.W., Davies, D.M., De La Rocha, C.L., Blain, S., 2015.
632 Phytoplankton morphology controls on marine snow sinking velocity. Mar. Ecol. Prog. Ser.
633 520, 35-56. doi: 10.3354/meps11116.
634 Leu, E., Søreide, J.E., Hessen, D.O., Falk-Petersen, S., Berge, J., 2011. Consequences of changing sea-
635 ice cover for primary and secondary producers in the European Arctic shelf seas: Timing,
636 quantity, and quality. Progr. Oceanogr. 90, 18-32. doi: 10.1016/j.pocean.2011.02.004.
637 Lundsgaard, C., M., O., Reigstad, M., Olli, K., 1999. Sources of settling material: aggregation and
638 zooplankton mediated fluxes in the Gulf of Riga. J. Mar. Syst. 23, 197–210. doi:
639 10.1016/S0924-7963(99)00058-5.
640 Mantoura, R.F.C., Wright, S.W., Barlow, R.G., Cummings, D.E., 1997. Filtration and storage of
641 pigments from microalgae. Monographs on Oceanographic Methodology, in: Jeffrey, S.W.,
642 Mantoura, R.F.C., Wright, S.W. (Eds.), Phytoplankton pigments in oceanography: guidelines
643 to modern methods. UNESCO Publishing, Paris.
644 McDonnell, A.M.P., Buesseler, K.O., 2010. Variability in the average sinking velocity of marine
645 particles. Limnol. Oceanogr. 55, 2085-2096. doi: 10.4319/lo.2010.55.5.2085.
646 Meinecke, G., Wefer, G., 1990. Seasonal pteropod sedimentation in the Norwegian Sea. Palaeogeogr.
647 Palaeocl. 79, 129-147. doi: 10.1016/0031-0182(90)90109-K.
648 Noji, T.T., Bathmann, U.V., Bodungen, B.v., Voss, M., Antia, A., Krumbholz, M., Klein, B., Peeken,
649 I., Noji, C.I.-M., Rey, F., 1997. Clearance of picoplankton-sized particles and formation of
650 rapidly sinking aggregates by the pteropod, *Limacina retroversa*. J. Plankton Res. 19, 863-
651 875. doi: 10.1093/plankt/19.7.863.
652 Noji, T.T., Estep, K.W., Macintyre, F., Norrbin, F., 1991. Image analysis of faecal material grazed
653 upon by three species of copepods: evidence for coprorhexy, coprophagy and coprochaly. J.
654 Mar. Biol. Assoc. UK 71, 465-480. doi: 10.1017/S0025315400051717.
655 Noji, T.T., Noji, C.I.-M., Barthel, K.-G., 1993. Pelagic-benthic coupling during the onset of winter in
656 a northern Norwegian fjord. Carbon flow and fate of suspended particulate matter. Mar. Ecol.
657 Prog. Ser. 93, 89-99.
658 Olli, K., Rieser, C.W., Wassmann, P., Ratkova, T., Arashkevich, E., Pasternak, A., 2002. Seasonal
659 variation in vertical flux of biogenic matter in the marginal ice zone and the central Barents
660 Sea. J. Mar. Syst. 38, 189-204. doi: 10.1016/S0924-7963(02)00177-X
661 Onarheim, I.H., Smedsrud, L.H., Ingvaldsen, R.B., Nilsen, F., 2014. Loss of sea ice during winter
662 north of Svalbard. Tellus A 66, 23933. doi: 10.3402/tellusa.v66.23933.
663 Otsu, N., 1979. A Threshold Selection Method from Gray-Level Histograms. IEEE T. Syst. Man Cyb.
664 9, 62-66. doi: 10.1109/TSMC.1979.4310076.
665 Parsons, T.R., Lalli, C.M., 1988. Comparative oceanic ecology of the plankton communities of
666 subarctic Atlantic and Pacific Oceans. Oceanogr. Mar. Biol. Annu. Rev. 26, 317-359.
667 Passow, U., 1991. Species-specific sedimentation and sinking velocities of diatoms. Mar. Biol. 108,
668 449-455. doi: 10.1007/BF01313655.
669 Passow, U., De La Rocha, C.L., 2006. Accumulation of mineral ballast on organic aggregates. Global
670 Biogeochem. Cy. 20, GB1013. doi: 10.1029/2005GB002579.
671 Peinert, R., von Bodungen, B., Smetacek, V.S., 1989. Food Web Structure and Loss Rate, in: Berger,
672 W.H., Smetacek, V.S., Wefer, G. (Eds.), Productivity of the ocean: present and past. Wiley,
673 Berlin, pp. 35-48.
674 Ploug, H., Iversen, M.H., Fischer, G., 2008. Ballast, sinking velocity, and apparent diffusivity within
675 marine snow and zooplankton fecal pellets: Implications for substrate turnover by attached
676 bacteria. Limnol. Oceanogr. 53, 1878-1886. doi: 10.4319/lo.2008.53.5.1878.

677 Rat'kova, T.N., Wassmann, P., 2002. Seasonal variation and spatial distribution of phyto- and
678 protozooplankton in the central Barents Sea. J. Mar. Syst. 38, 47-75. doi: 10.1016/s0924-
679 7963(02)00169-0.
680 Reigstad, M., Riser, C.W., Wassmann, P., Ratkova, T., 2008. Vertical export of particulate organic
681 carbon: Attenuation, composition and loss rates in the northern Barents Sea. Deep-Sea Res. II
682 55, 2308-2319. doi: 10.1016/j.dsr2.2008.05.007.
683 Reigstad, M., Wassmann, P., 1996. Importance of advection for pelagic-benthic coupling in north
684 Norwegian fjords. Sarsia 80, 245-257. doi: 10.1080/00364827.1996.10413599.
685 Reigstad, M., Wassmann, P., 2007. Does *Phaeocystis* spp. contribute significantly to vertical export of
686 organic carbon? Biogeochemistry 83, 217-234. doi: 10.1007/s10533-007-9093-3.
687 Reigstad, M., Wassmann, P., Ratkova, T., Arashkevich, E., Pasternak, A., Øygarden, S., 2000.
688 Comparison of the springtime vertical export of biogenic matter in three northern Norwegian
689 fjords. Mar. Ecol. Prog. Ser. 201, 73-80. doi: 10.3354/meps201073.
690 Rynearson, T.A., Richardson, K., Lampitt, R.S., Sieracki, M.E., Poulton, A.J., Lyngsgaard, M.M.,
691 Perry, M.J., 2013. Major contribution of diatom resting spores to vertical flux in the sub-polar
692 North Atlantic. Deep-Sea Res. I 82, 60-71. doi: 10.1016/j.dsr.2013.07.013.
693 Smayda, T.J., 1971. Normal and accelerated sinking of phytoplankton in the sea. Mar. Geol. 11, 105-
694 122. doi: 10.1016/0025-3227(71)90070-3.
695 Smetacek, V.S., 1985. Role of Sinking in Diatom Life-History Cycles - Ecological, Evolutionary and
696 Geological Significance. Mar. Biol. 84, 239-251. doi: 10.1007/bf00392493.
697 Smith, R.W., Bianchi, T.S., Allison, M., Savage, C., Galy, V., 2015. High rates of organic carbon
698 burial in fjord sediments globally. Nat. Geosci. 8, 450-453. doi: 10.1038/ngeo2421.
699 Stübner, E.I., Søreide, J.E., Reigstad, M., Marquardt, M., Blachowiak-Samolyk, K., Common
700 strangers – seasonal meroplankton dynamics at high latitudes in Adventfjorden, Svalbard.
701 Submitted to J. Plankton Res.
702 Sutherland, B.R., Barrett, K.J., Gingras, M.K., 2015. Clay settling in fresh and salt water. Environ.
703 Fluid. Mech. 15, 147-160. doi: 10.1007/s10652-014-9365-0.
704 Svensen, C., Wexels Riser, C., Reigstad, M., Seuthe, L., 2012. Degradation of copepod faecal pellets
705 in the upper layer: role of microbial community and *Calanus finmarchicus*. Mar. Ecol. Prog.
706 Ser. 462, 39-49. doi: 10.3354/meps09808.
707 Syvitski, J.M., 1980. Flocculation, Agglomeration, and Zooplankton Pelletization of Suspended
708 Sediment in a Fjord Receiving Glacial Meltwater, in: Freeland, H., Farmer, D., Levings, C.
709 (Eds.), Fjord Oceanography. Springer US, pp. 615-623.
710 Søreide, J.E., Leu, E., Berge, J., Graeve, M., Falk-Petersen, S., 2010. Timing of blooms, algal food
711 quality and *Calanus glacialis* reproduction and growth in a changing Arctic. Glob. Change
712 Biol. 16, 3154-3163. doi: 10.1111/j.1365-2486.2010.02175.x.
713 Thiele, S., Fuchs, B.M., Amann, R., Iversen, M.H., 2015. Colonization in the photic zone and
714 subsequent changes during sinking determines bacterial community composition in marine
715 snow. Appl. Environ. Microbiol. 81, 1463-1471. doi: 10.1128/aem.02570-14.
716 Thompson, R.J., Deibel, D., Redden, A.M., McKenzie, C.H., 2008. Vertical flux and fate of
717 particulate matter in a Newfoundland fjord at sub-zero water temperatures during spring. Mar.
718 Ecol. Prog. Ser. 357, 33-49. doi: 10.3354/meps07277.
719 Thornton, D., 2002. Diatom aggregation in the sea: mechanisms and ecological implications. Eur. J.
720 Phycol. 37, 149-161. doi: 10.1017/S0967026202003657.
721 Tommasi, D., Hunt, B.P.V., Pakhomov, E.A., Mackas, D.L., 2013. Mesozooplankton community
722 seasonal succession and its drivers: Insights from a British Columbia, Canada, fjord. J Mar.
723 Sys. 115–116, 10-32. doi: 10.1016/j.jmarsys.2013.01.005.
724 Townsend, D.W., Keller, M.D., Sieracki, M.E., Ackleson, S.G., 1992. Spring phytoplankton blooms in
725 the absence of vertical water column stratification. Nature 360, 59-62. doi: 10.1038/360059a0.
726 Tremblay, C., Runge, J., Legendre, L., 1989. Grazing and sedimentation of ice algae during and
727 immediately after a bloom at the ice-water interface. Mar. Ecol. Prog. Ser. 56, 291-300.
728 Tremblay, J.-É., Gagnon, J., 2009. The effects of irradiance and nutrient supply on the productivity of
729 Arctic waters: a perspective on climate change, in: Nihoul, J.C.J., Kostianoy, A.G. (Eds.),
730 Influence of Climate Change on the Changing Arctic and Sub-Arctic Conditions. Springer
731 Netherlands, pp. 73-93.

Turner, J.T., 2002. Zooplankton fecal pellets, marine snow and sinking phytoplankton blooms. Aquat. Microb. Ecol. 27, 57-102. doi: 10.3354/ame027057.
Turner, J.T., 2015. Zooplankton fecal pellets, marine snow, phytodetritus and the ocean's biological pump. Prog. Oceanogr. 130, 205-248. doi: 10.1016/j.pocean.2014.08.005.
Wassmann, P., 1984. Sedimentation and benthic mineralization of organic detritus in a Norwegian fjord. Mar. Biol. 83, 83-94. doi: 10.1007/BF00393088.
Wassmann, P., Peinert, R., Smetacek, V., 1991. Patterns of production and sedimentation in the boreal and polar Northeast Atlantic. Proceedings of the Pro Mare Symposium on Polar Marine Ecology, Trondheim, 12-16 May 1990. Pol. Res. 10, 209-228. doi: 10.1111/j.1751-8369.1991.tb00647.x.
Wassmann, P., Svendsen, H., Keck, A., Reigstad, M., 1996. Selected aspects of the physical oceanography and particle fluxes in fjords of northern Norway. J. Mar. Syst. 8, 53-71.
Węsławski, J.M., Kwasniewski, S., Wiktor, J., 1991. Winter in a Svalbard fjord ecosystem. Arctic 44, 115-123. doi: 10.14430/arctic1527115-123.
Węsławski, J.M., Szymelfenig, M., Zajączkowski, M., Keck, A., 1999. Influence of salinity and suspended matter of benthos of an Arctic tidal flat. ICES J. Mar. Sci. 56 Supplement, 194-202.
Wexels Riser, C., Wassmann, P., Reigstad, M., Seuthe, L., 2008. Vertical flux regulation by zooplankton in the northern Barents Sea during Arctic spring. Deep Sea Research Part II: Topical Studies in Oceanography 55, 2320-2329. doi: 10.1016/j.dsr2.2008.05.006.
Weydmann, A., Søreide, J.E., Kwaśniewski, S., Leu, E., Falk-Petersen, S., Berge, J., 2013. Ice-related seasonality in zooplankton community composition in a high Arctic fjord. J. Plankton Res. 35, 831-842. doi: 10.1093/plankt/fbt031.
Wiedmann, I., Reigstad, M., Sundfjord, A., Basedow, S., 2014. Potential drivers of sinking particle's size spectra and vertical flux of particulate organic carbon (POC): Turbulence, phytoplankton, and zooplankton. J. Geophys. Res.-Oceans 119, 6900-6917. doi: 10.1002/2013JC009754.
Zajączkowski, M., Nygård, H., Hegseth, E.N., Berge, J., 2010. Vertical flux of particulate matter in an Arctic fjord: the case of lack of the sea-ice cover in Adventfjorden 2006-2007. Polar Biol. 33, 223-239. doi: 10.1007/s00300-009-0699-x.
Zajączkowski, M., Włodarska-Kowalczuk, M., 2007. Dynamic sedimentary environments of an Arctic glacier-fed river estuary (Adventfjorden, Svalbard). I. Flux, deposition, and sediment dynamics. Estuar. Coastal Shelf S. 74, 285-296. doi: 10.1016/j.ecss.2007.04.015.

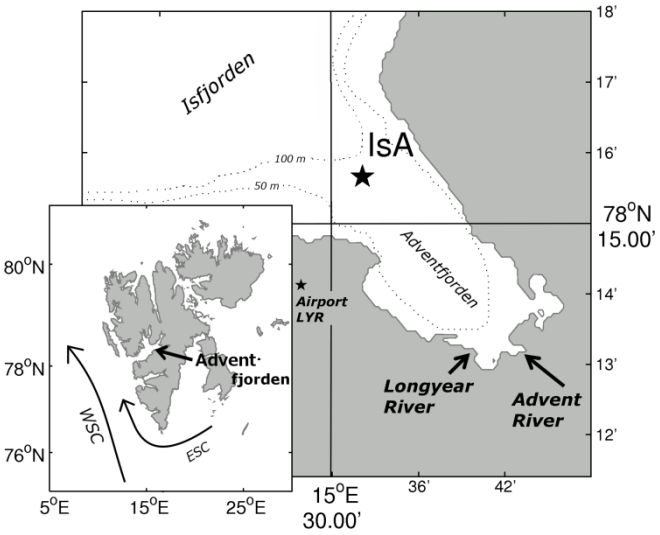

Figure 1: IsA station was located in the mouth of Adventfjorden, a side branch of the Isfjorden system, western Svalbard (main map, depth contour following Zajączkowski et al., 2010). Adventfjorden is influenced by the Atlantic derived, warm West Spitsbergen Current (WSC) and the Arctic derived, cold East Spitsbergen Current (ESC, small map), as well as glacial run-off from the Longyear and Advent River (during ice melting period in summer and autumn).

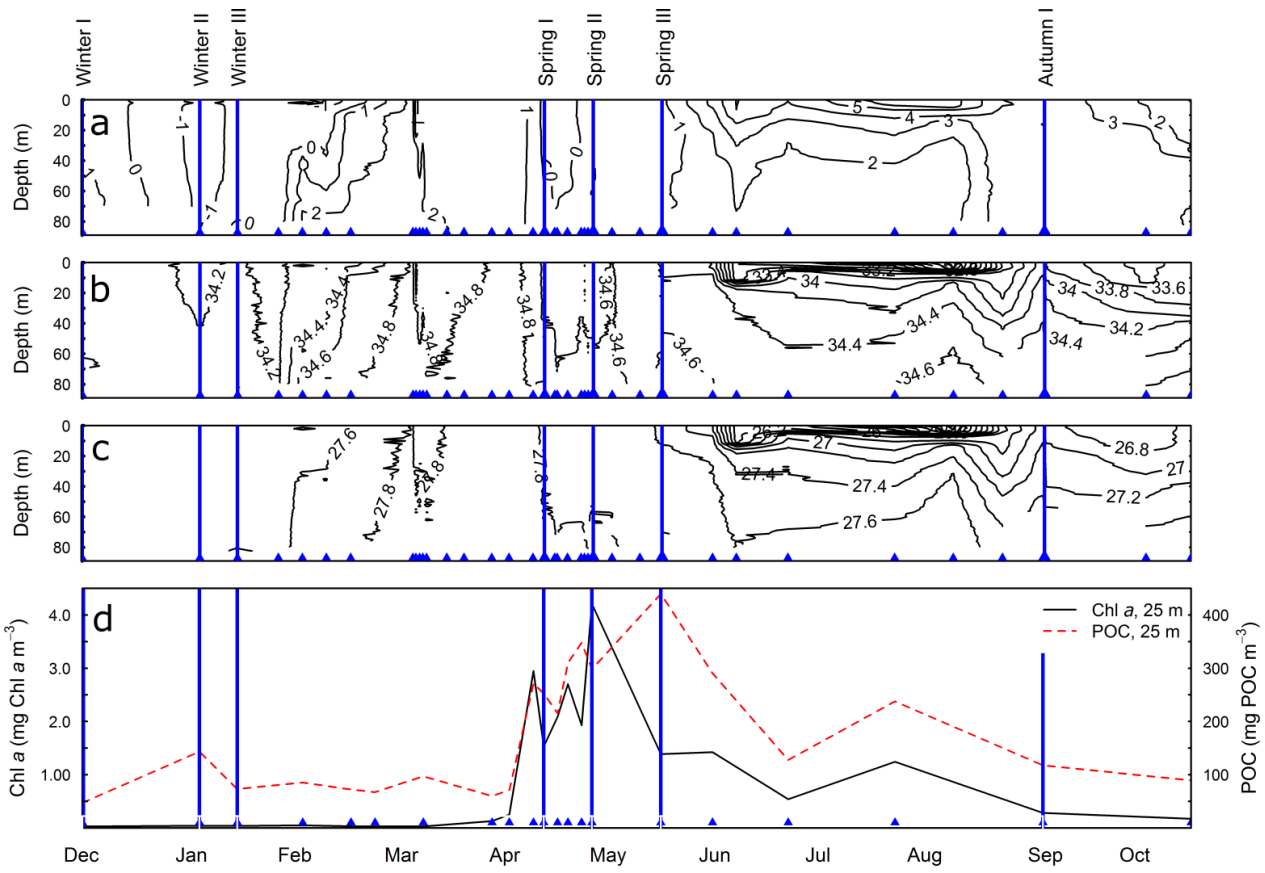

Figure 2: Temperature (a), salinity (b), density (c), and the seasonal development of suspended biomass is shown (d, black line: chlorophyll *a*, Chl *a*, red stippled line: particulate organic carbon, POC) at IsA during the sampling program (14.12.2011 - 31.10.2012). Sampling dates with the CTD are indicated by blue triangles. Sediment trap deployment took place at the dates indicated by blue vertical lines.

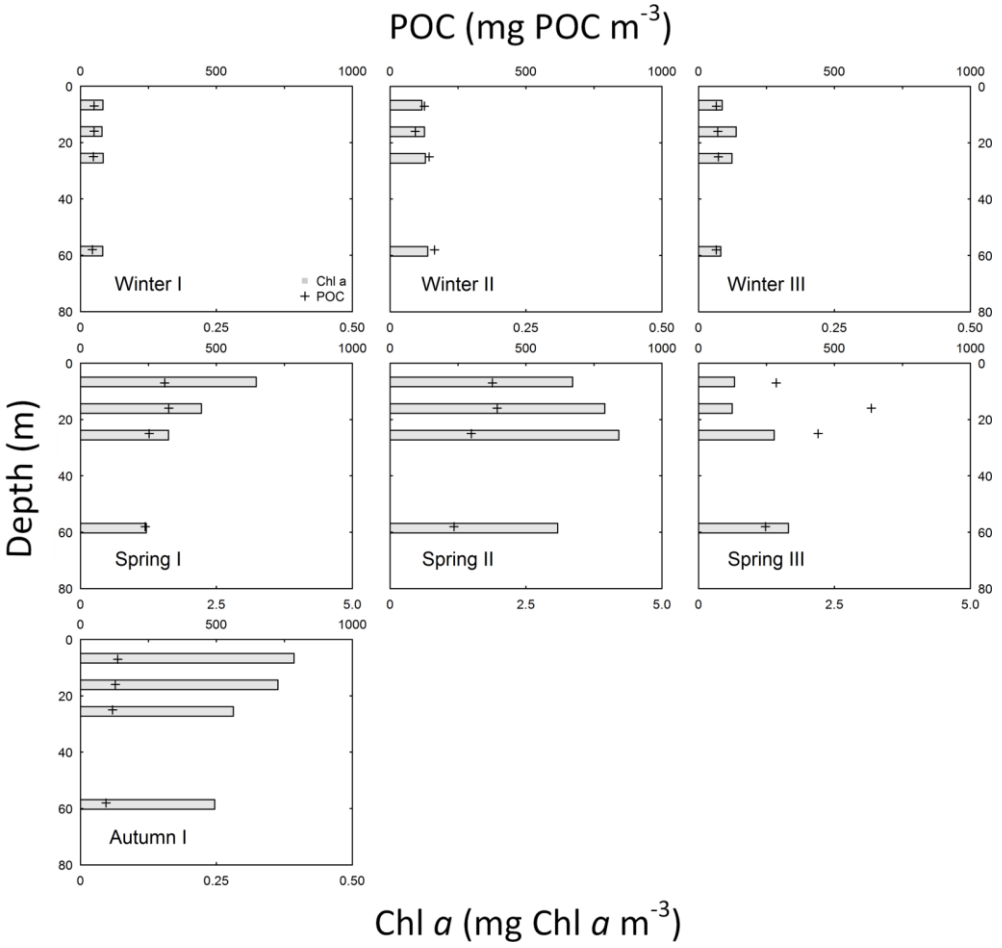

Figure 3: Suspended chlorophyll *a* (Chl *a*) (grey bars) and particulate organic carbon (POC, black cross) concentrations at 5, 15, 25 and 60 m during Winter I-III, Spring I-III and Autumn I. Note different scales on the lower x-axis for Spring I-III.

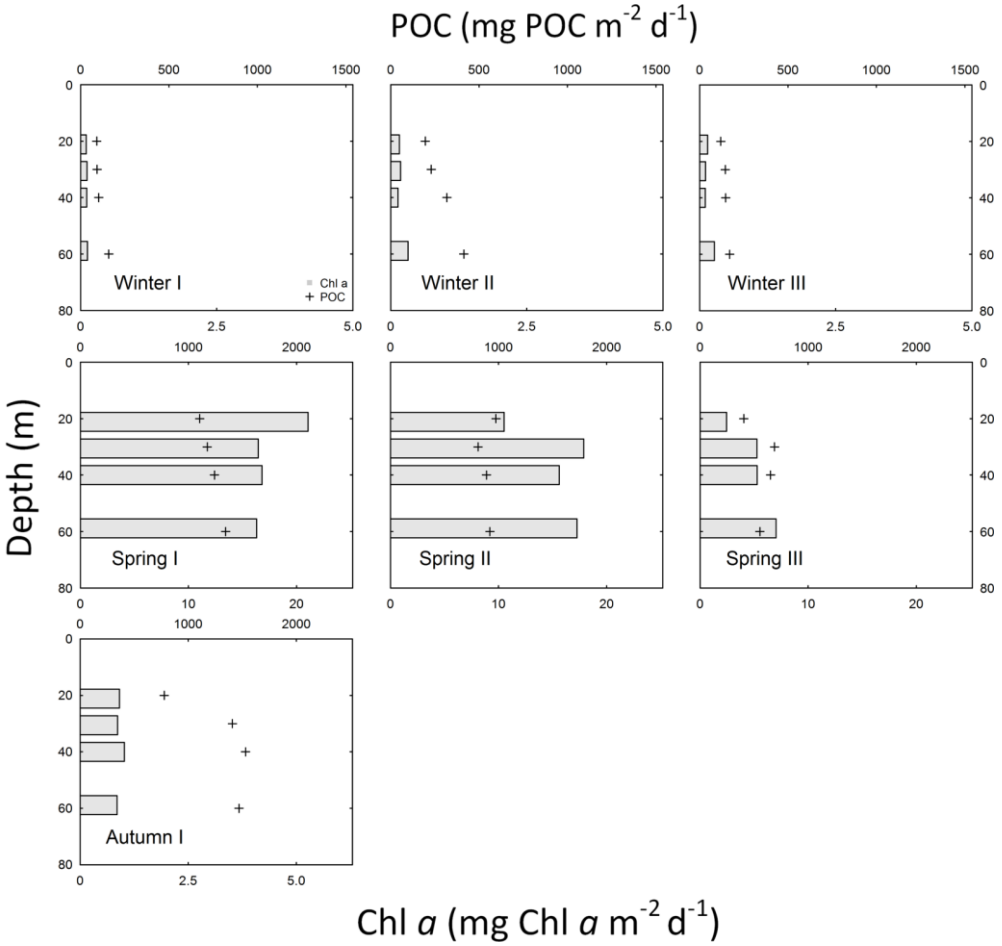

Figure 4: Vertical flux of chlorophyll *a* (Chl *a*, grey bars) and particulate organic carbon (POC, black cross) at 20, 30, 40, and 60 m during Winter I-III , Spring I-III, and Autumn I. Note different scale on the upper x-axis during Winter I-III and the lower x-axis for Spring I-III.

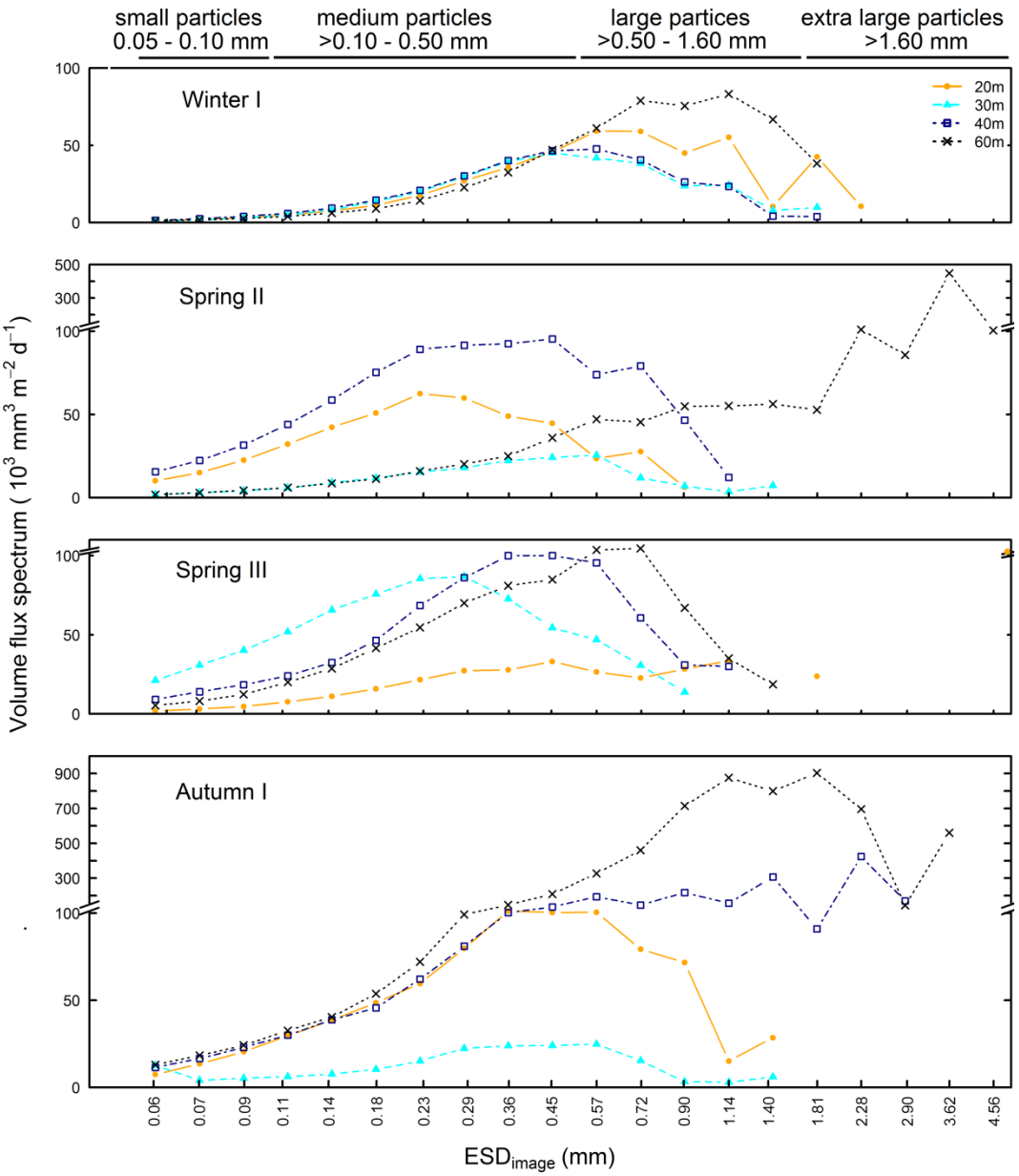

Figure 5: Volume flux spectra at the four trap deployment depths (20 m: orange solid, 30 m: turquoise stippled, 40 m: blue dotted/stippled, 60 m: black dotted) during Winter I, Spring II, Spring III, and Autumn I. The horizontal axis is logarithmic and displays the average size of the particle bins. The area under the curve reflects the total volume of particles sinking out per sampling depth, and the top line indicates the size classes of the particles. Note the broken y-axis in Spring II, Spring III and Autumn I.

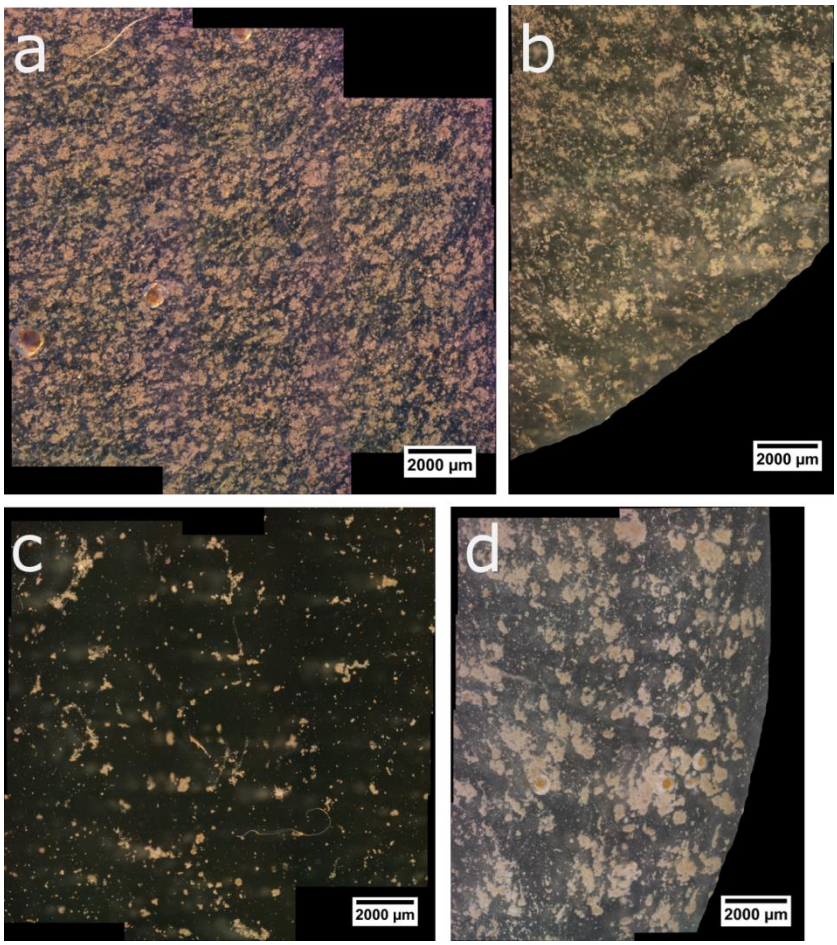

Figure 6: Example images (15 x magnification) demonstrating the different quality of sinking particles observed in the gel traps deployed at 60 m during Winter I (a), Spring II (b), Spring III (c) Autumn I (d). Note that the December sample was deployed for ~24 h, while the other samples were only deployed for ~2 h.

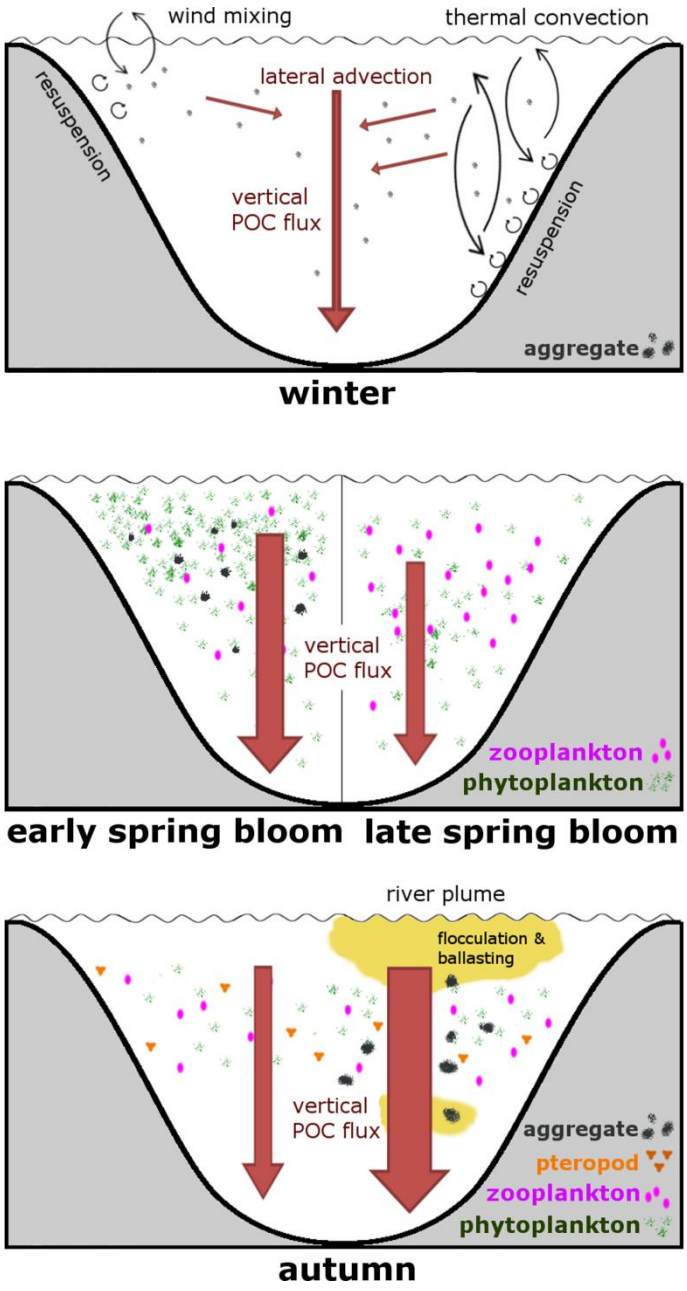

Figure 7: Conceptual model of vertical POC flux during the different seasons in the ice-free, high Arctic Adventfjorden. Resuspension of detritus from the bottom and lateral advection resulted in some vertical POC flux during winter. A strong flux event can take place during an early spring bloom situation, when aggregates of phytoplankton and detritus are formed and sink out. During a late bloom phase a stronger coupling between phytoplankton production and zooplankton diminishes the vertical POC flux. During autumn, the plume of glacial run-off can cause flocculation and aggregate formation. Entrained lithogenic material in-cooperated into sinking particles can enhance the sinking velocity of organic material, as well as high pteropod abundances.

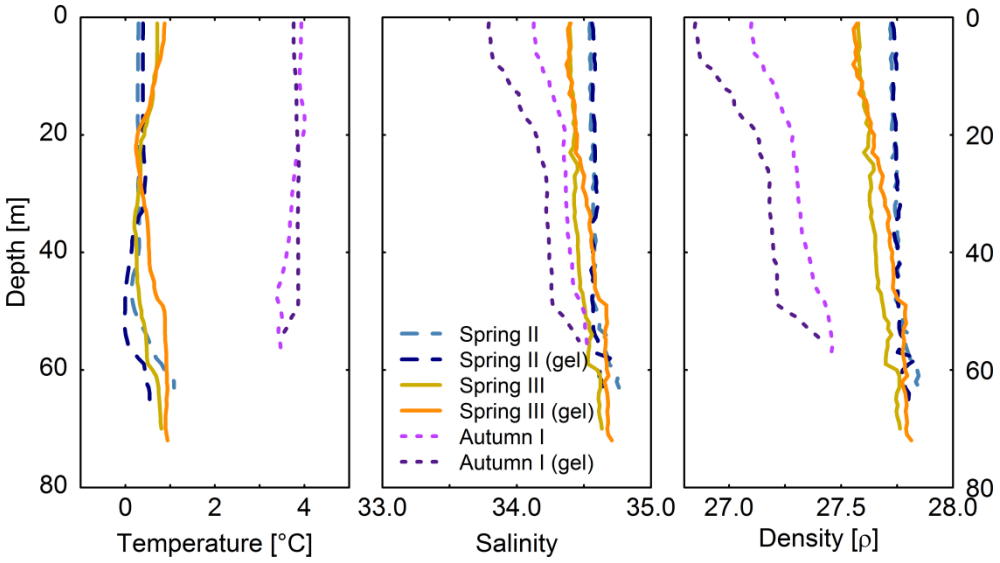

Supplement – Figure A.1: Temperature (left), salinity (middle) and density (right) plots from Spring II, Spring III and Autumn I, when CTD casts were conducted on two subsequent days (on first day, when the 24 h sediment traps array was deployed and on the second day, when the 2 h gel trap array was deployed), illustrating the variable impact of the glacial run-off on salinity during autumn.

Table 1: Sampling schedule for suspended water samples, sediment trap deployment and 'gel trap' deployment (sediment traps modified with a gel jar) at IsA station (78° 15.67' N, 15° 32.10' E). Research Vessel: 1: NorCGV Svalbard, 2: R/V Helmer Hanssen, 3: Polar Circle, 4: R/V Viking Explorer, 5: M/V Farm.

Label	Date	Boat	CTD	Euphotic zone (m)	Susp. Chl *a*, POC (mg m^{-3})	Susp. C/N	Deployment time (h)	Sediment trap** (m)	'Gel trap' (m)
Winter I	13./ 14.12.2011	1	X		5,15,25,60	5,15,25,60*	24:15	20,30,40,60	20,30,40,60
Winter II	17./ 18.01.2012	2	X		5,15,25,60	5,15,25,60	22:00	20,30,40,60	
Winter III	27./ 28.01.2012	1	X		5,15,25,60	5,15,25,60	25:00	20,30,40,60	
	09.02.2012	3	X		25				
	16.02.2012	3	X		25				
	23.02.2012	3	X		25				
	01.03.2012	3	X		25				
	08.03.2012	3			25				
	19.-22.03.2012***	3	X	34					
	29.03.2012	3	X	45	25				
	03.04.2012	3	X	40	25				
	11.04.2012	3	X	40	25				
	16.04.2012	3	X	45	25				
	23.04.2012	3	X	35	25				
Spring I	26./ 27.04.2012***	4	X	30	5,15,25,60	5,15,25,60	24:25	20,30,40,60	
	30.04.2012	3	X	30	25				
	03.05.2012	3	X	25	25				
	07.-09.05.2012***	3	X	25	25				
Spring II	10./ 11.05.2012***	4	X	25	5,15,25,60	5,15,25,60	23:25	20,30,40,60	
	11.05.2012	4					02:00		20,30,40,60
	16.05.2012	3	X						
	24.05.2012	3	X	30	25				
Spring III	30./ 31.05.2012***	4	X	20	5,15,25,60	5,15,25,60	23:45	20,30,40,60	
	31.05.2012	4					01:50		20,30,40,60
	14.06.2012	3	X		25				
	21.06.2012	3		25	25				
	06.07.2012	3	X	8	25				
	06.08.2012	3	X	30	25				
	23.08.2012	3	X	20	25				
	06.09.2012	3	X						
Autumn I	18./ 19.09.2012***	5	X	30	5,15,25,60	5,15,25,60	23:05	20,30,40,60	
	19.09.2012	5					02:30		20,30,40,60
	31.10.2012	3	X		25				

*PON samples not available
** analyzed for POC, PON and Chl *a*
*** daily sampling

Table 2: Loss rate and average sinking velocity of Chl *a* and POC.

	Winter I		**Winter II**		**Winter III**		**Spring I**		**Spring II**		**Spring III**		**Autumn I**	
	30 m	60 m	30 m	60 m	30 m	60 m	30 m	60 m	30 m	60 m	30 m	60 m	30 m	60 m
Loss rate (% d^{-1})														
- Chl *a*	9.5	5.1	9.6	8.1	6.0	8.3	-	-	15.5	7.8	19.7	9.6	6.6	3.7
- POC	6.3	5.6	6.8	5.5	6.9	4.1	13.2	8.3	7.6	5.0	5.1	2.4	36.8	21.2
Average sinking velocity (m d^{-1})														
- Chl *a*	2.8	3.1	2.8	4.6	1.7	6.6	-	-	4.2	5.6	3.8	4.2	2.4	2.8
- POC	2.0	3.7	1.6	3.0	2.0	2.6	4.6	5.6	2.7	3.9	1.6	2.2	12.0	15.7

Table 3: Quality of the sinking material denoted by the C/N ratio (PON values of Winter I not available) and the most frequent particle type (detritus = mainly small, unidentifiable particles, PP = phytoplankton, FP = fecal pellets) in the deployed gel jars. Dominant particle type in bold.

		Winter I	**Winter II**	**Winter III**	**Spring I**	**Spring II**	**Spring III**	**Autumn I**
C/N	20, 30, 40, 60 m		10.6-12.4	12.7-14.1	7.9-8.0	6.8-7.8	6.7-7.2	13.0-15.0
dominant particle type	20 m	detritus				detritus, FP	PP aggregates, detritus	**FP**, aggregates*, *Limacina* sp. (138)
	30 m	detritus, *Limacina* sp. (10)				detritus, aggregates*	PP aggregates, detritus	aggregates*, FP, *Limacina* sp. (63)
	40 m	detritus				detritus, aggregates*	aggregates*, FP	**detritus, aggregates***, FP, *Limacina* sp. (73)
	60 m	detritus, *Limacina* sp, (13)				detritus, aggregates	**FP**, aggregates*	**detritus**, aggregates, few FP, *Limacina* sp. (68)

* most likely phytoplankton aggregates

Table 4: Literature compilation of suspended POC and Chl *a* concentrations (mg m^{-3}) and the vertical flux of both parameters (mg m^{-2} d^{-1}) in high latitude fjords and the Barents Sea during winter, spring and autumn.

Place	Date	Depth (m)	Chl *a*	POC	C/N	Reference
Winter - suspended						
Adventfjorden – IsA, Svalbard	Dec 11/ Jan 12	5,15,25,60 m	<0.1	50-160	8.3-11.7	present study
Adventfjorden, Svalbard	Nov 06/ Feb 07	5,35 m	0.2-0.6	180-500	2.5-20[2]	Zajaczkowski et al. 2010
Kongsfjorden, Svalbard	Dec 06	0-50 m [1]	0.01	43	6.6	Iversen and Seuthe (2010)
Central Barents Sea	March 98	0-50 m [1]	<0.05	40-70	7.4-9.0	Olli et al. (2002)
Balsfjorden, N-Norway	Dec 08	20,63 m	0.05			Eilertsen and Degerlund (2010)
Malangen, N-Norway	Dec 08	20,417 m	0.03-0.04			Eilertsen and Degerlund (2010)
Ramfjorden, N-Norway	Nov/ Dec 89	0,10,30,50,70 m	0.03-0.20	70-270	13-25	Noji et al. (1993)
Spring - suspended						
Adventfjorden – IsA, Svalbard	Apr/ May 12	5,15,25,60 m	0.6-4.2	230-630	6.2-7.1	present study
Adventfjorden, Svalbard	Apr/ May 06	5,35 m	0.1-6.8	300-900	6-16	Zajaczkowski et al. (2010)
Kongsfjorden, Svalbard	Apr/ May 06	0-50 m [1]	0.2-10	310-670	4.6-5.3	Iversen and Seuthe (2010)
Central Barents Sea	May 98	0-50 m [1]	4.5-7.5	300-680	6.5-8.0	Olli et al. (2002)
Balsfjorden, N-Norway	Apr 92	0-36 m [1]	2.7-4.1	500-830		Reigstad et al. (1996)
Indrejord/ Tenneskjær, Malangen, N-Norway	Apr/ May 91	0-30 m [1]	0.5-2.1	410-610		Wassmann et al. (1996)
Conception Bay, Newfoundland fjord, Canada	May 98	30 m	2.5			Thompson et al. (2008)
Autumn – suspended						
Adventfjorden – IsA, Svalbard	Sept 12	5,15,25,60 m	0.3-0.4	90-130	8.5-10.5	present study
Adventfjorden, Svalbard	Oct 06	5,35 m	0.1	190-210	7.5-20 [2]	Zajaczkowski et al. (2010)
Kongsfjorden, Svalbard	Sept 06	0-50 m [1]	0.5	114	7.1	Iversen and Seuthe (2010)
Indrejord/ Tenneskjær, Malangen, N-Norway	Sept 91-Oct 91	0-30 m [1]	0.6-1.2			Wassmann et al. (1996)
Winter – sedimented						
Adventfjorden – IsA, Svalbard	Dec 11/ Jan 12	20,30,40,60 m	<0.26	90-400	10.6-14	present study
Adventfjorden, Svalbard	Nov 06/ Feb 07	35 m	0.22-0.33	500-750	6-25	Zajaczkowski et al. 2010
Central Barents Sea	March 98	30-200m[5]	<0.2	20-70		Olli et al. (2002)
Ramfjorden, N-Norway	Nov/ Dec 89	10,30,50,70 m	0.03-0.3	25-300	9-12	Noji et al. (1993)
Fanafjorden, W-Norway	Nov 79/ Feb 80	60,90 m		100-220	9-10	Wassmann (1984)
Spring – sedimented						
Adventfjorden – IsA, Svalbard	Apr/ May 12	20,30,40,60 m	2.5-20 [4]	900-1350 [4]	6.1-8.0	present study
Adventfjorden, Svalbard	Apr/ May 06	35 m	0.75-5	400-600	5-14	Zajaczkowski et al. (2010)
Central Barents Sea	May 98	30-200m[5]	10-30	200-2000		Olli et al. (2002)
Balsfjorden, N-Norway	Apr 92	30,60 m	0.5-5-5	180-630	6.5-13	Reigstad et al. (1996)

Indrejord/ Tenneskjær, Malangen, N-Norway	Apr/ May 91	30 m	0.1-13	250-750	5.5-10	Keck and Wassmann (1996)
Ullsfjorden, N-Norway	Apr 97	60 m	10-12	220-420	7.8-9.2	Reigstad et al. (2000)
Fanafjorden, W-Norway	Apr/ May 91	60,90 m		220-600	8-13	Wassmann (1984)
Conception Bay, Newfoundland fjord, Canada	May 98	40,80 m		300-700	8-9	Thompson et al. (2008)
Autumn - sedimented						
Adventfjorden – IsA, Svalbard	Sept 12	20,30,40,60 m	0.6-0.8 [4]	770-1530 [4]	13-15 [4]	present study
Adventfjorden, Svalbard	Oct 06	35 m	<0.1	500	7-16	Zajaczkowski et al. (2010)
Indrejord/ Tenneskjær, Malangen, N-Norway	Sept 91-Oct 91	30 m		130-190	7.5-8.0	Keck and Wassmann (1996)
Fanafjorden, W-Norway	Sept 80	60,90 m		300-420	9.5	Wassmann (1984)
Hudson Bay, Canada	Sept/ Oct 05	50 m	0.06-1.34	50-76.8		Lapoussière et al. (2013)

[1] Average concentration, not integrated
[2] different size fractions (0.4-2.7; 2.7-20; >20 µm)
[3] data from Reigstad and Wassmann (1996), another sampling station in the same fjord
[4] 2 h deployed traps not taken into account
[5] 30,40,50,60,90,120,150,200 m

Table A.1: Bin averages with the lower and upper limit and particle size categories, which were used to bin the particles

Bin average (mm)	Lower bin limit (mm)	Upper bin limit (mm)	Size category
0.056	0.050	0.063	
0.071	0.063	0.079	small particles
0.090	0.079	0.100	
0.113	0.100	0.126	
0.142	0.126	0.159	
0.179	0.159	0.200	
0.226	0.200	0.252	medium particles
0.285	0.252	0.318	
0.359	0.318	0.400	
0.452	0.400	0.504	
0.569	0.504	0.635	
0.717	0.635	0.800	
0.904	0.800	1.008	large particles
1.139	1.008	1.270	
1.435	1.270	1.600	
1.808	1.600	2.015	
2.278	2.015	2.539	
2.870	2.539	3.200	very large particles
3.616	3.200	4.031	
4.555	4.031	5.080	